Université d'Ottawa · University of Ottawa

Seismic Retrofit of Concrete Columns with Splice Deficiencies by External Prestressing

by

Pascal Beauséjour

A thesis submitted to Faculty of Graduate Studies and Research
in partial fulfilment of the requirements for the degree of

Master of Applied Science in Civil Engineering

The Master of Applied Science Program in Civil Engineering
is a joint program with Carleton University,
administrated by The Ottawa-Carleton Institute for Civil Engineering

University of Ottawa
Ottawa, Ontario, Canada
September 2000

0-612-57085-1

TO MY GIRLFRIEND ISABELLE AND MY PARENTS FOR THEIR LOVE AND CONTINUOUS SUPPORT

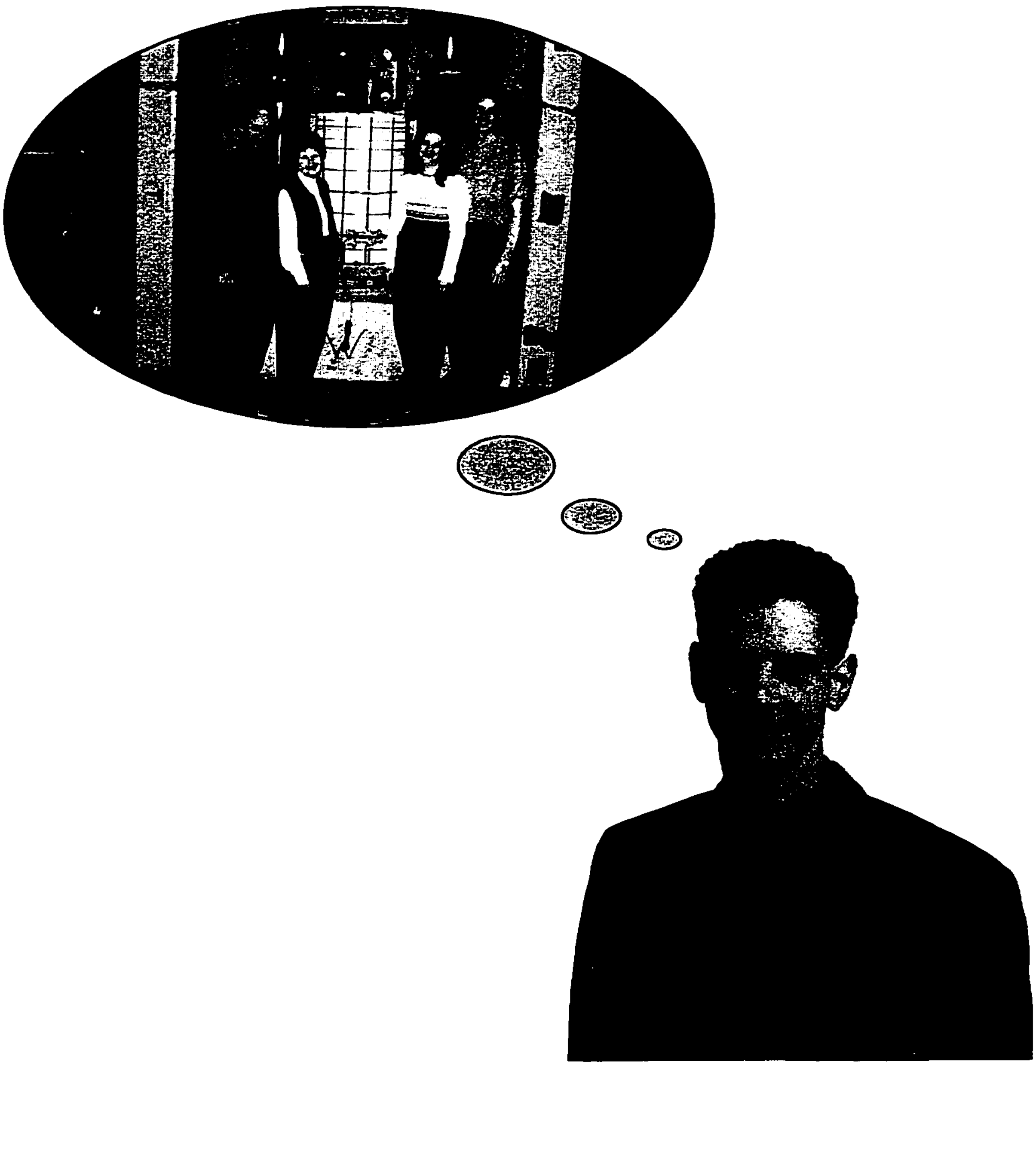

ABSTRACT

Engineers and designers have become aware of the seismic vulnerability of structures after recent earthquakes around the world. These events were responsible for improvements in design codes for the last three decades. According to the current design practice, reinforced concrete columns should have sufficient ductility to resist major earthquakes. The ductility allows a column to maintain its strength during inelastic response to earthquakes. However, many columns are not ductile, especially those built prior to the early 1970's. This is mainly because of lack of appropriate reinforcement detailing. These columns must be retrofitted for improved strength and ductility, if future disasters are to be prevented.

The research project reported in this thesis involves the use of a new retrofit strategy developed for concrete columns at the University of Ottawa. The new procedure consists of external prestressing existing columns with seven wire strands. External prestressing overcomes diagonal tension caused by shear, confines compression concrete, and may improve the behaviour of spliced reinforcement under reversed cyclic loading. Six large-scale bridge columns were built and tested under simulated seismic loading. Four long columns with a circular or a square cross-section of approximately 500 mm, and two short circular columns of 610 mm in diameter, were investigated. The columns all had lap spliced longitudinal reinforcement within the potential plastic hinge region. The splice length was equal to twenty times the bar diameter. The reinforcing details were typical of the pre-1970's design practice. The columns were subjected to a constant axial load of 15% of their concentric capacity.

Test data showed that the external prestressing provided sufficient confinement to significantly increase column ductility. The confinement in the splicing region had to be larger than everywhere else to avoid early slippage of spliced bars. The failures of retrofitted columns were ductile and occurred after the formation of plastic hinges near

the base. The drift capacities of strengthened columns were comparable to those with continuous reinforcement.

The columns were analysed with computer program ***COLA***, which did not incorporate the effects of reinforcement splicing. The analytical results were slightly lower than the strength values measured during testing. Similarly, column drift capacities were also underestimated when determined analytically.

RÉSUMÉ

À la suite des récents tremblements de terre survenus dans le monde, les ingénieurs et les concepteurs ont commencé à prendre conscience de la vulnérabilité séismique des structures. Ces événements ont entraîné plusieurs modifications aux codes de construction au cours des trente dernières années. Selon les codes actuellement en vigueur, les colonnes en béton armé devraient être ductiles afin de pouvoir résister à des séismes majeurs; la ductilité permet à la colonne de maintenir sa capacité lors de la réponse inélastique au tremblement de terre. Toutefois, plusieurs colonnes ne sont pas ductiles, spécialement celles qui ont été construites avant le début des années 1970, puisque les détails d'acier d'armature étaient inappropriés. À cette époque, les connaissances séismiques étaient inadéquates. Il faudrait donc renforcer ces colonnes en béton armé afin d'augmenter leur ductilité et ainsi améliorer leur comportement séismique.

Le projet de recherche avait pour but de renforcer des colonnes non ductiles en utilisant une nouvelle technique élaborée à l'Université d'Ottawa. Il n'était pas nécessaire de modifier les colonnes de béton existantes afin qu'elles soient renforcées; des câbles de précontraintes étaient installés autour des colonnes afin d'obtenir un confinement actif. Six colonnes de ponts à grande échelle ont été construits et mis à l'essai. Quatre colonnes longues avaient une section circulaire ou carrée d'une dimension extérieure d'environ 500 mm et deux colonnes courtes avaient une section circulaire de 610 mm de diamètre. L'acier d'armature longitudinal des six spécimens était chevauché à la base des colonnes sur une longueur représentant vingt fois le diamètre de la barre. Les détails d'acier d'armature étaient typiques des colonnes construites avant les années 1970. Les spécimens étaient testés sous une charge latérale simulant un séisme et une charge axiale correspondant à 15 % de la capacité de la colonne en compression pure.

Les résultats expérimentaux ont démontré que les câbles de précontrainte ont suffisamment confiné les colonnes pour augmenter leur ductilité de façon significative. Le confinement dans la région de chevauchement des barres devait toutefois être supérieur au confinement fourni ailleurs sur la colonne afin d'éviter le glissement hâtif de l'acier longitudinal. La rupture des colonnes renforcées étaient ductile et elle produite après la formation d'une rotule plastique à la base des colonnes. Le pourcentage de déformation des colonnes renforcées étaient comparable à celui des colonnes dotées de barres d'armature continues.

Les colonnes ont été analysées avec le programme COLA, même si le chevauchement des barres longitudinales ne pouvait pas être modélisé. Le logiciel a légèrement sous-estimé la résistance des colonnes longues non renforcées alors qu'il a sous-évalué la capacité des colonnes courtes non renforcées. Ce programme est un outil intéressant permettant d'évaluer s'il est nécessaire ou non de renforcer une colonne.

ACKNOWLEDGMENTS

I would like to express my sincere gratitude to my thesis supervisor Dr. Murat Saatcioglu for his guidance, help and support. Many thanks to Derek Mes for his assistance, availability and technical support as well as his suggestions during the construction and testing of specimens. I would also like to thank my fellow graduate students for their help in the laboratory. Mr. Derek Mes and Dr. Cem Yalcin are also acknowledged for providing assistance and test data on columns without lap splices.

Many special thanks to my girlfriend Isabelle and my parents Diane and Réal for their encouragement and continuous support during the years of my studies. The encouragement from my brother and his wife as well as from my parents-in-law and my grandparents are sincerely appreciated and not forgotten.

Finally, I gratefully acknowledge the following organisations for their financial support throughout my master's degree at the University of Ottawa: the National Sciences and Engineering Research Council (NSERC) of Canada, the Fonds pour la Formation de Chercheurs et l'Aide à la Recherche (FCAR) in collaboration with the Ministère des Transports du Québec, the University of Ottawa and Ciment Saint-Laurent.

FOREWORD

This thesis follows two others written by Dr. Cem Yalcin and Mr. Derek Mes on the same overall project, dealing with column retrofitting. It is based on a new method developed at the University of Ottawa under the supervision of Professor Murat Saatcioglu. The method involves externally prestressing concrete columns with specially developed hardware.

The current thesis forms *Phase 3* of the research program. With the completion of the third phase, 19 large-scale bridge columns will have been tested, including those critical in shear, flexure, and lap splices. The research program has led to a better understanding of column behaviour with and without the new retrofitting developed.

CONTENTS

LIST OF TABLES

LIST OF FIGURES

NOTATIONS

A_c	Area of the core section
A_g	Gross area of concrete section
A_{ps}	Nominal area of the prestressing strands
C_j	Modification factor for longitudinal reinforcement details
d_b	Longitudinal bar diameter
D	Column diameter or outside dimension of the column
E	Modulus of elasticity
f'_c	Cylinder compressive strength of concrete specimens
f_l	Lateral confinement pressure in columns
f_{ps}	Stress level applied on prestressing strands
f_{pu}	Ultimate strength of prestressing strands
f_u	Ultimate strength of reinforcing steel
f_y	Yield strength of reinforcing steel
F	Applied lateral load
h	Outside dimension of the column
L	Shear span (effective height of the column)
M	Applied moment
M_y	Yield moment capacity
P	Applied axial load
P_o	Axial capacity under pure compression
s	Spacing between transverse reinforcement
s_{ps}	Spacing between prestressing strands
t_j	Steel jacket thickness
Δ	Lateral tip displacement of the column
Δ_y	First yield displacement
ε_{sh}	Strain hardening strain of reinforcing steel
ε_u	Ultimate strain of reinforcing steel
ε_y	Yield strain of reinforcing steel
θ_h	Total rotation at h from the base of the column
$\theta_{h/2}$	Total rotation at h/2 from the base of the column
θ_0	Anchorage slip rotation at the base of the column
ρ_l	Longitudinal reinforcement ratio
μ	Displacement ductility ratio (Δ/Δ_y)

CHAPTER 1

INTRODUCTION

1.1 GENERAL

Each year, about 140 earthquakes occur around the world with a Richter magnitude of 6 or greater. Of these earthquakes about 20 have a magnitude exceeding 7. Such earthquakes may cause major damage, especially when the epicentre is located close to urban areas. Seismologists identify about 1500 earthquakes each year in Canada alone. Some of them cannot be felt, while others may cause significant damage. For instance, the 1988 Saguenay earthquake caused tens of millions of dollars in damage. It reminded Eastern Canadians of their vulnerability to major earthquakes. Figure 1.1 presents the Canadian seismicity in the 20^{th} century. Table 1.1 summarises significant earthquakes over the same period. Considering the urban areas, this data shows two major seismic zones: Eastern Canada and Western Canada. Western Canada is subjected to high seismic activity and is located in an

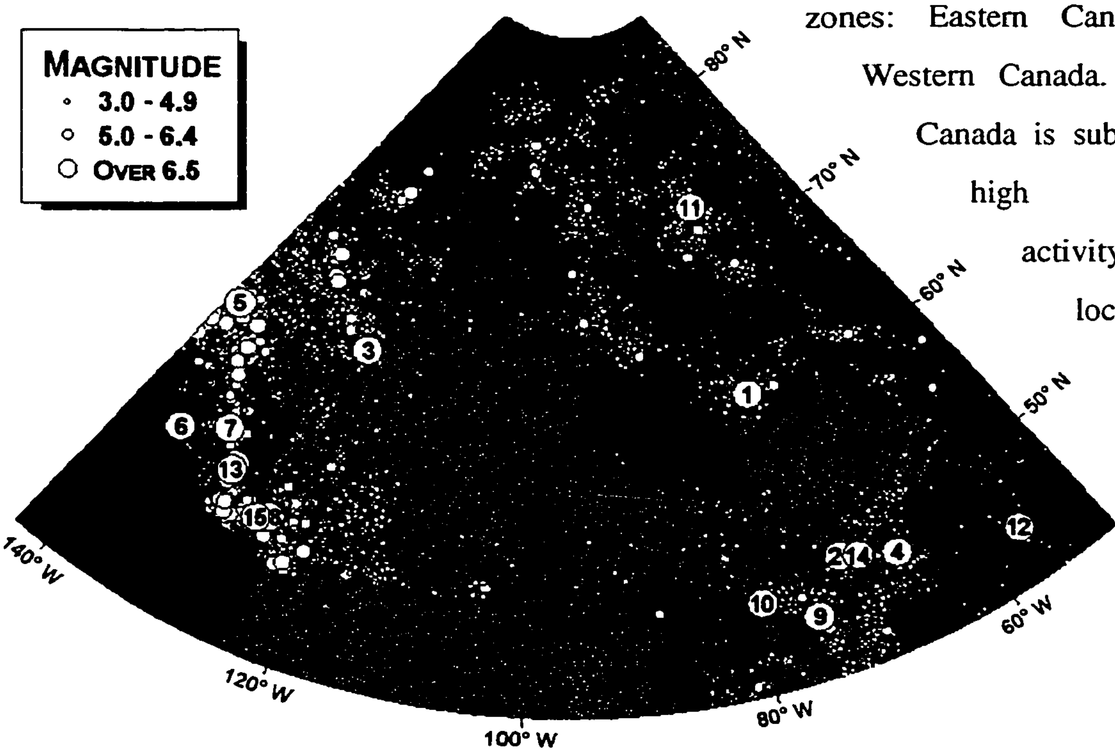

Figure 1.1 Canada Seismicity - 20^{th} century

active fault region. In comparison, Eastern Canada is considered a moderate seismic zone with high dominant frequency earthquakes due to the geological characteristics of the Laurentian shield.

Table 1.1 Major earthquakes in Canada - 20th century

No.	Year	M*	Region
1.	1989	6.3	Ungava
2.	1988	5.9	Saguenay
3.	1985	6.9	Nahanni
4.	1982	5.7	Miramichi
5.	1979	7.2	Yukon
6.	1970	7.4	Queen Charlotte Islands
7.	1949	8.1	Queen Charlotte Islands
8.	1946	7.3	Vancouver Island
9.	1944	5.6	Cornwall
10.	1935	6.2	Quebec
11.	1933	7.3	Baffin Bay
12.	1929	7.2	Antlantic (tsunami)
13.	1929	7.0	Queen Charlotte Islands
14.	1925	6.2	Charlevoix-Kamouraska
15.	1918	7.0	Vancouver Island

* M = Magnitude

Unfortunately, many structures are vulnerable to earthquakes. Figure 1.2 illustrates examples of structures that suffered damage during recent earthquakes. Seismic behaviour of reinforced concrete structures designed and built prior to early 1970's especially indicates inadequate seismic capacity because of lack of appropriate seismic provisions in the building codes of the era. The 1971 San Fernando earthquake revealed many shortcomings of pre-1971 designs which resulted in severe structural damage. Non-ductile behaviour of columns was one of the primary reasons for structural

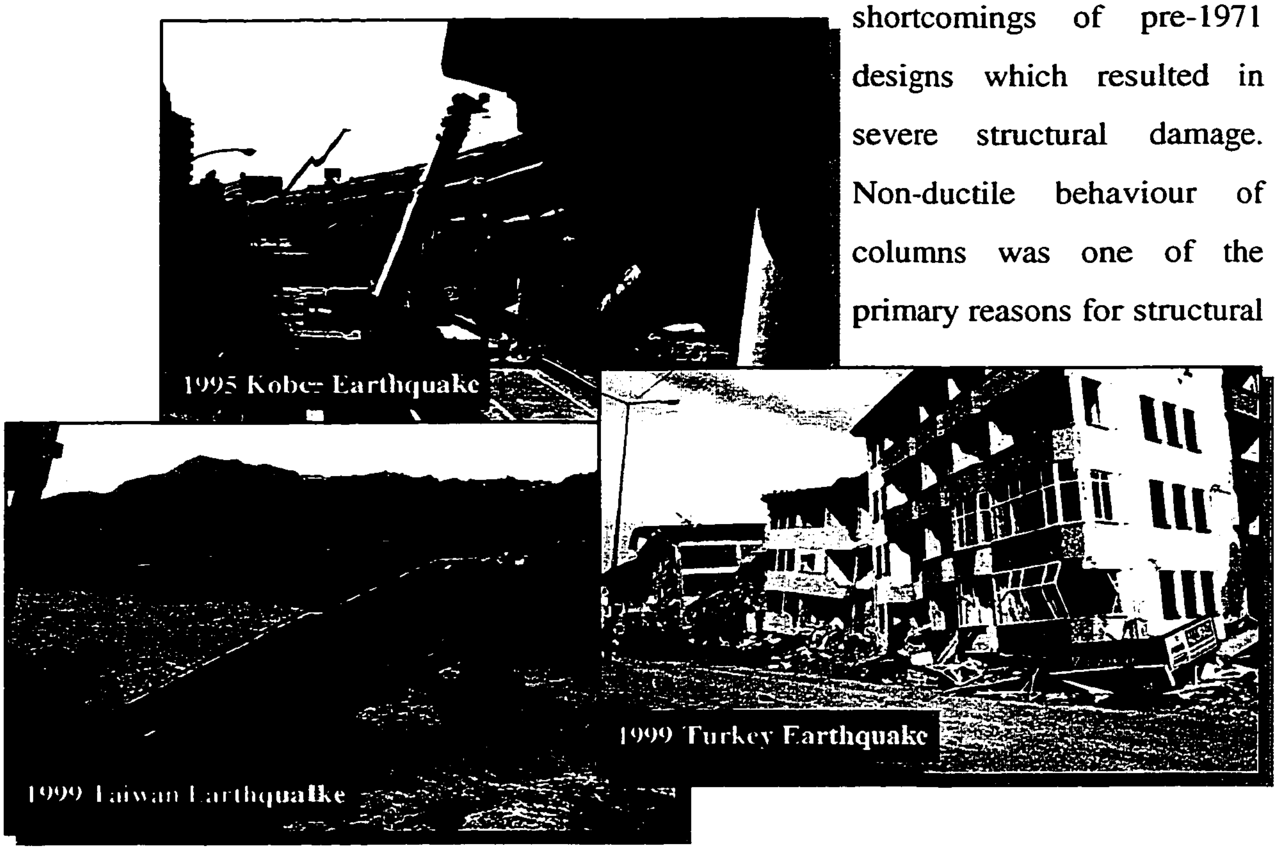

Figure 1.2 Recent earthquake damages

Figure 1.3 Effect of confinement; ① Poorly confined column; ② Adequately confined column

collapse. Concrete columns were poorly confined because of insufficient transverse reinforcement. Figure 1.3 presents two pictures of the Olive View Medical Centre taken after the 1971 San Fernando earthquake, illustrating the difference between poorly and adequately confined columns. The square column shown in Fig. 1.3.1 failed due to lack of transverse reinforcement (poor confinement) and lost its integrity. On the other hand, the circular column shown in Fig. 1.3.2, although of the same building, showed ductile behaviour, developing excessive lateral displacement because of the adequate confinement provided by spiral reinforcement. Furthermore, most bridge columns and first storey building columns designed prior to early 1970's had the longitudinal reinforcement lap spliced in the potential hinging region. This created additional weaknesses in seismic resistance of these structures.

The reinforcement details of Canadian bridge columns designed prior to 1971 are similar to those that failed during recent earthquakes in the United States (Yalcin, 1998). Building columns of the same era in Canada have similar designs, with inadequate lap splice and insufficient transverse reinforcement. Therefore, these columns, when located in seismically active regions have to be retrofitted to avoid potential collapses. Some structures, especially bridges, must be functional after an earthquake because they provide access to hospitals, fire stations and a variety of other post-disaster relief services. The research program presented in this thesis involves the investigation of a retrofit technique for non-ductile reinforced concrete columns developed at the University of Ottawa. The technique has been demonstrated to be more practical and economical compared to the majority of other retrofit strategies that have been used for concrete columns. Although the same technique is applicable to building columns, the emphasis in this research program was placed on bridge piers.

1.2 LITERATURE REVIEW

Recent major earthquakes; like the 1971 San Fernando, 1989 Loma Prieta, 1994 Northridge, and 1995 Kobe earthquakes provided many lessons to learn. Consequently, the structural design codes were improved in order not to repeat mistakes of earlier design practices. The main design deficiencies of the pre-1971 codes will be underlined in the literature review presented in this section. An overview of the state-of-the-art on seismic retrofitting of existing concrete columns will be highlighted. Also, the results of experimental research conducted in earlier phases of the current research program will be presented.

1.2.1 BACKGROUND AND PREVIOUS RESEARCH

The following is a summary of several papers published around the world on subjects related to reinforced concrete column retrofitting. Although it does not provide an exhaustive list of all the publications related to this thesis, the articles were chosen because of their quality in providing a good overview of the subject. The articles are presented in chronological order of publication.

Chai, Priestley and Seible (1991) reported various structural inadequacies in concrete bridge columns designed prior to early 1970's. Specifically, they reported that:

- Flexural strength was inadequate. The seismic design force coefficient of 10% that was previously employed resulted in high ductility demands during significant earthquakes.
- The use of No. 4 stirrups (12.7 mm diameter) spaced at 12" (305 mm), regardless of column dimensions, reduced flexural ductility and shear strength. This resulted in lower shear capacities than those corresponding to flexural yielding and produced brittle shear failures, especially in short columns.
- The lap length of 20 times the bar diameter was insufficient to develop yield strength in longitudinal bars.
- Pile caps and footings in older bridges were often provided with only bottom reinforcement. Top steel and shear reinforcement in these pile caps were considered unnecessary and routinely omitted.
- Joint regions were usually not designed to resist the high shear stresses that they could be exposed to during a severe earthquake.

Chai et al. (1991) built six long circular bridge columns of 24" (610 mm) in diameter and 12' (3.658 m) in height. The objective was to evaluate the enhancement of flexural strength and ductility by using a site-welded steel jacket around the potential plastic hinge region. They also observed the difference in behaviour between continuous and spliced longitudinal reinforcement (with 20 bar diameter splice length) within the plastic hinge region. Two types of footings were used in their experimental research, consisting of a strong and a weak footing. The lateral displacement history imposed on columns was based on displacement ductility ratio, μ, defined as the ratio of maximum displacement at a given cycle, Δ, to the displacement needed to cause first yielding in the longitudinal reinforcement, Δ_y. A reversed cyclic load was applied at the tip of columns involving three cycles at each value of $\mu = 1$, 1½, 2, 3, 4, etc. up to failure. Axial load was applied to represent gravity loads, and was equal to 17.7% $A_g f'_c$.

Chai et al. (1991) concluded that using continuous bars in the potential plastic hinge region of as-built columns resulted in failure due to lack of confinement. Those with lap splices failed due to the slippage of bars within the lap length, preventing the development of nominal flexural strength.

Adding a steel jacket around circular bridge columns was effective in increasing flexural ductility. A ductility ratio of $\mu = 7$, corresponding to a lateral drift ratio of $\Delta/L = 5.3\%$, was reached during tests of retrofitted columns. The stiffness was increased by about 10% to 15%. Steel jacketing was also effective in repairing a damaged column in restoring its flexural strength and deformability. However, the energy absorption of the repaired column was less than that for retrofitted columns. The researchers further noticed that footings designed on the basis of provisions of pre-1970 codes might be susceptible to joint shear failure. They emphasised their finding by stating, "the design and retrofit of such regions requires urgent attention."

Coffman, Marsh and Brown (1993) reported that circular concrete bridge columns with long shear spans, built between 1950's and mid-1970's were among seismically deficient structures. The transverse reinforcement provided in these columns was of minimum quantity, and its effectiveness was doubtful. This reinforcement could not provide sufficient confinement of the longitudinal lap splices in potential plastic regions.

The objective of Coffman et al. (1993) was to retrofit a typical column to improve its behaviour using prestressed external hoops around the column. Four circular bridge columns with pre-1971 details were built. The dimensions were 18" (457 mm) in diameter and 10' (3.048 m) high. Nine dowels were screwed and welded to a thick steel base plate under the column. The lap splice length was 35 times the longitudinal bar diameter. Only the region with spliced bars was retrofitted, which included the plastic hinge zone. The first column was tested without the retrofit as reference. The other three were retrofitted with No. 4 (12.7 mm diameter) prestressed external hoops placed at 3" (76 mm) or with No. 3 (9.5 mm diameter), placed either at 3" (76 mm) or 4" (102 mm). Each retrofit hoop was formed into semicircular pieces connected by swaged couplers and was prestressed to approximately 350 MPa. The columns were subjected to an axial load of 20% $A_g f'_c$. The lateral loading history for all columns was based on the ductility ratio, μ, and consisted of one cycle at $\mu = ¾$, two cycles at $\mu = 1$, two cycles at $\mu = 2$ and continued cycling at $\mu = 4$ until failure. This loading sequence was based on a suggestion made by Park, which was adopted in the New Zealand structural design code. Accordingly, the structure should be able to withstand "at least four times that at first yield, without the horizontal load-carrying capacity of the building being reduced by more than 20 percent."

The non-retrofitted column lost its strength after the first cycle at a ductility ratio of $\mu = 4$, corresponding to a drift ratio of $\Delta/L = 3.6\%$, whereas the retrofitted columns completed between 12 to 16 cycles at $\mu = 4$. The failure of the three retrofitted columns occurred by rupturing of the weld at the junction of dowel-steel base plate. The researchers concluded that this retrofitting technique did not affect the stiffness. It increased column strength and energy dissipation in a single cycle slightly, while also increasing the total number of cycles before failure. Also, based on these conclusions, the authors were confident in the use of this retrofit procedure on long columns of pre mid-1970's era, built in a moderately high shakings of long duration.

Mitchell, Sexsmith and Tinawi (1994) presented problems observed in old bridges designed with inadequate level of knowledge and awareness of seismic effects compared to our current understanding. The main problems involved reinforced concrete foundations, columns, cap beams and beam-column joints, as well as steel braces. These are listed in Table 1.2 with recommended corrective measures.

Table 1.2 Deficiencies of bridges designed before 1971

		PROBLEMS	SUGGESTIONS
REINFORCED CONCRETE	FOUNDATIONS	• Footings too small with inadequate number of piles for the actual seismic effects. • Insufficient flexural and shear strength. • Insufficient amount or lack of top reinforcement. • Inadequate embedment and anchorage of the reinforcement. • Insufficient amount of vertical reinforcement through the interface column-footing to resist to shear demand.	A footing must be stronger than the column to allow plastic hinging in the column. To retrofit a foundation properly, a designer has to make sure that this substructure is able to transfer the column resistance while remaining elastic.
REINFORCED CONCRETE	COLUMNS	• Insufficient lap splice length. • Splicing at the plastic hinge region. • Insufficient amount of transverse reinforcement resulting in poor confinement and insufficient shear strength. • Poor reinforcement details (large spacing and 90° bend anchorage). • Insufficient flexural strength and ductility.	Steel jacketing is a good technique to retrofit columns providing passive pressure. "This confinement increases the shear strength, decreases the tendency for buckling of longitudinal bars and improves the ductility [...] without significantly increasing the moment capacity."
REINFORCED CONCRETE	CAP BEAMS	• Insufficient flexural strength and shear strength of beam to allow plastic hinge formation in the columns. • Large spacing between stirrups. • Inadequate stirrup anchorage (90° hook). • Insufficient embedment for longitudinal bars.	In multi-storey buildings, beams dissipate most of the energy, whereas in bridges, the columns are the main energy dissipators. Cap beams must be over-designed, providing the plastic hinge in the columns.
REINFORCED CONCRETE	JOINTS	• Lower shear strength than flexural strength of the cap beam and the column. • Large bar spacing. • Lack of shear reinforcement. • Poor anchorage details. • Large bending radius for large bar sizes.	A reinforced concrete jacket with horizontal and vertical reinforcement is a good way to retrofit a weak joint as long as it enables the formation of plastic hinges in the column.
STEEL	BRACING	• Weaker connections than the members. • Too high slenderness. • K brace arrangements are vulnerable to progressive collapse. • Insufficient bracing capacity to resist seismic loads.	K and X bracing should be eliminated or greatly strengthened. The connections should be modified to make sure they are stronger than the members.

Mitchell et al. (1994) also reported deficiencies with regard to insufficient seat width. To prevent bridge girders from falling off the supports, restrainers were suggested as a suitable retrofit technique. This is probably the least expensive retrofitting strategy, preventing disastrous consequences. Furthermore, it was indicated that old bridge bearings were not designed to resist lateral seismic loads. The authors stated that the main retrofit objective for reinforced concrete bridges was to improve ductility of the columns. "Hence, the capacities of the foundations, beams and beam-column joints must exceed the demand from flexural hinging in the columns." For steel braced bridges, the importance of preventing brace buckling and brace connection failure was emphasised.

Rodriguez and Park (1994) conducted experimental research on reinforced concrete building columns designed and built prior to 1970. Major deficiencies found in building columns were the same as for bridge columns: inadequate flexural strength and ductility of columns and inadequate shear strength of beams, columns and beam-column joints. These shortcomings were mainly due to the insufficient amount of transverse reinforcement used and poor anchorage, especially in columns.

A total of four columns were built, representing the lower level of a seven-storey building constructed in the 1950's. Each column was 350 mm square and 3.3 m long corresponding to the region between the mid-height of two consecutive storeys. A stub at mid-height of specimens represented part of a two-way slab and beams. Two columns were repaired after being tested and the other two were retrofitted. The use of reinforced concrete jacket was chosen to improve the column behaviour. The authors reported that this technique gave an increase in lateral resistance, which is distributed throughout the structure without having to modify the foundation.

During the tests, a reversed cyclic load was applied at mid–height of the specimens combined with a constant axial load of 20% $A_g f'_c$. The columns were subjected to two cycles at each of $\mu = 1, 2, 3, 4$, etc. Results showed that the four reinforced specimens had a similar behaviour, no matter if the specimen had been damaged or not prior to the retrofit. Rodriguez et al. (1994) concluded that the strength and stiffness were increased up to three times compared with the as-built column. The ductility and the energy dissipation were also enhanced and a ductility ratio μ of 6 was reached, corresponding roughly to 2¾% drift, whereas the as-built column could develop only $\mu = 2$. The results of this research showed that a reinforced concrete jacket could be effective, but it is a labor-intensive retrofitting technique.

Mitchell, Bruneau, Williams, Anderson, Saatcioglu and Sexsmith (1995) presented some design deficiencies of bridges built prior to 1971 that were similar to the previous ones, such as low design lateral force levels, inadequate confining reinforcement, lack of longitudinal restraint across expansion joints and insufficient seat widths at joints and supports. In this article, problems with bridges during the 1994 Northridge earthquake were reported. The majority of problems were attributed to poor column performance and column failures, except for one case where the bridge collapse was due to loss of seating. Although this bridge was retrofitted with restrainers, it could not survive the earthquake. The authors explained that the bridge was subjected to torsion, probably because of an unsymmetric lateral support system and a large skew angle of 66°. Since the restrainers were parallel to the longitudinal axis of the bridge, instead of being perpendicular to the deck joints, they were inefficient to resist the lateral displacement. The other bridges retrofitted with restrainers behaved well. Relatively minor failures were attributed to restrainers, and these were blamed on early designs. Use of joint restrainers still appears to be economical and effective to prevent loss of span failures.

Mitchell et al. (1995) explained the failure modes of the columns that caused the collapse of six bridge structures during the 1994 Northridge earthquake. These bridges were designed in the 1960's and early 1970's. Two types of transverse reinforcement were used in columns. The first one was No. 4 (12.7 mm diameter) or No. 5 (16 mm diameter) hoops at 305 mm spacing, providing poor confinement and low shear capacity. The second one was No. 5 (16 mm diameter) spirals with 89 mm pitch that could not maintain the shear capacity after the formation of the plastic hinge. Because of the poor reinforcement details, the columns failed due to shear or to a combination of shear, flexure and compression. The behaviour of these columns could have been predicted and the columns could have been retrofitted to prevent collapse. In fact, the authors reported that over 100 bridges were retrofitted with steel jacket in this area and only a few of them were subjected to minor visible damage due to spalling at control joint locations.

Chai (1996) confirmed the effectiveness of steel jackets on columns during the 1994 Northridge earthquake. Their good performance motivated his analytical study. The aim was to investigate the influence of this retrofitting technique on the structural characteristics of circular bridge columns.

A steel jacket increases the confinement of concrete columns with insufficient transverse reinforcement. The California Department of Transportation (CALTRANS) specified a minimum jacket thickness of 6.4 mm to provide enough rigidity to be able to manipulate and install the steel jacket with ease in the field. This thickness, t_j, is required to increase with the size of the column according to the following relation:

$$t_j = C_j \left(\frac{D}{200}\right) \geq 6.4 \text{ mm} \qquad [1.1]$$

where, D = Column diameter

C_j = Modification factor for longitudinal reinforcement details

The factor C_j adjusts the thickness of the steel jacket to take into consideration inadequate lap splices at the base of the column:

$$C_j = \begin{cases} 1.0, & \text{for continuous longitudinal reinforcement} \\ 1.2, & \text{for lapped longitudinal reinforcement} \end{cases} \qquad [1.2]$$

Chai (1996) reported that the thickness proposed in Eq. 1.1 provided an effective confinement pressure of 2.0 MPa for concrete. It resulted in an enhancement of the tensile strain of longitudinal reinforcement and also in an increase of the ultimate compressive strain of concrete, reaching about four to nine times the spalling strain of unconfined concrete. Hence, the curvature ductility and the flexural strength were both enhanced. Simulations showed that the ultimate limit state was generally governed by ultimate compressive strain of the concrete when the design jacket thickness specified in Eq. 1.1 was used. For a thickness larger than twice the provision, a low-cycle fatigue fracture of the longitudinal reinforcement would occur.

Steel jacket also increased the column stiffness due to three factors: i) the bond strength between the jacket and the column, ii) the thickness and iii) the length of jacketting. For example, the CALTRANS specifications would enhance the stiffness by 35% to 60% for long columns with full-height steel jackets. Based on this study, the thickness provision of CALTRANS was adequate and it would be useless to choose a thicker steel jacket.

Jaradat, McLean and Marsh (1996) reported the same shortcomings presented in other literature about column bridges designed before 1971. Typically, No. 3 (9.5 mm diameter) or No. 4 (12.7 mm diameter) hoops at 12" (305 mm) were used providing low shear capacity and poor confinement. Therefore, the full flexural strength could not have been reached and the longitudinal reinforcement was susceptible to buckling. Current code provisions are about eight times the transverse reinforcement present in pre-1971 designs. Another problem was splicing main reinforcement at the bottom of the columns with a splice length of only 20 times the longitudinal bar diameter. The lap splice length was too small to be effective within this potential hinging region. The vulnerability of pre-1971 bridges was evident in the 1971 San Fernando, the 1987 Whittier Narrows, the 1989 Loma Prieta and the 1994 Northridge earthquakes.

The authors tested four as-built columns to characterise the load and displacement capacities of bridge columns designed prior to 1970's. The scaled models were circular with a 254 mm in diameter and either a 1020 mm or a 1780 mm height. Shear span-to-depth ratios of 2.0 and 3.5 were studied, in combination with two longitudinal reinforcement ratios of 1% and 2%. The main reinforcement was continuous at the top of the columns and was spliced at the bottom, over a length of 20 times the bar diameter.

During testing, each column had fixed-fixed end conditions. A constant axial load of 5% $A_g f'_c$ was applied, while accompanied by a variable lateral load applied at the tip. The loading pattern consisted of three cycles for each value of μ = 1, 2, 3, 4, 5 and 6 unless failure occurred earlier. The authors reported that the plastic hinge regions without splices maintained an acceptable level of flexural strength and failed because of longitudinal bar buckling. For plastic hinge regions with lap splices, the strength decreased rapidly because of concrete cracking and splice slippage. "Despite the splice degradation, the splice region was able to transfer shear and axial loads through large displacement levels."

Two columns were expected to have flexure dominant behaviour and two others, shear dominant behaviour. However, only one column failed in shear. To compute theoretical shear and flexure strengths, Jaradat et al. (1996) used the following models:

THEORETICAL SHEAR STRENGTH

- American Concrete Institute (ACI) equations
- American Association of States Highways and Transportation Officials (AASHTO) specifications
- University of California at San Diego (UCSD) model
- University of California at Berkeley (UCB) model

THEORETICAL FLEXURAL STRENGTH

- Priestley and Seible model

The conclusions made by the authors about the theoretical shear strength were that all the models gave conservative values except the UCSD model, which gave slightly unconservative strength prediction. The ACI and AASHTO equations did not predict shear strength degradation as the displacement ductility increased. The predicted flexural strength was close to the experimental results for plastic hinge, with or without splices.

Aboutaha, Engelhardt, Jirsa and Kreger (1996) tested and retrofitted eleven reinforced concrete building columns with details of the 1950's and 1960's. At the time, buildings were mainly designed for gravity loads and were not adequately detailed to resist earthquake loads in regions of high seismicity. The shear strength and the confinement in flexural hinge zones were insufficient. The column bar splices were generally above the floor level, in the potential plastic hinge region. Furthermore, the splice lengths were mostly designed as compression splices.

Aboutaha et al. (1996) strengthened long rectangular building columns with inadequate lap splices at the bottom of columns through the use of rectangular steel jackets and adhesive anchor bolts. Details of the specimens were based on provisions of old ACI building codes (1956 and 1963). The splice length was 24 times the bar diameter. The columns were 9' (2.75 m) high with a cross-section of 18" $\times$ 36" (457 mm $\times$ 914 mm), 18" $\times$ 27" (457 mm $\times$ 686 mm) or 18" $\times$ 18" (457 mm $\times$ 457 mm). A reversed cyclic loading was applied with ½% drift increments until failure. Two cycles were completed for each drift ratio. The columns were not subjected to axial load because it was considered more critical to test the splice region.

Six variables were analyzed using retrofitted specimens. These included number and location of adhesive anchor bolts, spacing between adhesive anchor bolts, concrete strength, column width and steel jacket height. The test results showed an improvement of the column behaviour, maintaining flexural strength up to a drift ratio of 4%. The adhesive anchor bolts were essential in attaining good performance for large columns. According to Aboutaha et al. (1996), small columns could be successfully retrofitted without these bolts. The authors developed a simplified analytical model and elaborated some design recommendations to retrofit rectangular building columns with rectangular steel jackets.

Saadatmanesh, Ehsani and Jin (1996) retrofitted old columns with fiber reinforced plastic (FRP) composite straps in order to increase the column ductility. The advantages of this material are its high strength, good fatigue life, light-weight, maintenance cost and ease of transportation and handling.

A total of five $^1/_5$-scale models were built based on the existing highway bridge columns that were designed before 1971. All the specimens were circular with a 12" (305 mm) diameter. Although the column height was not specified, it seemed to have been around 71" (1.8 m). The longitudinal reinforcement was continuous for two columns and was spliced at the bottom of the other three columns over a length of 20 times the bar diameter. The strengthened columns were wrapped with six layers of high performance FRP for a total thickness of 0.2" (5 mm). Unidirectional glass fibers in the FRP composite straps were used to provide passive or active confinement. A gap between the column and the straps was filled with pressurised epoxy resin to attain active pressure. During the tests, the columns were subjected to an axial load of 100 kips (445 kN) corresponding approximately to 16% $A_g f'_c$. The applied lateral displacement history was two complete cycles for each ductility ratio of μ = 1, 1½, 2, 3, 4, etc.

The non-retrofitted columns sustained lateral loads of up to a low ductility level of μ = 1½ (about 2.2% drift) for the column with lap splices, and μ = 3 (approximately 3.7% drift) for the column with continuous bars. The strengthened columns developed stable hysteresis loops up to $\mu \approx 6$ (roughly 6½% drift). Saadatmanesh et al. (1996) concluded that columns wrapped with FRP in the potential plastic hinge region increased the strength and the ductility. Both passive and active confinement improved the behaviour of columns in a similar way, so the active pressure did not seem to justify additional costs.

Seible, Priestley, Hegemier and Innamorato (1997) reported three different types of failures that could occur in reinforced concrete columns with insufficient transverse reinforcement, when subjected to seismic loads. These included shear failure, confinement failure of the hinging region and lap splice de-bonding. These three problems were the result of the following deterioration:

SHEAR FAILURE

- Development of diagonal cracks once the concrete tensile strength is exceeded
- Opening of diagonal cracks
- Cover concrete spalling
- Opening of transverse reinforcement
- Buckling of longitudinal reinforcement
- Disintegration of the core concrete

CONFINEMENT FAILURE OF THE HINGING REGION

- Formation of horizontal flexural cracks
- Crushing and spalling of the concrete cover
- Buckling of longitudinal reinforcement
- Compression failure of the core concrete initiating the deterioration of the plastic hinge

LAP SPLICE SLIPPAGE

- Development of vertical cracks
- Debonding of lap splices

Shear failure was indicated to be brittle and even explosive, whereas confinement failure was classified to be less destructive and more desirable. Slippage of splices was associated with flexural capacity deterioration and could occur rapidly for a poorly confined column with short lap splices. It was suggested that, to strengthen a column, none of these problems should be considered separately because retrofitting for only one could shift the problem elsewhere and create another failure mode.

Seible et al. (1997) also introduced general guidelines for retrofitting reinforced concrete columns with carbon fiber jackets based on the failure modes mentioned earlier. The authors showed the validation of the guidelines by testing seven bridge columns. Each column was subjected to an axial load and a lateral force. The lateral loading scheme consisted essentially of three cycles at each ductility ratio of $\mu = 1$, 1½, 2, 3, 4, 6, 8, 10, 12, or until failure. Test results were compared with three previously tested columns that were retrofitted with steel jackets. Two of the rectangular columns tested were 610 mm × 406 mm in cross-section with 2.4 m height. The shear span was 1.2 m because the end conditions were fixed-fixed. The column aspect ratio was selected so that shear dominant behaviour could be obtained. The longitudinal reinforcement was continuous from the footing up to the column top. An axial load of 507 kN was applied corresponding to 5.9% $A_g f'_c$. One of the columns, without any retrofit, could only develop a displacement ductility ratio of $\mu = 3$ (2.7% drift), although the other, with a carbon fiber jacket, was able to sustain $\mu = 10$ (7.4% drift).

The second pair of rectangular columns had a 730 mm × 489 mm cross-section and 3.7 m height, showing flexure dominant behaviour. They were built without splices. With an axial load of 1780 kN (14.5% $A_g f'_c$), the control column failed after a ductility ratio of $\mu = 3$ (2½% drift), while the column retrofitted with fiber carbon jacket maintained a constant load level up to $\mu = 7$ (5.7% drift).

Three other columns were built with a circular cross-section of 610 mm in diameter and a height of 3.658 m. The longitudinal reinforcement was spliced at the bottom of the column, over a length of 20 times the bar diameter. Each column was tested under constant axial load of 1780 kN (17.7% $A_g f'_c$). The first column was tested with a fiber carbon jacket retrofit, but results showed de-bonding of the lap splice after a displacement ductility ratio of $\mu = 5$ (4½% drift). After the test, Seible et al. (1996) realised that the actual jacket thickness was 20% less than the design jacket thickness. Subsequently, another test was conducted with a slightly higher thickness than the requirements called for. The results of this last column showed that a ductility ratio of $\mu = 10$ (6.8% drift) was achieved without a significant strength decay. The conclusion made by the authors was that a composite jacket is just as effective as conventional steel jacket in improving the structural characteristics of reinforced concrete columns with poor details.

Saadatmanesh, Ehsani and Jin (1997) investigated a method utilizing fiber reinforced plastic (FRP) straps to retrofit rectangular bridge columns. The straps wrapped around the columns provided external confinement, prevented concrete crushing and spalling, and prevented buckling of the longitudinal reinforcement. The aim was to evaluate the effectiveness of FRP straps on columns with inadequate splicing or insufficient transverse reinforcement. Five scaled models were built reflecting the pre-1971 designs. The rectangular columns had a cross-section of 241 mm × 368 mm and a height of 1.8 m. An axial load of 15% $A_g f'_c$ was applied on the columns. The lateral loading pattern consisted of two reversed cycles for each ductility level of $\mu = 1, 1½, 2, 3, 4, 5, 6$ until failure.

Two specimens had lap splices of 254 mm long at the bottom of the column, corresponding to a length of 16 times the bar diameter. The non-retrofitted column failed due to the slippage of the splices once the ductility level reached $\mu = 1½$ (2% drift). The other column was strengthened with eight plies of FRP in the potential plastic hinge region. The straps had a rectangular shape. Pressurized epoxy resin was introduced between the FRP straps and the concrete cover to create active confinement. The column sustained lateral load up to $\mu = 5$ (6.4% drift).

Three models were designed as shear dominant columns without the splicing of longitudinal reinforcement. One of the columns represented as-built conditions, without a retrofit. This column was able to sustain a ductility ratio of $\mu = 2$ (2.8% drift) and failed due to shear, as anticipated. The other two columns were strengthened either with rectangular shaped straps or with oval shaped straps providing passive pressure in both cases. These specimens were wrapped with eight plies in the hinging region and three plies everywhere else, to increase the shear capacity. Test results showed stable load-displacement hysteresis loops up to $\mu \approx 6$ (7½% drift), without significant structural deterioration. The tests were stopped because the actuator reached its maximum stroke. It was concluded that the columns were strengthened effectively with FRP straps, which increased their strength, ductility and energy dissipation. No major differences were observed between rectangular and oval shaped columns. It was suggested to conduct additional tests to establish the effectiveness of modifying the cross-section.

Xiao and Ma (1997) evaluated the efficiency of prefabricated composite jackets to retrofit reinforced concrete bridge columns. This type of prefabricated jackets offers better quality control and curing of the composite jacket in a plant, and quicker installation in the field. The researchers constructed three specimens with a circular cross-section of 610 mm diameter and a height of 2.44 m. The longitudinal reinforcement bars were spliced over a length of 20 times the bar diameter near the bottom of the column. The first specimen was tested as-built and repaired with four layers of prefabricated composite jacket, applied on the bottom half of column. Each layer was made of unidirectional glass fiber sheets arranged in such a way that 90% of the fibers were in the circumferential direction and 10% in the longitudinal direction. The layer thickness was approximately 3.2 mm. Another specimen was retrofitted with three layers, placed over 1220 mm, and a fourth one over 610 mm, whereas the last column had five layers applied on the first 1220 mm and three layers on the next 991 mm. "The upper portion retrofit was mainly for construction demonstration, rather than required by design."

Typical axial load on multi-column bents in California bridges is about 5% of the concentric capacity. Therefore, an axial load of about 5% P_o (5¼% $A_g f'_c$) was applied with a lateral loading scheme, consisting of three cycles at each displacement ductility factor of $\mu = 1$, 1½, 2, 3, 4, 6, 8, etc. until failure. The tests showed enhancement of hysteretic response and ductility. The retrofitted columns maintained stable hysteresis loops up to the first cycle of ductility ratio $\mu = 6$ (near 4% drift), whereas the control column could barely withstand the capacity up to $\mu = 1$ (less than 1% drift) with a lower flexural strength. The repaired column slightly increased the flexural capacity and failed at $\mu = 4$ (3% drift). Xiao et al. (1997) modelled each column and compared the results. The estimated values proposed by the analytical model were close to the experimental results. The authors are confident that this analytical model could be used to retrofit columns with prefabricated composite jackets.

Aboutaha, Engelhardt, Jirsa and Kreger (1999) evaluated different methods of repairing damaged building columns made of reinforced concrete. They built six rectangular specimens according to the provisions of the 1950's and 1960's building codes of the United States. The longitudinal reinforcement of each column was spliced just above the top of the footing over a length of 24 times the bar diameter. Four columns were tested and repaired with rectangular steel jackets, steel jackets with anchor bolts, steel jackets with through rods or welded lap splices. The rectangular specimens were 9' (2.75 m) high with a cross-section of 18" × 36" (457 mm × 914 mm). The columns were tested without axial load because this was considered to be more critical for the splice region. Lateral load was applied at the tip of specimens consisting of two complete cycles for each drift ratio, which increased in increments of ½%. The hysteretic response of the as-built columns showed very poor ductility and low energy dissipation. The failure was brittle and occurred after drift ratios of 1% to 2% because of splice slippage. Each of the previously mentioned repairing techniques provided an improvement of the strength and ductility compared to the as-built column behaviour. The repaired columns withstood lateral forces up to drift ratios of 3% to 5%, depending on the technique used in repairing damaged columns. The most effective technique was the use of a thin jacket with through rods. According to the results, welding the lap splices improved the general behaviour of column, but it was suggested that further investigations should be done before using it in the field, especially to evaluate the performance of welded reinforcement under inelastic cyclic loading.

Daudey and Filiatrault (2000) judged that many existing bridges in highly populated urban areas of Eastern Canada were vulnerable to seismic effects and their associated seismic risk could not be neglected. The authors built a scaled model of an existing bridge pier in the Montreal region, to evaluate its capacity and its ductility under reversed cyclic loading. Four other columns were built and retrofitted with steel jackets to increase ductility and energy dissipation. The geometry of the jacket, size of the gap at the base of pier, and the properties of fill material between the jacket and the original cross-section were investigated experimentally. The specimens had a grooved rectangular cross-section with overall dimensions of 223 mm × 362 mm and a height of 835 mm. The reinforcement details were typical of bridges designed before 1971 in Eastern Canada. Lap splice of 250 mm, corresponding to 26 times the bar diameter, was located near the footing. The tests consisted of applying a lateral load to complete two cycles for a displacement ductility ratio of $\mu = ½$, one cycle for $\mu = 1$ and two cycles for $\mu = 2, 4, 6, 7, 8, 9, 10$. An axial compressive load of 120 kN was also applied corresponding to about 4½% $A_g f'_c$.

The as-built column failed once the ductility level exceeded $\mu = 1$ (less than 1% drift) because the lap splices started to slip. The columns retrofitted with steel jackets performed very well and allowed displacement ductility ratios of $\mu = 6$ (4.9% drift) before observing a significant strength decay. Daudey et al. (2000) concluded that the geometry of the steel jacket (circular or elliptical) did not affect the hysteretic behaviour. Also, the gap size between the jacket and the footing of 50 mm, used in practice, appeared to be adequate. The active confinement provided from expansive grout was not achieved properly. Based on the test results, filling the region between the jacket and the original section with this material did not improve significantly the behaviour of the column. An analytical model was proposed to evaluate the envelop of the displacement hysteresis loops for the as-built column, with lap splices and the analytical curve agreed very well with the experimental response.

1.2.2 CURRENT RESEARCH PROGRAM

The current thesis follows two other research projects, conducted by Dr. Cem Yalcin and Mr. Derek Mes, as part of the same overall research program at the Structures Laboratory of the University of Ottawa. The objective was to develop a new and economical technique to retrofit reinforced concrete columns with insufficient seismic capacity. This new method involved external prestressing concrete columns in the transverse direction. Tests of large-scale columns were conducted. The columns had different cross-sections, aspect ratios and reinforcement details. The retrofit strategy consisted of applying active confinement with external prestressing strands. The target was to enhance the ductility by favouring the formation of plastic hinges at the bottom of the columns. The shear capacity had to be high enough so that the column could develop its flexural capacity prior to premature shear distress. These factors would increase the energy dissipation and would allow a column to resist the inertia forces induced during strong earthquakes.

Yalcin (1998) did not find any literature presenting an inventory of existing bridges in Canada. With the collaboration of provincial Ministries of Transportation, the author conducted a cross-Canada survey on bridges. Much data emerged from this investigation, especially on geometric and structural properties of bridges. For instance, reinforced concrete columns designed before the early 1970's in Canada had typical details of this period when compared with other countries like the United States or Japan. Typically, No. 3 (9.5 mm diameter) and No. 4 (12.7 mm diameter) were used as transverse reinforcement spaced at 12" (305 mm), regardless of the column size.

Yalcin (1998) used computer software named ***DRAIN-RC*** to evaluate lateral displacement demand on bridge columns under different ground motions. A ***COL***umn ***A***nalysis software (***COLA***) was developed by the author to compute the envelope (backbone curve) of force-displacement hysteresis loops. It incorporated the modelling of inelastic behaviour of reinforced concrete columns including P-Δ effects, confinement of core concrete, anchorage slip and buckling of reinforcement. The program allowed determination of the column drift capacity. Several simulations were carried out with software ***COLA*** to study the effect of structural properties on drift capacity.

Very little research had been conducted on shear dominant columns. However, many columns have failed in shear during recent earthquakes, so Yalcin (1998) decided to build and test seven full-scale models with shear dominant behaviour. The height of each specimen was 1.485 m. Five columns had a 610 mm diameter circular section, and were identified as BR-C1 to BR-C5. Two columns were of square cross-section, 550 mm × 550 mm, and were labelled as BR-S1 and BR-S2. The longitudinal reinforcement consisted of twelve No. 25 bars uniformly distributed along the perimeter. Each bar was continuous from the footing to the top of column. The hoops were No. 10 bars spaced at 300 mm with overlapping ends for the circular columns, and 135° hooked ends for the square columns. The reinforcement detailing was typical of the pre-1970's designed practice.

The columns were retrofitted either with high strength steel packaging straps or with prestressing strands. The spacing and the effect of initial prestressing were investigated. The high-strength steel straps were about 19.1 mm ($^3/_4$") wide and 1.2 mm ($^3/_{64}$") thick. Yield and the ultimate strengths were 910 MPa and 1015 MPa, respectively. The prestressing strands were designated as size 9, grade 1860 MPa, seven-wire strands. Their nominal diameter was 9.53 mm, nominal area was 51.6 mm², and the ultimate strength, f_{pu}, was about 1860 MPa. The strands were placed around the column, and the ends were joined with Dywidag twisted ring anchors to form individual prestressed hoops.

To retrofit the square column, three raisers were introduced between each strand and the column face on each side, and one raiser disk at each corner. The objective of these spacers was to confine the column as uniformly as possible. Table 1.3 summarizes the columns tested, and the retrofit technique used.

Each column was subjected to an axial load of 15% of column concentric capacity under pure compression, P_o. The loading program consisted of three full cycles at each drift ratio of ½%, 1%, 2%, 3%, etc. up to failure.

Table 1.3 Summary of columns tested by Yalcin (1998)

COLUMN	DIMENSION (mm)	ASPECT RATIO*	RETROFITTING TECHNIQUE			REFERENCE
			TYPE	STRESS	SPACING	
BR-C1**	610, diam.	2.4	—	—	—	Control
BR-C2	610, diam.	2.4	Strands	25% f_{pu}	150 mm	BR-C1
BR-C3	610, diam.	2.4	Strands	5% f_{pu}	150 mm	BR-C1
BR-C4	610, diam.	2.4	Strands	25% f_{pu}	300 mm	BR-C1
BR-C5	610, diam.	2.4	Straps	Snug tight	150 mm	BR-C1
BR-S1**	550 × 550	2.7	—	—	—	Control
BR-S2	550 × 550	2.7	Strands & Raisers	25% f_{pu}	150 mm	BR-S1

* Aspect ratio is equivalent to shear span-to-depth ratio
** BR is for bridge column; C, circular cross-section; S, square cross-section

The as-built columns, with a circular and a square cross-section, could not withstand deformation reversals beyond 1% drift, and failed in shear when forced to deform to 2% drift. The circular and square columns which were retrofitted with strands at 150 mm spacing, and prestressed to either 5% f_{pu} or 25% f_{pu} were able sustain deformation reversals up to 5% and higher drifts. When the prestress level was 25% f_{pu}, the failure mode was no longer governed by shear but by flexure. When it was 5% f_{pu}, the response was the same up to 4% drift, but at later stages of loading, the hysteresis loops showed some pinching, indicating a shear contribution to overall response. Columns retrofitted with high strength steel straps or prestressing strands spaced at 300 mm failed at 3% drift. These two strategies were not as effective as the previous ones.

The author concluded that the best behaviour came from columns retrofitted with strands prestressed to 25% f_{pu} and spaced at 150 mm. It was stated that the new retrofitting technique developed in the research program offered a number of practical advantages, including ease, speed and economy of construction.

Mes (1999) further investigated the effectiveness of the new retrofitting technique on columns with different aspect ratios. A total of six large-scale models were built and tested. Again, the drift level was used to control lateral displacements during testing. The loading history consisted of reversed cyclic loading, with three cycles at each drift ratio of ½%, 1%, 2%, 3%, etc. until failure. A constant compression load of 15% P_o was applied during the entire test. This value was a good representation of the actual gravity load of the superstructure on bridge columns.

Four specimens were built with an effective height of 2.0 m. Two of them were circular with a diameter of 508 mm and two others were square with a cross-section of 500 mm × 500 mm. The corresponding aspect ratios were around 4.0 to give the columns a flexural dominant behaviour. Twelve No. 20 longitudinal bars were uniformly distributed along the perimeter, and were continuous from the footing to the tip of columns. The transverse reinforcement consisted of No. 10 hoops placed at 300 mm. The circular hoops had overlapping ends, whereas the square hoops had 135° bends at the ends. The reinforcement details of these four long columns were typical of the construction practice prior to the 1970's.

A pair of short circular columns was also built with details of the 1970's. The two columns had a No. 10 spiral with a pitch of 75 mm. The longitudinal reinforcement consisted of twelve No. 20 bars continuous from the footing to the top of columns. The effective height of these columns was 1.55 m, and the cross-section was 610 mm in diameter. These two specimens were labelled as BR-SP1 and BR-SP2.

All the columns were retrofitted with the same prestressing strands used by Yalcin (1998). The seven-wire strands had an ultimate strength f_{pu} of 1860 MPa. Their nominal diameter and nominal area were 9.53 mm and 51.6 mm² respectively. The strands were placed at 150 mm and were prestressed to about 25% of the ultimate strength f_{pu}. The strands around the retrofitted square specimens were raised at three points on each column face to provide more uniform confinement.

The short column BR-SP2 was also retrofitted with prestressing strands but a fiber-reinforced concrete shell of 25 mm was used as a cover over the strands. Such a practice could be used to protect the strands against corrosion and to improve the æsthetics. The objective of this test was to investigate the behaviour of a concrete cover placed over the retrofitting hardware to protect them against corrosion. Table 1.4 presents a summary of the columns tested by Mes (1999) in this phase of the investigation.

Table 1.4 Summary of the columns tested by Mes (1999)

COLUMN	DIMENSION (mm)	ASPECT RATIO*	RETROFITTING TECHNIQUE			REFERENCE
			TYPE	STRESS	SPACING	
BR-C6**	508, diam.	3.9	—	—	—	Control
BR-C7	508, diam.	3.9	Strands	25% f_{pu}	150 mm	BR-C6
BR-S3**	500 × 500	4.0	—	—	—	Control
BR-S4	500 × 500	4.0	Strands & Raisers	25% f_{pu}	150 mm	BR-S3
BR-SP1**	610, diam.	2.5	—	—	—	Control
BR-SP2	610, diam.	2.5	Strands & Shell	25% f_{pu}	150 mm	BR-SP1

* Aspect ratio is equivalent to shear span-to-depth ratio

** BR is for bridge column; C or S, circular or square column with stirrups; SP, circular column with spiral reinforcement

The results showed that long columns with a circular or a square cross-section failed similarly at about the same drift level. The flexure dominant columns without the retrofit withstood the load up to 2% drift, but they lost their strength very quickly in the following cycles. The circular specimen failed after the first cycle at 3% drift and the square one, at the third cycle at 3% drift. The failure of the retrofitted columns was more gradual. The circular specimen lost its strength after the first cycle at 5% drift and the square one, during the last cycle at 5% drift.

The as-built column with spiral reinforcement exhibited ductile hyteretic response and failed at 6% drift. The companion column was retrofitted and covered with a concrete shell. The shell behaved well during the test and maintained its integrity until 5% drift. It was shown that a thin concrete jacket would be a good way to provide corrosion protection for the strands. Mes (1999) concluded that the retrofitting technique developed at the University of Ottawa was effective in improving the strength and ductility of test columns. The material costs and the labour to retrofit columns with this strategy would be reduced as compared to steel jacket, while attaining similar improvement in column behaviour.

1.2.3 DISCUSSION AND CONCLUSIONS FROM LITERATURE REVIEW

Many engineers became aware of the seismic vulnerability of structures after the magnitude 6.6, 1971 San Fernando earthquake. Since this event, code provisions have been reviewed, leading to a better understanding of the non-linear dynamic behaviour of structures. The current methods for detailing reinforcement control the failure mode. It favours ductile flexural response to brittle shear failure and provides high-energy dissipation.

One of the problems with the designs prior to the early 1970's was the low seismic lateral design force. It led to non-conservative shear demands and insufficient transverse reinforcement. Figure 1.4 presents a bridge column photographed after the 1994 Northridge earthquake showing typical reinforcement details. Generally, No. 3 (9.5 mm diameter) or No. 4 (12.7 mm diameter) hoops were placed at 12" (305 mm), regardless of the column dimensions.

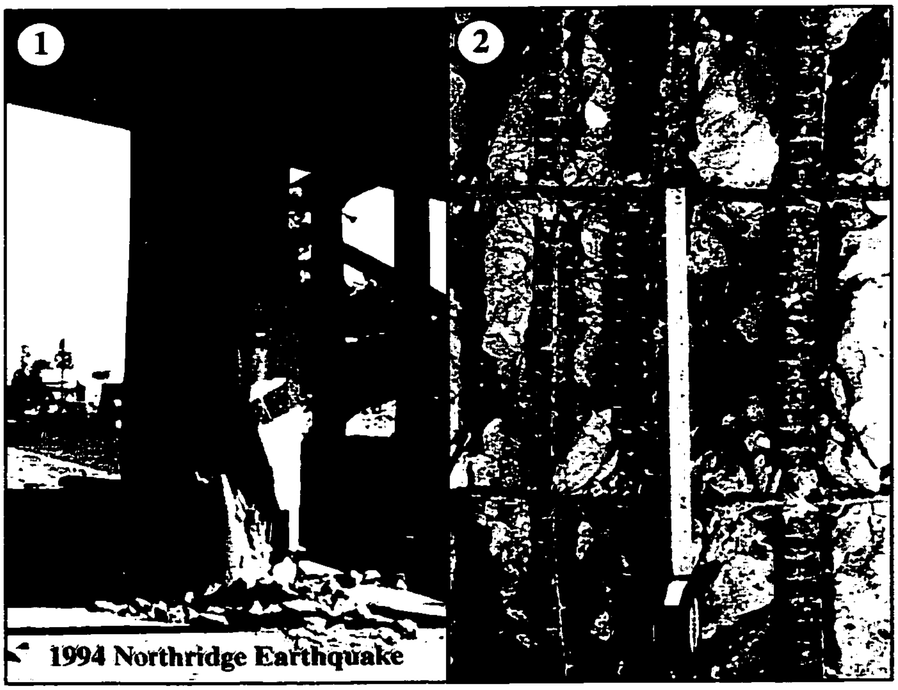

Figure 1.4 Typical reinforcement details; ① Overall view; ② Close-up view

Such a practice provided low confinement. This fact is illustrated in Fig. 1.5 taken from Yalcin (1998). A column properly confined would have a ratio of spacing, s, to longitudinal bar diameter, d_b, smaller than 4½ in order to develop strain hardening in the longitudinal reinforcement before buckling. However, the spacing of 12" (305 mm) used in the pre-1970's designs could not provide a ratio of $s/d_b < 4½$. Actually, the longitudinal reinforcement could only reach yielding before the failure occurred, resulting in a poorly confined column with low flexural capacity.

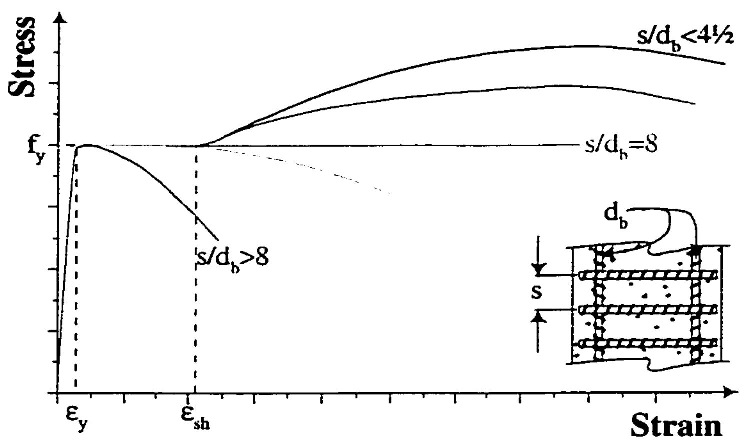

Figure 1.5 Effect of tie spacing and longitudinal bar diameter on stress-strain relationship of reinforcement in compression.

The splicing of longitudinal reinforcement was another problem. The starter bars were at the bottom of columns where the development of plastic hinges was expected. Also, the lap splice length was insufficient to develop the (yield) strength of reinforcement. A length of 20 times the bar diameter was frequently used and was based on the requirements for compression reinforcement.

These deficiencies caused three types of damage during recent earthquakes; shear failure, compression crushing of concrete due to lack of confinement, and reinforcement splicing failure as shown in Fig. 1.6. To retrofit columns designed prior to the early 1970's, a jacketing strategy is effective. The most frequently used is the steel jacket. However, studies on concrete and composite jackets showed their efficiency to improve the seismic response of reinforced concrete columns. The current research program investigates a new retrofitting strategy, consisting of applying active confinement with external prestressing strands. So far, this strategy is effective and improves the behaviour of shear and flexure dominant columns with different cross-sections and aspect ratios.

Figure 1.6 Failure modes; ① Shear failure; ② Confinement failure of the hinging region; ③ Lap splice failure (slippage)

1.3 OBJECTIVE

The objective of this research project is to study the effectiveness of external prestressing on seismic performance of concrete bridge columns with inadequate longitudinal reinforcement lap splices. The objective also includes the development of a new seismic retrofit methodology for seismic rehabilitation of concrete columns, consisting of external prestressing.

1.4 EFFICIENCY CRITERIA

The purpose of the new retrofitting strategy to be developed is to provide clamping pressure in the splice region, preventing the slippage of reinforcement while confining the core concrete. An effective retrofit will avoid early shear failure, while delaying flexural failure or reinforcement slippage in the splice region. To evaluate the efficiency of the technique, three criteria will be considered; ductility enhancement, preservation of strength and energy dissipation.

1.5 SCOPE

The scope of this research project includes the literature review, followed by the steps outlined below:

- Design, construction and instrumentation of six large-scale reinforced concrete columns.
- Retrofitting of the columns with prestressing strands.
- Preparation of test set-up for testing columns under simulated seismic loading.
- Testing of the columns under constant axial compression and lateral deformation reversals.
- Evaluation of test data.
- Analysis of column response and drawing conclusions for the retrofit strategy employed.
- Preparation of thesis and presentation of results.

CHAPTER 2

SPECIMENS AND TEST APPARATUS

2.1 GENERAL

An experimental investigation was conducted to develop a retrofit strategy for non-ductile concrete bridge columns. It involved testing six large-scale reinforced concrete columns under simulated seismic loading. The specimens were built in pairs in order to test one as a control column (without any retrofit) and the other as a retrofitted column. A total of three pairs were prepared with different cross-sections (circular or square) and aspect ratios (long or short columns). The reinforcement detailing represented typical bridge designs employed prior to the early 1970's. For instance, No. 10 hoops were placed at 300 mm and longitudinal reinforcement was spliced at the bottom of the columns over a length equal to 20 times the bar diameter. The retrofitting strategy consisted of confining the columns with external prestressing strands.

During each test, the column was subjected to combined axial load and reversed lateral cyclic loading, while test data were recorded by a data acquisition system. The axial compression represented typical gravity load of superstructure, acting on the bridge columns. The specimen details, material properties and test setup are described in this chapter, as well as the loading scheme and instrumentation. The following chapters contain illustrative figures. For convenience, these figures are grouped at the end of each chapter, instead of placing them throughout the text.

2.2 CONSTRUCTION OF COLUMN SPECIMENS

Test specimens was constructed at the Structures Laboratory of the University of Ottawa. Concrete and reinforcing steel were ordered from local companies. The steel reinforcement was supplied in pre-bent form.

2.2.1 FOOTINGS

The construction of a footing started with the installation of strain gauges on bars before assembling the footing cage. Starter bars were kept in place by a template to make sure they were uniformly distributed along the perimeter of the specimen. The footings were well reinforced, making them very rigid to provide full fixity (see Fig. 2.1). The footings were cast in pairs reusing the same formwork each time. Figure 2.2 shows the six reinforced concrete footings cast.

2.2.2 COLUMNS

Concrete surface on the footings, where the column concrete is to be cast, was roughened with a small compressed air chisel before assembling the steel cages for columns. Sona tubes or plywood pieces were used for the formwork. Some ropes and pieces of wood were used to hold the formwork in an up-right position when necessary. The footing concrete was soaked and surface dried just before the columns were cast. Column concrete was subjected to a wet cure for almost a week after casting. The specimens were painted white, to make cracks more visible during testing. Black lines were drawn on the specimens to indicate the location of reinforcement inside the concrete. The sequence of construction is illustrated in Fig. 2.3.

2.2.3 INSTALLATION OF PRESTRESSING STRANDS

The prestressing strands were wrapped around three test specimens and stressed to the desired level. Two jacks, made by Enerpac, were used to prestress them. Figure 2.4 illustrates the hardware involved for prestressing, including a load cell, a jack extension, an anchor and some wedges. The procedure to install the strands is shown in Fig. 2.5. The strands were first prestressed with jack No. 1. Once the load cell indicated that the required stress was reached, jack No. 2 was used to push the wedges into the anchor. The prestressing strand was then cut and the jacks were removed. Note that the load cell shown in Figs. 2.4 and 2.5 was prepared to expose the movement of the jack extension and the wedges.

Two different anchors were used to retrofit circular and square columns. Dr Cem Yalcin designed the anchors used for the circular columns (smaller anchors). For the retrofitted square column, the prestressing strands were stressed using Dywidag twisted ring anchors. Both anchors are illustrated in Fig. 2.6.

2.3 SPECIMEN DETAILS

A total of six specimens were designed and built using pre-1970's practice. The first pair was long circular columns, labelled BR-C8 and BR-C9. The labelling scheme followed the earlier phases of the same investigation (Yalcin, 1998 and Mes 1999). The second pair was also long columns, but with a square cross-section. The square specimens were labelled as BR-S5 and BR-S6. The last pair was labelled BR-C10 and BR-C11, and consisted of two short columns with a circular cross-section. All six specimens are shown in Fig. 2.7.

The specimens were tested with fixed end condition at the base and pin end condition at the top. By doing so, the height of the test specimen represented the shear span and corresponded to half the column height for an actual fixed-fixed column, assuming the inflection point occurring at mid-height. Such a practice is common for testing columns.

Each column had No. 10 hoops spaced at 300 mm, with the first hoop placed at 75 mm from the top surface of the footing. The circular columns had circular hoops with overlapping ends. The square columns had square ties with 135° bent ends. At the top of the specimens, stress concentration was anticipated because of the test setup. In order to avoid a premature failure of this region, transverse reinforcement spacing was reduced to 65 mm or 90 mm near the tip of the columns. The reinforcing steel was of grade 400 MPa. For the longitudinal reinforcement, twelve No. 20 bars were equally distributed along the perimeter of the cross-section. Each bar was spliced at the bottom of the column. The lap splice length was 390 mm, corresponding to 20 times the bar diameter. On top of each column, eight bolts of 19 mm in diameter were embedded into the concrete. The bolts were used to connect the column tip to the test setup.

2.3.1 LONG CIRCULAR COLUMNS

Columns BR-C8 and BR-C9 were 1.7 m high. The effective height, also known as shear span, was 2.0 m, since the point of application of the horizontal load was 275 mm above the tip of the reinforced concrete specimen. The cross-section was circular with a diameter of 508 mm and a clear cover of close to 50 mm. Figure 2.8 shows the steel cage prior to concrete casting. Column geometry and reinforcement details are illustrated in Figure 2.9.

Column BR-C8 was tested as-built, whereas BR-C9 was retrofitted with prestressing strands prior to testing. The strands were 9 mm in diameter, and were spaced at 150 mm, with the first one placed at 75 mm above the footing. They were prestressed to 25% of their ultimate tensile capacity, f_{pu}. The smaller anchors were used for this circular column. Figure 2.10 illustrates the retrofit details.

2.3.2 LONG SQUARE COLUMNS

Square columns BR-S5 and BR-S6 had the same height as the previous two circular columns, i.e., 1.7 m. The effective height was 2.0 m. The columns had a 500 mm square cross-section with a clear cover of 45 mm. Figures 2.11 and 2.12 show the reinforcement cage and steel detailing for square columns.

Column BR-S5 was tested without retrofitting. The other column, BR-S6, was retrofitted with prestressing strands placed at every 100 mm in the splicing region, starting at 75 mm from the column base. The stress level was 50% of the ultimate strength, f_{pu}. Other strands above the potential hinging region were installed at every 150 mm, and prestressed to 25% f_{pu}. The top part of the column did not have to be retrofitted because the hoop spacing was 90 mm. To retrofit the square column, raisers were placed between the face of the column and the prestressing strands, consisting of semi-circular disks of different diameter. The purpose of these spacers was to confine the square column as uniformly as possible by applying well distributed lateral forces on the column face. The raisers consisted of three half-discs installed on a hollow structural section (HSS), forming a frame around the column. A small piece of steel, covered with grease, was placed at each corner in between the strand and the HSS, so the strand could slide on this piece while being prestressed. The prestressing force was sustained by a Dywidag twisted ring anchor. Retrofitting details are presented in Fig. 2.13.

2.3.3 SHORT CIRCULAR COLUMNS

The last pair of columns were labelled as BR-C10 and BR-C11, and had a circular cross-section. The outside diameter was 610 mm leaving a clear cover of 55 mm. The specimen height was 1.2 m in order to have an effective height (shear span) of 1.5 m. Figure 2.14 shows the steel cages prior to casting, whereas Fig. 2.15 illustrates the column details.

Specimen BR-C10 was not retrofitted, whereas its companion BR-C11 was strengthened similarly to the retrofitted square column. The strands were at 100 mm spacing in the splicing region and were prestressed to 50% f_{pu}. Other wires were installed in the remaining portion of the column every 150 mm with a stress level of 25% f_{pu}. The smaller anchors designed by Dr Cem Yalcin were used to retrofit this circular column. Figure 2.16 shows the retrofitting details of the column BR-C11.

Tables 2.1 and 2.2 summarize the specimen details. The transverse reinforcement and lap splice details are omitted in these tables because they were the same for all columns. The transverse reinforcement consisted of No. 10 hoops, spaced at 300 mm, and the longitudinal bars were spliced near the base over a length equal to 20 times the bar diameter (390 mm). The symbols A_g, A_c and ρ_l used in Table 2.1 are the gross area of concrete section, the area of the core section and the longitudinal reinforcement ratio, respectively.

Table 2.1 Column geometry and reinforcement

Column	Dimension (mm)	Shear Span (m)	Aspect Ratio*	A_g/A_c	ρ_l
BR-C8** and BR-C9	508, diam.	2.0	3.9	1.61	1.78%
BR-S5** and BR-S6	500×500	2.0	4.0	1.56	1.44%
BR-C10 and BR-C11	610, diam.	1.5	2.5	1.55	1.23%

* Aspect ratio is equivalent to shear span-to-depth ratio
** BR is for bridge column; C, circular cross-section; S, square cross-section

Table 2.2 Column retrofit details

Column			Retrofitting (Splice Region)			Reference
Label	Type	Cross-section	Type	Stress	Spacing	
BR-C8	Long	Circular	—	—	—	Control
BR-C9	Long	Circular	Strands	25% f_{pu}	150 mm	BR-C8
BR-S5	Long	Square	—	—	—	Control
BR-S6	Long	Square	Strands & Raisers	50% f_{pu}	100 mm	BR-S5
BR-C10	Short	Circular	—	—	—	Control
BR-C11	Short	Circular	Strands	50% f_{pu}	100 mm	BR-C10

2.4 MATERIAL PROPERTIES

The material properties were established through standard tests. Concrete cylinders and steel coupons were tested to determine the actual strength of concrete and steel used in this project. Each time, three cylinders or three steel coupons were tested in order to obtain a more accurate result.

2.4.1 CONCRETE

Standard concrete cylinders of 152 mm in diameter and 305 mm in height were cast to evaluate the strength of concrete in the footings and columns. Each cylinder was capped with a sulphur compound to ensure uniform loading. The cylinders were tested using a

Fourney testing machine with 2225 kN capacity, as shown in Fig. 2.17. The average strength of the footings was evaluated after 28 days, and was found to be 35 MPa, 38 MPa and 37 MPa for the footings of long circular, long square and short circular columns, respectively. The difference in strength for the concrete footings was very small and resulted from the use of different batches. The columns were all cast at the same time with the same batch of concrete. Twenty-eighth days after casting, the cylinder compressive strength of column concrete, f'_c, was 35.4 MPa. The average strength during the testing period was 36 MPa. Figure 2.18 and Table 2.3 present concrete stress development over time. The stress-strain relationship of concrete is shown in Fig. 2.19.

Table 2.3 Development of concrete strength over time

Time (Days)	Average Strength (MPa)
3	16
7	22
14	29
21	34
28	35
150	37

2.4.2 REINFORCING STEEL

Tension tests were performed on steel coupons to establish the stress-strain relationship of reinforcing steel used in columns. The coupon tests were performed using a Tinius Olsen testing machine, as shown in Fig. 2.20. This figure also shows the deformed shape of reinforcement after the test. Two different sizes of bars were used: No. 10 bars with a nominal diameter of 11.3 mm and No. 20 bars with a nominal diameter of 19.5 mm.

The No. 10 bars used for the hoops yielded at 445 MPa, and reached an ultimate strength of 576 MPa. Two different types of steel were used for the longitudinal bars because they were ordered from two different suppliers. For the long columns with a circular or a square cross-section, the No. 20 bars had yield strength of 439 MPa and ultimate strength of 644 MPa. The No. 20 bars used for the short columns yielded at 418 MPa and failed at an ultimate strength of 717 MPa. Table 2.4 summarizes the main characteristics for the three types of steel used. Figures 2.21 to 2.23 show their stress-strain relationships. Although the ultimate strain for each bar exceeded 12%, it was not possible to record the strains over this value due to the limitations of test setup.

Table 2.4 Properties of the reinforcing steel

	E	**f_y**	ε_y	ε_{sh}	**f_u**	ε_u
No. 10	225 GPa	445 MPa	0.2%	2.1%	576 MPa	Larger than 12%
No. 20 (long columns)	225 GPa	439 MPa	0.2%	1.2%	644 MPa	Larger than 12%
No. 20 (short columns)	215 GPa	418 MPa	0.2%	0.7%	717 MPa	Larger than 12%

2.4.3 PRESTRESSING STRANDS

The seven-wire strands used to retrofit the columns were designated as size 9 and grade 1860 MPa. The nominal diameter and nominal area were 9.53 mm and 51.6 mm^2, respectively. Three prestressing strands were tested on a Tinius Olsen testing machine of 1500 kN capacity and the results were recorded with a data acquisition system. Figure 2.24 presents the machine used as well as the strand coupons before and after testing. The results showed that the modulus of elasticity was 240 GPa. The prestressing strands yielded around 1775 MPa at a strain level of 0.74%. The ultimate tensile strength was 2195 MPa. Stress-strain relationships of the three strands tested are illustrated in Fig. 2.25.

Although the actual ultimate strength of prestressing strands f_{pu} was 2195 MPa, the designated value of 1860 MPa was used in the calculation. Since the retrofitting strategy consisted of applying either 25% f_{pu} or 50% f_{pu} for each strand, the corresponding stress levels were 465 MPa or 930 MPa, respectively.

2.5 TEST SETUP

The test setup for columns was oriented in the East-West direction and consisted essentially of five parts: a concrete specimen, three actuators, an A-frame, as well as a loading beam to apply the axial load and two steel frames to restrain large out-of-plane displacements. Figure 2.26 shows an overall view of the test setup.

Concrete specimens were attached to the laboratory strong floor with four high-strength bolts of 75 mm diameter. Three servo-computer controlled MTS hydraulic actuators, with 508 mm-stroke, and 960 kN tension and 1460 kN compression capacity were used. A schematic view illustrates the main characteristics of actuators in Fig. 2.27. There was one actuator on each side of the column (see Fig. 2.28) to apply uniform axial compression, simulating gravity loading. Each vertical actuator was attached to the footing and to the loading beam assembly. The third actuator was mounted horizontally on an A-frame that was bolted to the strong floor (see Fig. 2.29). One end of the actuator was attached to the A-frame and the other end to the tip of column. This horizontal actuator applied the reversed cyclic loading to the column tip, simulating seismic loading. All the actuators were attached with four high-strength bolts at each end.

The entire setup was symmetrical to avoid eccentric loading (see Figs. 2.28 and 2.30). The schematic drawings shown in Figs. 2.28 to 2.30 present the details of test setup. Figure 2.31 shows two yellow steel frames, made of HSS and located on either side of the test specimen. These frames provided additional safety against unexpected out-of-plane movements.

Although all the diagrams illustrating the test setup showed a long column, the same setup was used for short columns as well. There were only two differences; the horizontal actuator was lowered by 500 mm for the short columns and a reinforced concrete spacer block of 965 mm height was used instead of the 460 mm-spacer block (see Fig. 2.32).

2.6 LOADING PROGRAM

Constant axial load was applied to each specimen during testing. This load represented the gravity load of superstructure on the column. Bridge columns are usually subjected to a gravity load of 10% to 20% their axial capacity under pure compression P_o (Yalcin, 1998). In the current test program, the axial load used was 15% P_o. Table 2.5 presents the compressive load applied to each column.

Table 2.5 Constant axial load applied to the columns

COLUMN		COMPRESSIVE LOAD APPLIED		
LABEL	DESCRIPTION	VALUE	LOAD / P_o	LOAD / A_g f'_c
BR-C8 and BR-C9	Long circular column	1114 kN	15%	15.5%
BR-S5 and BR-S6	Long square column	1327 kN	15%	15.0%
BR-C10 and BR-C11	Short circular column	1518 kN	15%	14.7%

The horizontal loading was applied in displacement controlled mode. As shown in Fig. 2.33, three complete cycles were applied at each drift ratio of ½%, 1%, 2%, 3%, 4%, etc. until failure. The test was conducted under quasi-static load conditions, and the laboratory engineer controlled the displacement.

2.7 INSTRUMENTATION

The specimens were well instrumented. Data during testing were recorded by a data acquisition system. Four types of instruments were used for this purpose:

- Calibrated load cells of actuators (see Fig. 2.27).
- Electrical-resistance strain gauges bonded on reinforcing bars and prestressing strands.
- Linear Variable Differential Transducers (LVDT) of 50 mm-stroke.
- Temposonic LVDTs.

A total of 14 strain gauges were placed on the longitudinal reinforcement of each column. For the transverse reinforcement, the first two hoops were instrumented with two strain gauges. Figure 2.34 illustrates the position of the strain gauges on reinforcing steel of the circular columns, and Fig. 2.35 on the square columns. One gauge was also placed on each prestressing strand, as shown in Fig. 2.36, although the bottom three had two strain gauges.

A total of four LVDTs were used to evaluate the flexural rotation at h and h/2 from the footing, where h was the cross-sectional dimension of the column. They were fixed to threaded rods, which had been cast into the concrete columns. The flexural rotation θ_h or $\theta_{h/2}$ were calculated using Eq. 2.1.

$$\theta = \mathrm{Arc\,tan}\left(\frac{\Delta_1 - \Delta_2}{d_{LVDT}}\right) \cong \frac{\Delta_1 - \Delta_2}{d_{LVDT}}, \text{ for small angles} \qquad [2.1]$$

where, Δ_1 = Displacement measured by LVDT No. 1

Δ_2 = Displacement measured by LVDT No. 2

d_{LVDT} = Horizontal distance between LVDT No.1 and LVDT No. 2

Two Temposonic LVDTs were used to evaluate the anchorage slip rotation θ_0 at column-footing interface along with Eq. 2.1. Both measured displacements within 25 mm gauge length, just above the footing, because it was not practical to take readings closer to the footing. A third temposonic LVDT was placed to measure the horizontal displacement at the point of application of horizontal load corresponding to the effective height of the column. Figure 2.37 shows the location of the LVDT and the temposonic LVDT. Note that Fig. 2.37 illustrates the locations of LVDTs for long columns. The only difference for the short columns was that the point of application of the horizontal load was lowered by 500 mm in order to obtain an effective height of 1.5 m.

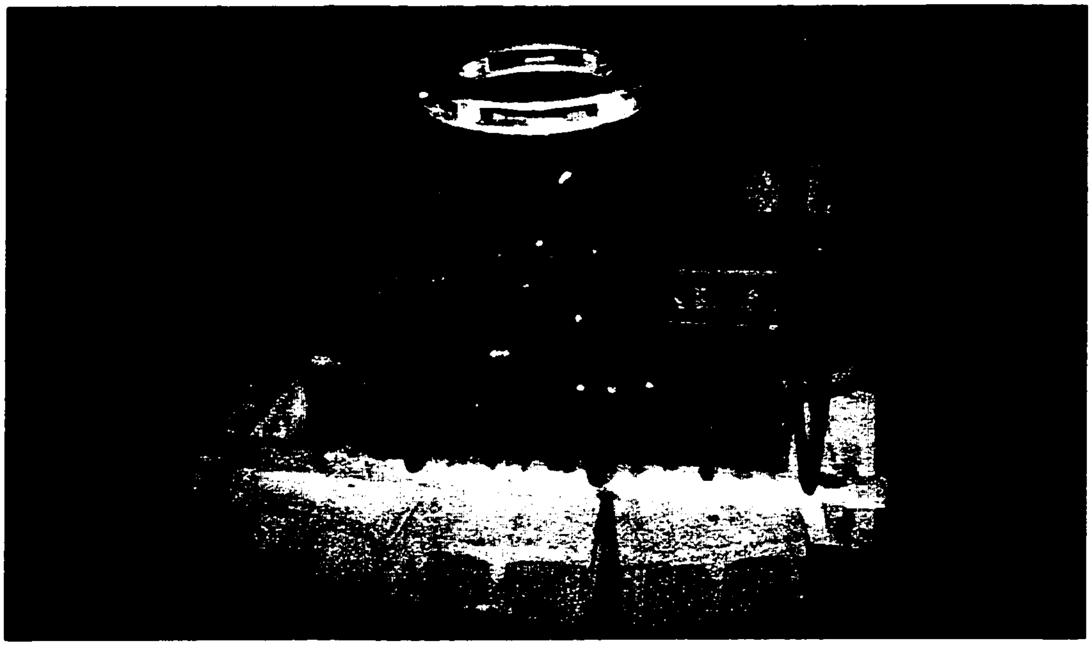

(a) Building of the cage

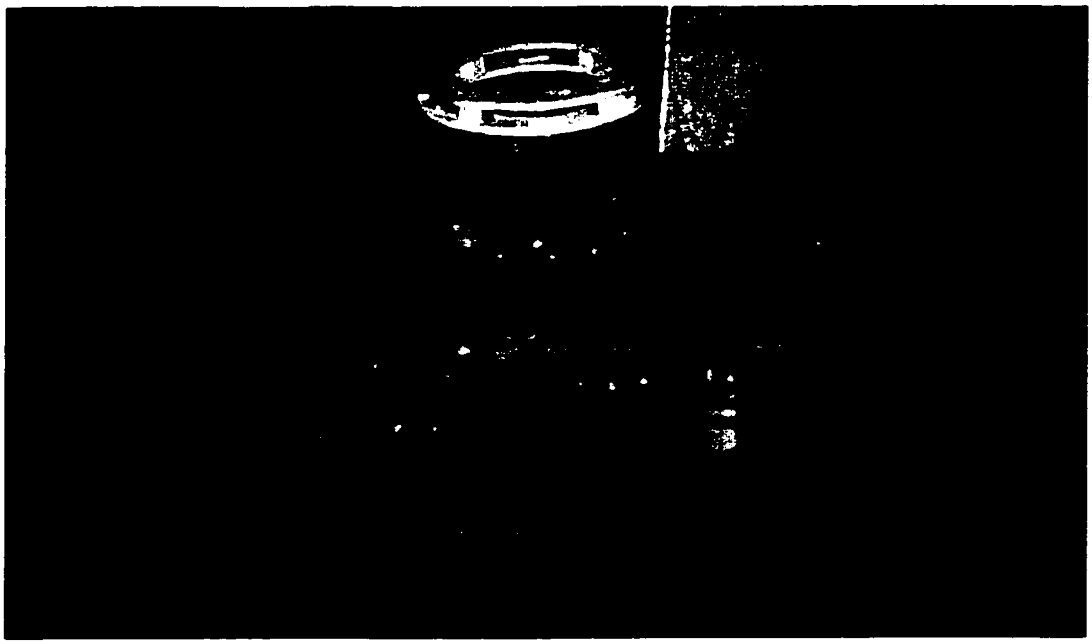

(b) Steel cage completed

Figure 2.1 Construction of steel cage for footings

(a) Long column footings

(b) Short column footings

Figure 2.2 Reinforced concrete footings with dowels

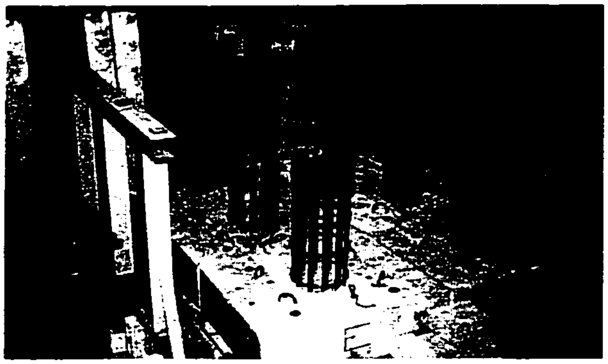

(a) Steel cages

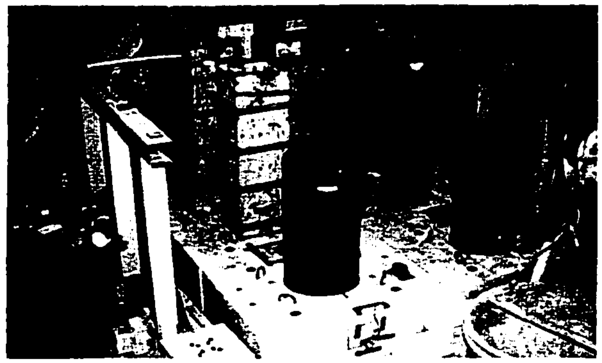

(b) Formwork

(c) Wet cure

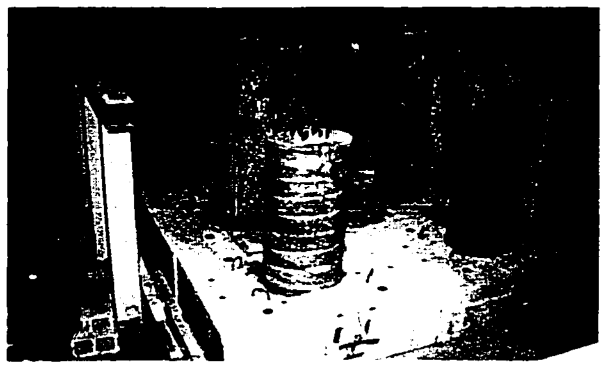

(d) End of the cure

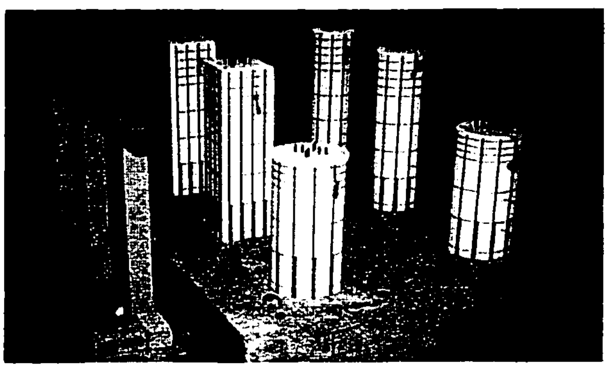

(e) Painting

Figure 2.3 Steps for the construction of the columns

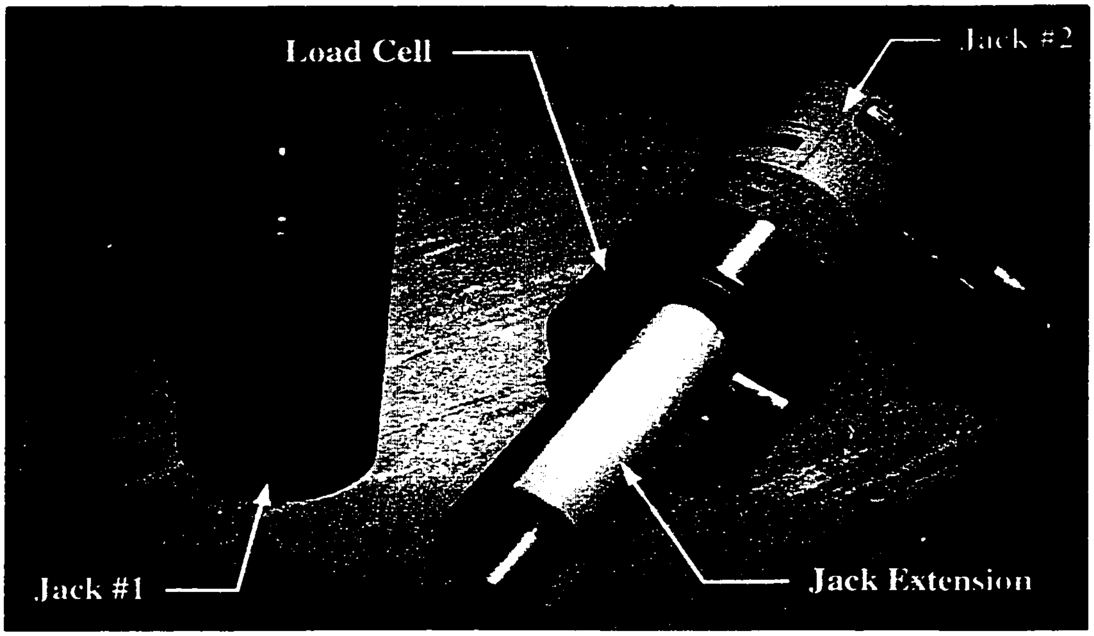

(a) Two jacks with a load cell and a jack extension

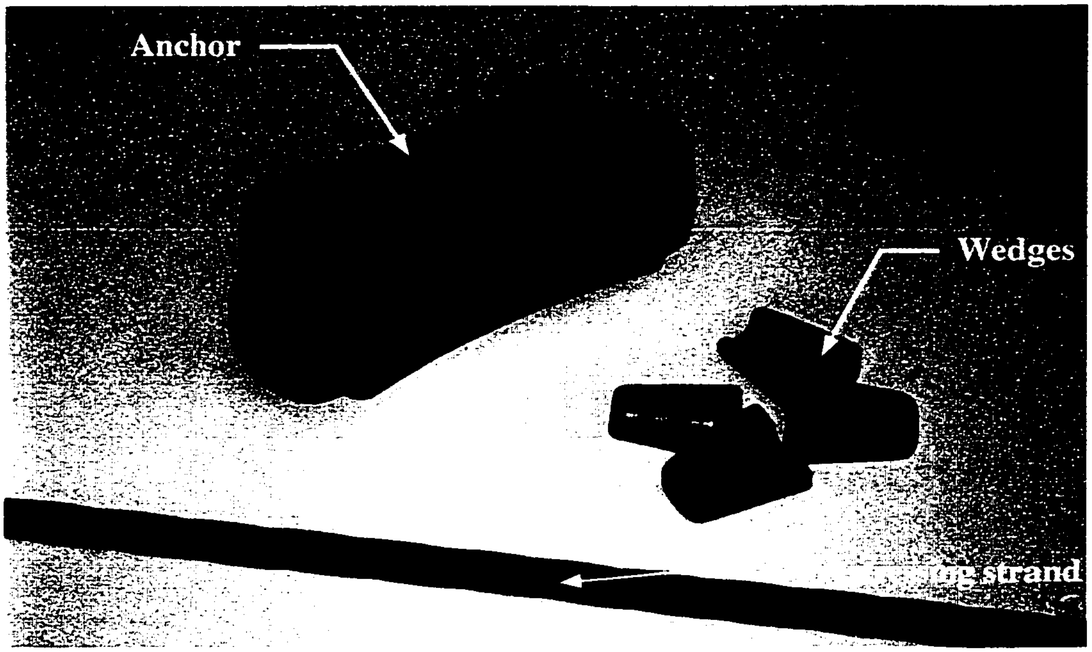

(b) Prestressing strand with an anchor and some wedges

Figure 2.4 Hardware required for the installation of prestressing strands

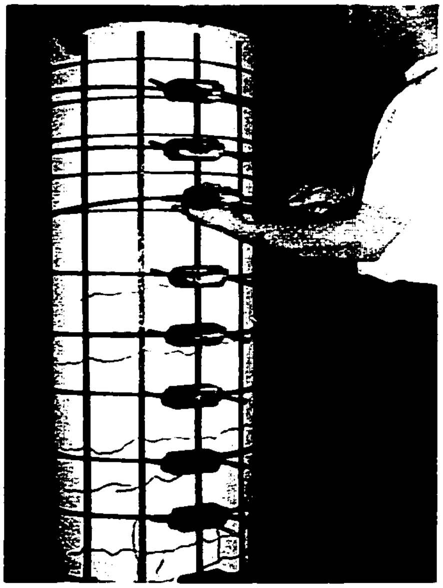

STEP 1 Positioning the strand

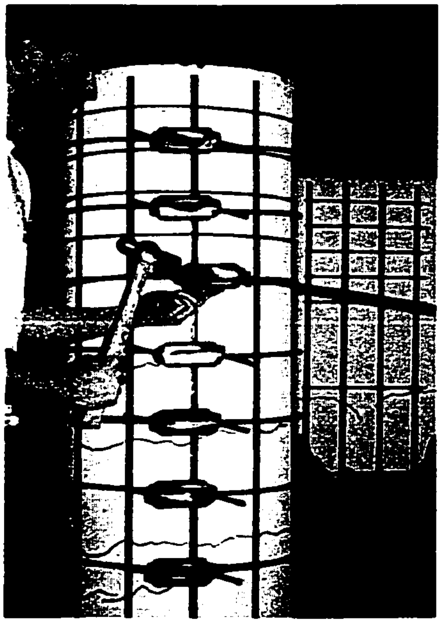

STEP 2 Inserting and hammering the wedges

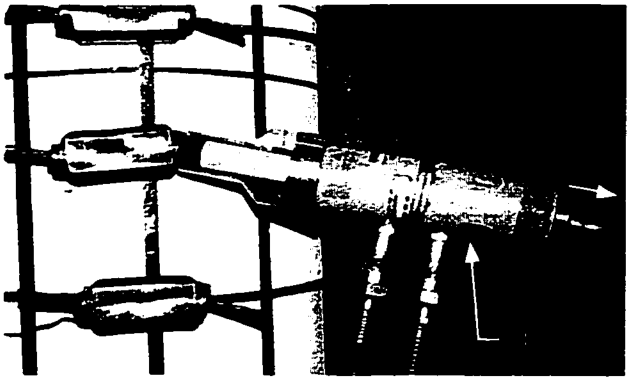

STEP 3 Prestressing the strand with jack no. 1

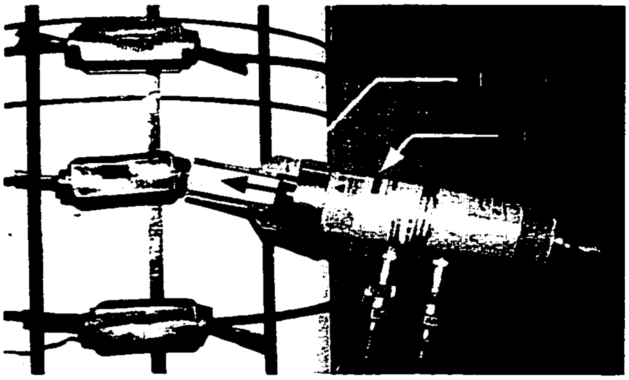

STEP 4 Pushing the wedges with jack no. 2

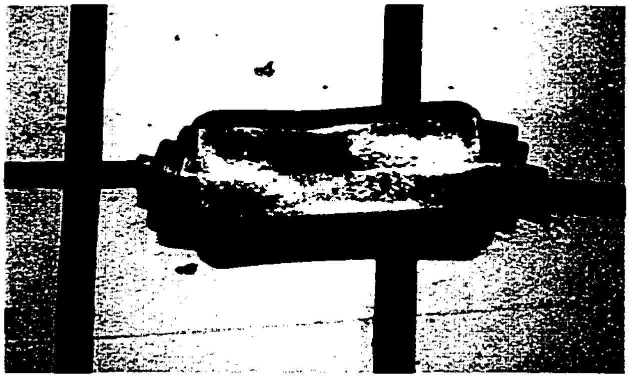

STEP 5 Cutting the strand and removing the jacks, the load cell and the jack extension

Figure 2.5 Installation of prestressing strands

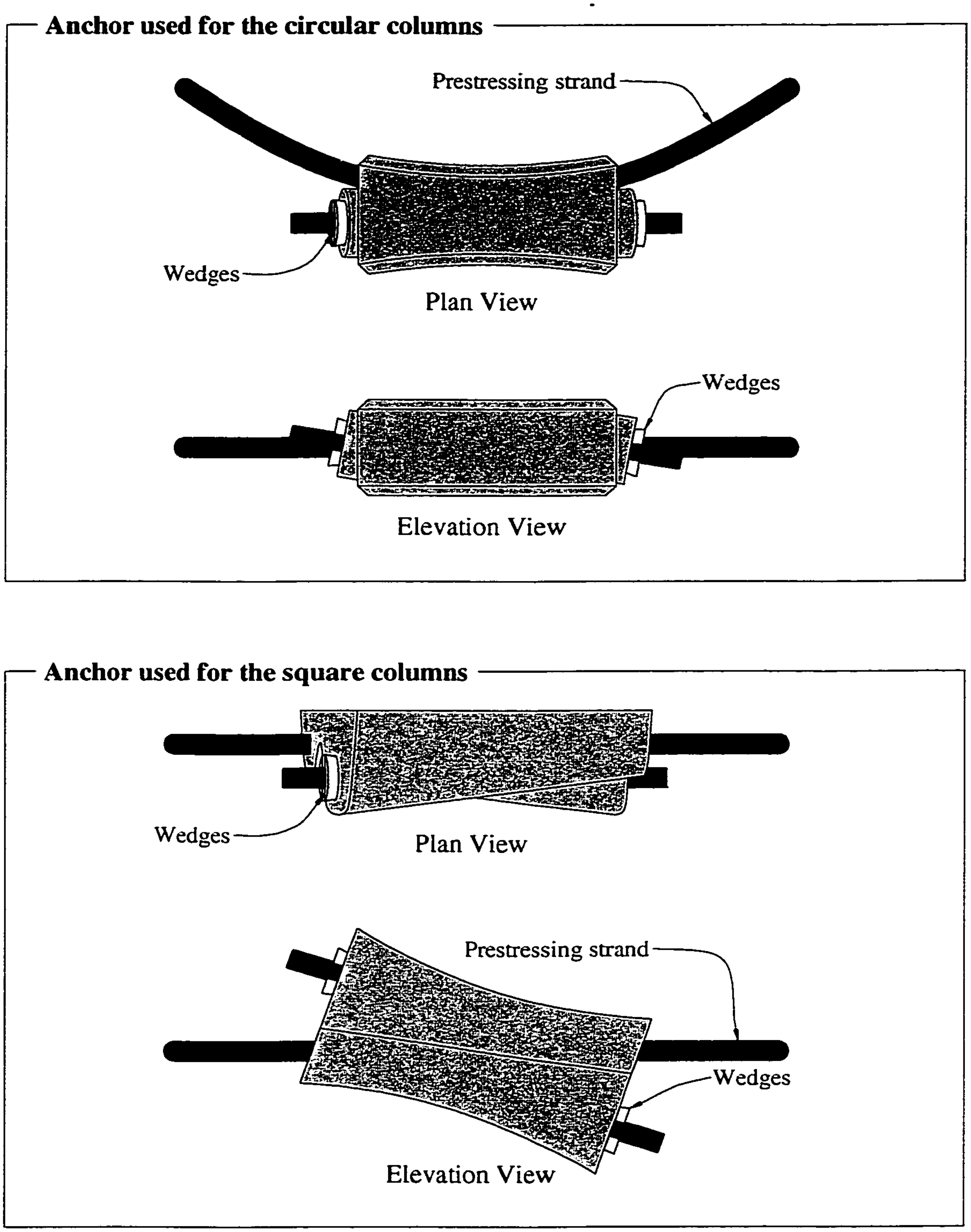

Figure 2.6 Schematic drawing of the anchors used

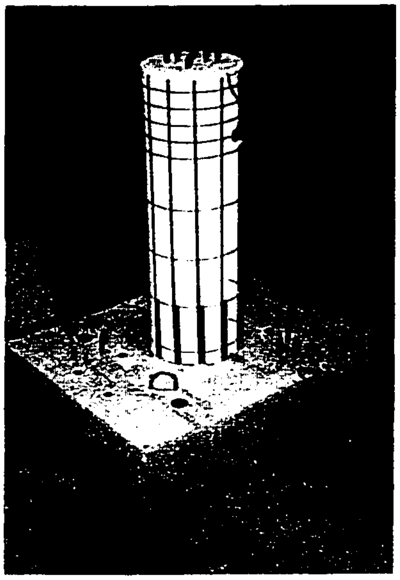

(a) BR-C8
(Long circular column without retrofitting)

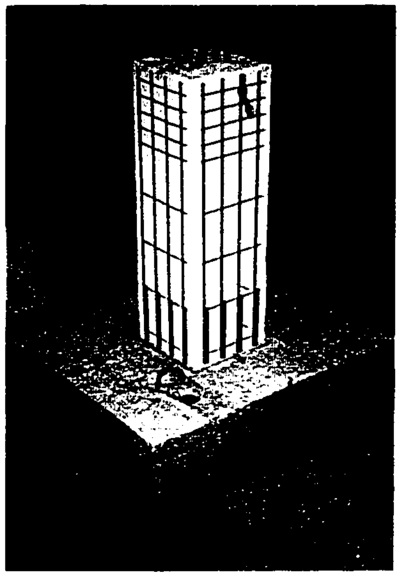

(b) BR-S5
(Long square column without retrofitting)

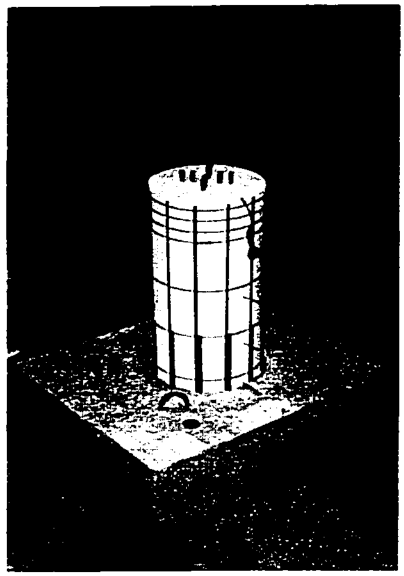

(c) BR-C10
(Short circular column without retrofitting)

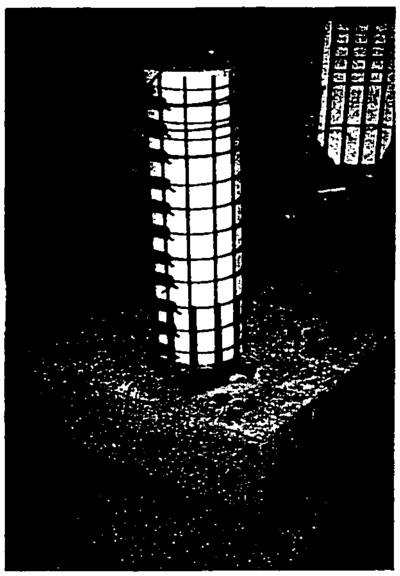

(d) BR-C9
(Long circular column with retrofitting)

(e) BR-S6
(Long square column with retrofitting)

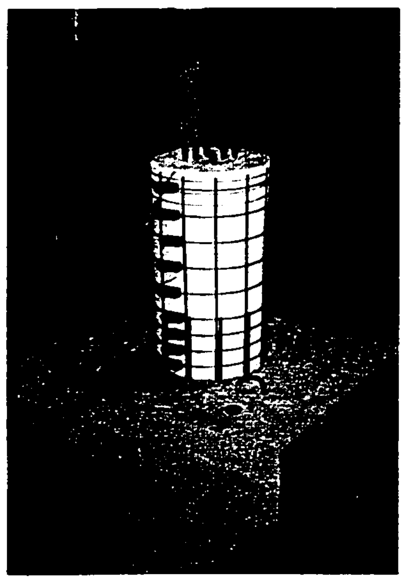

(f) BR-C11
(Short circular column with retrofitting)

Figure 2.7 Test specimens

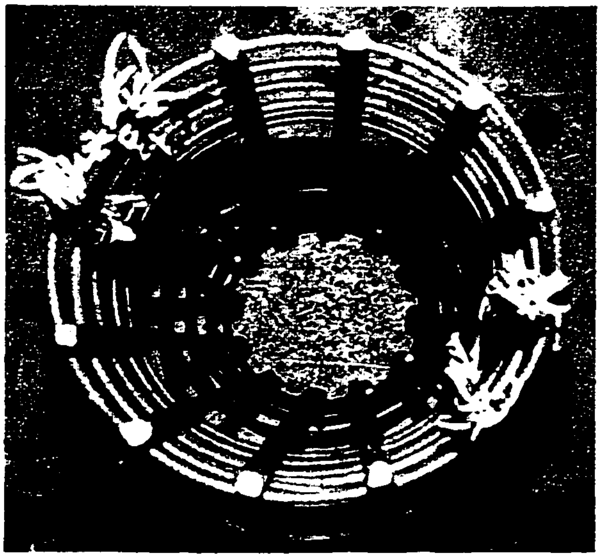

(a) Cross-sectional view

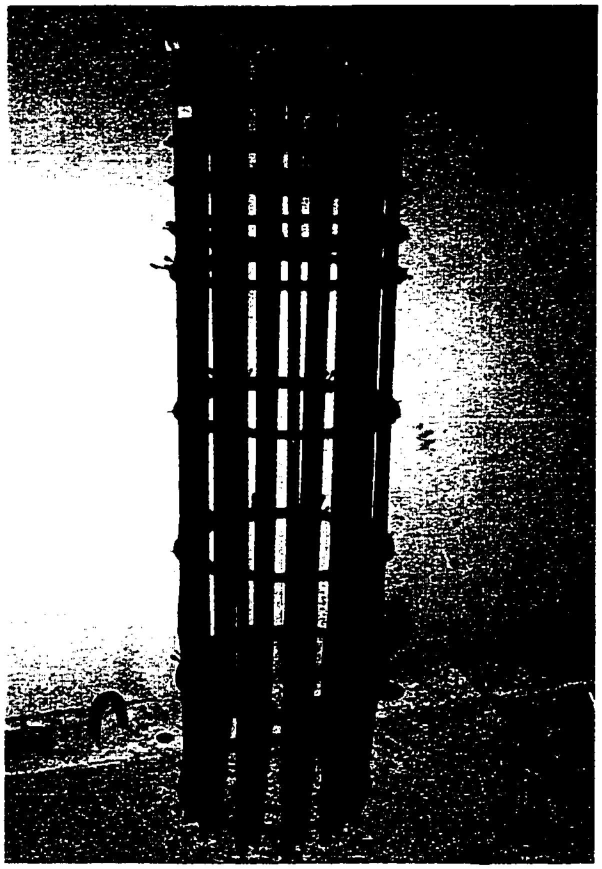

(b) Side view

Figure 2.8 Reinforcement cage of long circular column

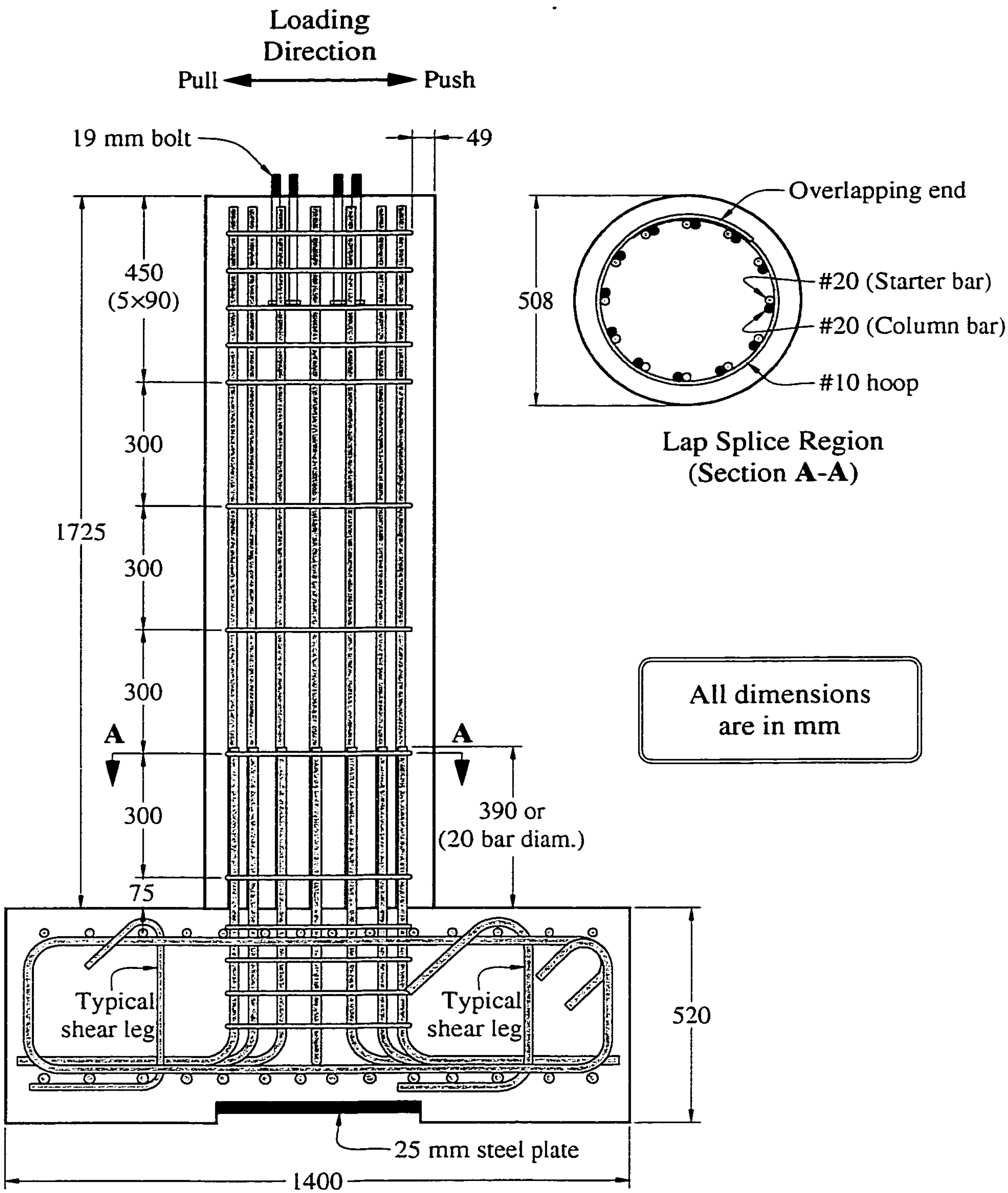

Figure 2.9 Dimensions and reinforcement details for columns BR-C8 and BR-C9

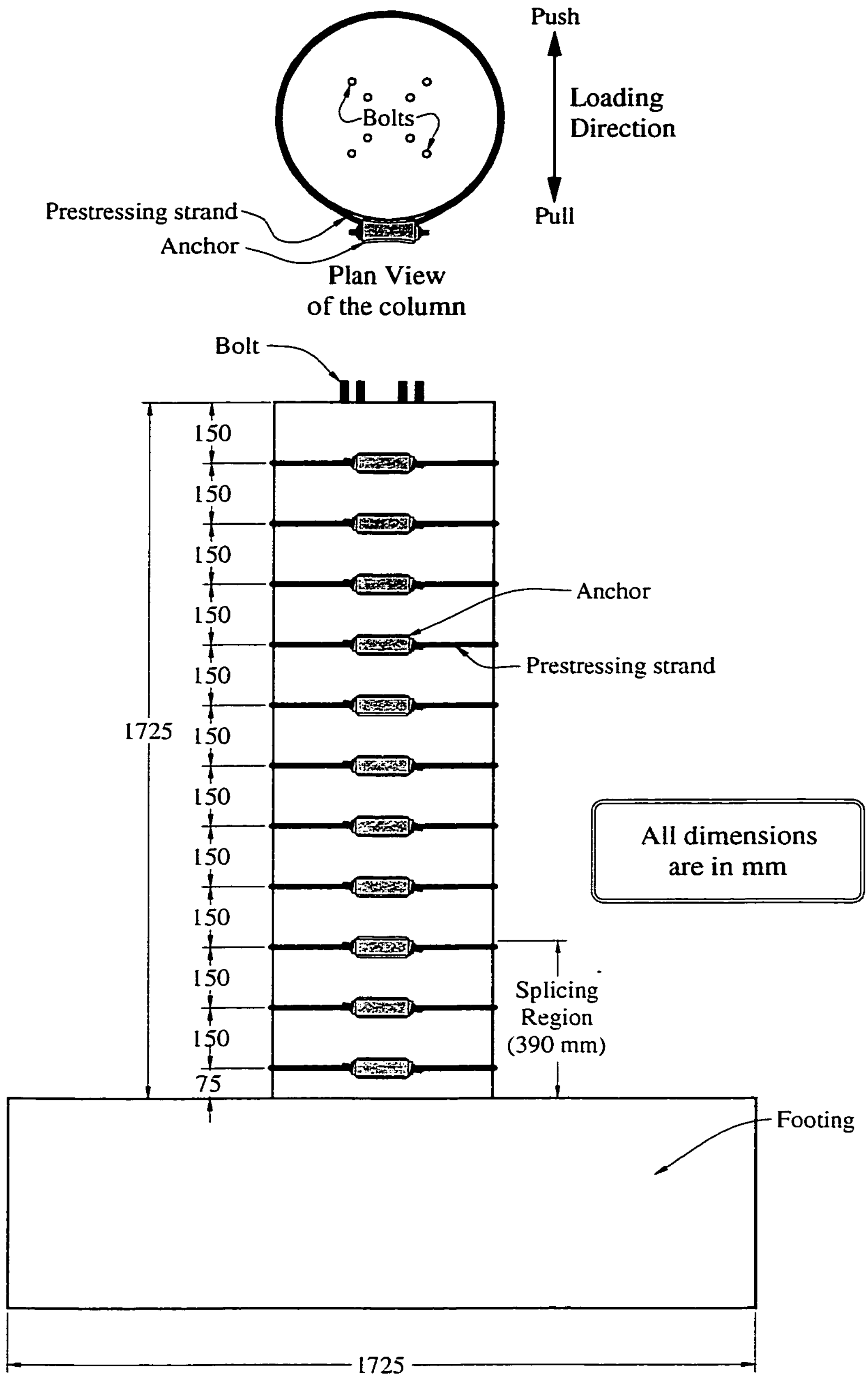

Figure 2.10 Retrofitting details for column BR-C9

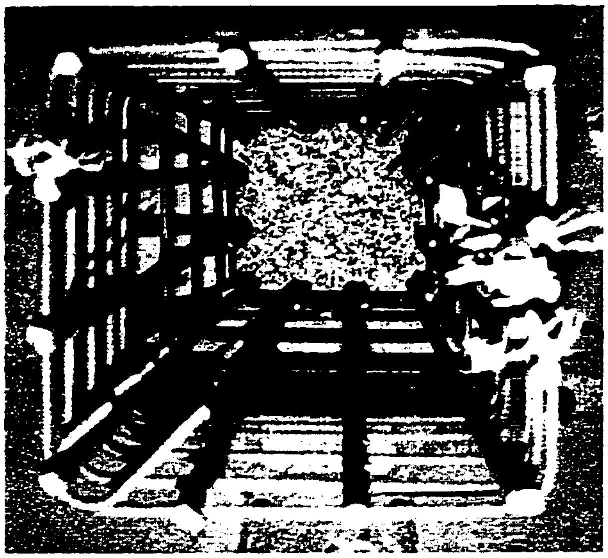

(a) Cross-sectional view

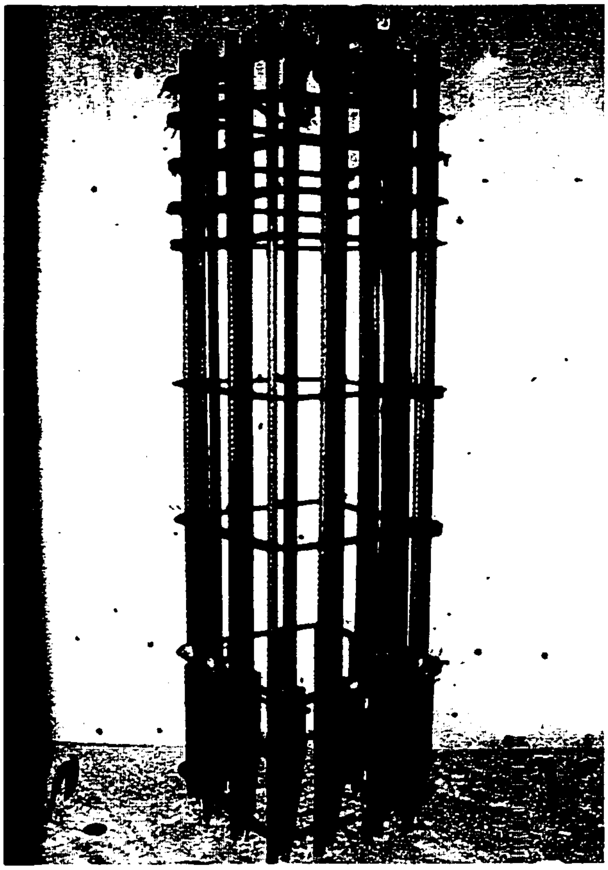

(b) Side view

Figure 2.11 Reinforcement cage of long square column

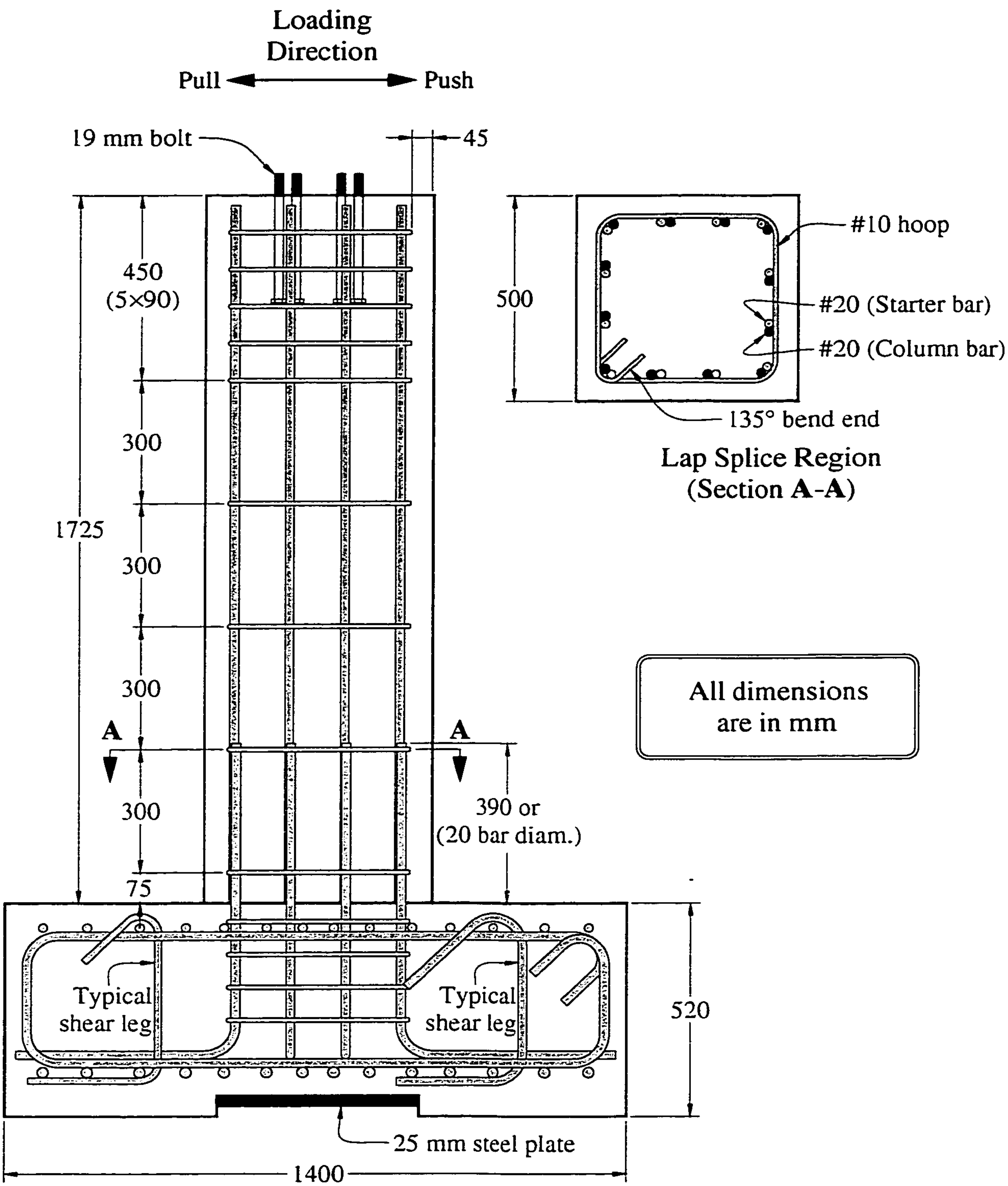

Figure 2.12 Dimensions and reinforcement details for columns BR-S5 and BR-S6

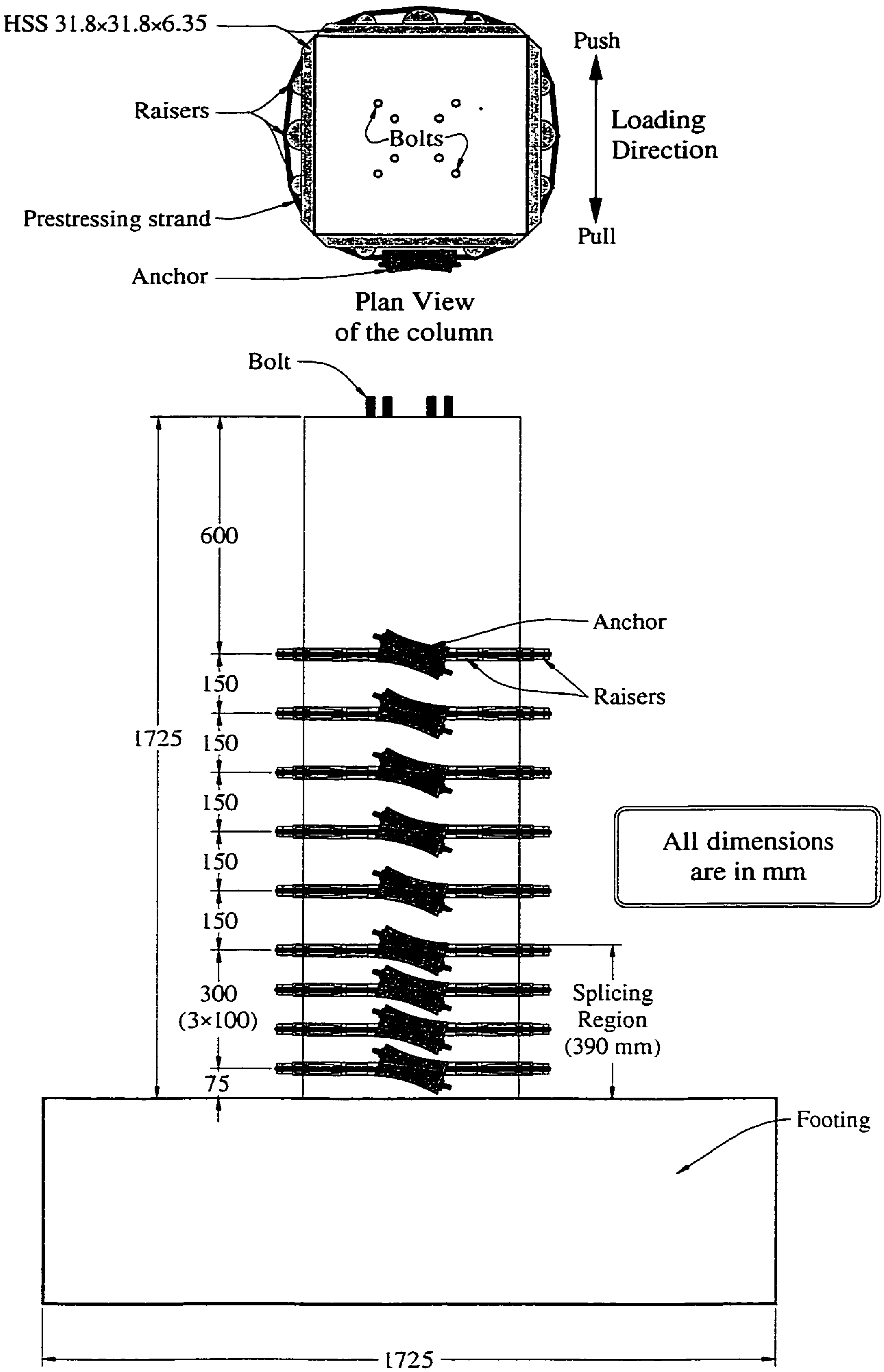

Figure 2.13 Retrofitting details for column BR-S6

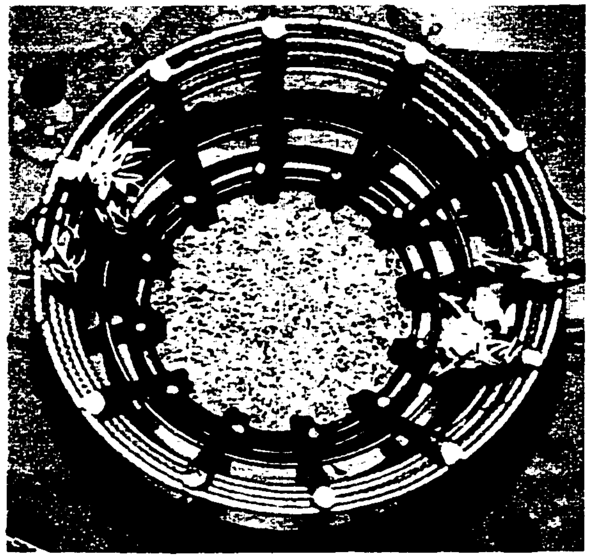

(a) Cross-sectional view

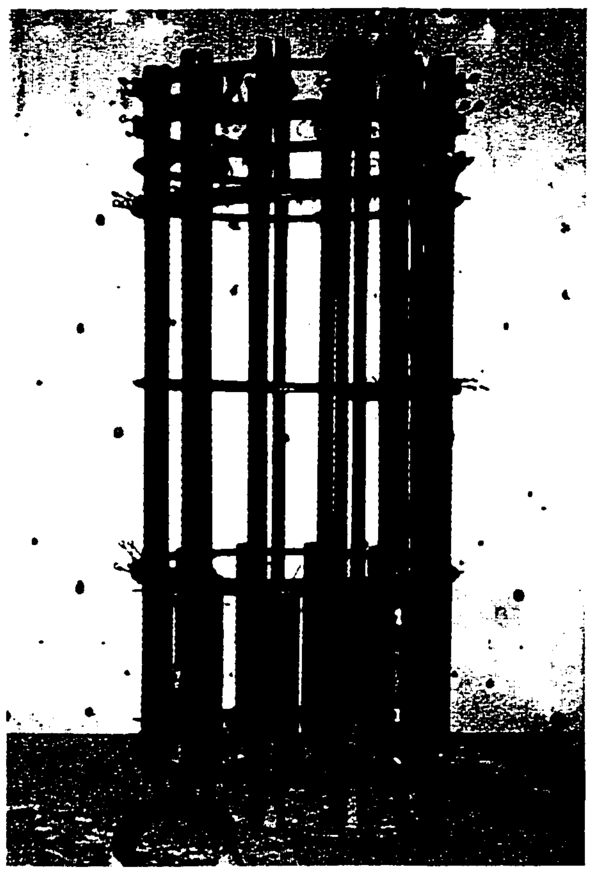

(b) Side view

Figure 2.14 Reinforcement cage of short circular column

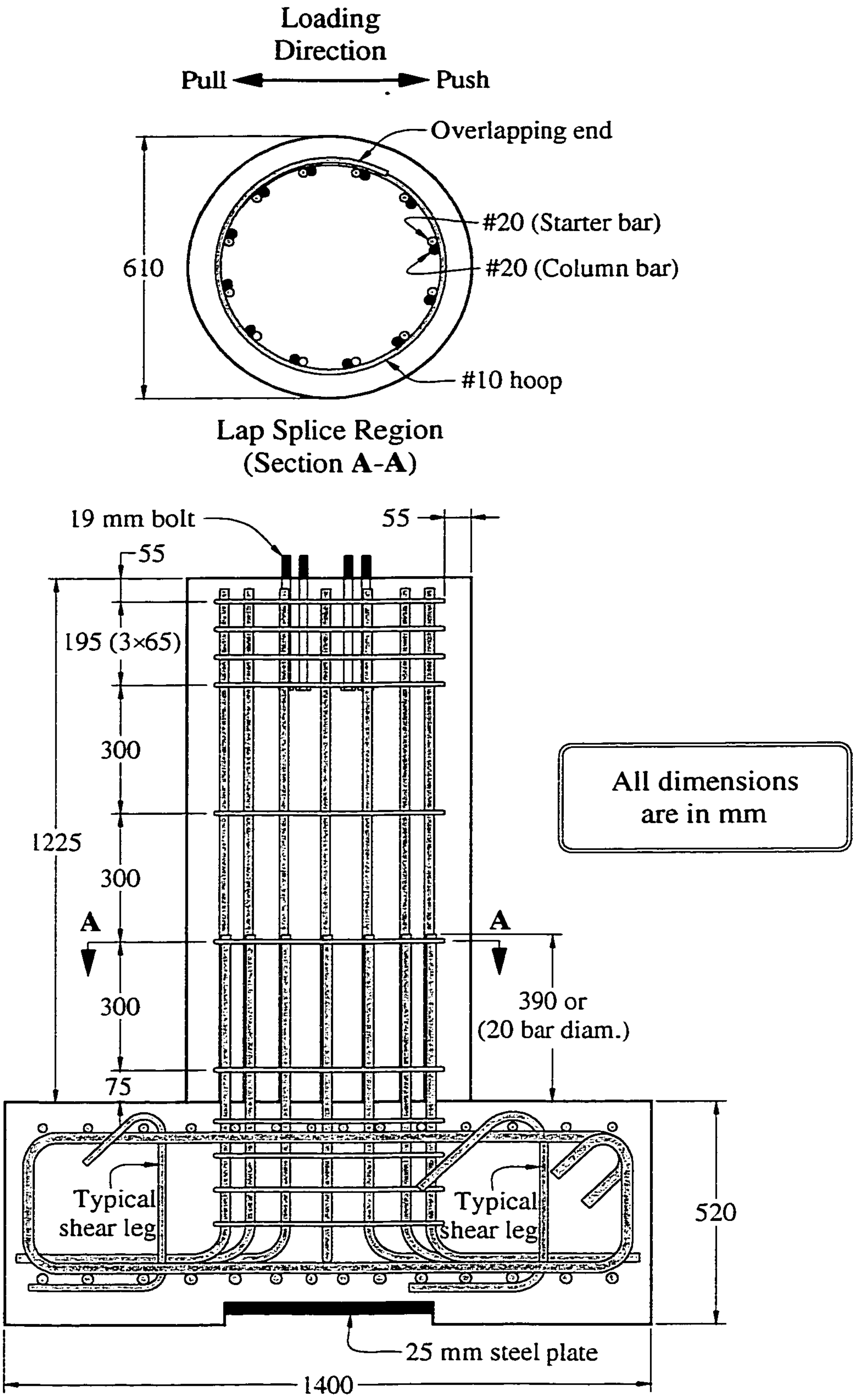

Figure 2.15 Dimensions and reinforcement details for columns BR-C10 and BR-C11

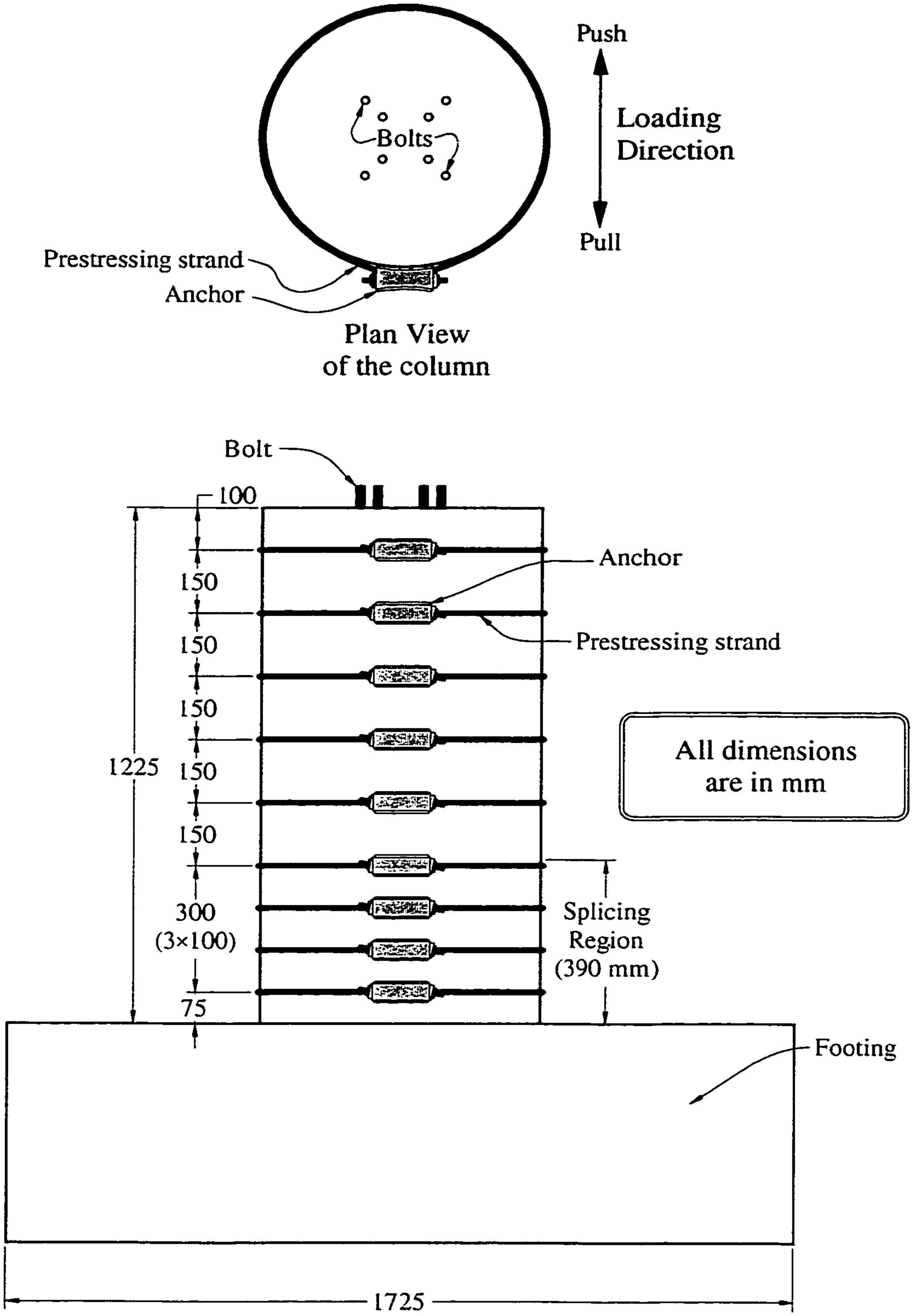

Figure 2.16 Retrofitting details for column BR-C11

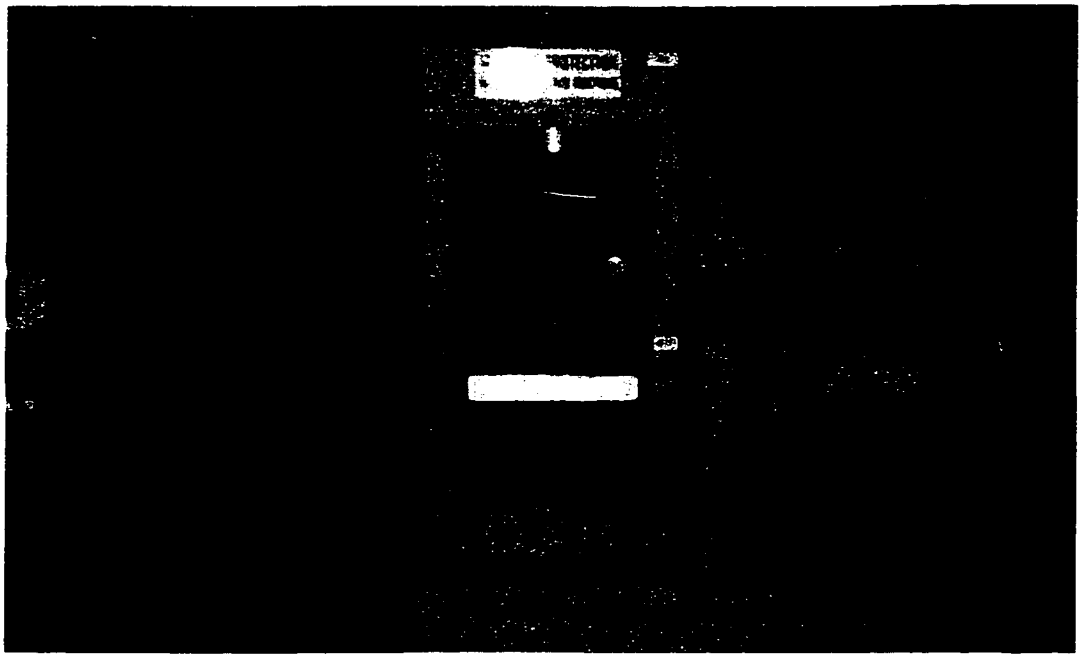

(a) Fourney testing machine

(b) Before testing

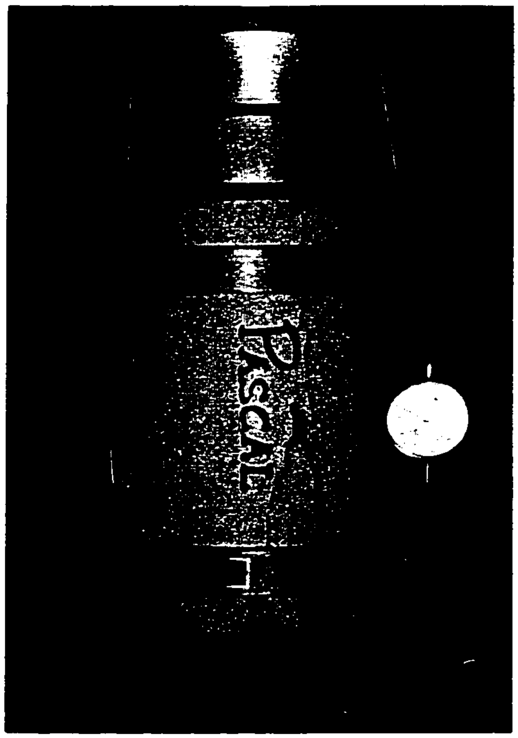

(c) After testing

Figure 2.17 Testing of standard concrete cylinders

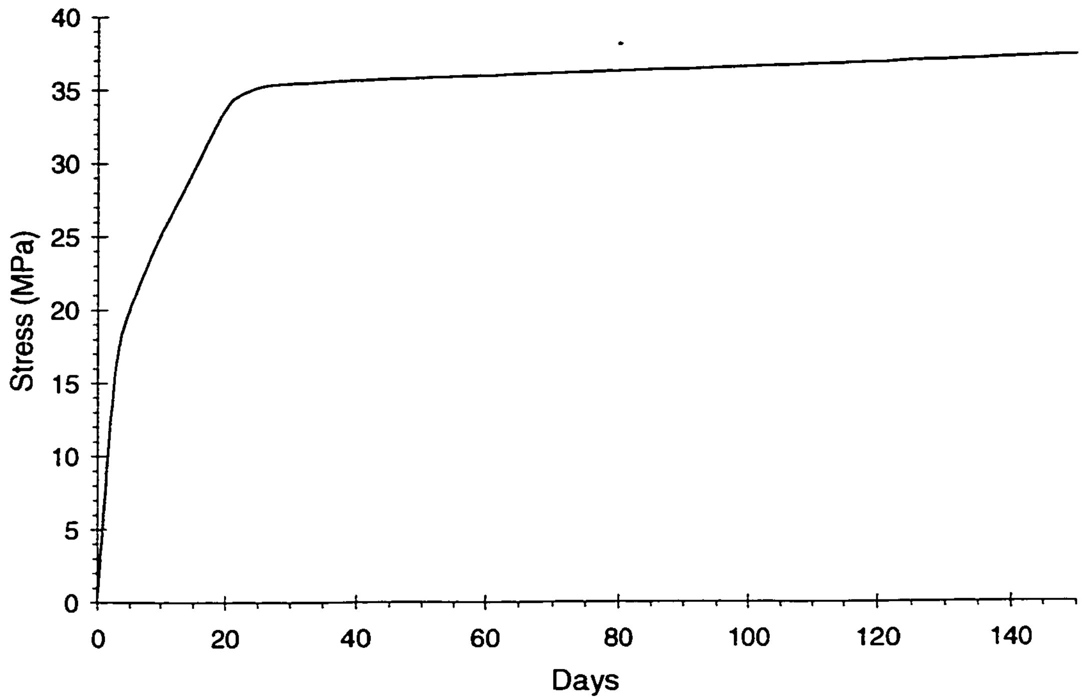

Figure 2.18 Stress development over time of concrete test cylinders

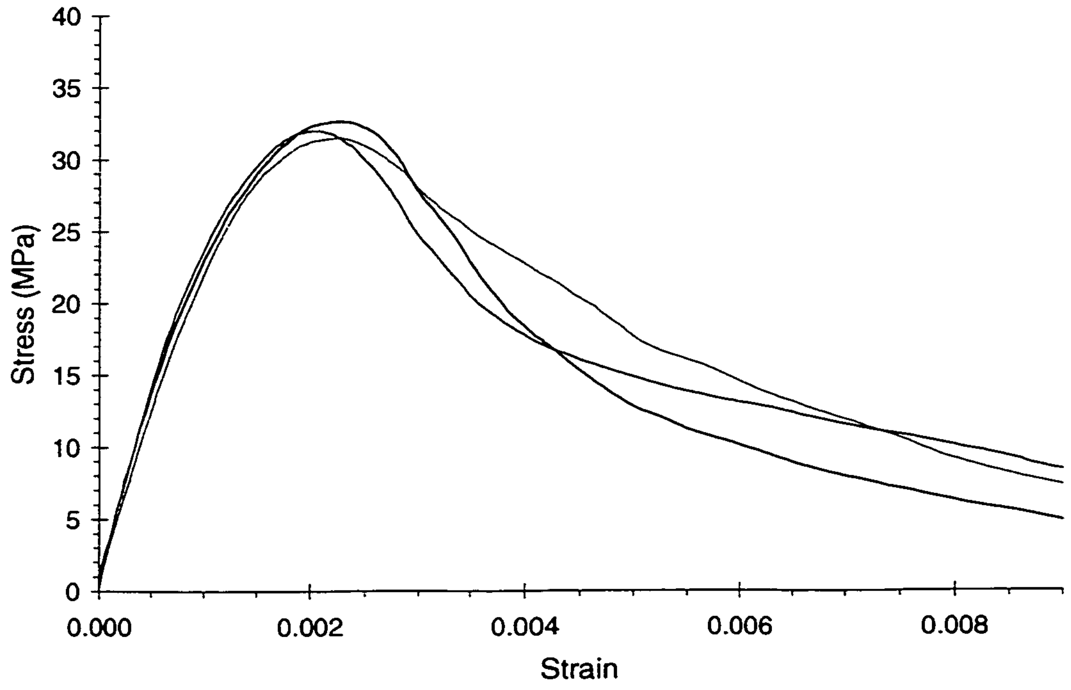

Figure 2.19 Stress-strain relationship of concrete test cylinders

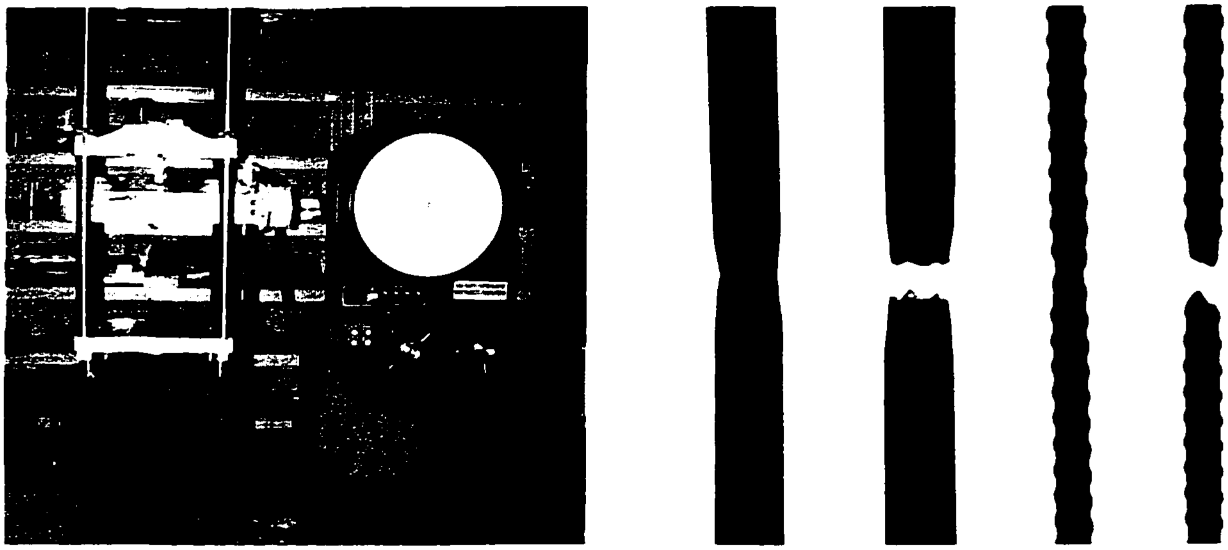

(a) Tinius Olsen testing machine (b) Deformed reinforcement after testing

Figure 2.20 Testing of longitudinal and transverse reinforcing steel

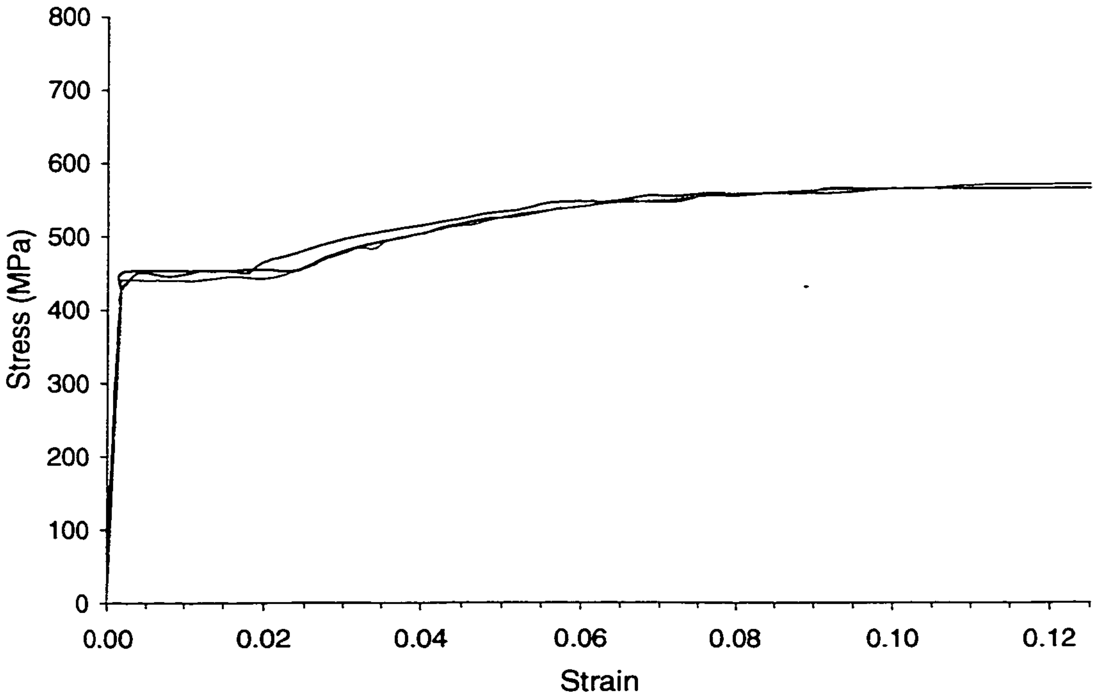

Figure 2.21 Stress-strain relationship of grade 400, No. 10 reinforcing steel bar

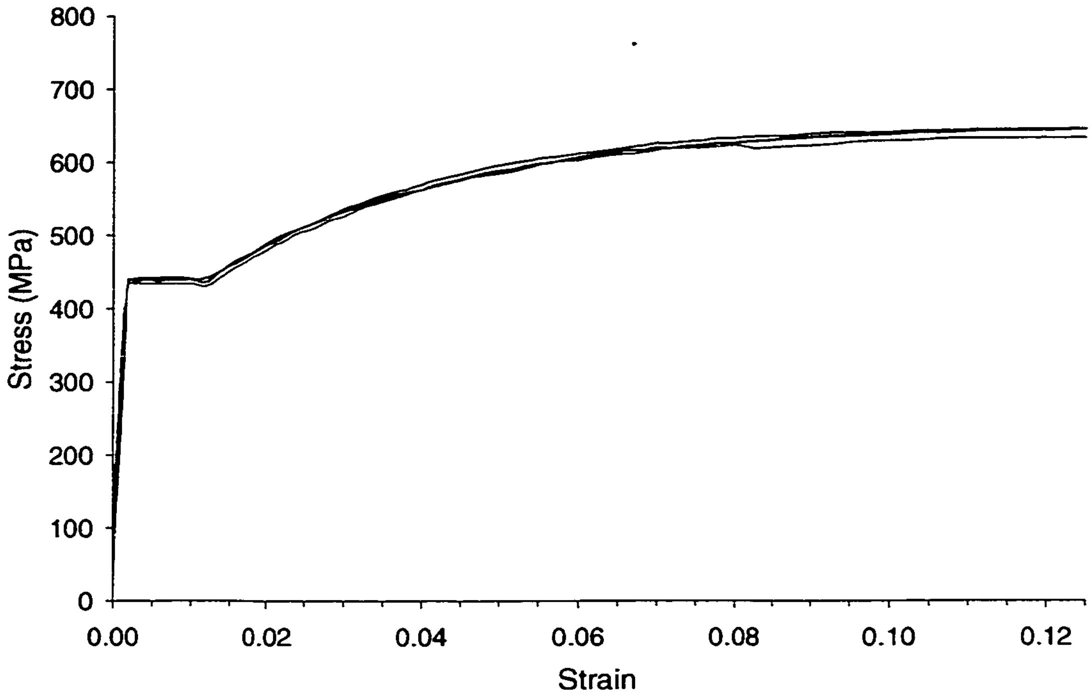

Figure 2.22 Stress-strain relationship of grade 400, No. 20 reinforcing steel bar used for long columns

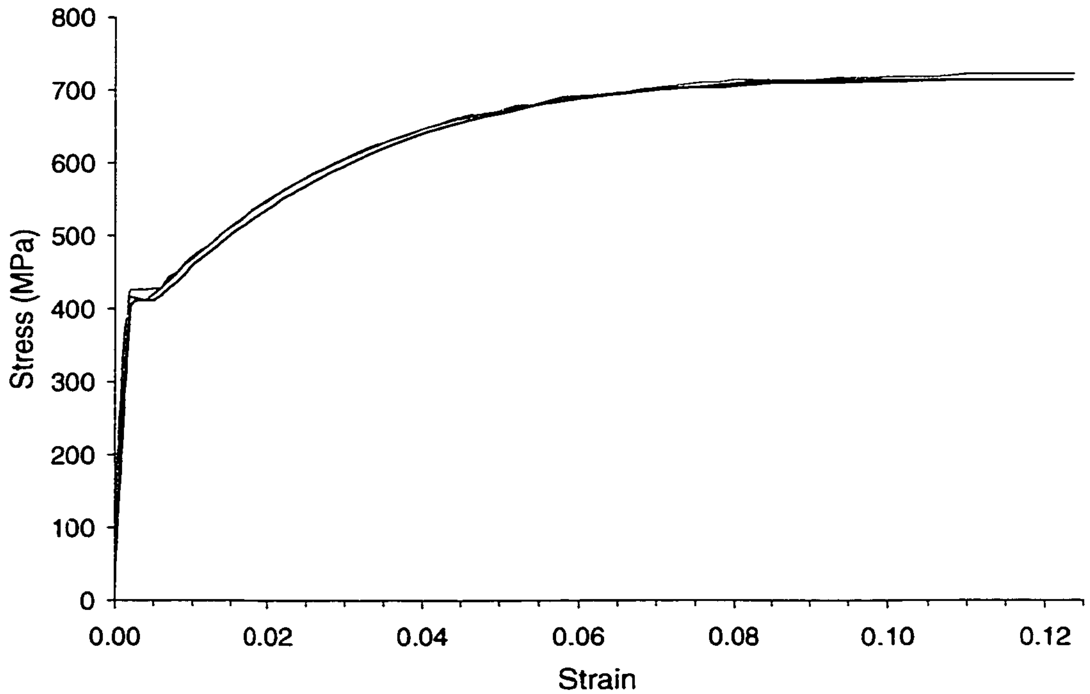

Figure 2.23 Stress-strain relationship of grade 400, No. 20 reinforcing steel bar used for short columns

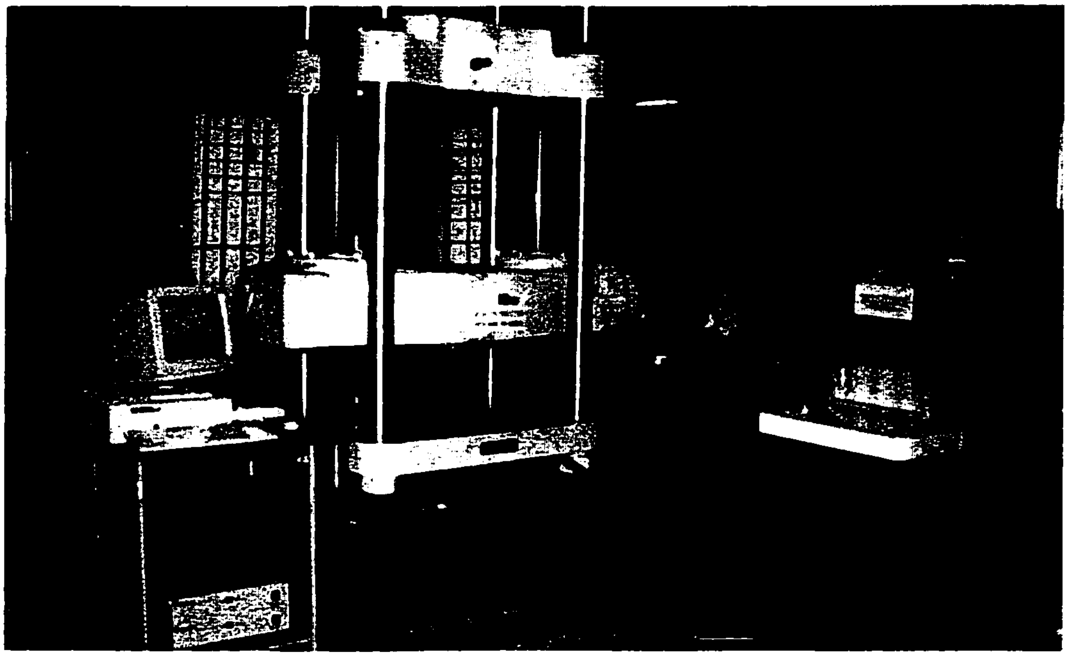

(a) Tinius Olsen testing machine

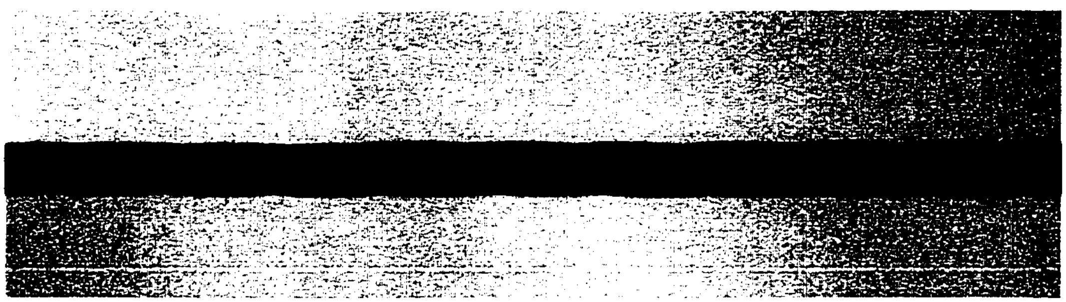

(b) Prestressing wire before testing

(c) Prestressing wire after testing

Figure 2.24 Testing of size 9 prestressing strands

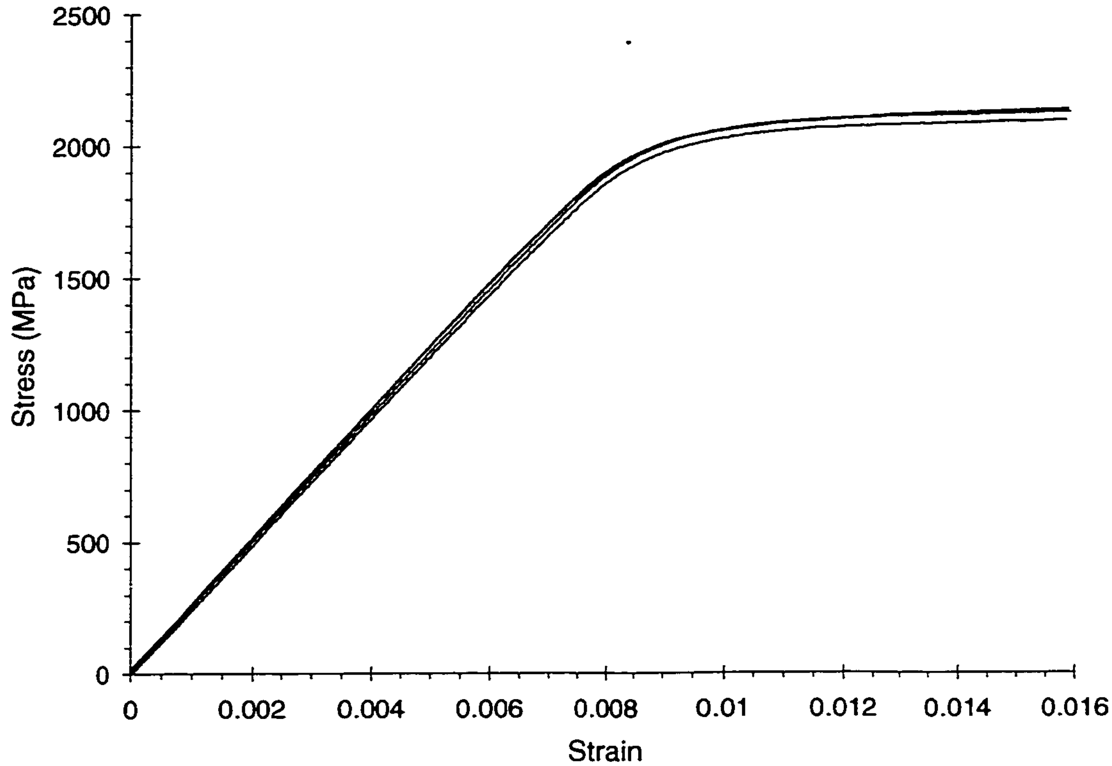

Figure 2.25 Stress-strain relationship of size 9, grade 1860, seven-wire prestressing strands

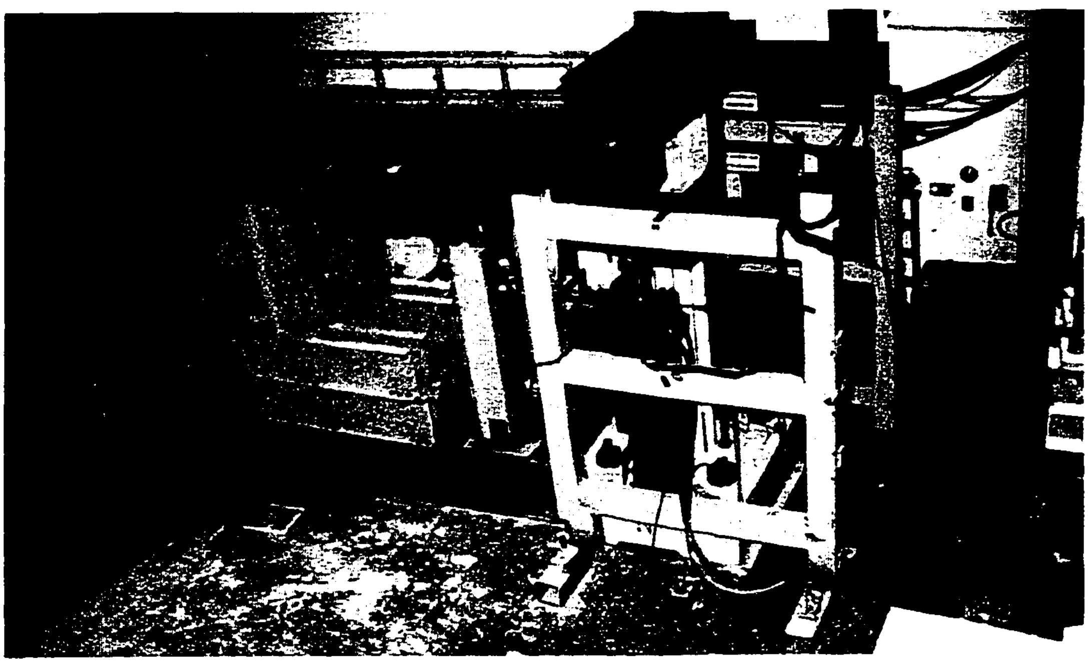

Figure 2.26 Overall view of the setup used to test the columns

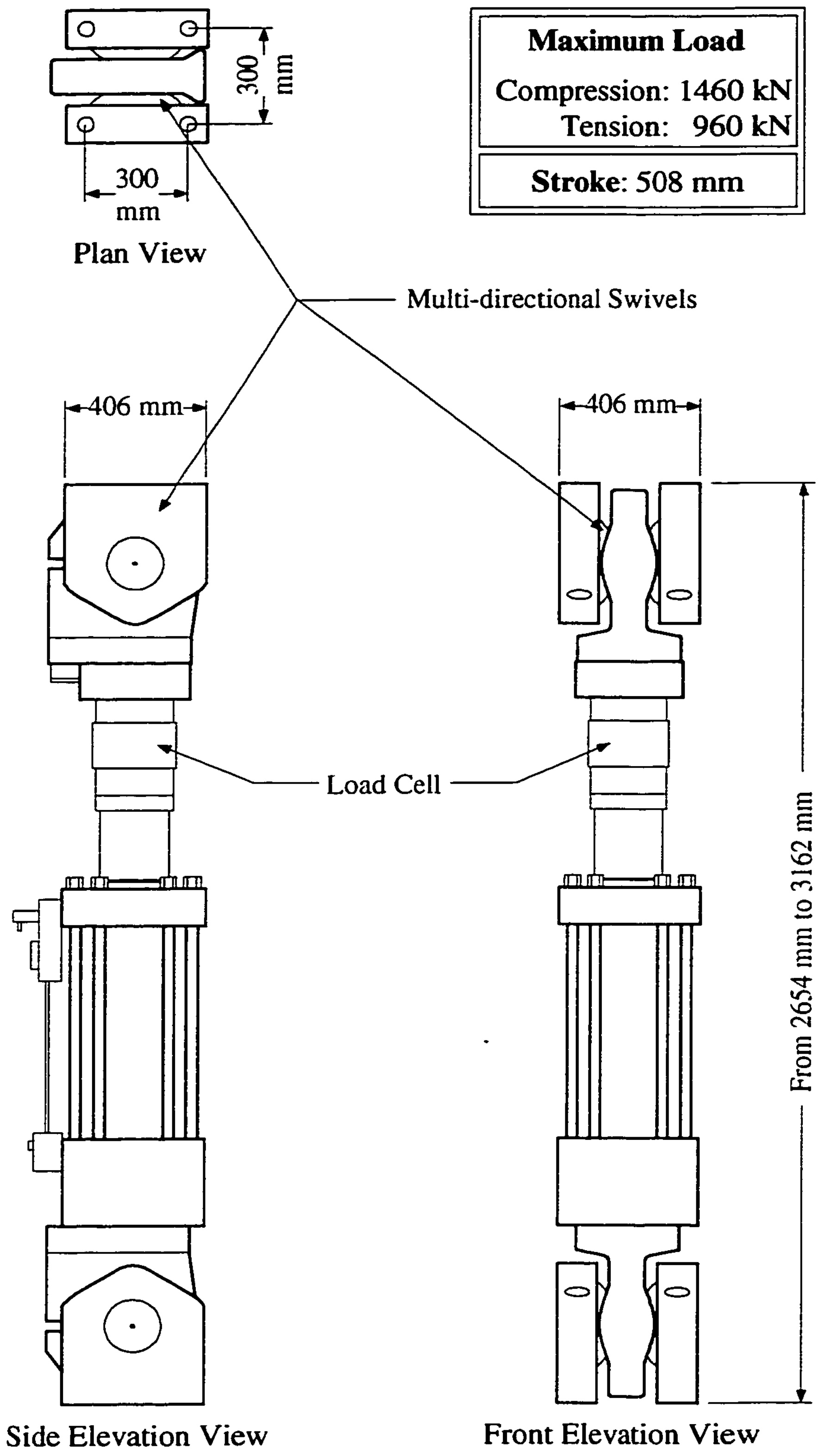

Figure 2.27 Details of the MTS hydraulic actuators

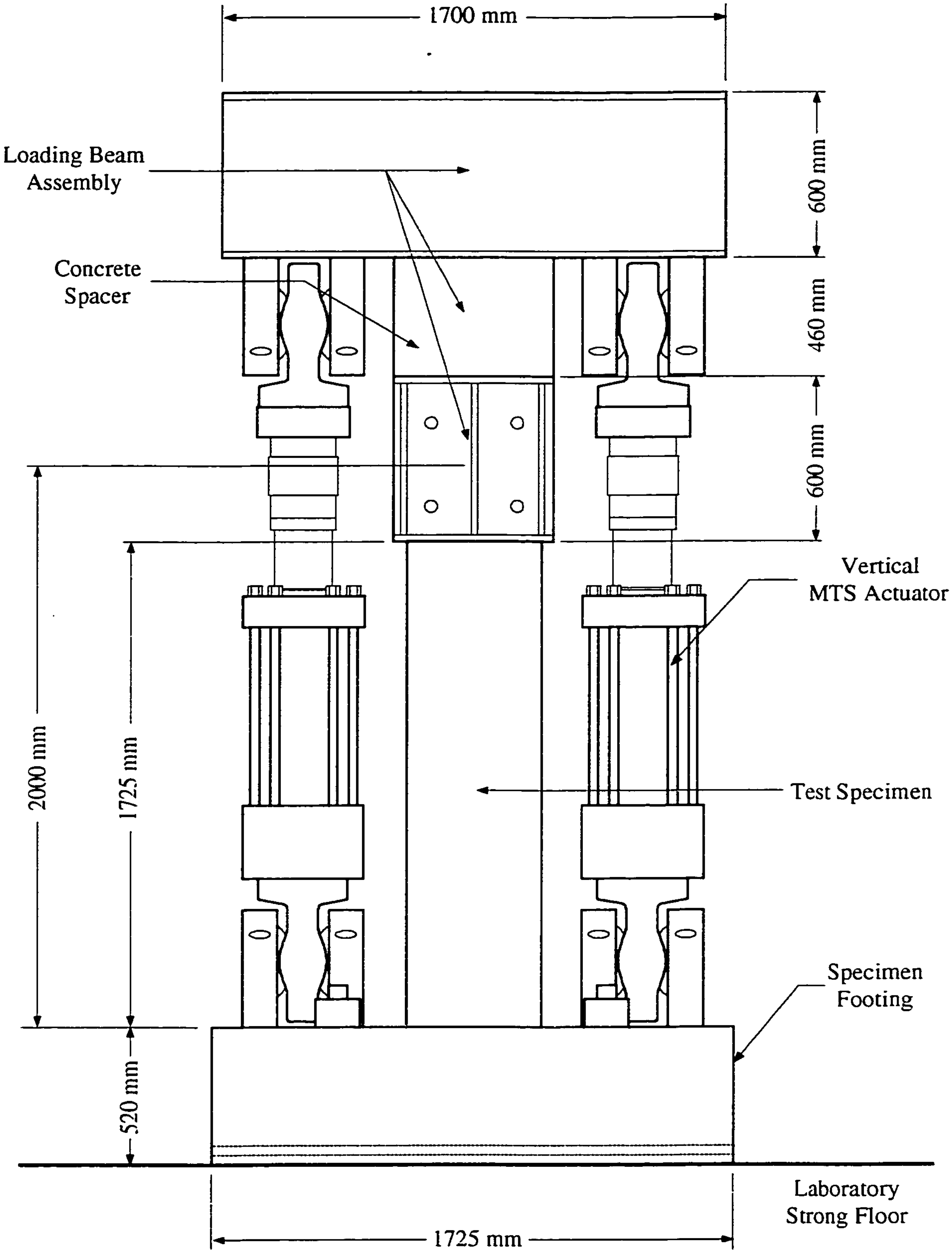

Figure 2.28 Front Elevation of Test Setup

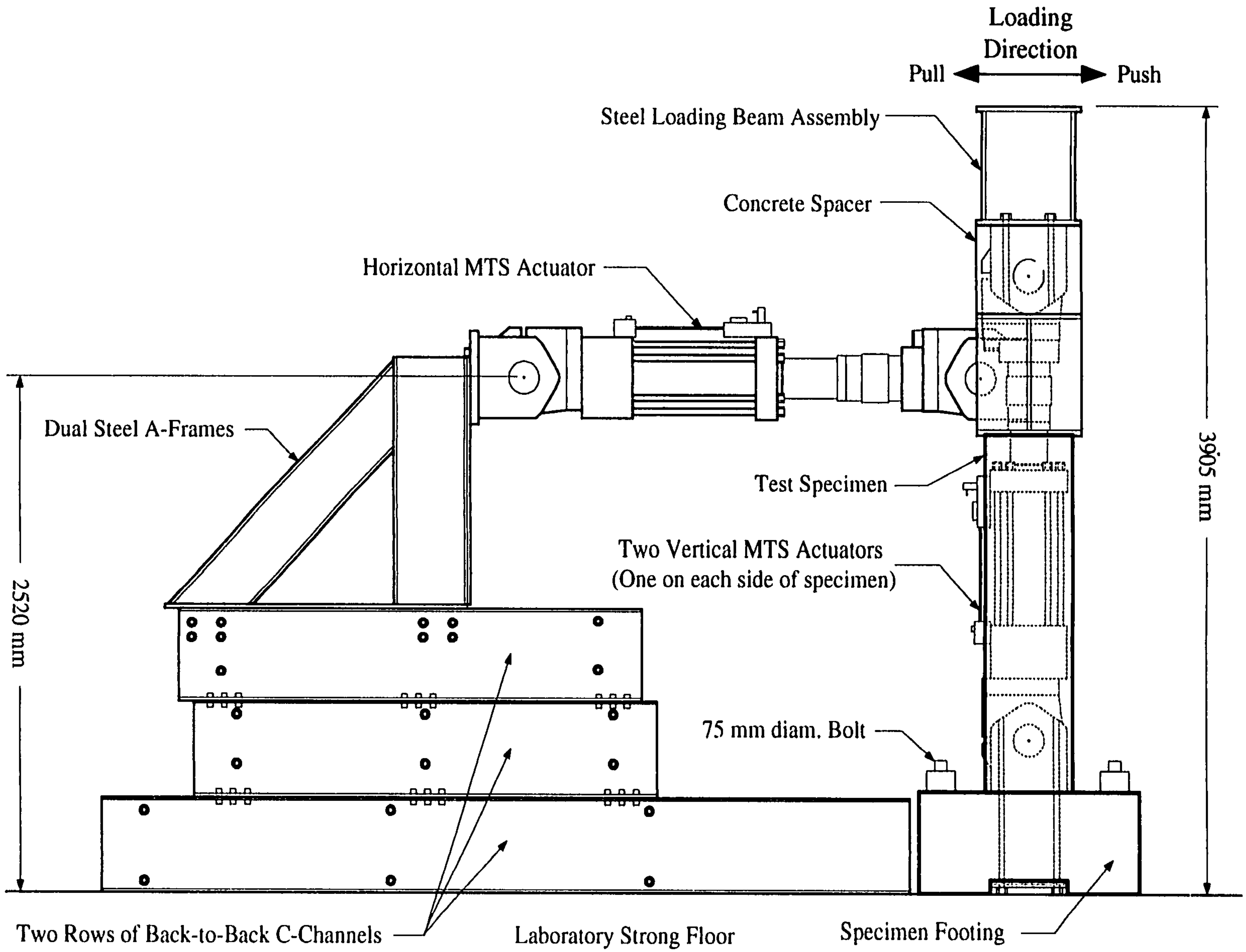

Figure 2.29 Side Elevation of Test Setup

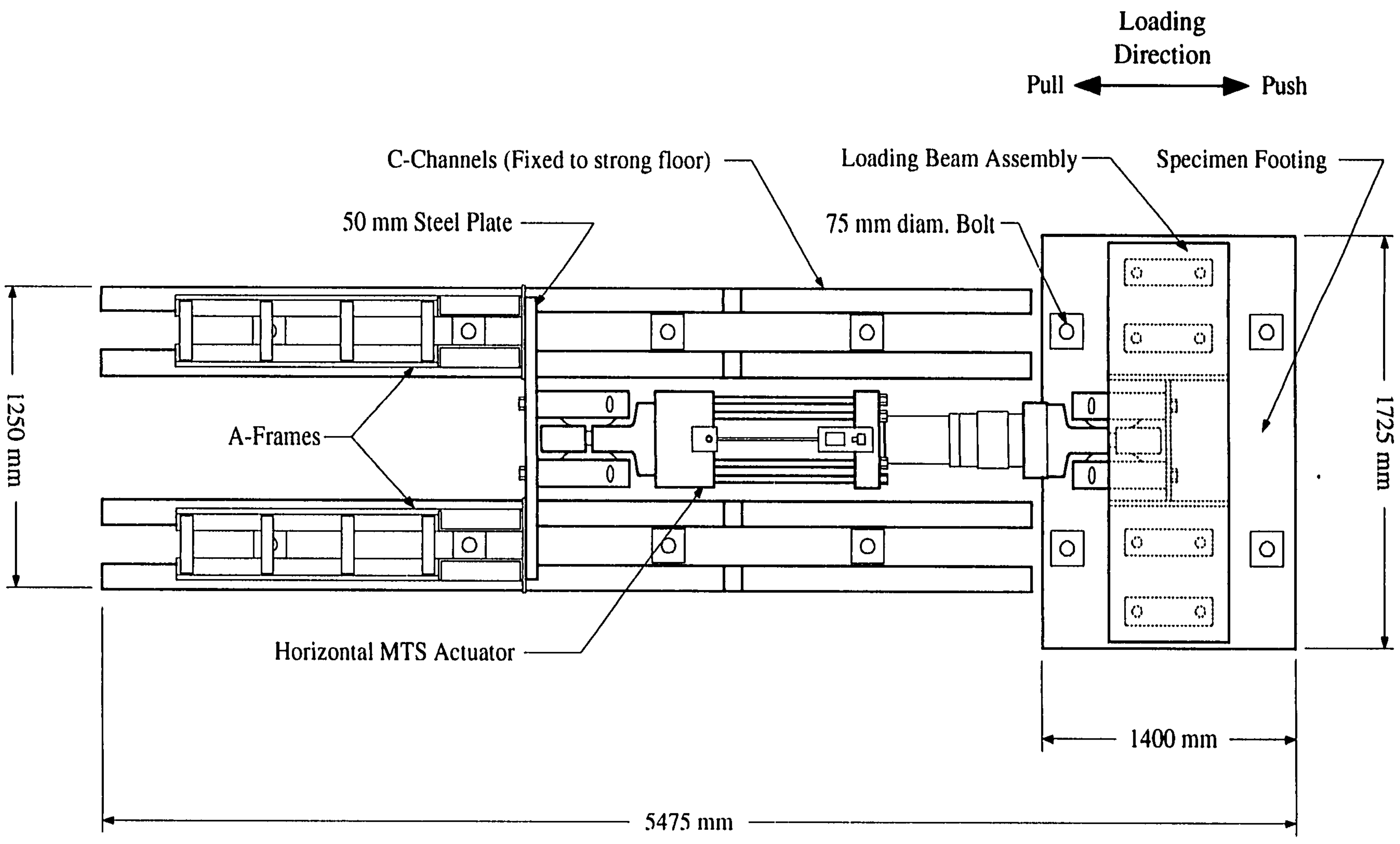

Figure 2.30 Plan View of Test Setup

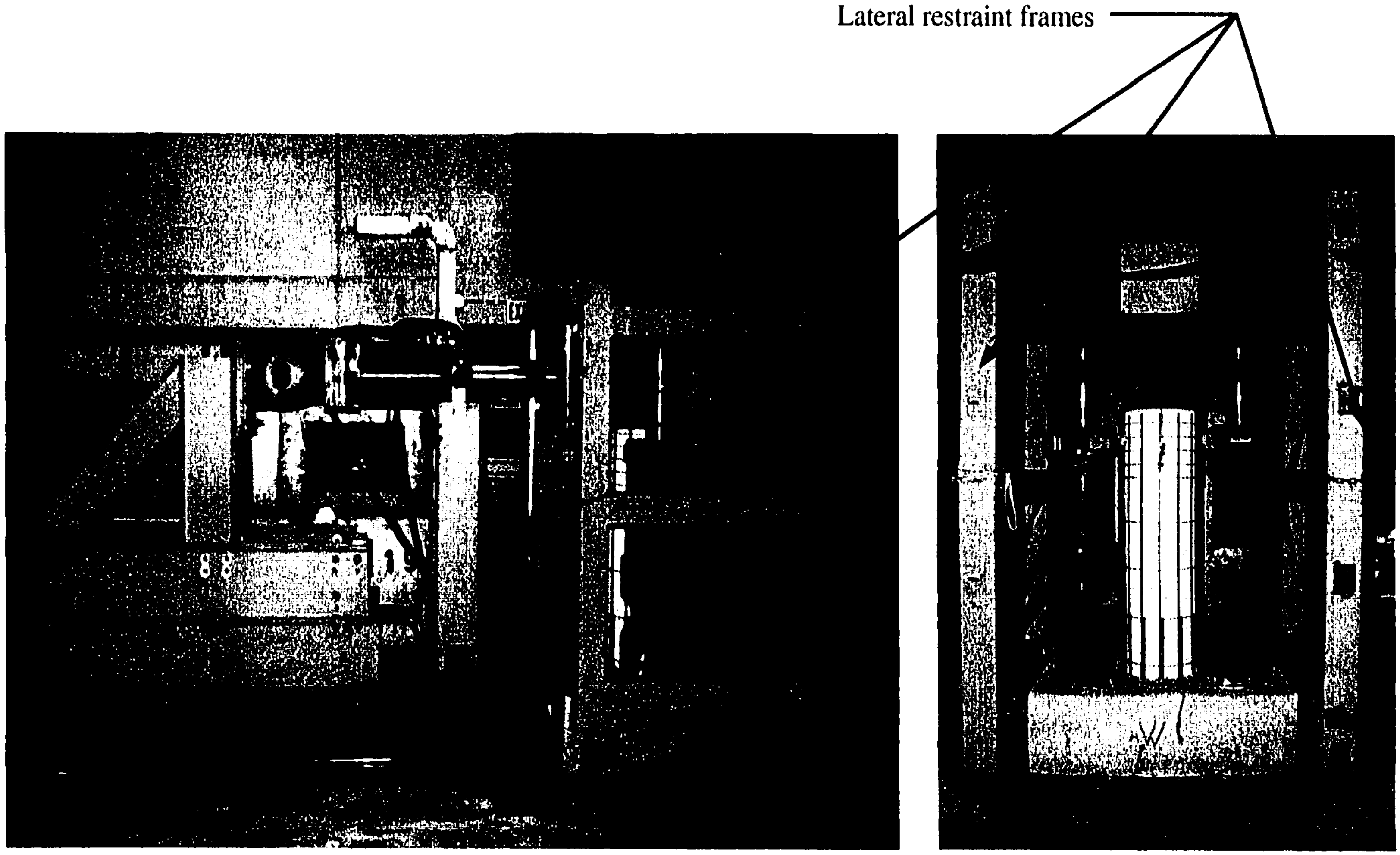

(a) Side view of the test setup

(b) Front view of the test setup

Figure 2.31 Lateral restraint frames

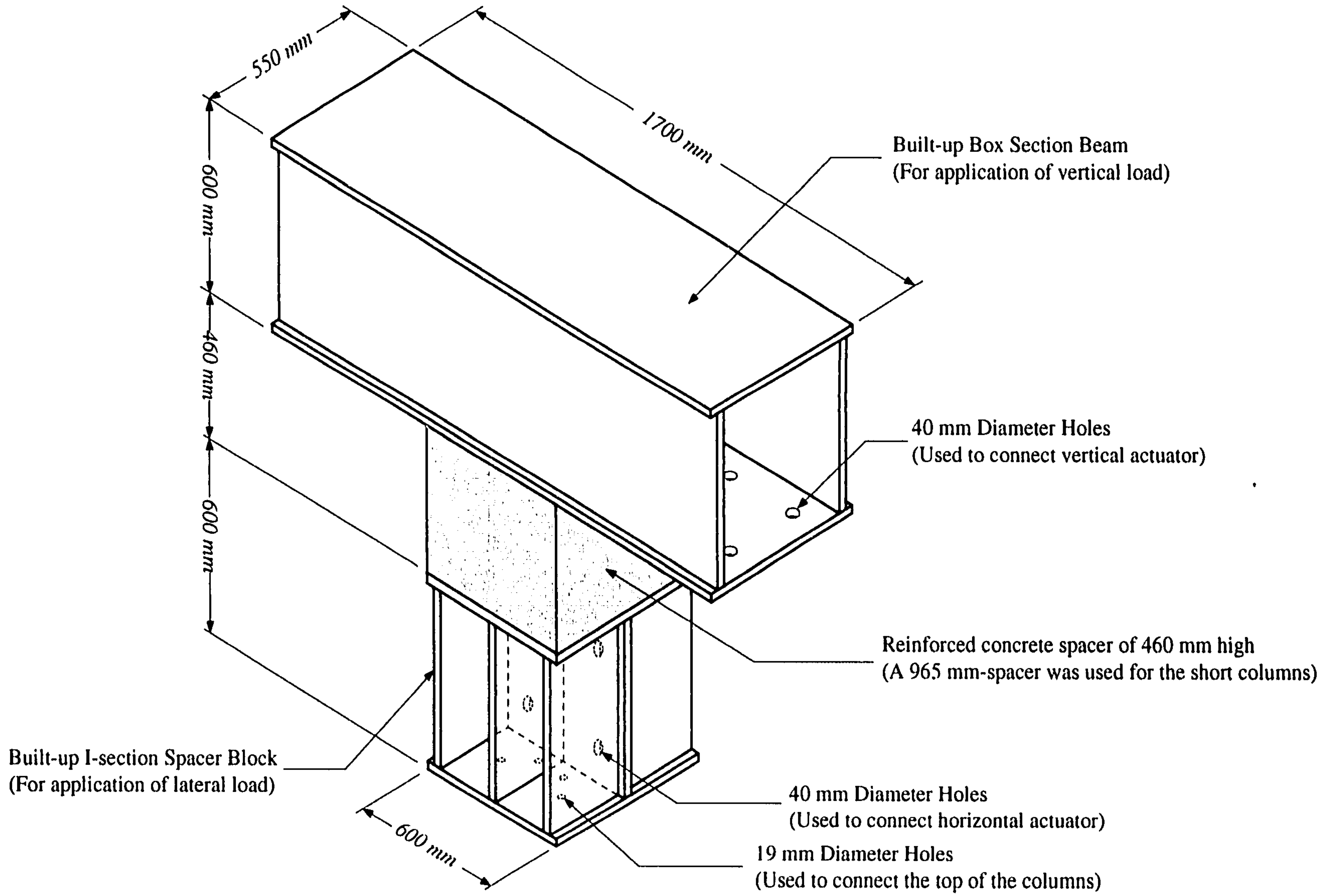

Figure 2.32 Details of the loading beam assembly

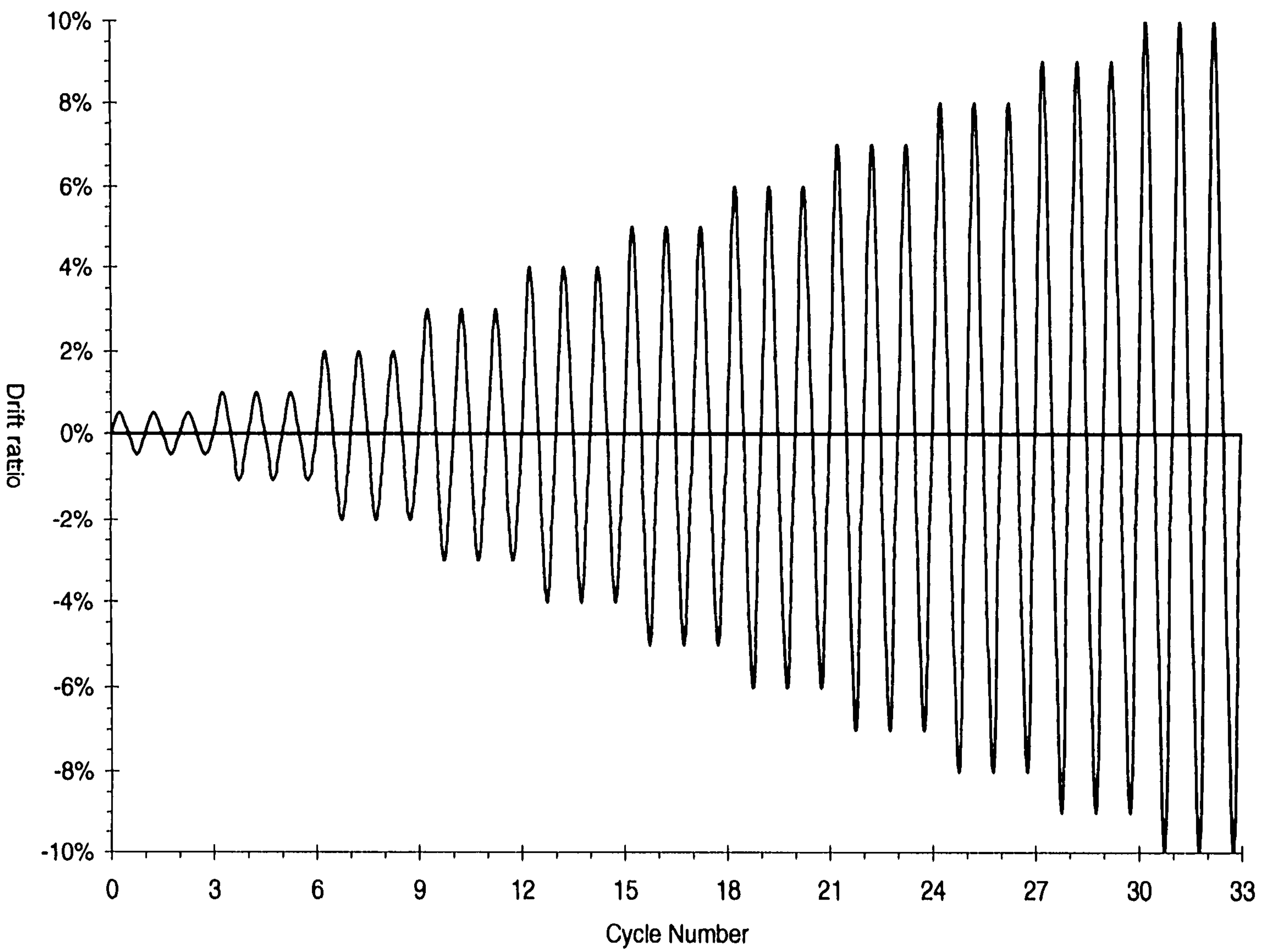

Figure 2.33 Loading Program

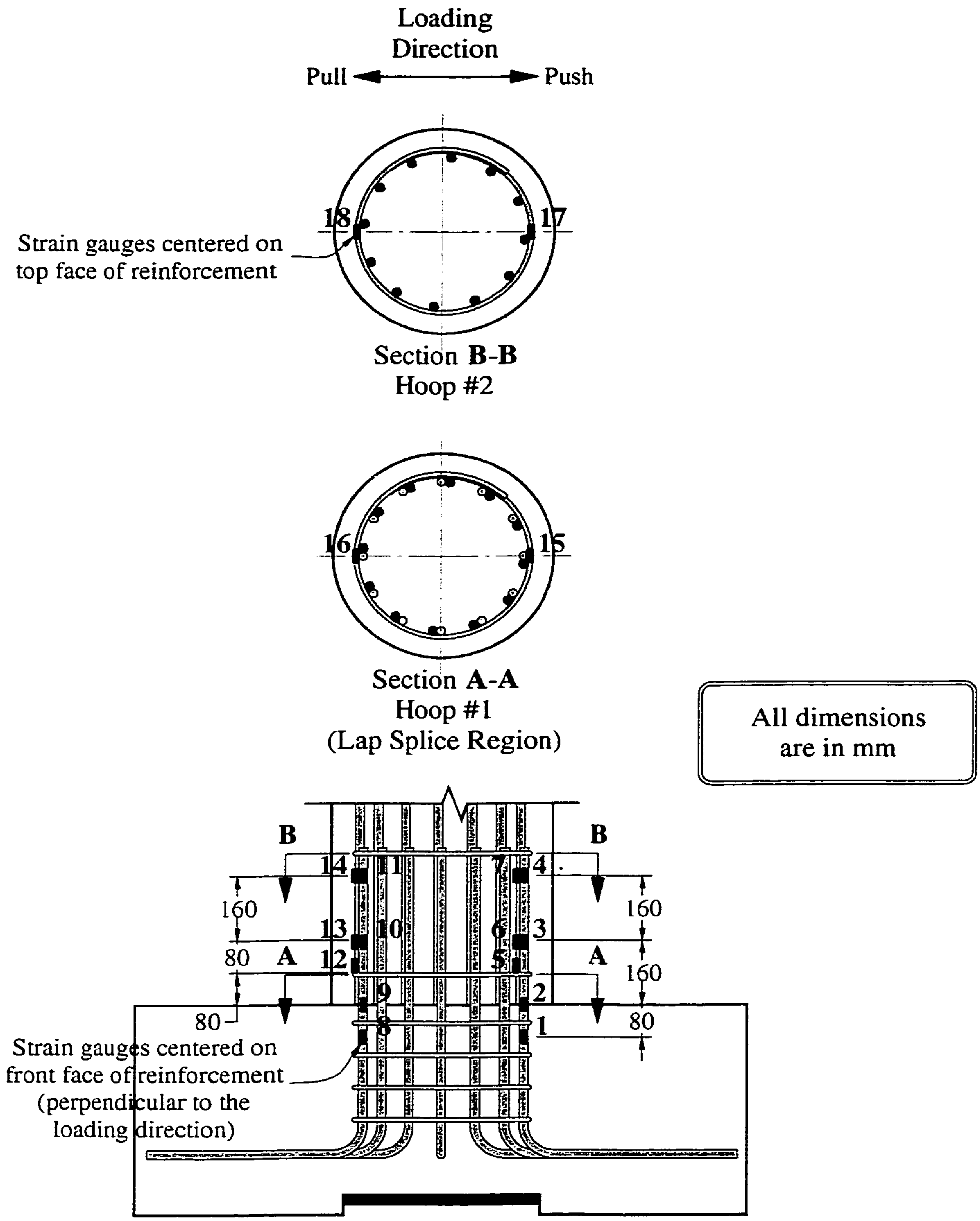

Figure 2.34 Strain gauge location on reinforcing steel for circular columns

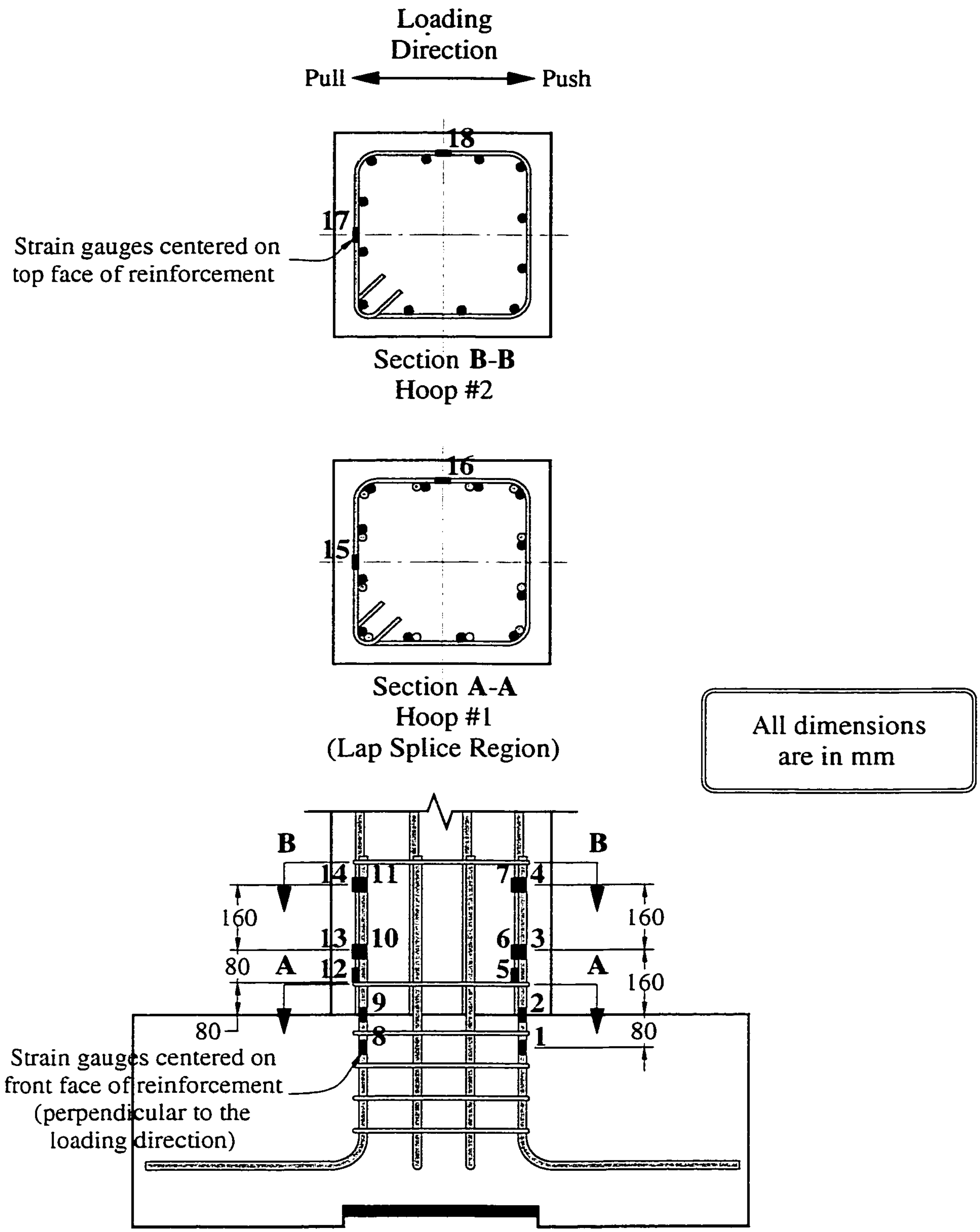

Figure 2.35 Strain gauge location on reinforcing steel for square columns

Long circular column (**BR-C9**)

Location of strain gauge	
A	**B**
All the prestressing strands	First three prestressing strands

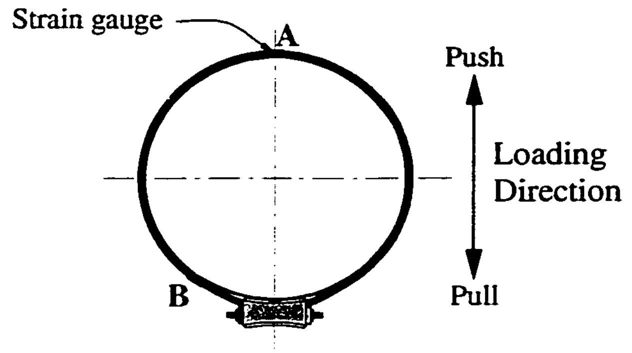

Long square column (**BR-S6**)

Location of strain gauge	
A	**B**
All the prestressing strands	First three prestressing strands

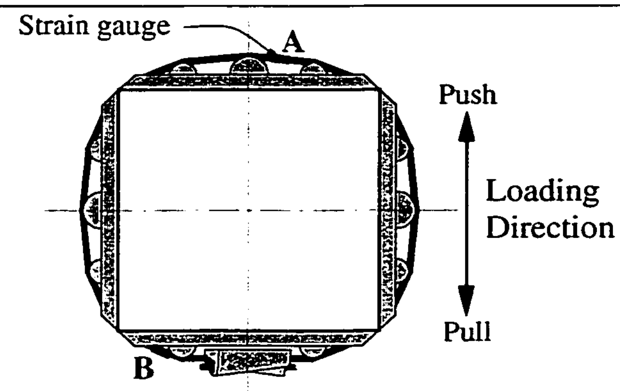

Short circular column (**BR-C11**)

Location of strain gauge	
A	**B**
All the prestressing strands	First three prestressing strands

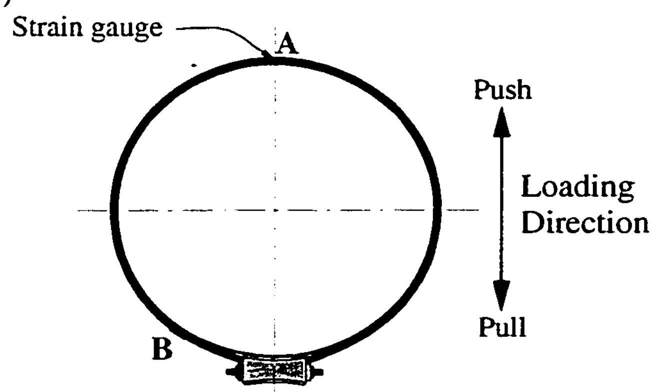

Figure 2.36 Strain gauge location on prestressing strands

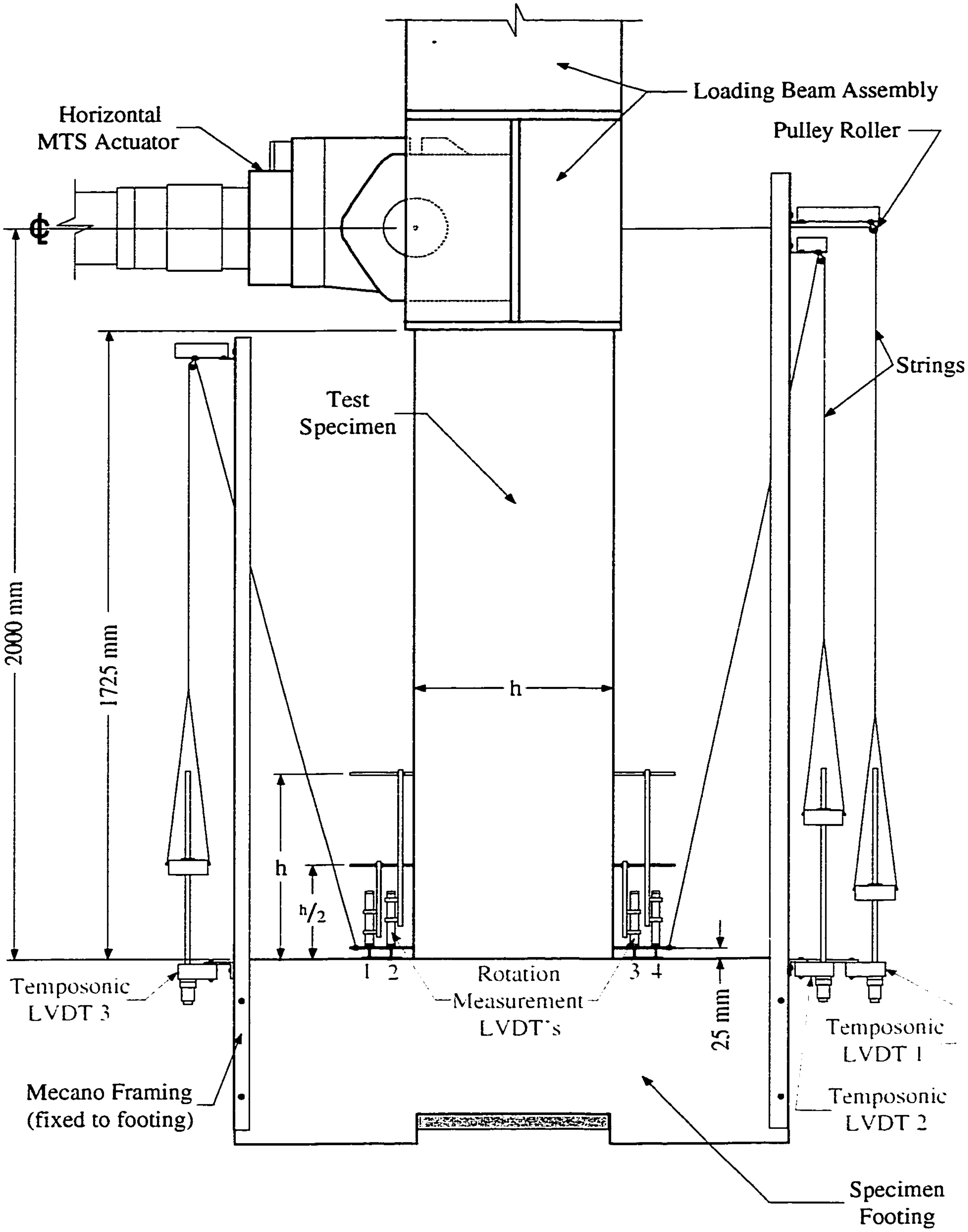

Figure 2.37 Location of LVDT

CHAPTER 3
EXPERIMENTAL RESULTS

3.1 GENERAL

This chapter summarises the results obtained from six reinforced concrete column tests. The recorded test data as well as the observations made are explained. The specimens representing existing bridge columns, without any retrofit, are compared with those retrofitted with external prestressing. The columns are considered failed once the lateral load drops down to 80% of the peak load. Many researchers use this criterion to determine column failure. The drift level at which three cycles are completed just before a strength decay of greater than 20% is experienced, is referred to as the drift capacity. The drift capacity illustrates the effectiveness of the retrofitting strategy adopted, as compared to those without the retrofit. Lateral force-drift and moment-drift hysteretic relationships are used to illustrate column behaviour. The force-drift relationship also includes degradations caused by P-Δ moment, whereas the moment-drift relationship only shows degradations in column load resisting mechanism.

The failure mechanism, as well as all recorded data are presented and discussed for each column specimen. Unfortunately, some instruments either experienced technical problems or could not collect data up to the end of the test because the wires were cut or the instruments were damaged as the specimens experienced distress, although this occurred in very few cases. The main graphs were plotted using the same scale for each pair of columns to facilitate direct comparison. Note that the positive sign for a strain gauge on reinforcing steel or prestressing strands indicates tension and the negative sign compression.

The test setup was such that the horizontal actuator was orientated in the East-West direction. At each deformation level, the column was first pushed towards West, and pulled towards East. Pushing was considered to generate positive deformations (right side of the graphs), and pulling was considered negative. Several photographs were taken at the end of each drift level from East and West sides. Additional photographs were taken when a significant change occurred in column behaviour. Red lines, showing the evolution of cracking during testing marked the crack pattern. The test photographs are shown at the end of the chapter.

3.2 LONG CIRCULAR COLUMNS

This section reports on the failure mechanism and the recorded data for the 2 m-circular columns, BR-C8 and BR-C9.

3.2.1 NON-RETROFITTED COLUMN BR-C8

The observed behaviour of specimen BR-C8 is illustrated in Fig. 3.1. Some flexural cracks appeared on the tension side, during cycling at ½% drift. The maximum lateral load resistance at ½% drift and 1% drift were 142 kN and 192 kN, respectively. At 1% drift, first hairline vertical cracks and new flexural cracks formed while existing cracks became wider. The starter bars yielded at 1% drift (see Fig. 3.5) causing vertical cracks in the splice region. According to the data, the longitudinal bars did not yield (see Fig. 3.4). A peak load resistance of 195 kN and a peak flexural capacity of 420 kN·m were reached during the first cycle at 2% drift. At that stage, flexural cracks widened and coalesced with vertical cracks. A diagonal shear crack appeared, and the first two hoops yielded (see Fig. 3.6). The concrete crushed at column base, and the bars started to slip. Lateral load dropped to 111 kN during the second cycle, corresponding to 57% of peak load resistance. The column was considered failed because the lateral resistance was lower than 80% of the peak capacity. It was a flexural bond failure caused by the slippage of longitudinal reinforcement. Figure 3.2 illustrates the Force-Drift and Moment-Drift hysteretic relationships. Pinching effect observed in hysteresis loops, at 2% drift, is mostly attributed to the slippage of vertical bars.

Even if the column was considered to have failed, the test was not stopped. Flexural cracks became wider during subsequent cycles, while the cover concrete spalled off. The lateral resistance dropped to 95 kN at 3% drift, corresponding to a strength decay larger than 50% of the peak load. At 4% drift, it was possible to see a 12 mm gap under the bars due to slippage, as shown in Fig. 3.1(e). The test was stopped at a drift ratio of 6% because there was no lateral resistance left, and the column started to tilt towards South. The longitudinal bars were buckled and there was no concrete cover left within the splice region (see Fig. 3.1(g)).

The rotation of the hinging region and anchorage slip rotation are shown in Fig. 3.3. LVDT No. 1 and LVDT No. 3 were used to evaluate total rotation at h/2 from the base, but a technical problem was experienced with LVDT No. 1 during testing. Therefore, the rotation was only calculated using the data obtained from LVDT No. 3, assuming similar behaviour of both LVDTs. Based on that assumption, much of the rotation occurred within the first 254 mm, as the graphs for θ_h and $\theta_{h/2}$ are quite similar in magnitude. Only a small part of the total rotation was developed at the interface of the column and the footing due to anchorage slip (θ_0).

Figures 3.4 and 3.5 illustrate the behaviour of column longitudinal bars and starter bars, respectively. These graphs are shown in two colours to illustrate when the bars started to slip. The blue line shows the behaviour of longitudinal reinforcement up to slippage during the first cycle of 2% drift, whereas the green line indicates that there was no more bond strength between the steel and concrete in the splice region. The green lines are mainly horizontal because once the slippage started, the bars could not elongate anymore. Diagonal green lines towards the compression side of the graphs indicate that the tip of the bars came into contact with concrete in compression. Note that two different scales were used for these graphs; the gridlines are either at 1000 $\mu\varepsilon$ or 4000 $\mu\varepsilon$.

The strain recorded in the first two hoops is shown in Fig. 3.6. The hoops yielded at the first cycle of 2% drift, because the strain exceeded 0.2% or 2000 $\mu\varepsilon$, and the bars started to slip. It agrees very well with Seible (1996) who showed that the "onset of lap splice debonding or relative slippage starts when measured hoops or dilation strain levels are between 1000 to 2000 $\mu\varepsilon$." Figure 3.1 shows that the second hoop was bent by a starter bar, when the column was pulled. It would explain the sudden enhancement in strain of the hoop after 4% drift.

The analysis of data showed that the overall behaviour of column was symmetrical. The drift capacity of column BR-C8 was 1%, before failing due to the slippage of longitudinal reinforcement.

3.2.2 RETROFITTED COLUMN BR-C9

Column BR-C9 was retrofitted with external prestressing hoops, spaced at 150 mm. The photographs shown in Fig. 3.7 illustrate the behaviour of column during testing. The initial cycles at ½% drift resulted in some flexural cracks between the strands placed in the bottom half of the specimen. The lateral load resistance at this stage of deformation reached 147 kN. The load resistance subsequently increased to 199 kN at 1% drift. The existing flexural cracks lengthened and widened, while others formed in the upper half of the column. The yield moment capacity, M_y, was exceeded during cycles at 1% drift because the longitudinal reinforcement had yielded (see Figs. 3.10 and 3.11). The significant elongation of the vertical reinforcement was responsible for the formation of a vertical crack in the splice region. Fig. 3.10 indicates that the starter bar on the West side entered into strain hardening, during the first cycle at 2% drift, because the strain gauges No. 1 and No. 2 exceed ε_{sh} of 1.2% or 12000 $\mu\varepsilon$. At this stage, some vertical cracks formed from the footing to the tip of starter bars. The crushing of concrete occurred near the base. The peak capacity reached 221 kN, corresponding to moment capacity of 481 kN·m. Bond strength started to deteriorate at 2% drift, and caused progressively increasing slippage of reinforcement (see Figs. 3.10 and 3.11). Figure 3.8 shows Force-Drift and Moment-Drift hysteretic relationships. A little pinching could be observed during the last cycle at 2% drift.

The cycles at 3% drift resulted in the widening of flexural and vertical cracks, some reaching to a width of 3 mm. The third prestressing strand, located close to the top of the starting bars started to penetrate into the cover concrete, as the concrete expanded and the strand exerted pressure to overcome this expansion. This is shown in Fig. 3.7(c). The interior hoops were observed to yield, reaching ε_y of 2000 $\mu\varepsilon$, as indicated in Fig. 3.12. The pinching effect was obvious at 3% drift, and was essentially caused by slippage. The column resisted a lateral load of 185 kN during the first cycle, and 144 kN during the second cycle at 3% drift, which corresponded to 84% and 65% of the peak load, respectively. The specimen was considered to have failed after the first cycle at 3% drift. Deformations of the starting bars and the column longitudinal reinforcement are illustrated in two colours in Figs. 3.10 and 3.11, respectively. Blue lines in the figure represent the segment of test from the beginning up to the slippage of the bars at 2% drift. Green lines correspond to the segment of test where there was no more bond strength beyond 3% drift, until the end of testing. Note that two different scales are used for the gridlines of these graphs: 1000 $\mu\varepsilon$ and 5000 $\mu\varepsilon$.

The test continued even if the resistance dropped by more than 20% of the peak load at 3% drift. The column was pushed to 4% drift, resisting 120 kN of lateral force. The lateral resistance dropped to 75 kN or 34% of the peak load at 5% drift. Some bars were visible at this stage, and it was possible to see a gap under some longitudinal bars because of the slippage experienced. This is shown in Fig. 3.7(d). Figure 3.11 indicates that the strain readings recorded by gauge No. 12 on longitudinal reinforcement remained in tension after 6% lateral drift. This could be explained by the buckling of reinforcement in compression, with the strain gauge that happened to be located on the tension side. Figure 3.7(i) shows a photograph of this bar taken after the test.

No significant change was observed during cycles at higher drift levels, except that the lateral resistance further dropped down to almost zero during the first cycle at 9% drift. The test was stopped at that point. Note that some free pieces of concrete were removed at 8% drift. Also, at the same deformation level, a very large crack was visible as illustrated in Fig. 3.7(f). It was possible to insert the first 170 mm of a steel ruler into the concrete. In other words, this crack had a depth over 220 mm from the original concrete surface, considering the cover that had been spalled off.

The rotation at h and h/2 from the footing surface, as well as anchorage slip rotation, are plotted in Fig. 3.9. The major part of the rotation was due to anchorage slip, up to 3% drift. Over this drift level, the rotation was concentrated within the first 254 mm (h/2) from the base of the column. It was obvious that the large crack shown in Fig. 3.7(f) was responsible for the rotation after 3% drift. The rotation between h/2 of 254 mm and h of 508 mm was almost zero since the magnitude of the rotation for θ_h and $\theta_{h/2}$ were very similar.

Unfortunately, no data was recorded for the prestressing strands due to a problem at the beginning of the test. Only three pieces of information could be gathered during testing regarding the strands. The maximum deformation occurred at 3% drift in the first prestressing strand and reached 3200 $\mu\varepsilon$. It corresponded to an increase of 60% of the initial strain. The stress in this first strand dropped to zero at about 6% drift because some free pieces of concrete fell down. For the other strands, it was noted during the test that the deformations were lower than 2700 $\mu\varepsilon$.

The flexure dominant column BR-C9 failed due to the slippage of longitudinal reinforcement. The drift capacity of this specimen was 2%, and failed during the second cycle at 3% drift because the maximum lateral load dropped to 65% of peak resistance.

3.2.3 COMPARISON

Both specimens BR-C8 and BR-C9 failed due to slippage. The as-built column had a drift capacity of 1% and the retrofitted column was able to develop a drift capacity of 2%. The strengthened column BR-C9 was also less damaged than its companion BR-C8, as shown in Fig. 3.13. The position of the anchors did not seem to significantly affect the column behaviour even if they were all on the East side, since the data recorded on the East and West side were similar.

The envelope curves of the Moment-Drift hysteretic relationships shown in Fig. 3.14 illustrate some improvement provided by the retrofitting technique. Ductility and strength were enhanced, as well as the energy dissipation capacity. However, the retrofitting strategy did not modify the column stiffness.

Although the use of prestressing strands improved the behaviour of column and even allowed the starting bars to develop strain hardening at 2% drift, a significant strength decay occurred during 3% drift, due to slippage. It was clear that the clamping force provided by the level of external prestressing applied, was not sufficient to attain further improvement in column deformability. Therefore, it was decided to increase the level of prestressing in the subsequent column test, while also reducing the strand spacing to 100 mm.

3.3 LONG SQUARE COLUMNS

The failure mechanism and performance of two square columns, BR-S5 and BR-S6, are presented in this section. The effectiveness of external prestressing is discussed by comparing two companion columns with and without retrofit.

3.3.1 NON-RETROFITTED COLUMN BR-S5

Column BR-S5 was representative of a flexure dominant square column with a lap splice in the potential hinging region. The damage observed during testing is shown in Fig. 3.15. Initial flexural cracks occurred upon loading to ½% drift, mostly in the bottom half of the column. Further cycling at this deformation level lengthened the cracks. The maximum lateral load resistance at ½% drift was 206 kN, and increased to the peak load of 271 kN (corresponding to peak flexural resistance of 569 kN·m) during the first cycle to 1% drift. The vertical reinforcement exceeded the yielding strain (ε_y) at 1% drift. Upon reaching yielding moment M_y, the horizontal flexural cracks started to become inclined on the side faces due to shear. The length of diagonal cracks ranged from 75 mm to 100 mm. Vertical cracks lengthened and intersected with flexural cracks during the last cycle at 1% drift. The portion of the column above the starting bars seemed to slip laterally by less than 1 mm. The specimen maintained lateral resistance of 268 kN during the first cycle at 2% drift. Concrete started to crush in the splicing region and the column slipped horizontally in the loading direction by about 2 mm. These were accompanied by the widening of vertical cracks up to 3 mm. Debonding of the lap splice also started during the first cycle at 2% drift. At that stage the pinching effect could be observed in force-drift and moment-drift hysteretic relationships (see Fig. 3.16). Pinching was attributed to the slippage of reinforcement longitudinally and the slippage of column as a whole laterally. There was no bond between the reinforcement and concrete during the second cycle at 2% drift. The horizontal green lines in Figs. 3.18 and 3.19 illustrate the slippage of bars whereas the blue lines depict the portion of the test up to the debonding of the lap splice. Diagonal green lines indicate that the reinforcement was once again in compression because the tip of the bar was back to its original position, bearing against concrete. During the second cycle at 2% drift, some concrete spalled off and it was possible to see the second hoop. The maximum lateral load dropped to 138 kN, representing 51% of the peak load resistance so the column was considered failed. The load further decreased to 119 kN during the third cycle. Significant amount of rotation occurred at column footing interface, up to 2% drift, due to anchorage slip. This is shown in Fig. 3.17. Due to a technical problem, LVDT No. 1 and LVDT No. 3 readings were not reliable beyond the 2% drift level. It is conceivable that from 3% drift up to the end of testing, the rotations were mainly taking place within a segment between h/2 (250 mm) and h (500 mm), since a large crack formed in this region at the second hoop level. Figure 3.15(c) illustrates the effect of this crack, showing part of the column inclined above the crack.

The column slipped in the loading direction by approximately 5 mm, and pieces of concrete were removed at 3% drift. The lateral load was 111 kN and continued to diminish to 84 kN during cycles of 4% drift. The square hoops did not yield up to 4%

drift. The strain gauges No. 15 was the only gauge that exceeded 2000 $\mu\varepsilon$ at this deformation level. This is shown in Fig. 3.20. The bar with strain gauges on the West side buckled inelastically during the second cycle at 4% drift. Figure 3.19 indicates that strain gauges No. 5 and No. 6 recorded compressive strains of up to 6% (60000 $\mu\varepsilon$). Figure 3.15(f) shows a photograph taken after the test of the bar that had these strain gauges located on the compressive side, while the bar buckled. The same thing happened on the East side, during the third cycle when strain gauge No. 12 was subjected to tension because it was glued on the tensile side of the buckling bar. This is illustrated in Figs. 3.15(g) and 3.19.

An explosive failure occurred during the second cycle at 5% drift. All the column longitudinal bars buckled as well as the cover concrete over a length of 950 mm (see Fig. 3.15(e)). Core concrete slipped along a large 60° crack shown in Fig. 3.15(i). After the test, the entire column shortened by 10 to 15 mm and the top part of the column was offset by 40 mm relative to the bottom part.

Specimen BR-S5 obviously had a flexural dominant behaviour but failed due to the slippage of lap splice during the second cycle at 2% drift. The drift capacity of this column was 1%.

3.3.2 RETROFITTED COLUMN BR-S6

Column BR-S6 was the only retrofitted square column. The photographs taken during the test, showing the degree of damage at various stages of loading are shown in Fig. 3.21. The experimentally recorded Force-Drift and Moment-Drift hysteretic relationships are illustrated in Figure 3.22. Hairline cracks were formed due to flexure during the initial cycles at ½% drift. The maximum lateral load for this drift level was 203 kN, and increased to 261 kN at 1% drift. The yield moment, M_y, was developed at 1% drift, since the vertical reinforcement exceeded 2000 $\mu\varepsilon$ in tension (see Figs. 3.24 and 3.25). Although the flexural cracks lengthened and widened, no other signs of deterioration was noted up to 2% drift. The peak lateral load was 295 kN and was reached during the first cycle at 2% drift. The starter bars entered into strain hardening at 2% drift, exceeding ε_{sh} of 1.2% or 12000 $\mu\varepsilon$. This is illustrated in Fig. 3.25. The crushing of concrete started at the base during the same deformation level. Some hairline shear cracks formed on side faces of column. The peak flexural resistance reached 661 kN·m during the first cycle of 3% drift, and the lateral load was maintained at 293 kN. Shear cracks became longer while flexural cracks widened up to 1 mm. There was no vertical crack observed. Reinforcement slippage was monitored, and no sign of slippage was observed until 3% drift. During the initial cycle at 4% drift, the first hairline vertical crack of 50 mm long, formed. The second hoop strains approached yield strain ε_y (see Fig. 3.26). A wide crack of 10 mm width and 75 mm depth was observed at column footing interface. This is shown in Fig. 3.21(c). A little damage was observed on the surface of footing, as evidenced by some chipping and minor cracking on the top of footing (see Fig. 3.21(d)). The column withstood 91% of the peak load resistance or 269 kN during the cycles of 4% drift. The load gradually decreased to 239 kN (81% of peak), 212 kN (72% of peak) and 202 kN (68% of peak) during the three cycles of 5% drift. The column was considered to have failed during the second cycle at 5% drift.

Bond strength deteriorated under cyclic loading, starting at about 3% drift, up to the first cycle at 6%, as the slippage of longitudinal reinforcement increased progressively. Two other vertical cracks formed at 6% drift. The bond between steel and concrete was totally lost after the first cycle at 6% drift, as illustrated by the green lines in Figs. 3.24 and 3.25. Note that two different scales are used for the graphs shown in Figs. 3.24 and 3.25. The gridlines are either spaced at 1000 $\mu\varepsilon$ or 5000 $\mu\varepsilon$.

The load resistance continued to drop to 193 kN at 6% drift and 122 kN at 7% drift. At this stage, the column capacity was already lower than 50% of peak resistance. The strains recorded by gauges Nos. 12 to 14, illustrated in Fig. 3.24, showed that at 7% drift the longitudinal bar started to strain harden in compression. A dowel located at the Northeast end of column fractured during the first cycle of the same drift level. This is illustrated in Fig. 3.21(e).

Figure 3.21(f) illustrates the inclination of the column at +8% drift as well as at -8% drift. Figure 3.23 shows the total rotation of the hinging region at the base of column, as well as at h/2 and at h from the base. It can be concluded from these three graphs that the main part of the rotation took place at the bottom of the column because they all had a similar magnitude for a given drift level. If all the rotation was due to anchorage slip at the column-footing interface, the calculated value of θ_0 at 8% drift would have been 80×10^{-3} rad. In fact, the maximum rotation θ_0 recorded was 68×10^{-3} rad at 8% drift, indicating that about 85% of the rotation was due to anchorage slip at the end of testing. Figure 3.21(g) illustrates the rotation of the hinging region at 9%. The test was stopped at 10% drift, because the lateral resistance was very low.

Strain gauges No. 15 and No. 17 were on the East side of the first and the second hoops respectively, whereas strain gauges No. 16 and No. 18 were on the South side. By analysing the graphs illustrated in Fig. 3.26, it can be concluded that the first hoop was mainly subjected to confinement and the second one to shear. Similar behaviour was observed in the as-built column, BR-S5, but it was not as obvious as for this retrofitted column BR-S6.

The graphs for the prestressing strands presented in Fig. 3.27 include a green line, which represents the initial stress applied on the strand to retrofit the column. The first four were pretressed to 50% f_{pu}, corresponding to a deformation of about 4000 $\mu\varepsilon$ and the last five were prestressed to 25% f_{pu} or an elongation of close to 2000 $\mu\varepsilon$. The stress in prestressing strands remained approximately constant during testing most likely because the failure was governed by debonding of lap splices. It seems that bond failure did not require significant expansion as opposed to diagonal shear cracks or compression crushing. Furthermore the prestressing strand spacing was reduced in the lap splice region, resulting in a distribution of strains amoung the prestressing strands. The largest strain deformation was in the first prestressing strand. At 5% drift, the deformation reached 4590 $\mu\varepsilon$ or 14% higher than its initial strain, and it went down to 4150 $\mu\varepsilon$ at 10% drift.

Column BR-S6 had a drift capacity of 4%. This specimen had flexure dominant behaviour but failed due to lap splice slippage during the second cycle at 5% drift.

3.3.3 COMPARISON

Failure of the non-retrofitted column BR-S5 was very different then its companion BR-S6. The failure of BR-S5 was brittle and even explosive. The drift capacity was 1%, whereas the drift capacity of the retrofitted specimen BR-S6 was 4%. The failure of the strengthened column was ductile and much more gradual. A lot of damage occurred on column BR-S5, as shown in Fig. 3.28, but almost nothing happened to BR-S6, except for some cracks and crushing of concrete within the first 75 mm segment near the base.

Figure 3.29 illustrates the envelope curves of the Moment-Drift hysteretic relationships for columns BR-S5 and BR-S6. Once the peak resistance was reached for the as-built column, the degradation was fast and the capacity dropped quickly. For the retrofitted column, the flexural capacity was maintained up to approximately 5% drift. The specimen BR-S6 was more ductile due to the confinement effect, allowing the formation of a plastic hinge at the bottom of the column. The flexural capacity increased by more than 12% when compared with the as-built column. The energy dissipation was also considerable for the strengthened column. The stiffness of both columns was quite similar.

The active confinement that was provided by external prestressing strands benefited the long square column, by improving its seismic behaviour. The retrofitting strategy delayed debonding of lap splice from 1% drift for the as-built column to 4% drift for the retrofitted one. Use of raisers for square columns seemed to behave very well during the entire test. Position of the anchors did not seem to significantly affect the column behaviour, even if they were all on the East side, since results reported by measuring instruments installed on the East side and on the West side were similar.

The improvement in the square column BR-S6 over BR-S5 was greater than the improvement of the circular column BR-C9 over BR-C8. This can be explained by comparing BR-C9 and BR-C8. The bond strength deterioration in BR-C9 started at 2% drift, whereas it started at 4% drift in BR-S5. The retrofitting scheme used for the square column would be more effective than the one used for the circular column. The short circular specimen will be strengthened using the same scheme as for the retrofitted square column; the prestressing strands will be spaced at 100 mm, prestressed to 50% f_{pu} in the splicing region and will be placed at 150 mm elsewhere, with a stress level of 25% f_{pu}.

3.4 SHORT CIRCULAR COLUMNS

This section presents the failure mechanism of the short columns tested, as well as the recorded test data. Column BR-C10 was tested without any retrofit, whereas its companion column BR-C11 was tested after retrofitting by external prestressing.

3.4.1 NON-RETROFITTED COLUMN BR-C10

The progression of damage observed during the test of column BR-C10 is illustrated in Fig. 3.30. The hysteretic behaviour is shown in Fig. 3.31 in terms of Force-Drift and Moment-Drift relationships. A maximum lateral load of 357 kN was reached during the initial cycles of ½% drift. Flexural cracks formed near the first three hoops and extended further under cyclic loading. Dowels started to yield as shown in Fig. 3.33. The first shear crack formed during the second cycle at ½% drift. Horizontal flexural cracks became wider during the third cycle, reaching a width of 1 mm.

The lateral resistance at 1% drift was recorded to be 450 kN. The longitudinal reinforcement yielded during the first cycle, as indicated in Fig. 3.34, developing the yielding moment M_y. At that stage, there was no slippage of the bars at the bottom of the column, even if some vertical cracks appeared during the first cycle. These cracks were likely the result of yielding of the vertical bars. The effect of shear became more obvious as some diagonal cracks formed on the side of the column during the initial cycle at 1% drift. Diagonal shear cracks lengthened during the second cycle and horizontal flexural cracks widened up to 2 mm. During the third cycle, shear cracks started to widen and other vertical cracks formed in the splicing region.

Many vertical cracks formed at the bottom of the column during the first cycle at 2% drift. Also, steep diagonal cracks appeared on the side of the column up to an angle of approximately 70° and were intersecting the horizontal cracks. Cover concrete started to spall off. Widths of the horizontal and vertical cracks were 3 mm and 2 mm, respectively. The column experienced shear yielding at 2% drift because the strain gauges on hoops recorded deformations exceeding the yielding strain, ε_y, during the first cycle (see Fig. 3.35). Bond strength was observed to deteriorate during the first cycle at 2% drift and slippage of the longitudinal bars was clear during the second cycle. Graphs of the vertical bar strains, illustrated in Figs. 3.33 and 3.34 are blue until debonding, and they are denoted in green beyond bar slippage. Note that the green lines are mainly horizontal due to lap splice slippage unless the bar was in compression, in which case the green lines became diagonal.

Pinching of hysteresis loops was observed, starting with 2% drift until the end of testing. This is attributed to the combination of shear and slippage of reinforcement. Peak resistances of 470 kN and 746 kN·m were developed during the first cycle of 2% drift. The resistance dropped to 271 kN (58% of the peak load capacity) during the second cycle and further decreased to 221 kN during the third cycle. The latter was lower than 50% of the peak lateral resistance. The specimen BR-C10 was considered to have failed during the second cycle at 2% drift.

Until the onset of debonding of reinforcement at the first cycle of 2% drift, the curvature was quite uniform from the base to a distance h from the footing (see Fig. 3.32). After the second cycle at the same drift level, about one third of the total rotation was produced by anchorage slip that accumulated at the column-footing interface. The remaining rotation was essentially taking place within the first 305 mm (h/2) segment from the base.

Three complete cycles were applied on the column at 3% drift. The cracks continued to widen and some pieces of concrete fell down. South side of the column was subjected to crushing over a height of about 500 mm, as shown in Fig. 3.30(e). It was the first sign of a sudden failure that occurred on the way to 4% drift. Figure 3.30(f) illustrates the damaged column. The second hoop opened up, and its diameter increased by 9%, from 500 mm to 545 mm; bars buckled; and chunk of concrete fell down. The column was about 10 mm shorter. It was also possible to see a large crack at the same level of the second hoop, as shown in Fig. 3.30(i).

The Force-Drift and Moment-Drift hysteretic relationships shown in Fig. 3.31 are not symmetrical about the origin. The peak lateral resistance of the column was larger when it was pushed, by approximately 18%. Also the peak load occurred at 1% drift when the column was pulled but at 2% drift when it was pushed. The only reasonable explanation is that the column was first pushed, creating first damage in this direction, and its capacity was already reduced when it was pulled. The same phenomenon would have occurred up to the last cycle at 2% drift. From that point, the hysteretic relationships became symmetrical about the origin.

According to the test data and the observed behaviour, this short column had flexure dominant behaviour and failed due to the slippage of reinforcing steel during the second cycle at 2% drift. The drift capacity of the specimen BR-C10 was 1%.

3.4.2 RETROFITTED COLUMN BR-C11

The observed behaviour of BR-C11 is illustrated in Fig. 3.36 with photographs taken at various stages during testing. Hairline flexural cracks appeared during the first cycle at ½% drift. Strain gauges on starter bars were damaged early during testing, and therefore the results shown in Fig. 3.39 are limited. Though strain gauge No. 8 did not rupture during testing, it fluctuated when it was in tension. At least, the overall result recorded by gauge No. 8 seems to be reliable and it gives an idea of the deformation range. According to strain gauge Nos. 2, 8 and 9, shown in Fig. 3.39, the starter bars yielded at ½% drift.

Figure 3.37 illustrates the Force-Drift and Moment-Drift hysteretic relationships. The maximum lateral load reported at ½% drift was 353 kN and it increased to 448 kN at 1% drift. A hairline 45° crack formed at 1% drift and the flexural cracks became slightly longer. The fourth prestressing strand from the base of the column started to embed into the cover concrete. Although it is not obvious in Fig. 3.40, strain gauges 7 and 14 recorded yielding of longitudinal bars starting at 1% drift, exceeding the yielding moment M_y. Some new diagonal shear cracks and flexural cracks formed under cyclic loading at 2% drift. The lateral capacity continued to increase up to 498 kN at 2% drift and reached lateral peak resistance of 507 kN at 3% drift. The peak flexural capacity was 825 kN·m. Some new cracks formed during cycles at 3% drift. The embedment of the fourth prestressing strand caused spalling of the cover concrete as illustrated in Fig. 3.36(b).

Data recorded by strain gauges placed on the hoops showed that the first hoop yielded at 4% drift (see Fig. 3.41). Width of all the cracks was still smaller than 2 mm at this drift level. Concrete of the footing crushed since cracks formed into the footing, as illustrated in Fig. 3.36(c). The opening at column-footing interface reached 12 mm. A steel ruler could be inserted under the column up to a depth of 150 mm, showing that a significant rotation took place at the base of the column. The maximum lateral load decreased to 465 kN, 439 kN and 409 kN during the first, second and third cycles at 4% drift respectively.

The column was considered to have failed at 5% drift because the lateral resistance of 397 kN was smaller than 80% of the peak load. Figure 3.36(e) shows that the opening at the bottom of the column, measured by a steel ruler, was at least 255 mm deep. The rotation at the bottom of the column is illustrated in Fig. 3.38. According to this figure, most part of the column rotation was due to the anchorage slip at column-footing interface. The hysteretic relationship plot for the anchorage slip rotation θ_0 is not as smooth as for the flexural rotation $\theta_{h/2}$ and θ_h. This was attributed to the setup of instrumentation, rather than the actual column behaviour. As presented in the previous chapter, the rotation θ_0 was recorded by two Temposonic LVDT (Nos. 2 and 3), whereas the rotation $\theta_{h/2}$ and θ_h was measured by two LVDT. A technical problem also occurred with Temposonic LVDT No. 3, so the hysteretic relationship for the anchorage slip rotation θ_0 was only evaluated with Temposonic LVDT No. 2, assuming a similar behaviour in both Temposonics. This assumption seemed to be realistic because a few values were recorded by Temposonic LVDT No. 3 and they were close to the one measured by Temposonic LVDT No. 2.

Debonding of the vertical bars started around 3% drift and continued up to 5% drift. There was virtually no bond left between the steel and concrete at 6% drift. This is illustrated by the green lines in Fig. 3.39 and 3.40. Note that two different scales of 2000 $\mu\varepsilon$ and 5000 $\mu\varepsilon$ were used in these graphs.

At 6% drift, the lateral load resistance dropped to 62% of its peak. The second hoop started to yield. A new vertical crack formed at 6% drift as shown in Fig. 3.36(f). This crack appeared during the first cycle on the compression side. The lateral load dropped below 40% of the peak load during cycles at 7% drift. Figure 3.36(g) shows that the opening under the column was wider. Slippage of the longitudinal bar is also visible on this photograph. There was no concrete cover left up to the first prestressing strand level at 75 mm from the base. The test was stopped after the third cycle at 10% drift because the resistance of the column was very low. The photograph shown in Fig. 3.36(i) was taken after the test. One of the starter bars had buckled and pieces of concrete were removed from the footing. Depth of the hole in the footing was about 40 mm corresponding to the clear cover thickness on the top of footing. Figure 3.36(j) illustrates the sinking of the fourth prestressing strand into the cover concrete near the end of testing as concrete expanded laterally.

The graphs for the prestressing strands are plotted in Fig. 3.42 and included a green line to represent the initial stress applied on the strand. The first four were pretressed to 50% f_{pu} corresponding to a deformation of about 4000 $\mu\varepsilon$. The last five were prestressed to 25% f_{pu} or an elongation close to 2000 $\mu\varepsilon$. The strain in the prestressing strands was not as steady as for the square retrofitted column. The deformation of many strands increased by almost 30% and their maximum stress was reached between 4% and 6% drift. The first prestressing strand exceeded 5000 $\mu\varepsilon$ at 3% drift. Prestressing strand No. 5 was the first wire from the bottom of the column to be prestressed to 25% f_{pu} (2000 $\mu\varepsilon$) and reached a maximum strain of 3500 $\mu\varepsilon$ at 10% drift.

Column BR-C11 reached the flexural yielding capacity at 1% drift and failed at 5% drift due to the debonding of lap splice. The drift capacity of the specimen was 4%.

3.4.3 COMPARISON

Figure 3.43 shows a photograph for specimens BR-C10 and BR-C11, taken after the test. The as-built column sustained extensive visible damage. Main damage on the retrofitted column was limited to the first 75 mm at the bottom of the column.

Failure of specimen BR-C10 was brittle and sudden. Its drift capacity was 1%, whereas its companion column BR-C11 sustained the capacity up to 4% drift and demonstrated ductile behaviour with gradual failure. The comparison of strength degradation is illustrated in Fig. 3.44, which shows the Moment-Drift envelope for both columns. Retrofitting the short column increased the flexural strength by 10% and considerably enhanced the energy dissipation. Strengthening the column with prestressing strands did not modify the stiffness, but significantly increased the column ductility. Although all the anchors were located on the same side of the column, it did not affect the results because the Moment-Drift envelope was similar, irrespective of whether the column was pushed or pulled.

Cover concrete of BR-C11 footing crushed near the column. This did not affect the results, however, since the footing was over-designed. It is advisable to make sure that the footing is always stronger than the column so that the footing remains intact when a plastic hinge forms in the column.

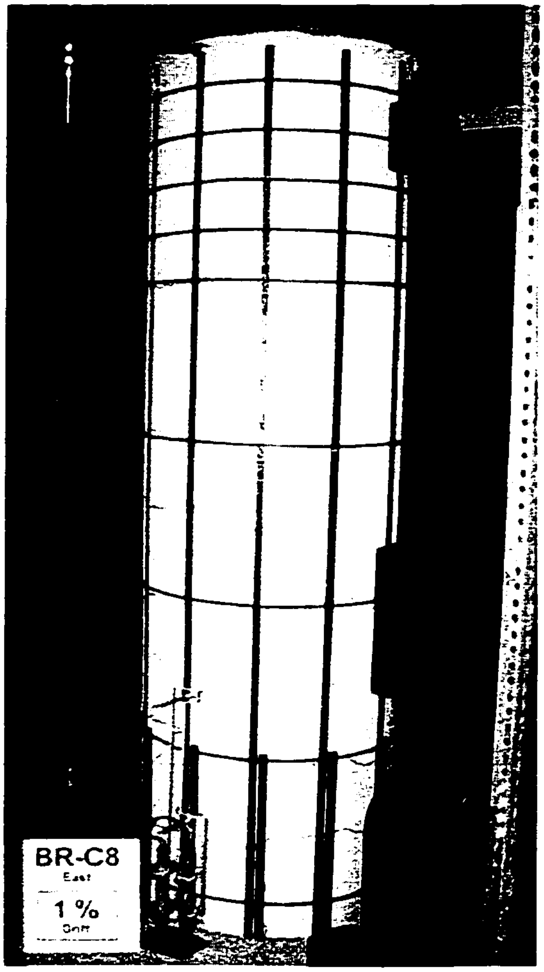

a) 1% drift

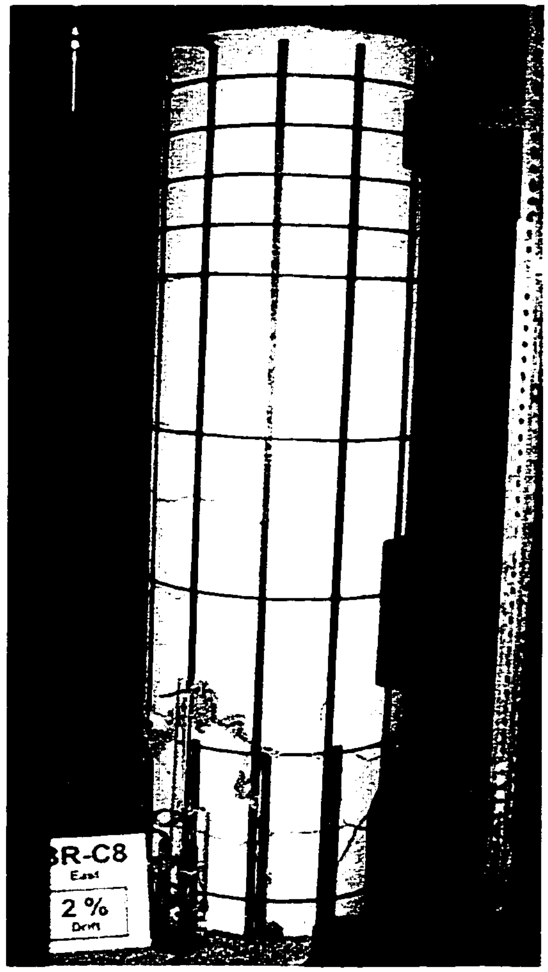

b) 2% drift

c) 3% drift

d) 4% drift

Figure 3.1 Behaviour of column BR-C8

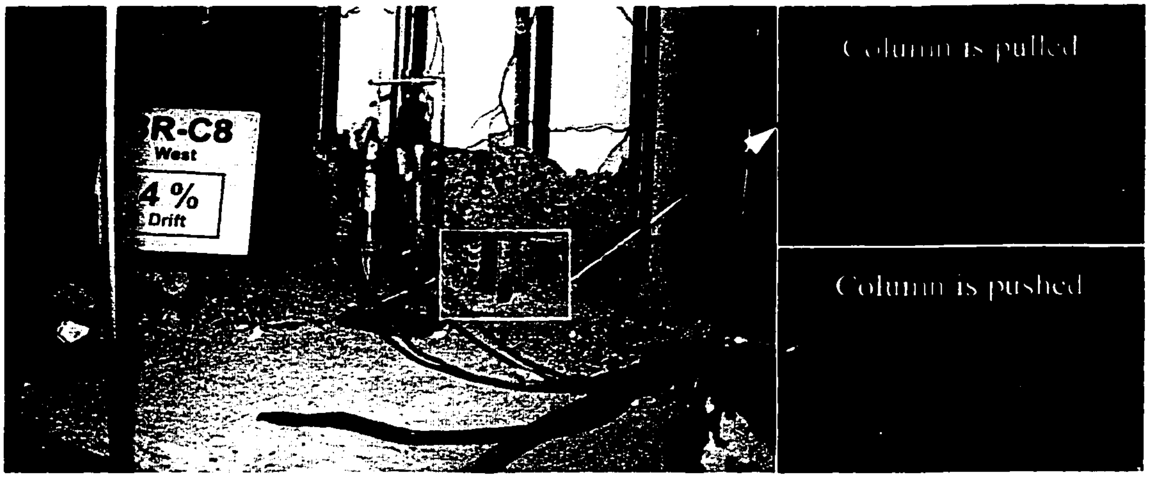

e) 4% drift, slippage of longitudinal reinforcement

f) 5% drift

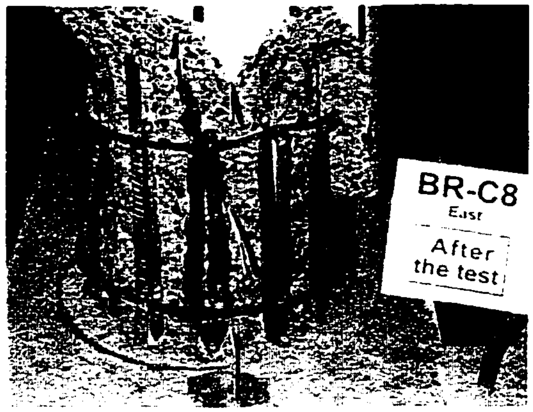

g) After the test

h) 6% drift (Hoop bended by a dowel in compression)

Figure 3.1 Behaviour of column BR-C8 (Continued)

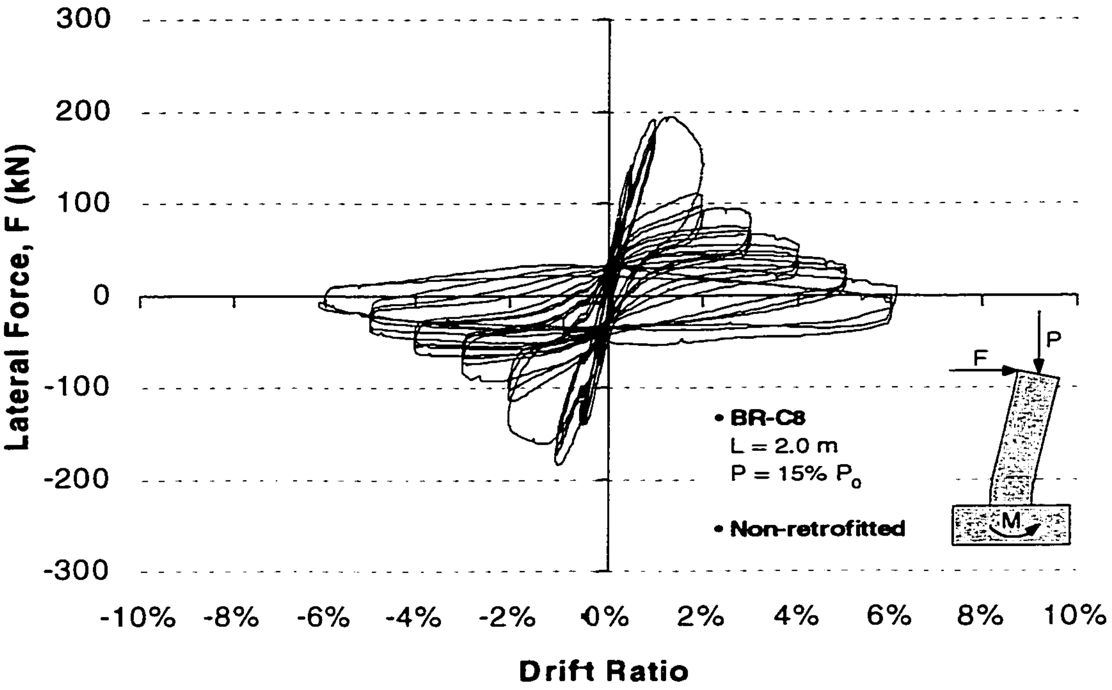

a) Force-Drift relationship

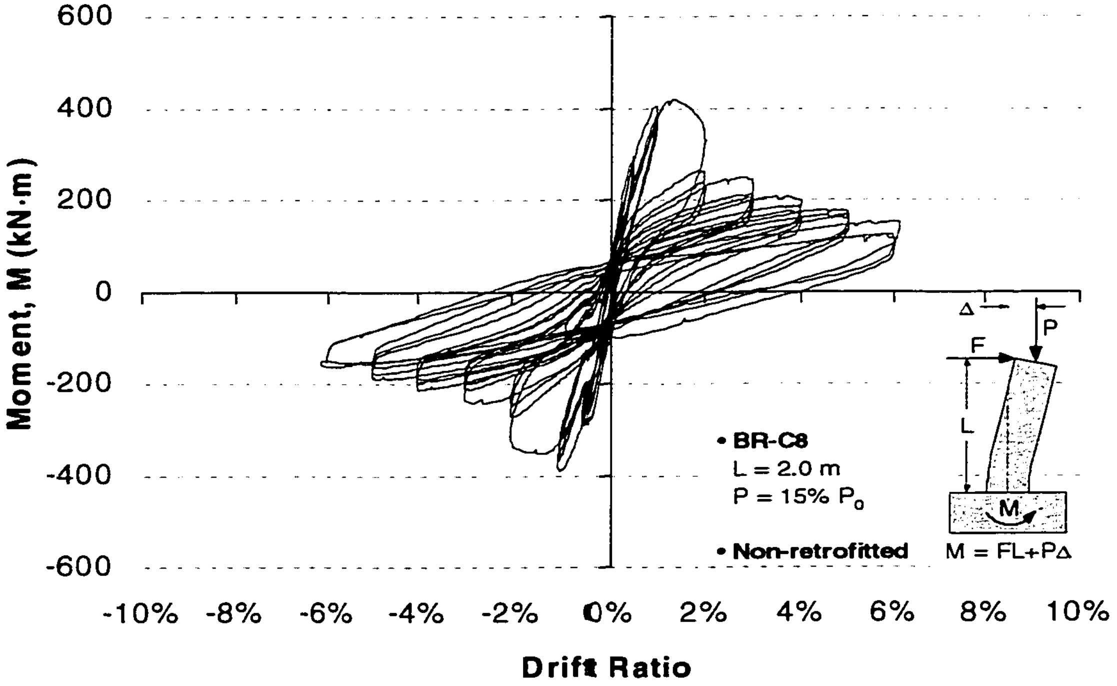

b) Moment-Drift relationship

Figure 3.2 Hysteretic relationships for column BR-C8

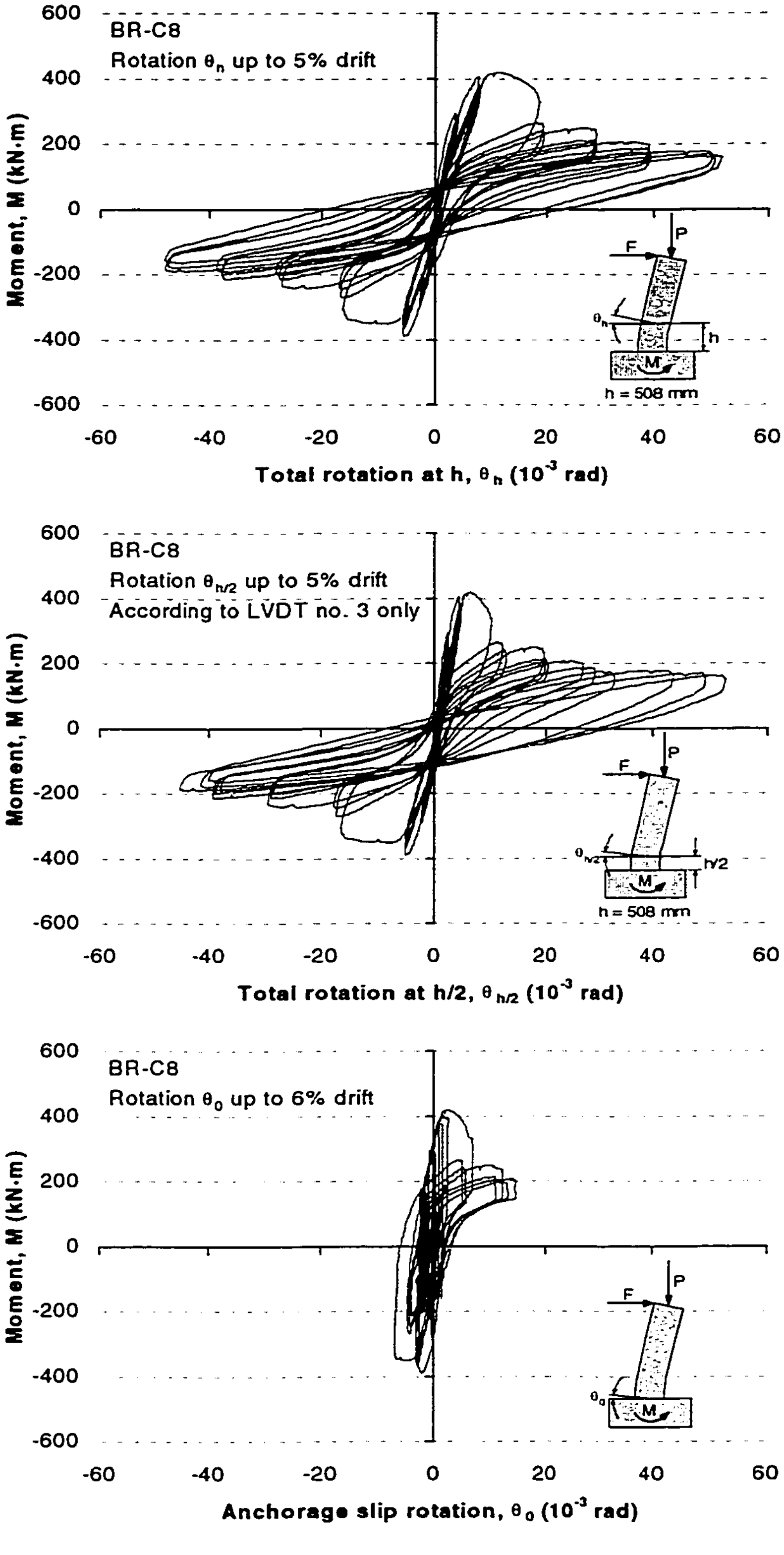

Figure 3.3 Rotation of the hinging region for column BR-C8

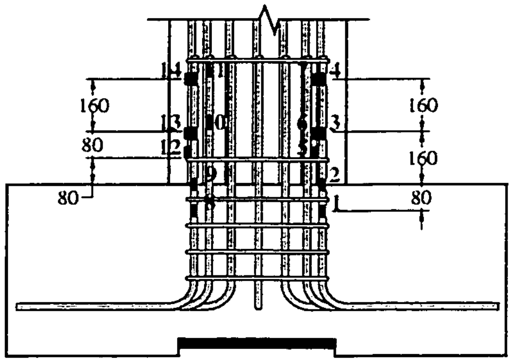

a) Strain gauge location on vertical bars

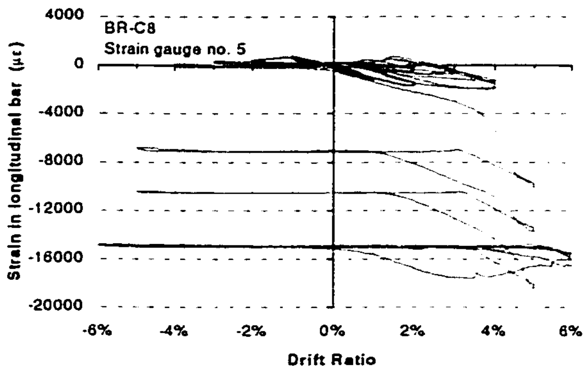

b) Strain gauge no. 5

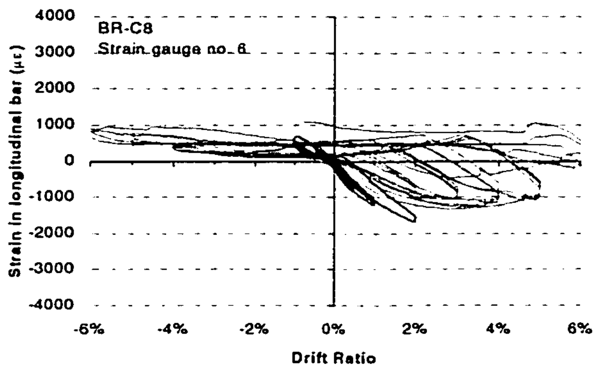

c) Strain gauge no. 6

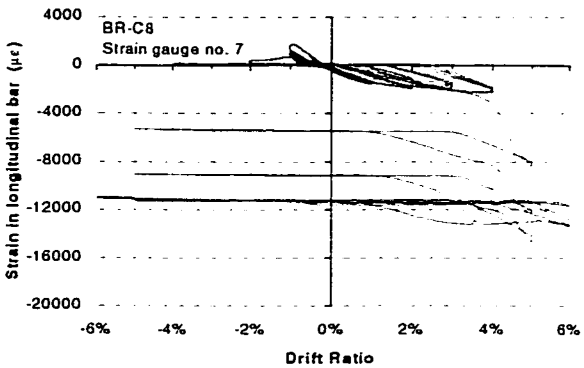

d) Strain gauge no. 7

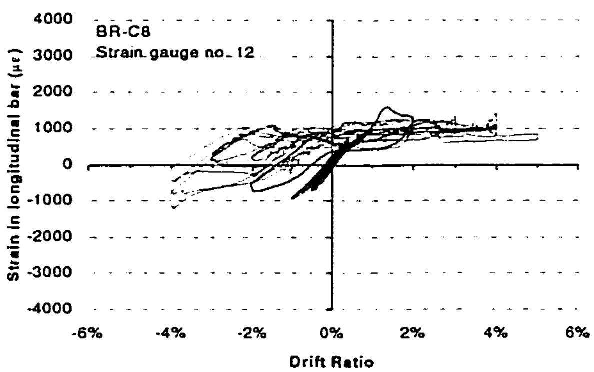

e) Strain gauge no. 12

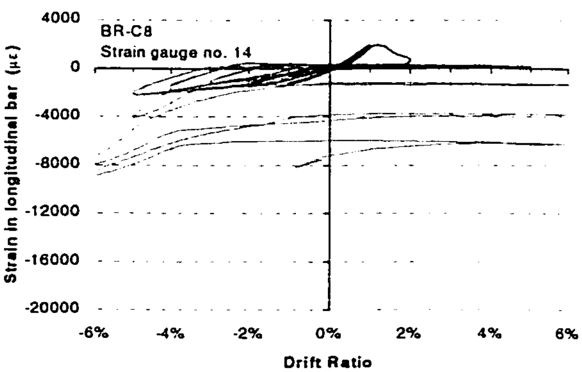

f) Strain gauge no. 14

Figure 3.4 Longitudinal reinforcement steel strains for column BR-C8

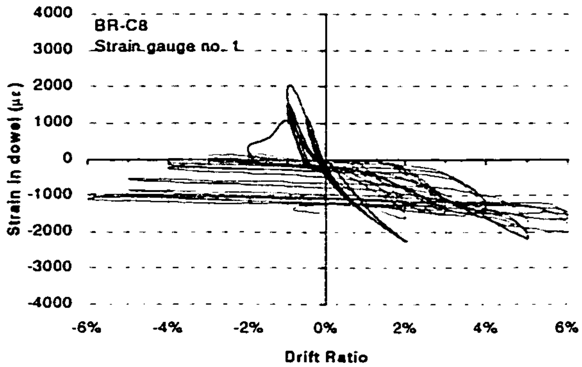

a) Strain gauge no. 1

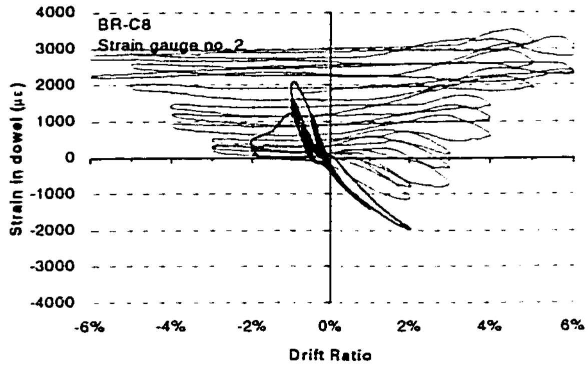

b) Strain gauge no. 2

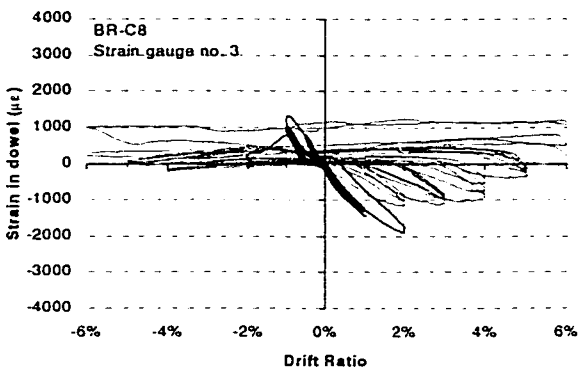

c) Strain gauge no. 3

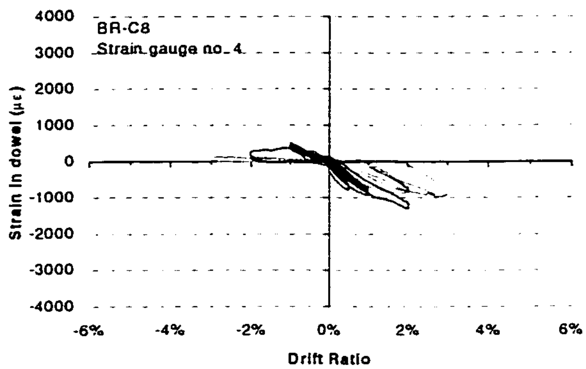

d) Strain gauge no. 4

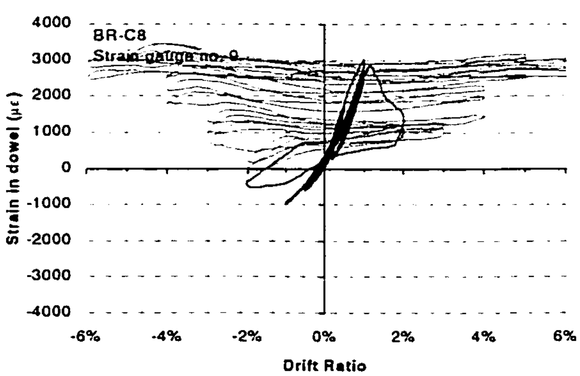

e) Strain gauge no. 9

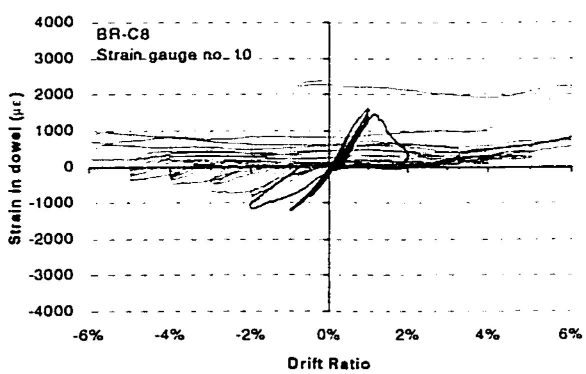

f) Strain gauge no. 10

Figure 3.5 Dowel strains for column BR-C8

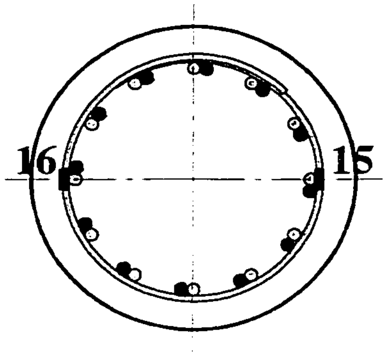

a) Strain gauge location on the 1st hoop

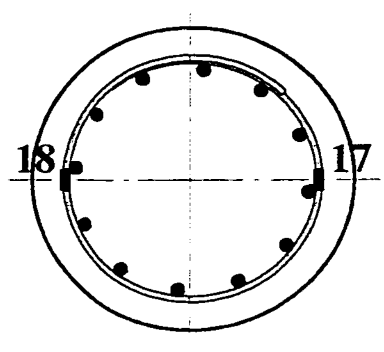

b) Strain gauge location on the 2nd hoop

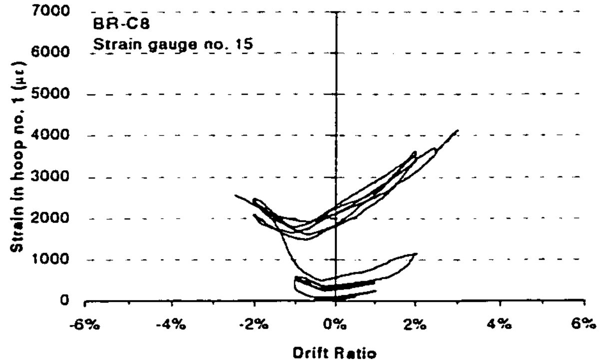

c) Strain gauge no. 15

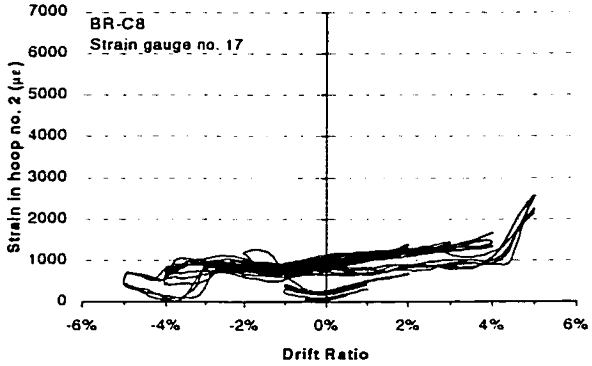

d) Strain gauge no. 17

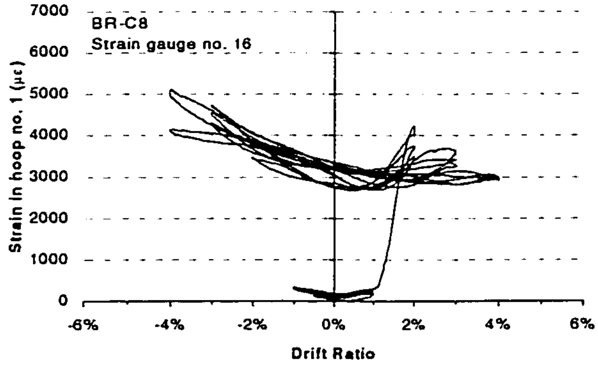

e) Strain gauge no. 16

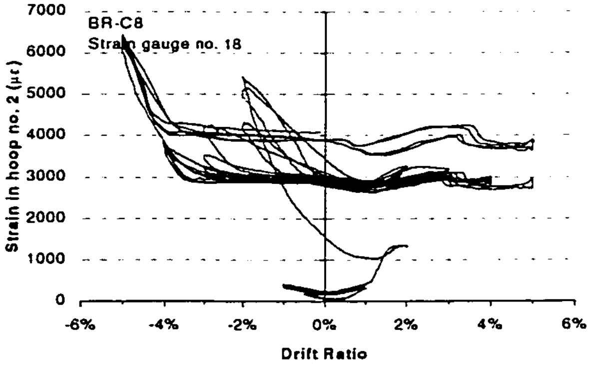

f) Strain gauge no. 18

Figure 3.6 Transverse reinforcement steel strains for column BR-C8

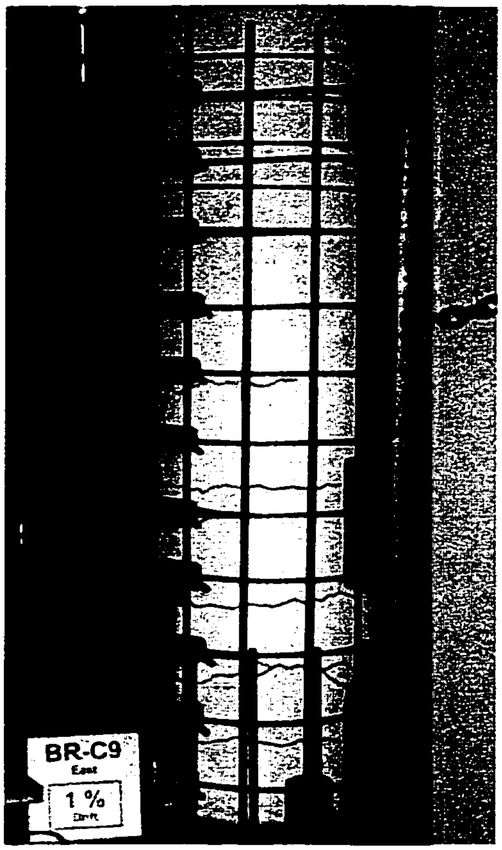

a) 1% drift

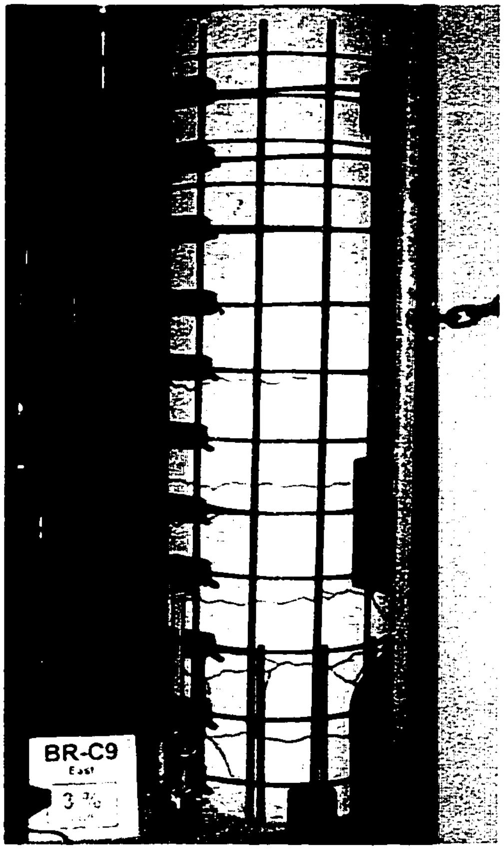

b) 3% drift

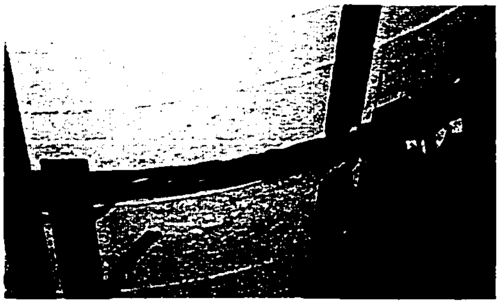

c) 3% drift, strand into concrete

d) 5% drift, gap due to slippage

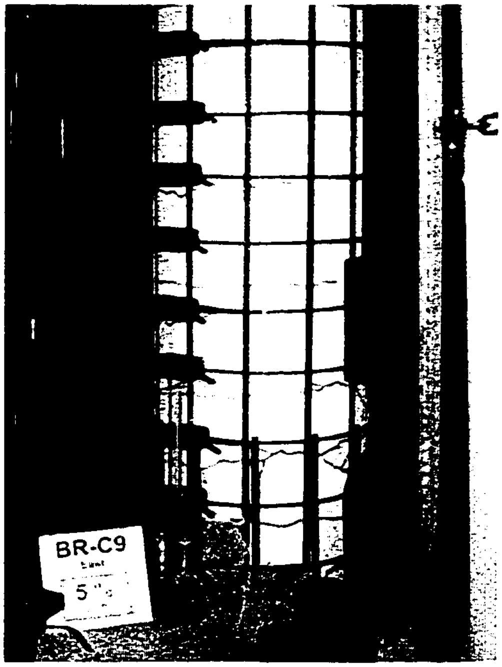

e) 5% drift

Figure 3.7 Behaviour of column BR-C9

f) 8% drift, opening of 170 mm deep

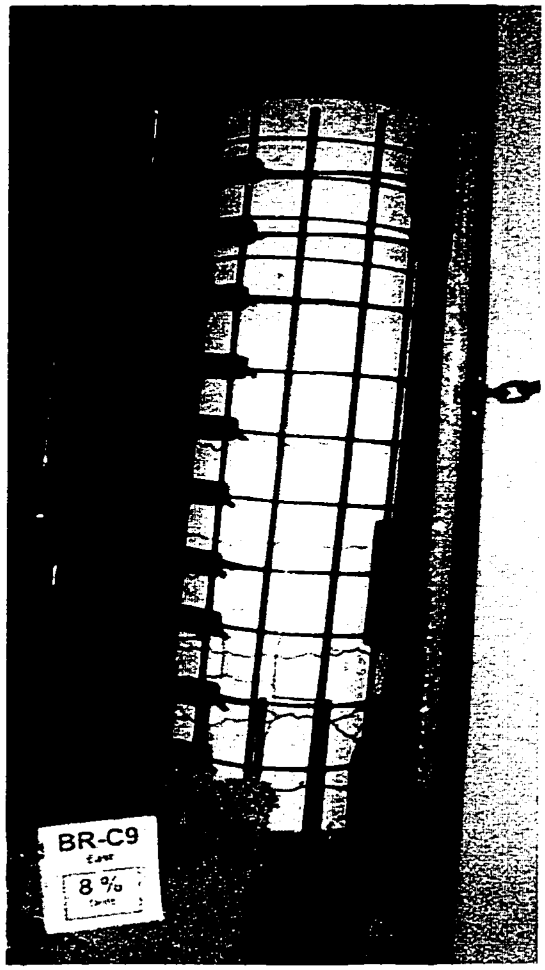

g) 8% drift

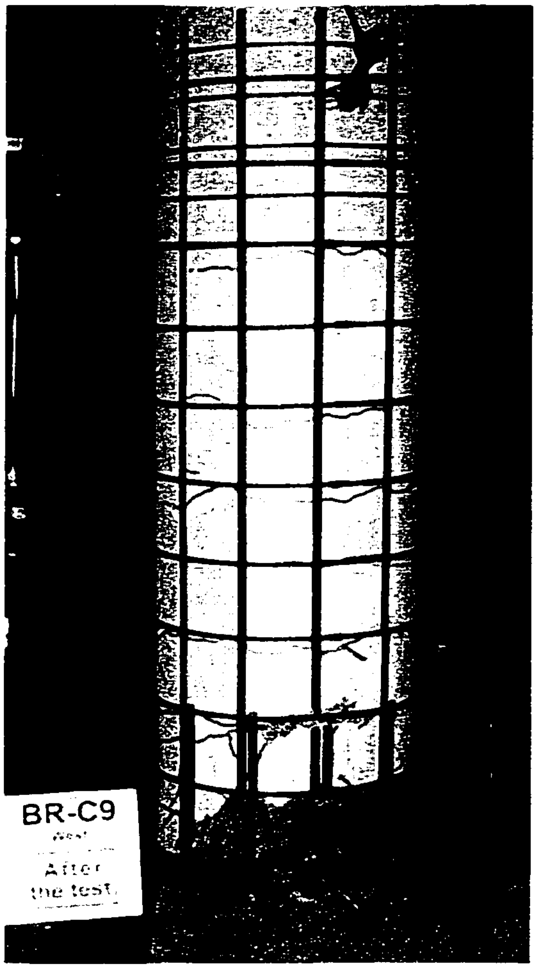

h) After the test (West side)

i) After the test

Figure 3.7 Behaviour of column BR-C9 (Continued)

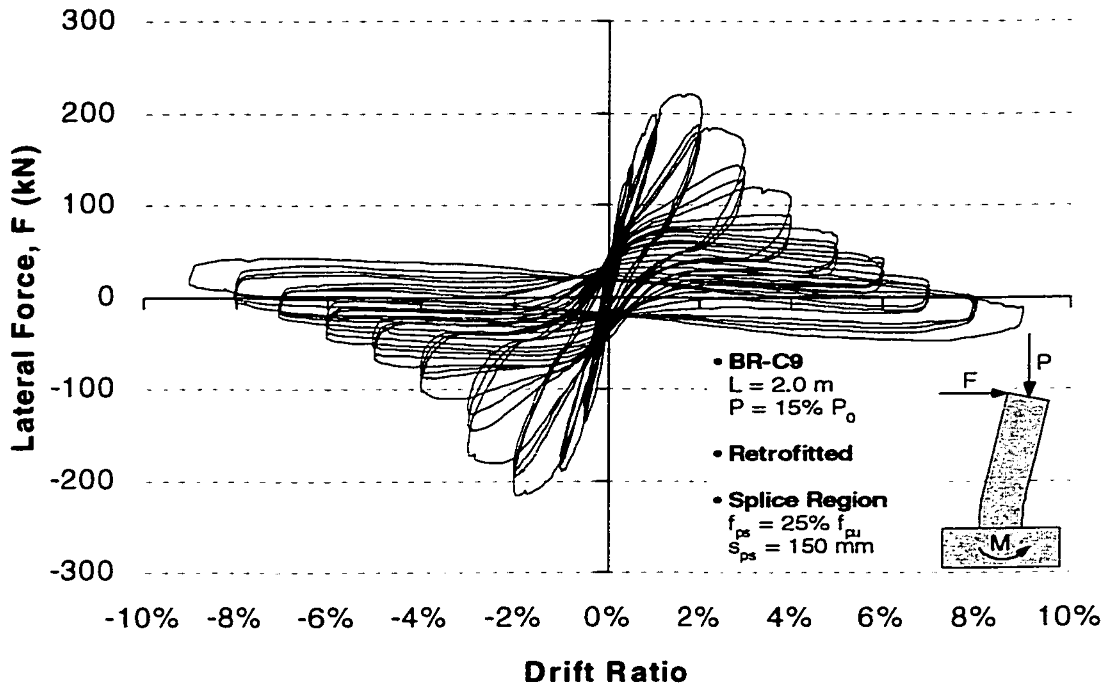

a) Force-Drift relationship

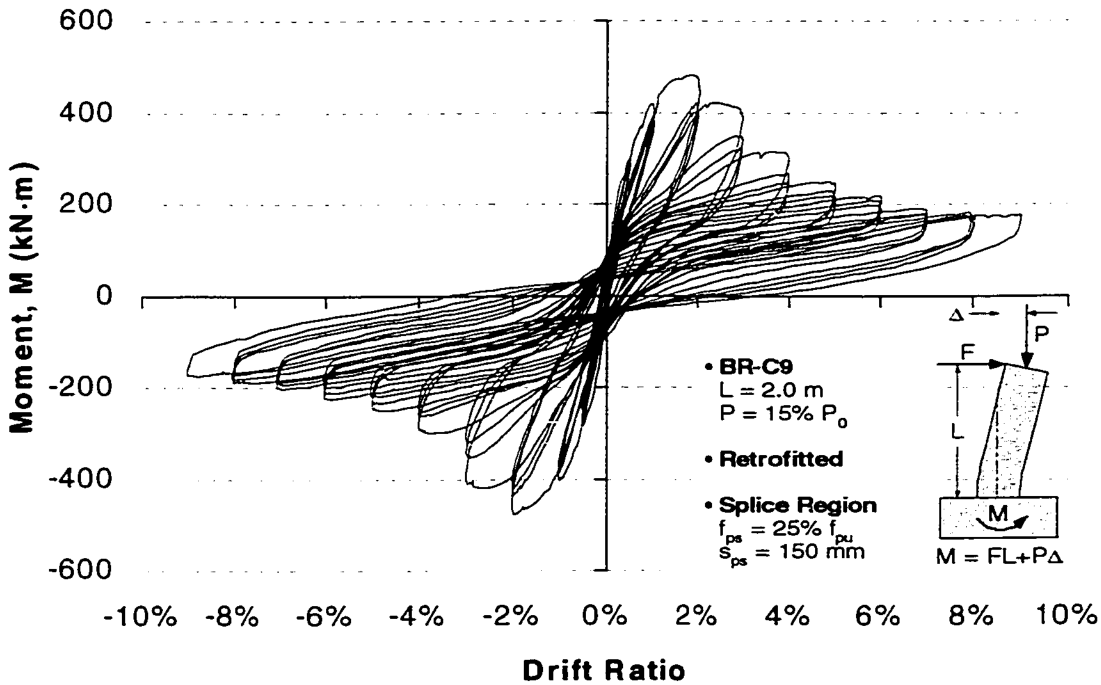

b) Moment-Drift relationship

Figure 3.8 Hysteretic relationships for column BR-C9

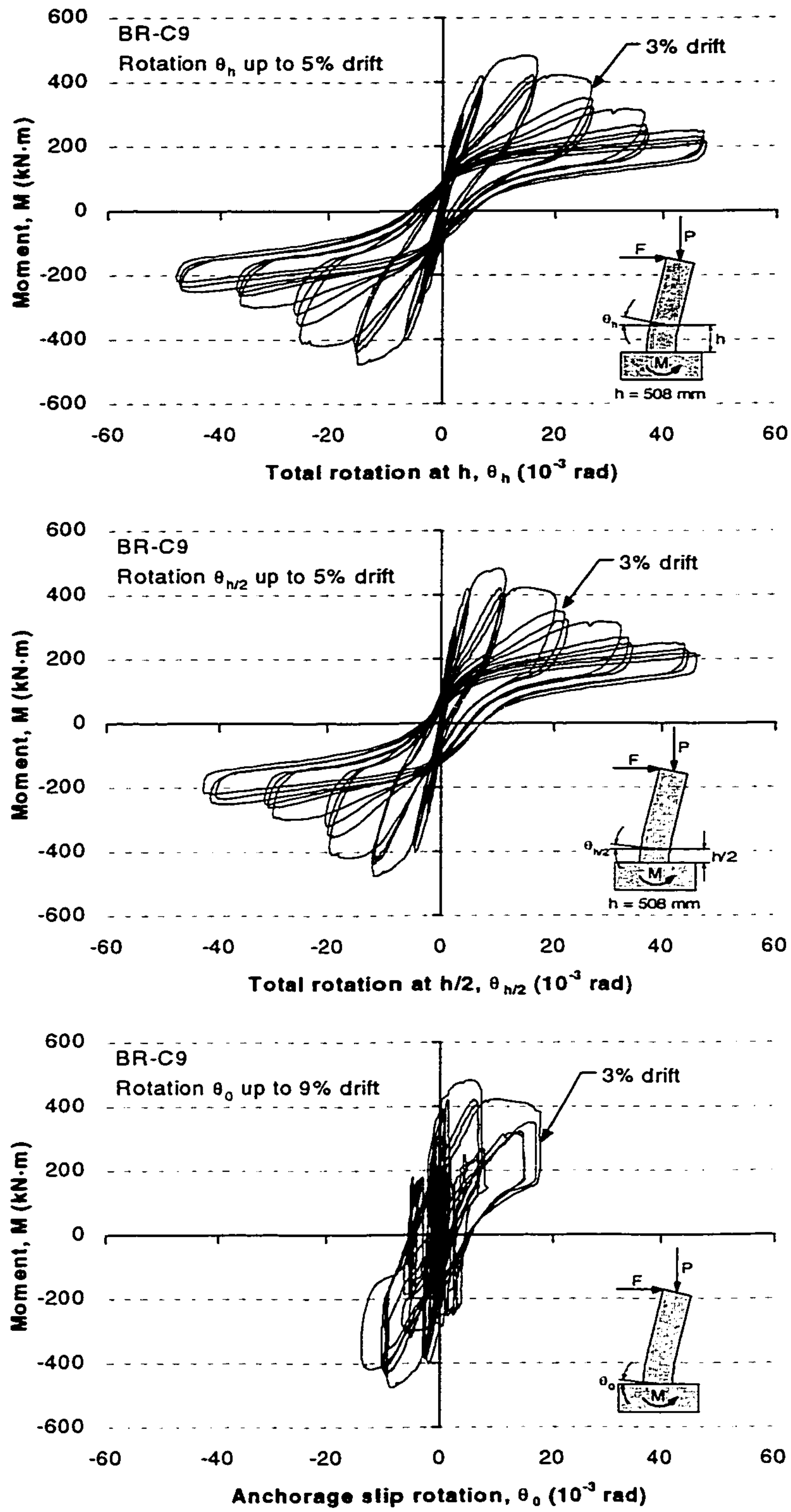

Figure 3.9 Rotation of the hinging region for column BR-C9

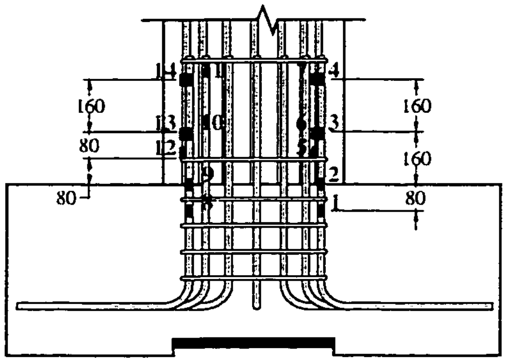

a) Strain gauge location on vertical bars

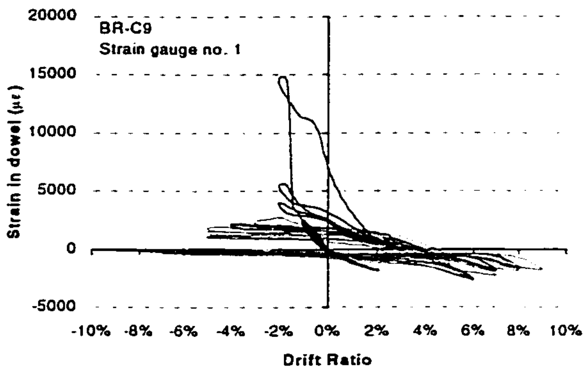

b) Strain gauge no. 1

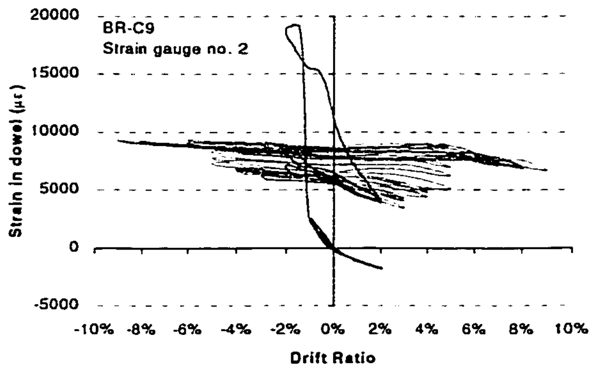

c) Strain gauge no. 2

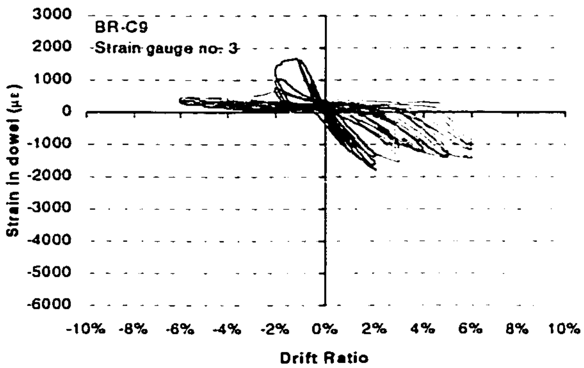

d) Strain gauge no. 3

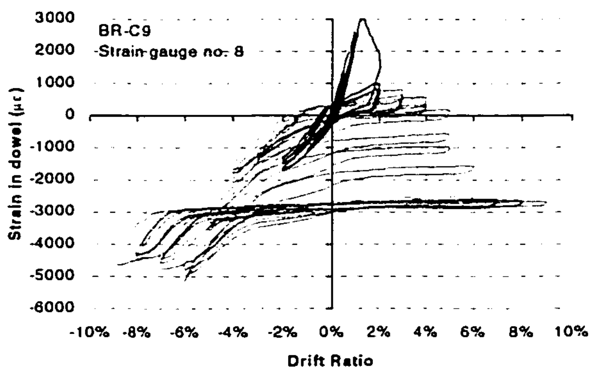

e) Strain gauge no. 8

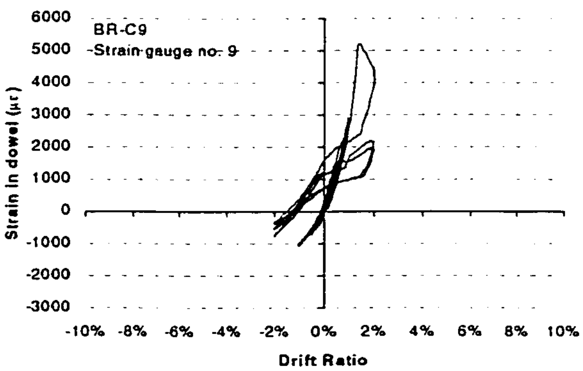

f) Strain gauge no. 9

Figure 3.10 Dowel strains for column BR-C9

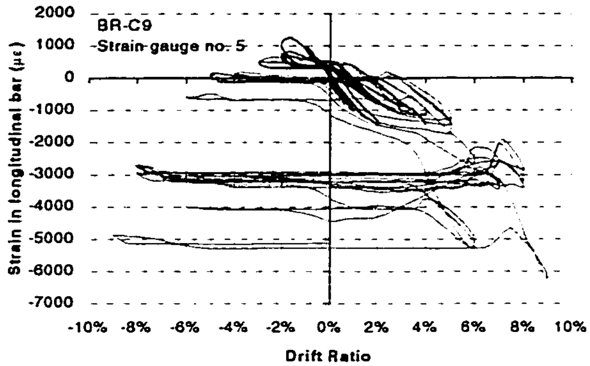

a) Strain gauge no. 5

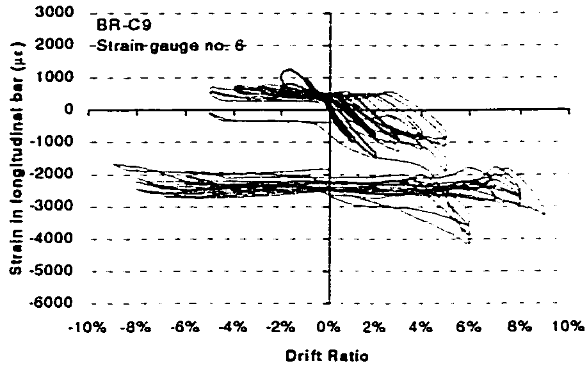

b) Strain gauge no. 6

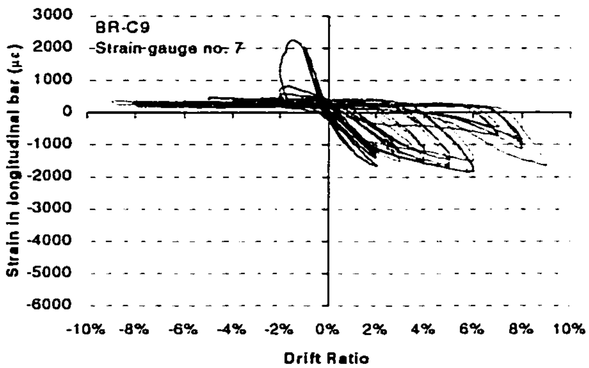

c) Strain gauge no. 7

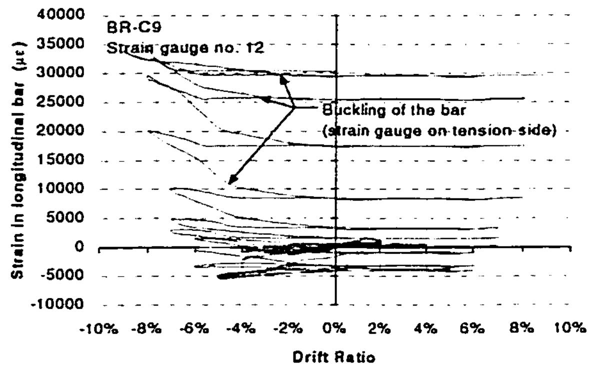

d) Strain gauge no. 12

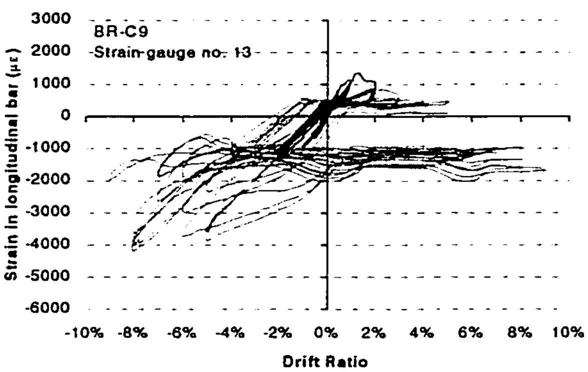

e) Strain gauge no. 13

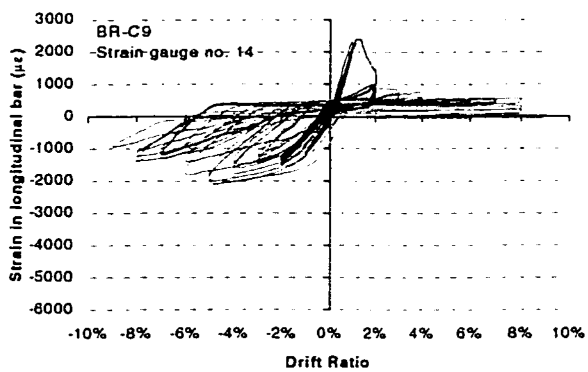

f) Strain gauge no. 14

Figure 3.11 Longitudinal reinforcement steel strains for column BR-C9

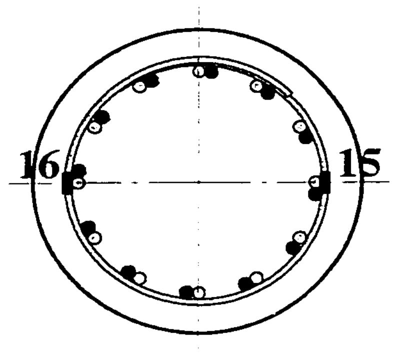

a) Strain gauge location on the 1st hoop

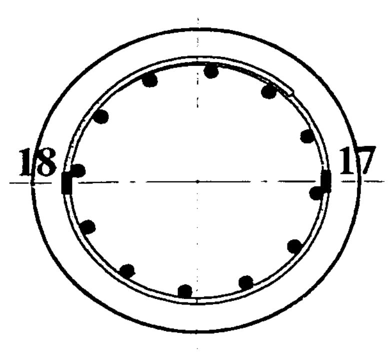

b) Strain gauge location on the 2nd hoop

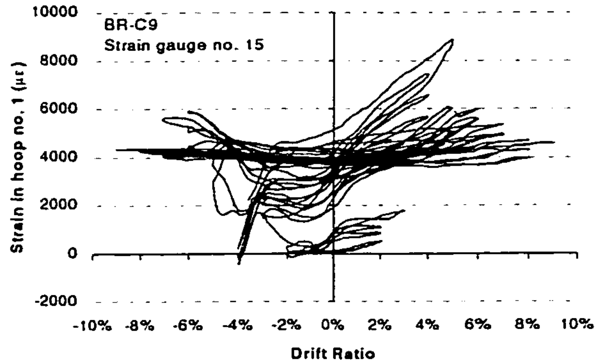

c) Strain gauge no. 15

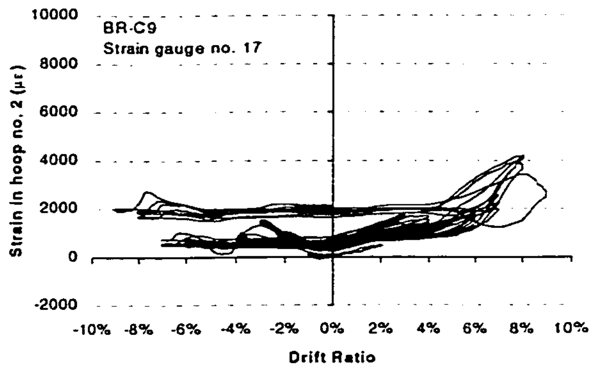

d) Strain gauge no. 17

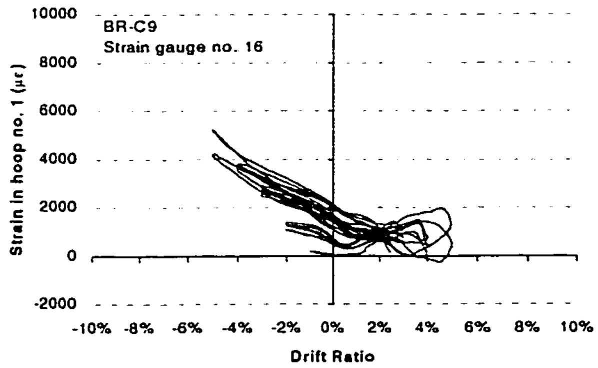

e) Strain gauge no. 16

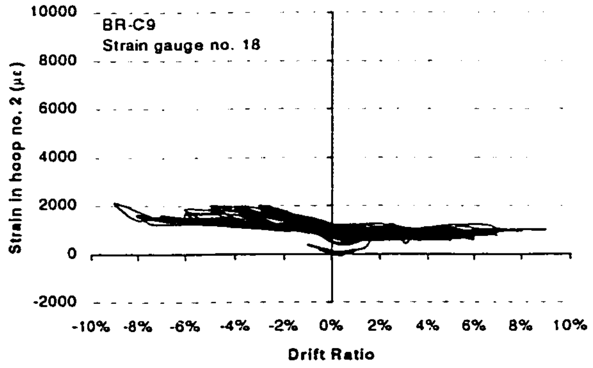

f) Strain gauge no. 18

Figure 3.12 Transverse reinforcement steel strains for column BR-C9

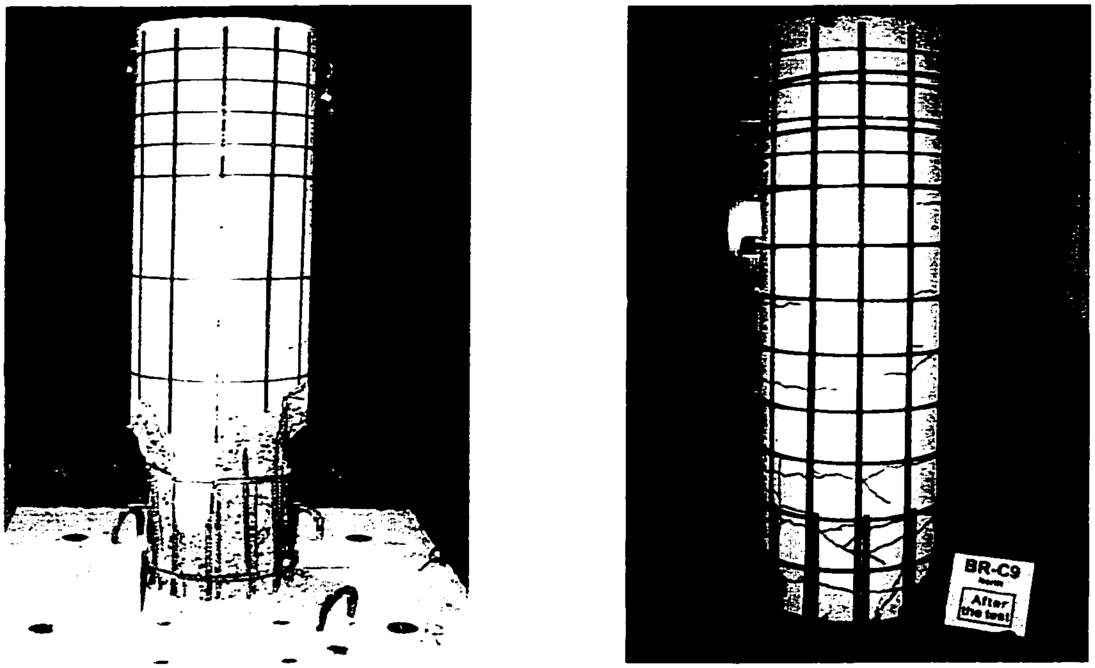

a) Column BR-C8 (North)　　**b)** Column BR-C9 (North)

Figure 3.13 Comparison of columns BR-C8 and BR-C9 (After the test)

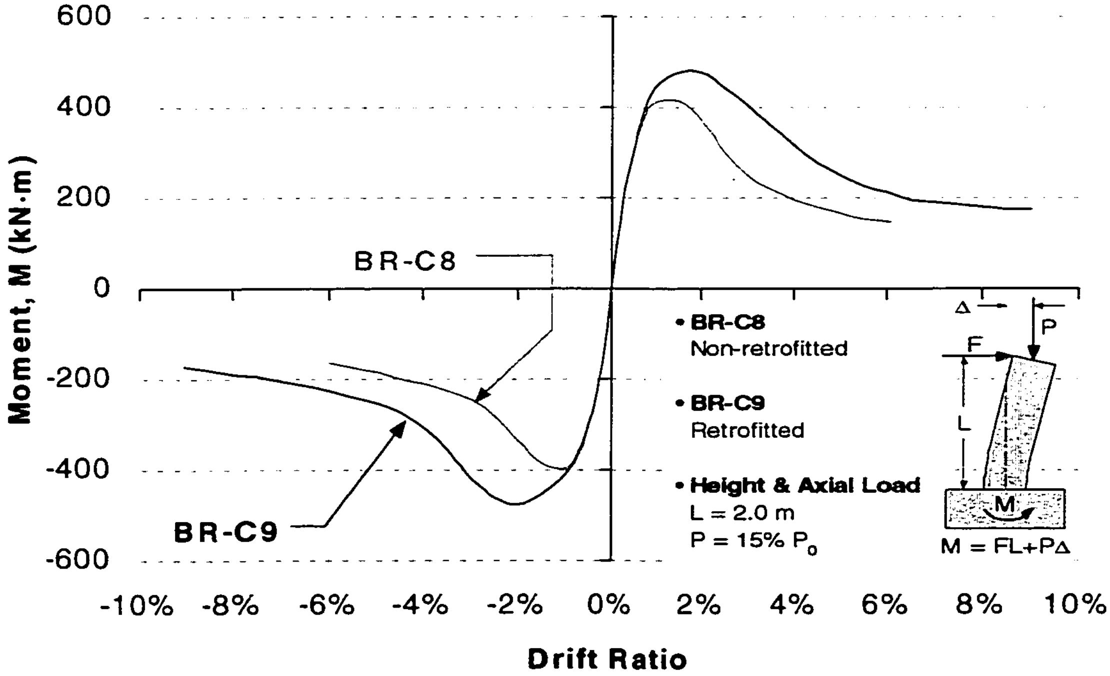

Figure 3.14 Moment-Drift envelope of columns BR-C8 and BR-C9

a) 1% drift

b) 2% drift

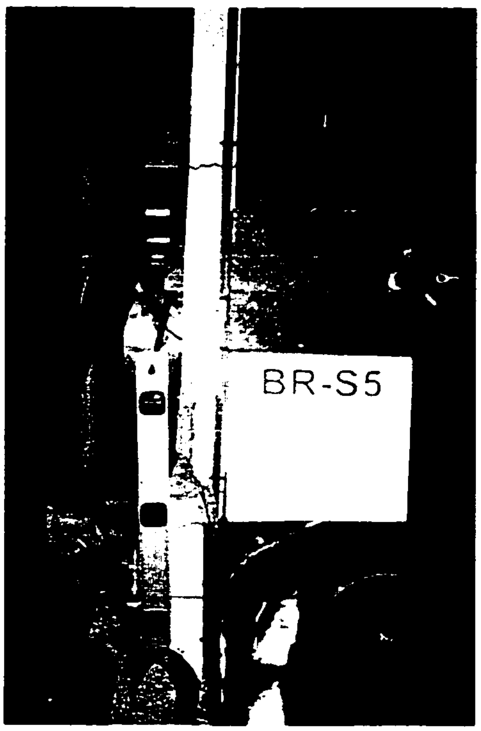

c) 3% drift, 2nd cycle (North)

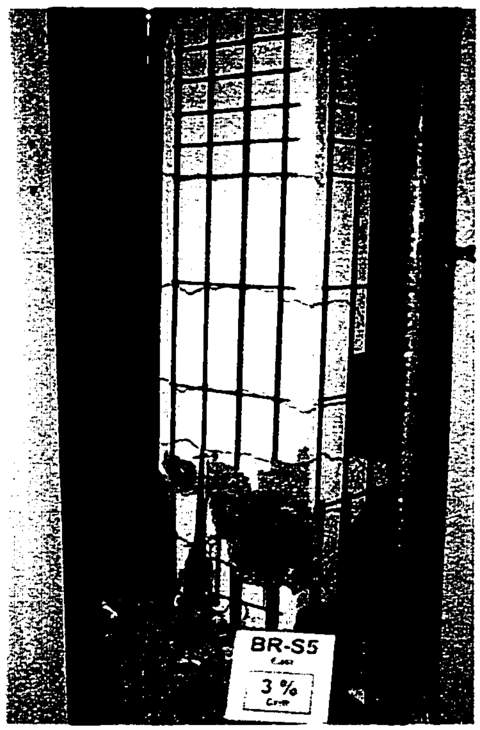

d) 3% drift, 3rd cycle

Figure 3.15 Behaviour of column BR-S5

e) 5% drift, 2nd cycle

f) After the test (West)

g) After the test (East)

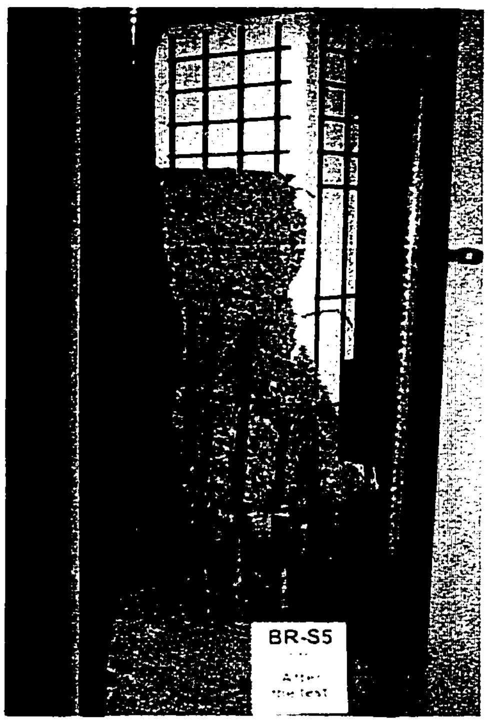

h) After the test

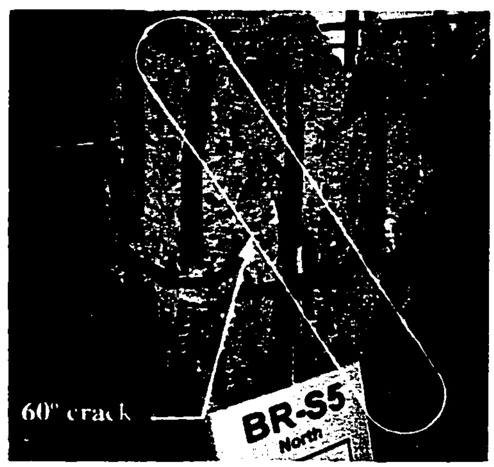

i) After the test (North-East)

Figure 3.15 Behaviour of column BR-S5 (Continued)

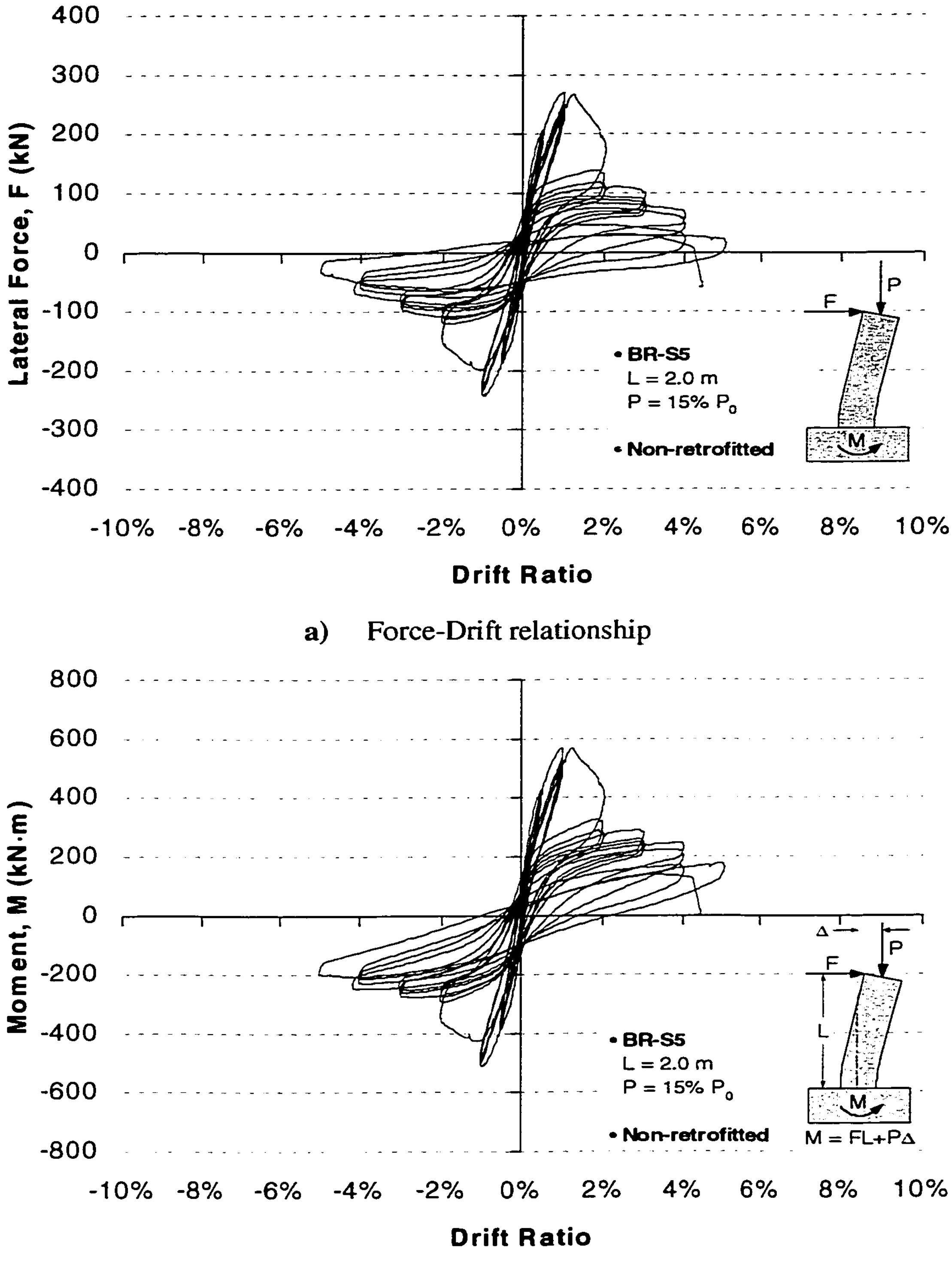

a) Force-Drift relationship

b) Moment-Drift relationship

Figure 3.16 Hysteretic relationships for column BR-S5

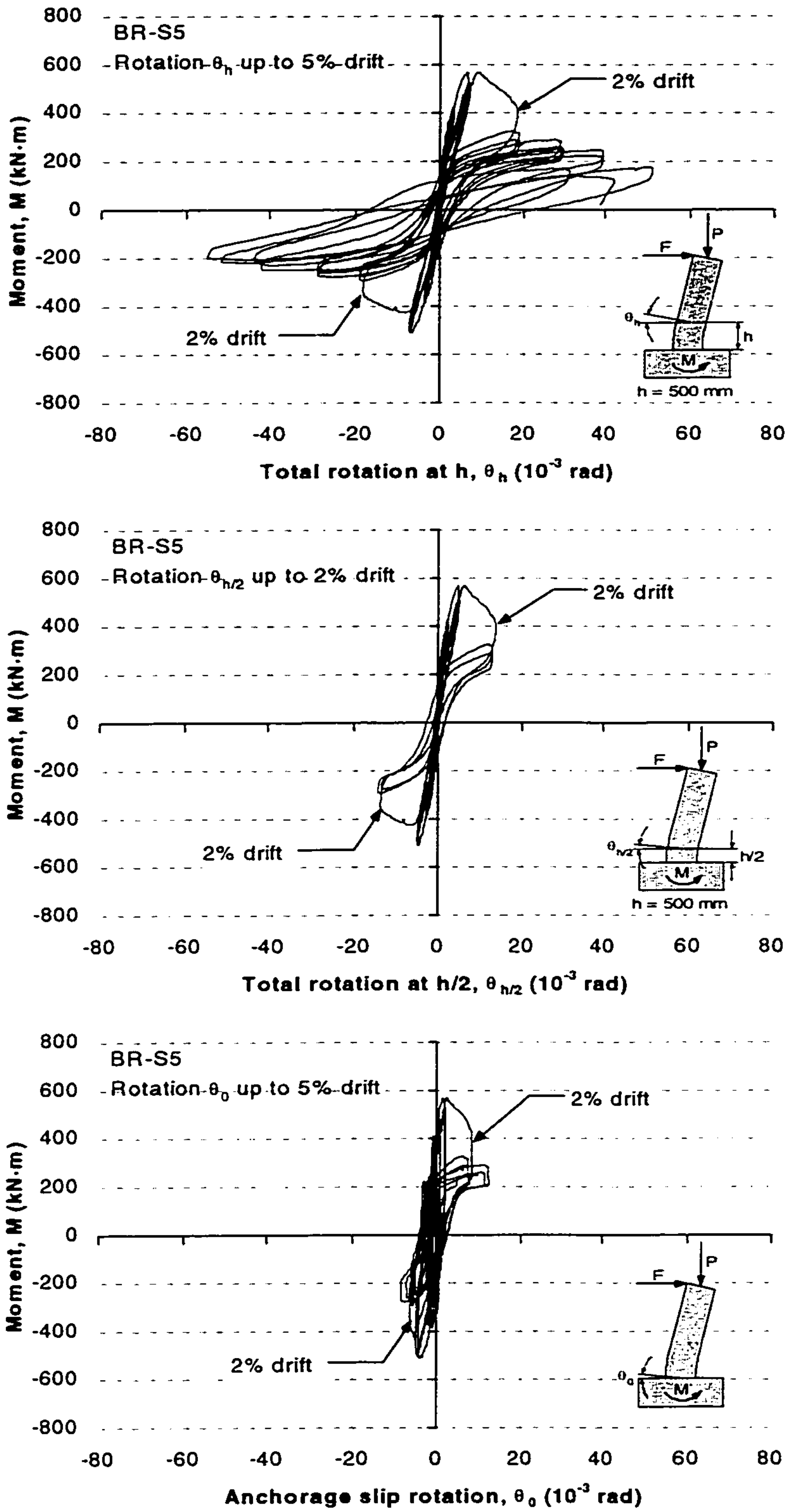

Figure 3.17 Rotation of the hinging region for column BR-S5

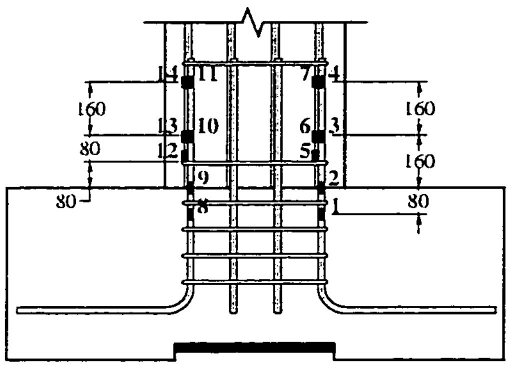

a) Strain gauge location on vertical bars

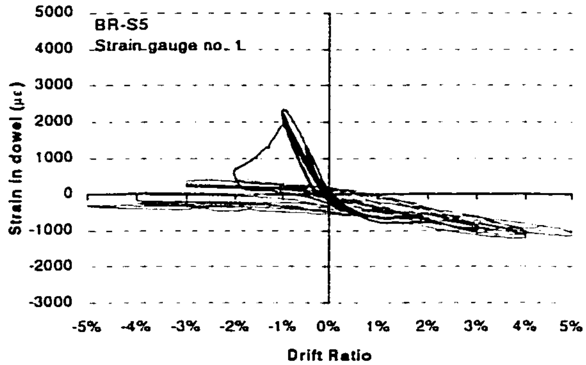

b) Strain gauge no. 1

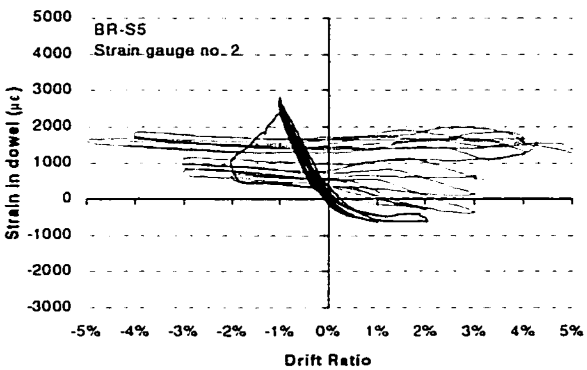

c) Strain gauge no. 2

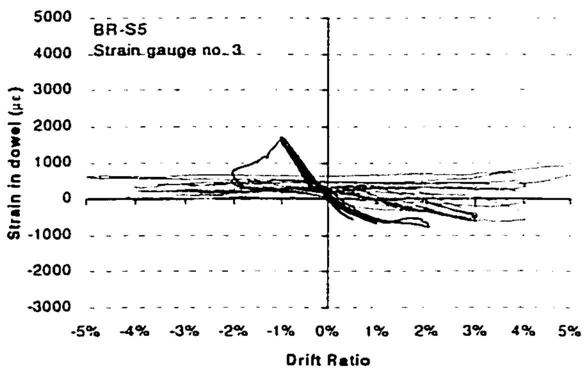

d) Strain gauge no. 3

Figure 3.18 Dowel strains for column BR-S5

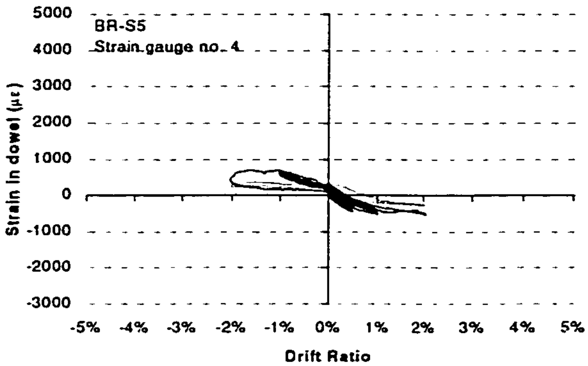

e) Strain gauge no. 4

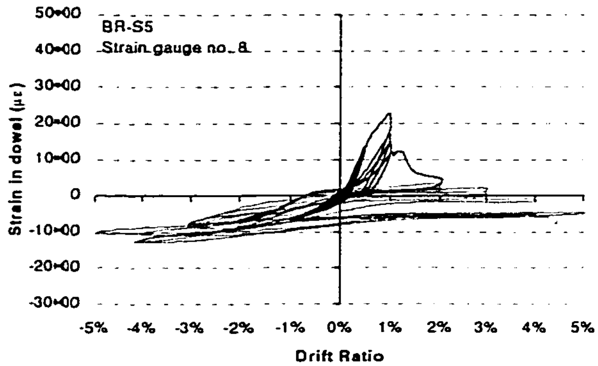

f) Strain gauge no. 8

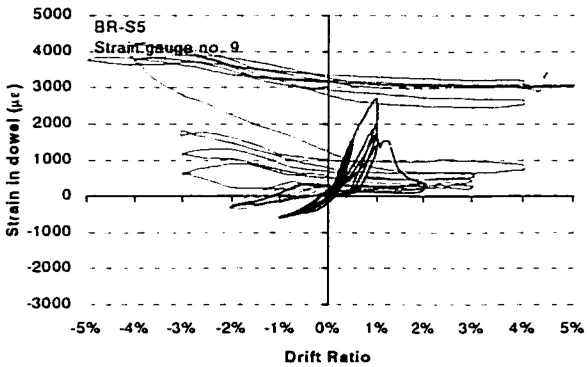

g) Strain gauge no. 9

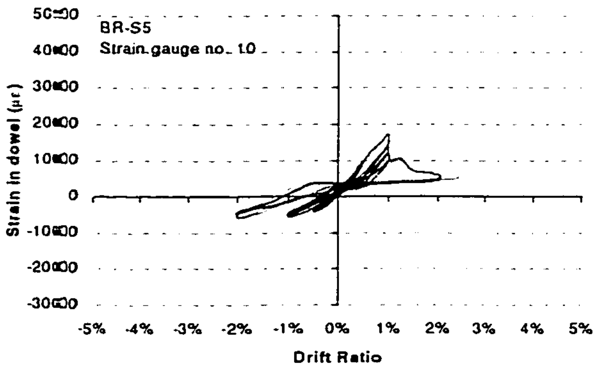

h) Strain gauge no. 10

Figure 3.18 Dowel strains for column BR-S5 (Continued)

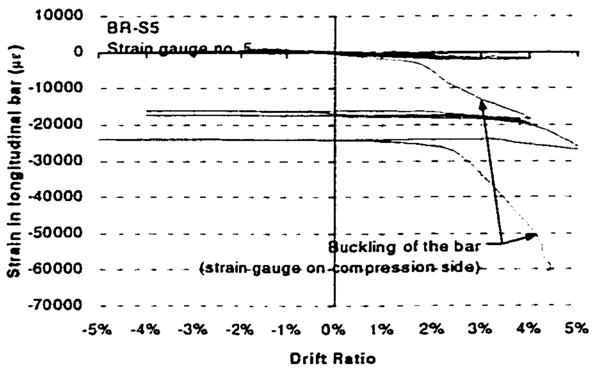

a) Strain gauge no. 5

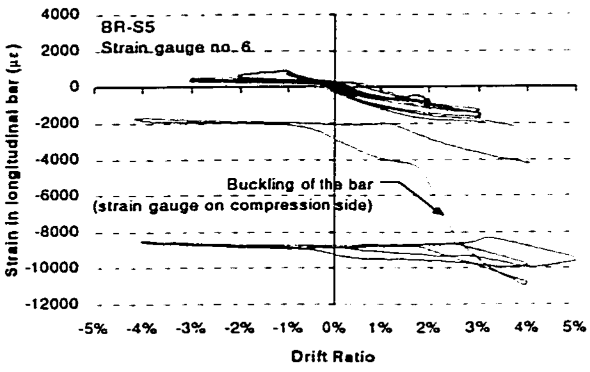

b) Strain gauge no. 6

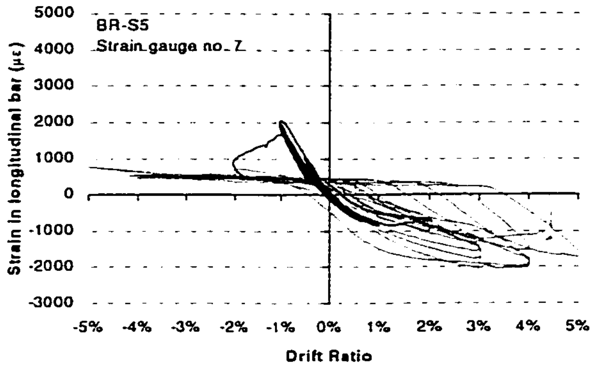

c) Strain gauge no. 7

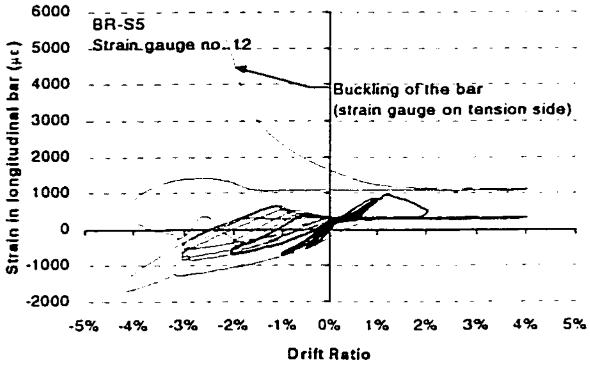

d) Strain gauge no. 12

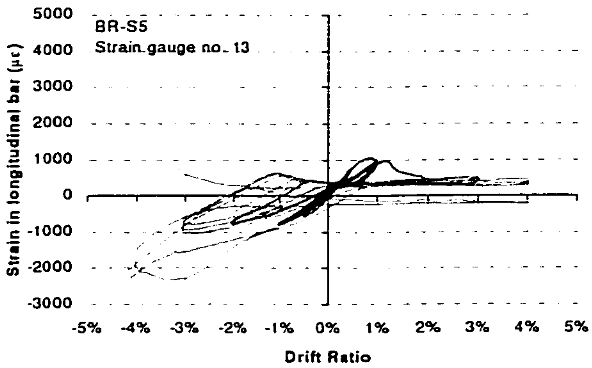

e) Strain gauge no. 13

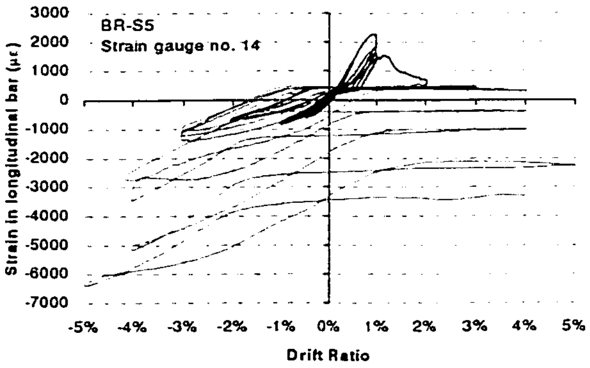

f) Strain gauge no. 14

Figure 3.19 Longitudinal reinforcement steel strains for column BR-S5

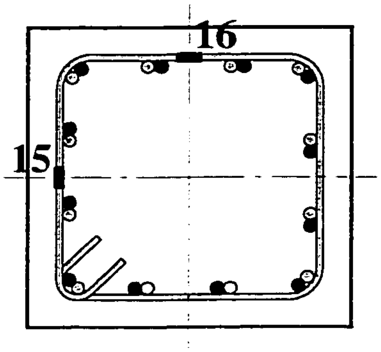

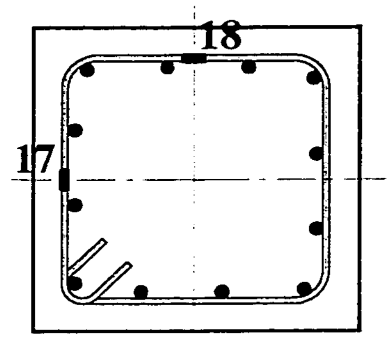

a) Strain gauge location on the 1st hoop **b)** Strain gauge location on the 2nd hoop

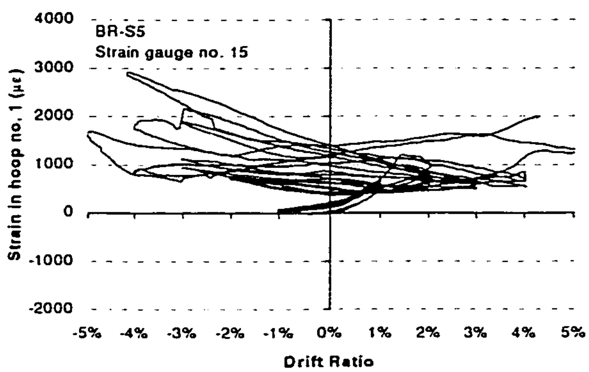

c) Strain gauge no. 15

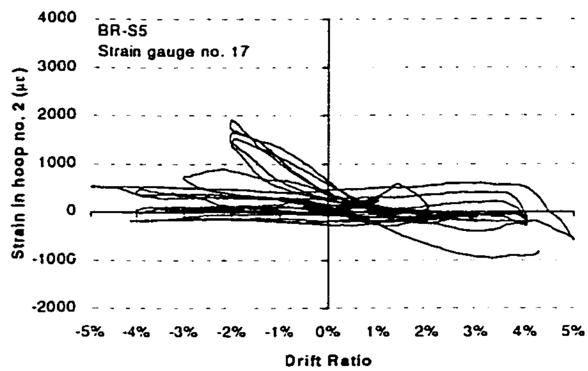

d) Strain gauge no. 17

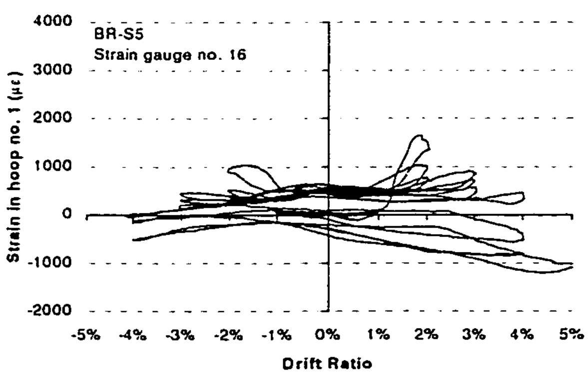

e) Strain gauge no. 16

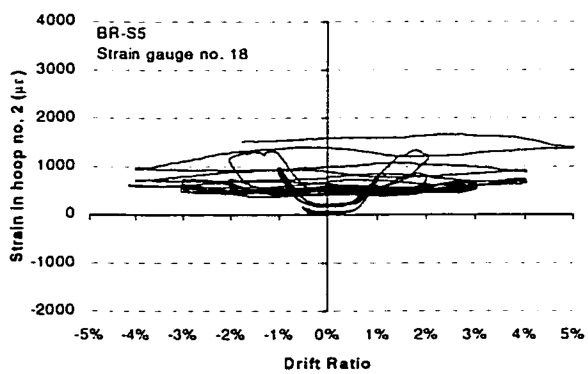

f) Strain gauge no. 18

Figure 3.20 Transverse reinforcement steel strains for column BR-S5

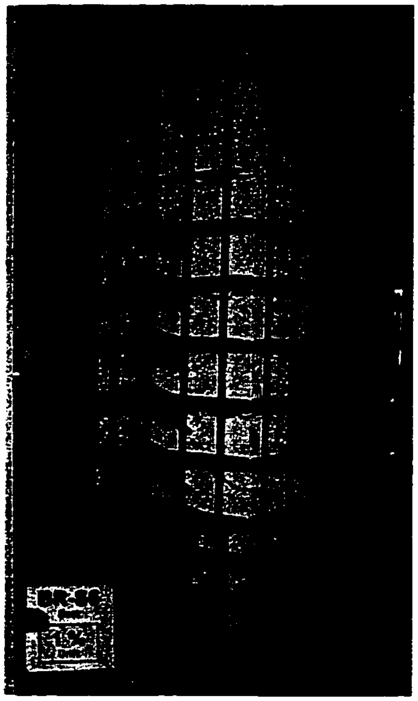

a) 1% drift

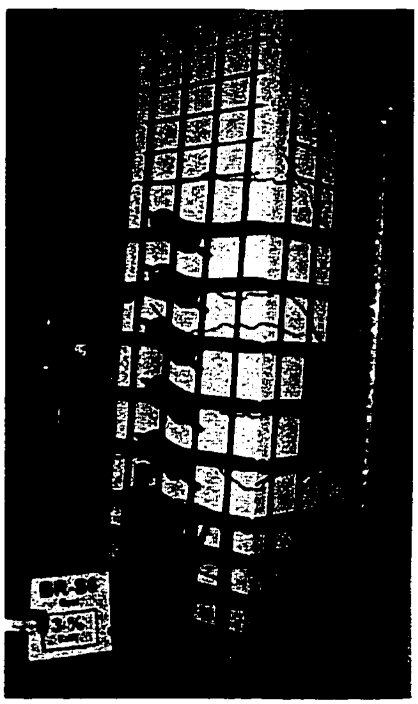

b) 3% drift

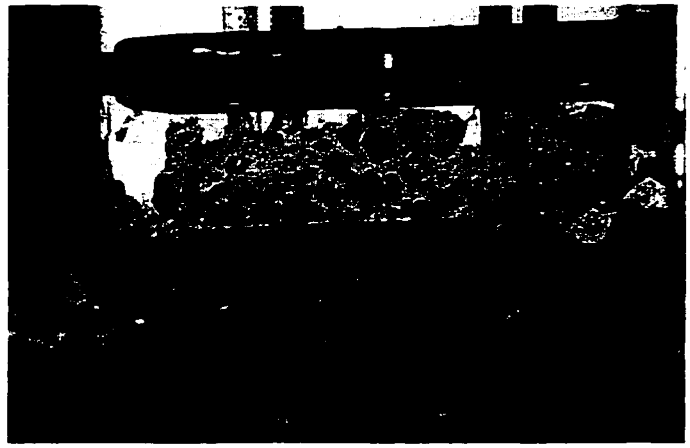

c) 4% drift, 10 mm gap with a depth of 75 mm

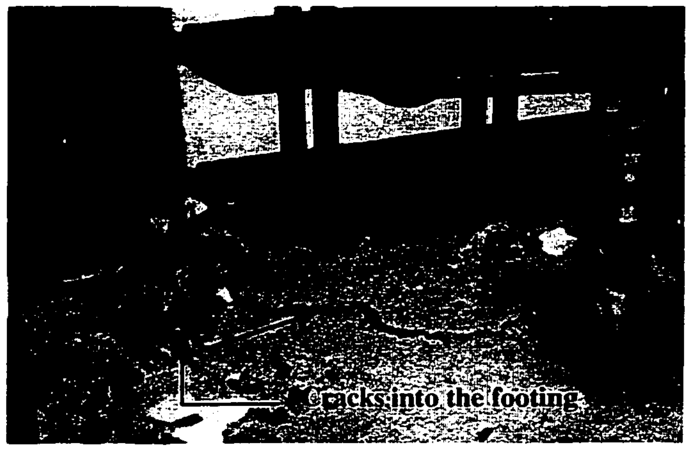

d) 4% drift, crushing of the footing

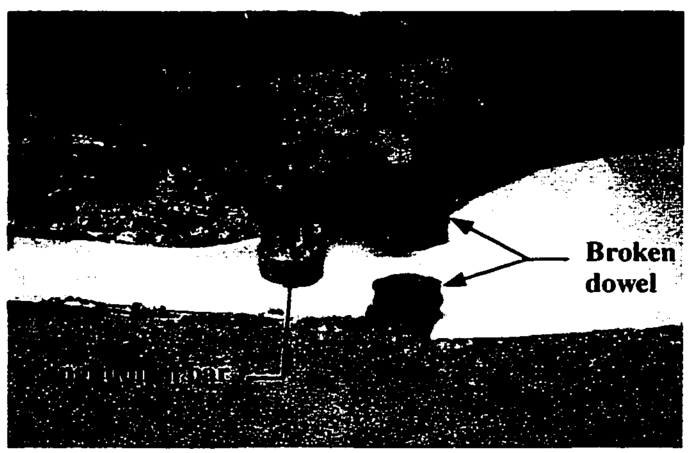

e) 7% drift, failure of a corner dowel

Figure 3.21 Behaviour of column BR-S6

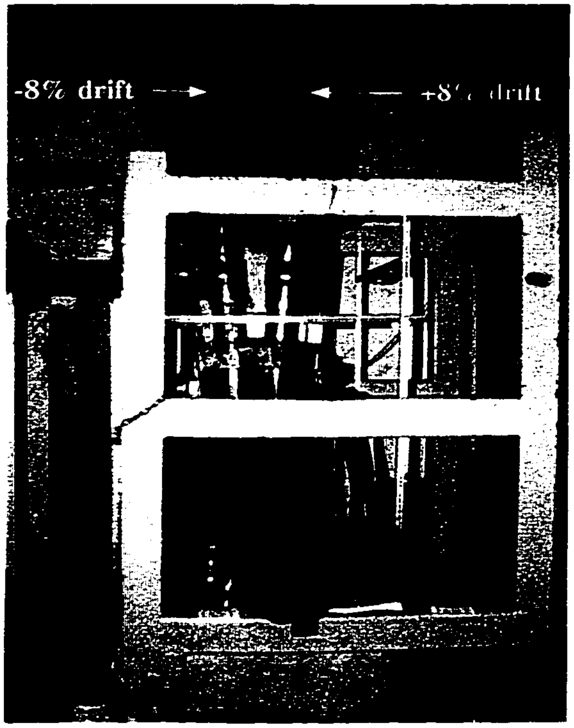

f) 8% drift (North)

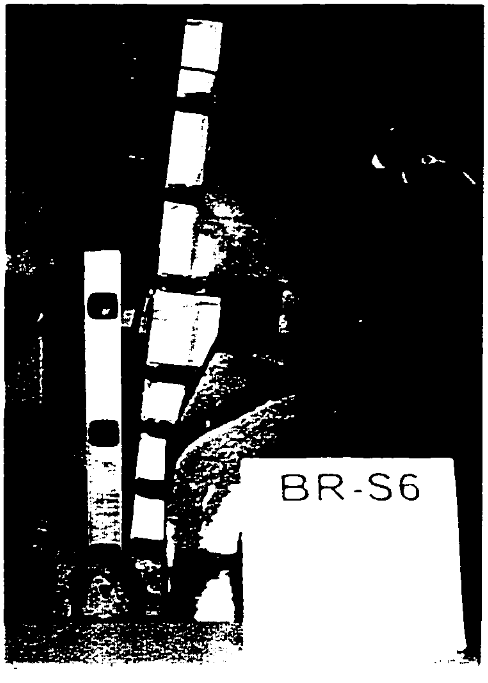

g) 9% drift (North)

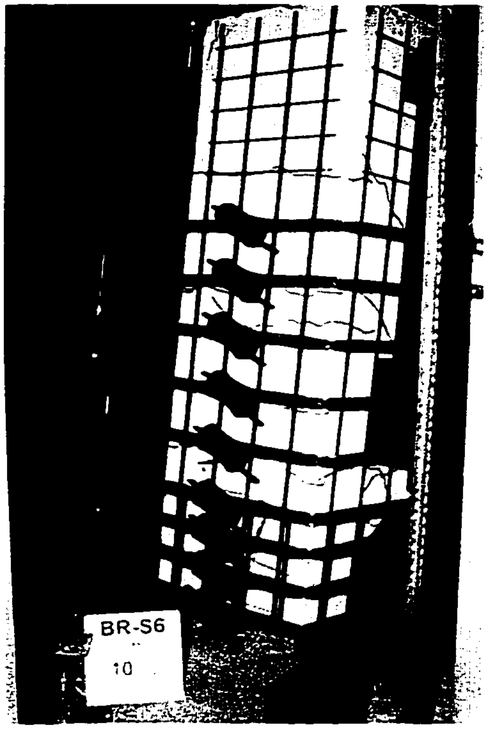

h) 10% drift (End of the test)

Figure 3.21 Behaviour of column BR-S6 (Continued)

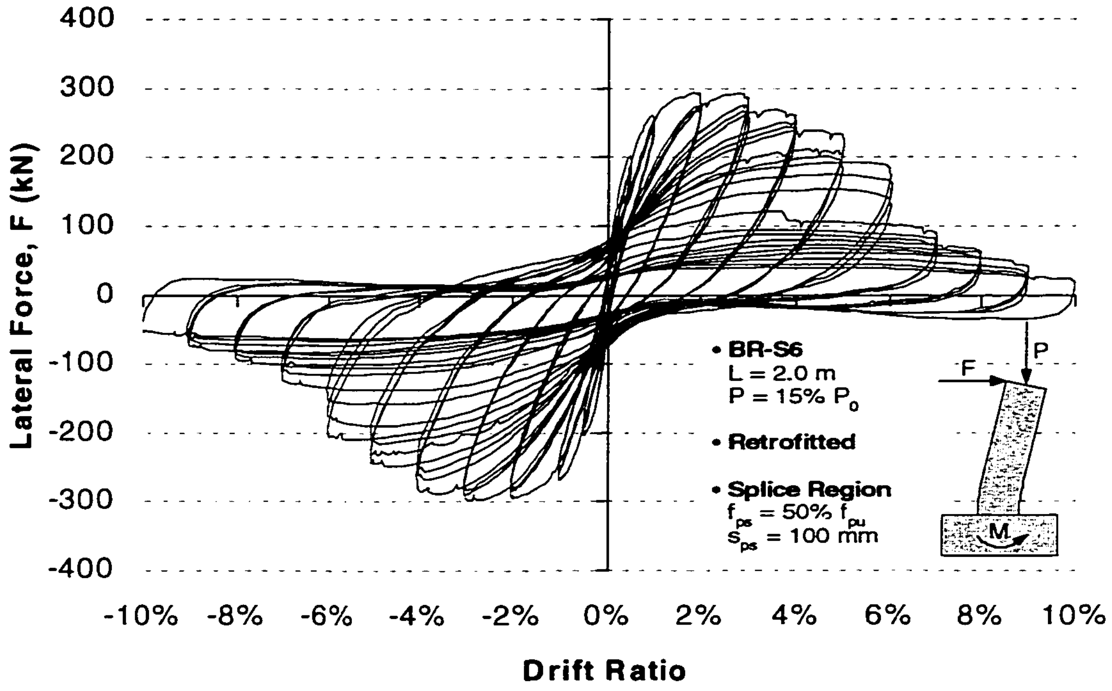

a) Force-Drift relationship

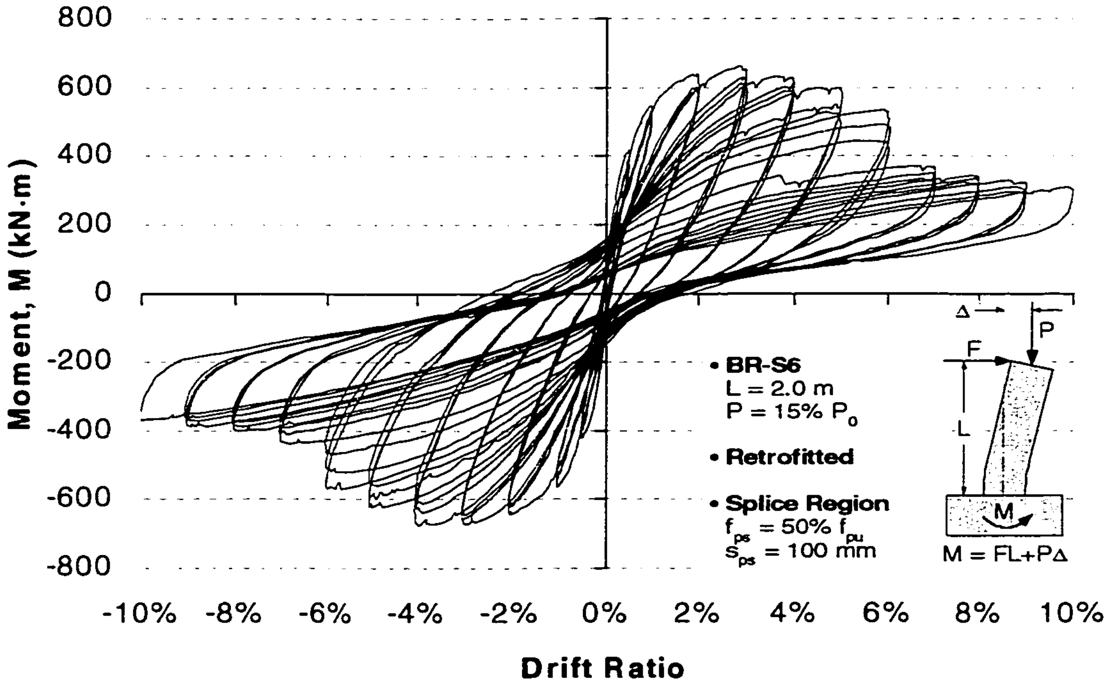

b) Moment-Drift relationship

Figure 3.22 Hysteretic relationships for column BR-S6

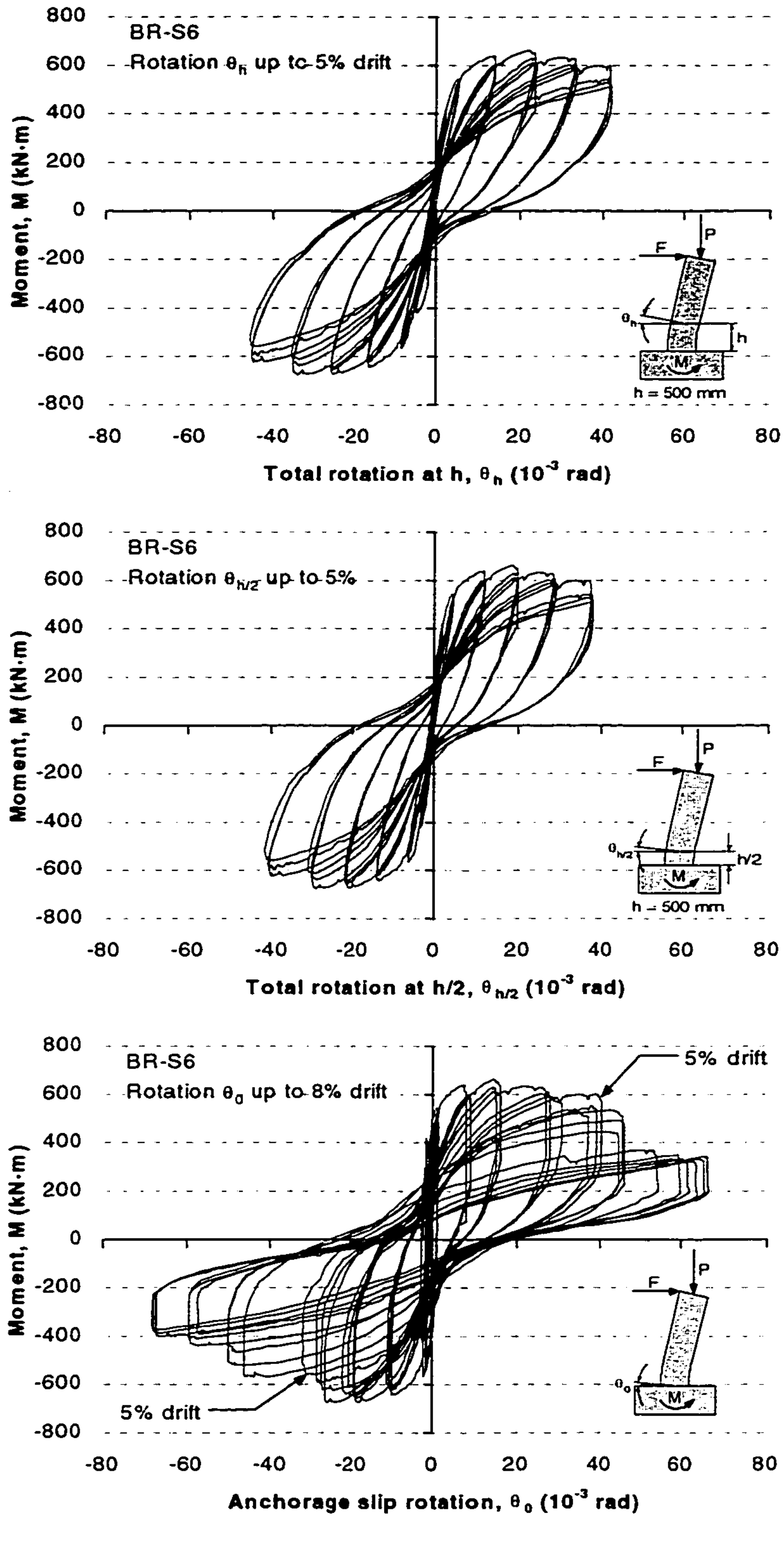

Figure 3.23 Rotation of the hinging region for column BR-S6

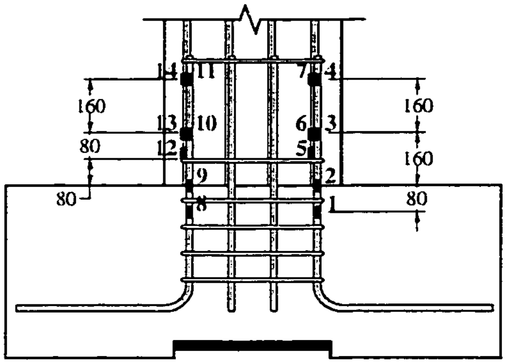

a) Strain gauge location on vertical bars

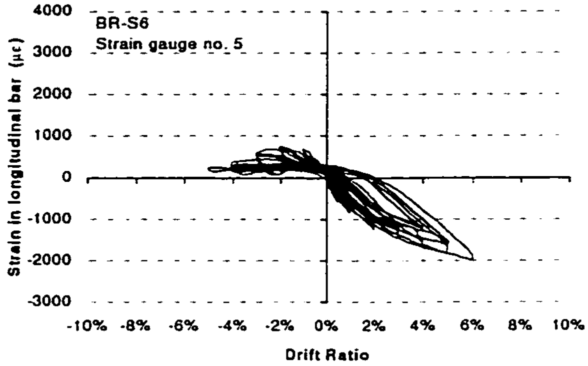

b) Strain gauge no. 5

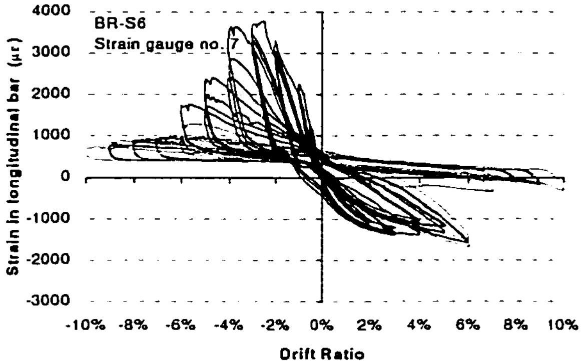

c) Strain gauge no. 7

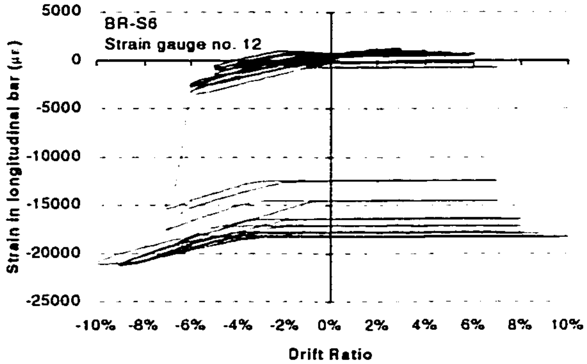

d) Strain gauge no. 12

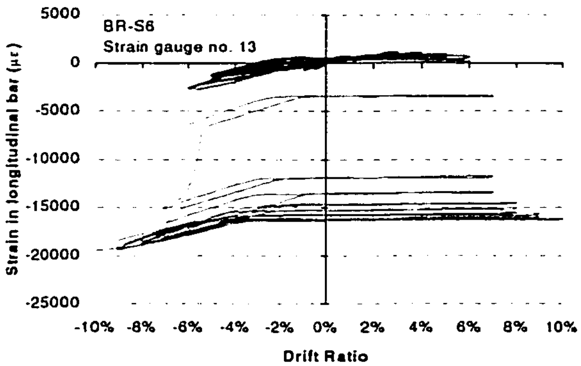

e) Strain gauge no. 13

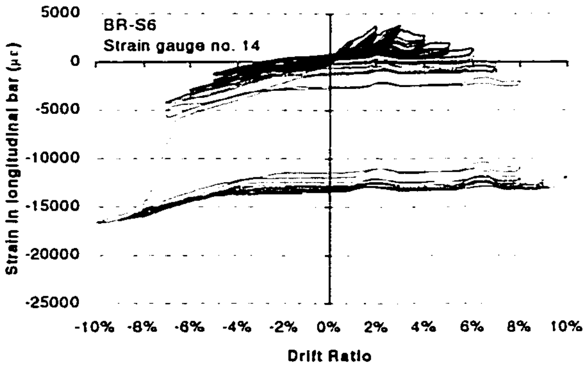

f) Strain gauge no. 14

Figure 3.24 Longitudinal reinforcement steel strains for column BR-S6

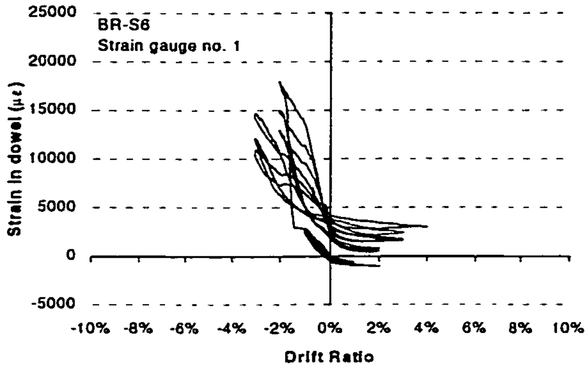

a) Strain gauge no. 1

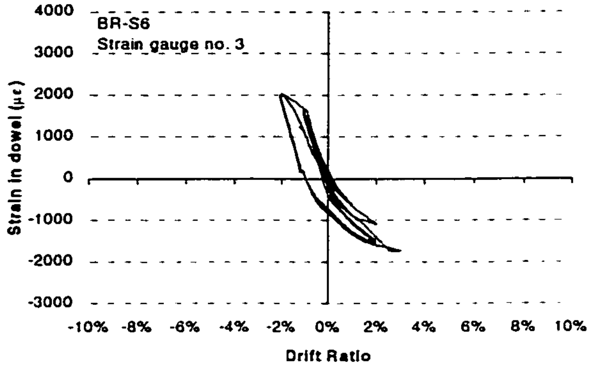

b) Strain gauge no. 3

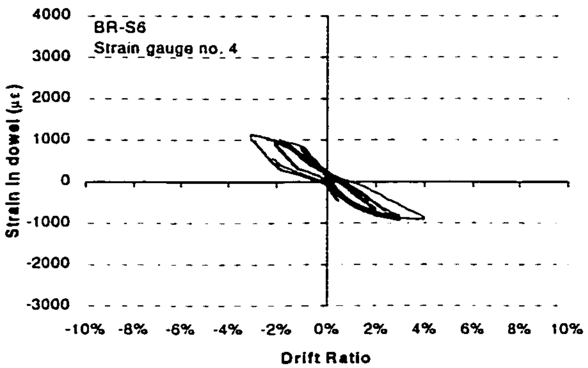

c) Strain gauge no. 4

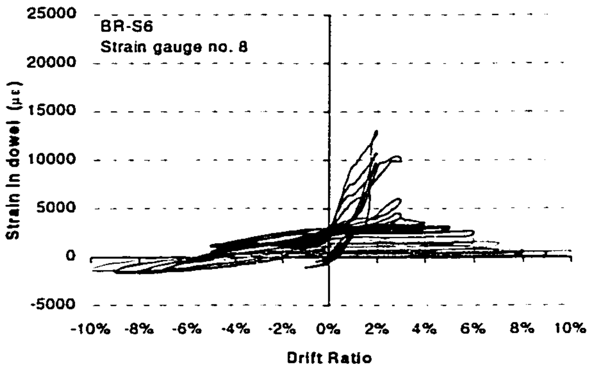

d) Strain gauge no. 8

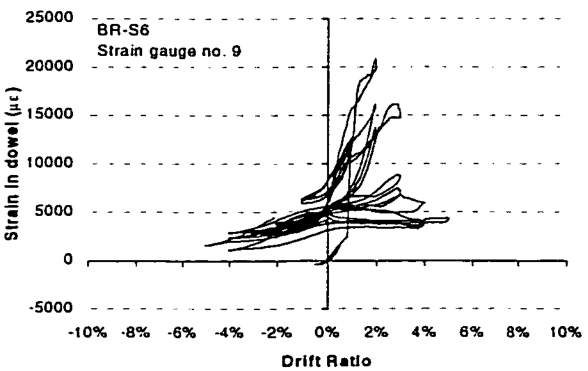

e) Strain gauge no. 9

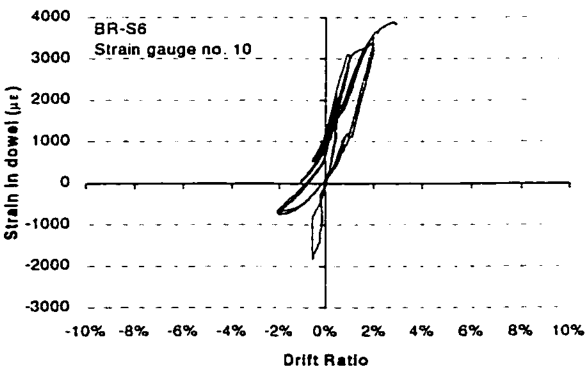

f) Strain gauge no. 10

Figure 3.25 Dowel strains for column BR-S6

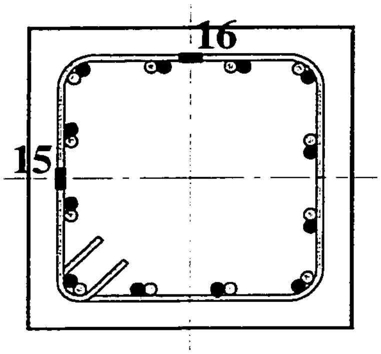

a) Strain gauge location on the 1st hoop

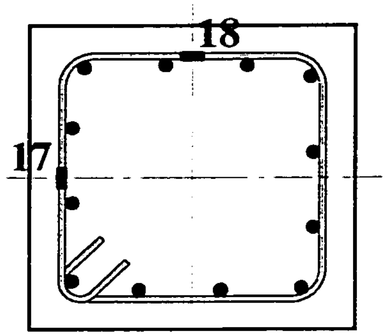

b) Strain gauge location on the 2nd hoop

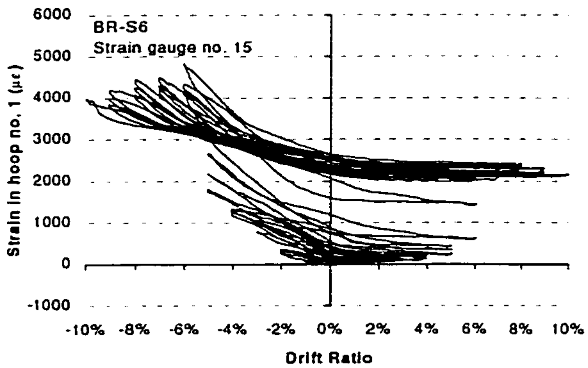

c) Strain gauge no. 15

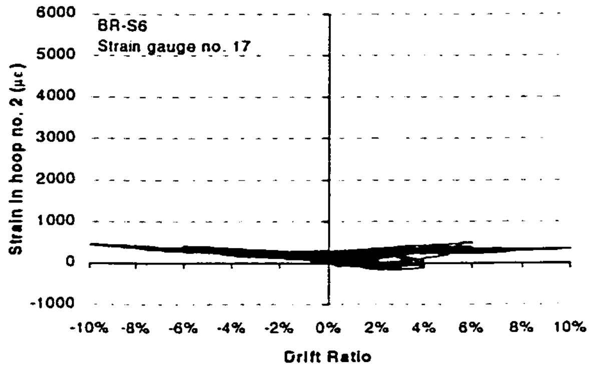

d) Strain gauge no. 17

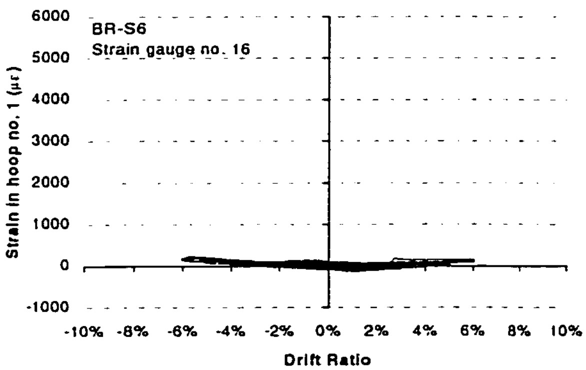

e) Strain gauge no. 16

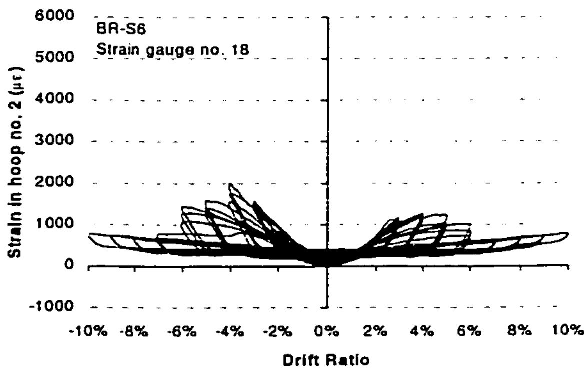

f) Strain gauge no. 18

Figure 3.26 Transverse reinforcement steel strains for column BR-S6

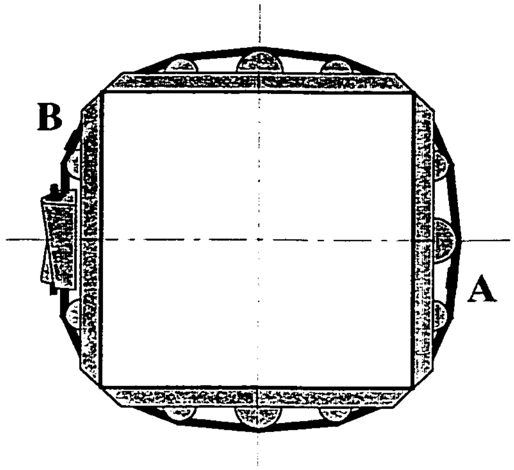

a) Strain gauge location on prestressing strands

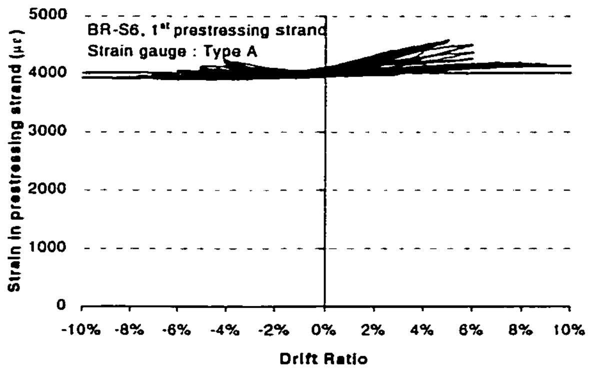

b) 1st strand (Gauge: type A)

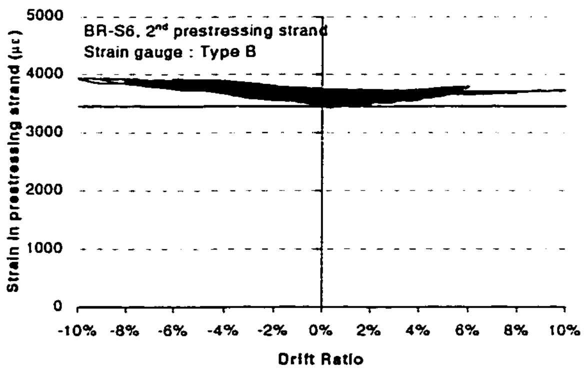

c) 2nd strand (Gauge: type B)

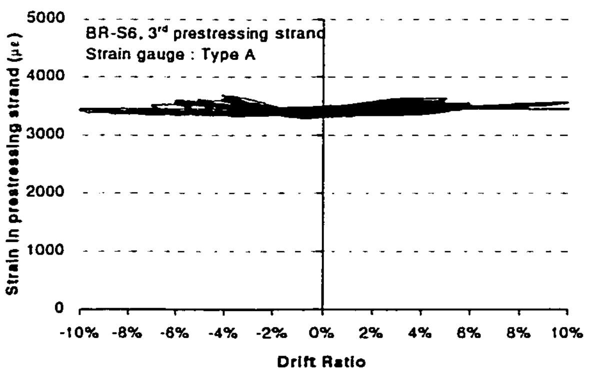

d) 3rd strand (Gauge:Type A)

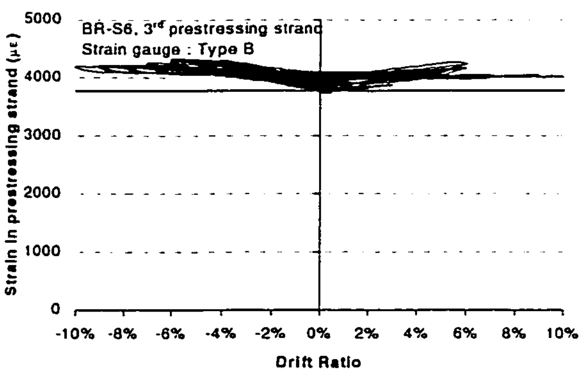

e) 3rd strand (Gauge:Type B)

Figure 3.27 Prestressing strand strains for column BR-S6

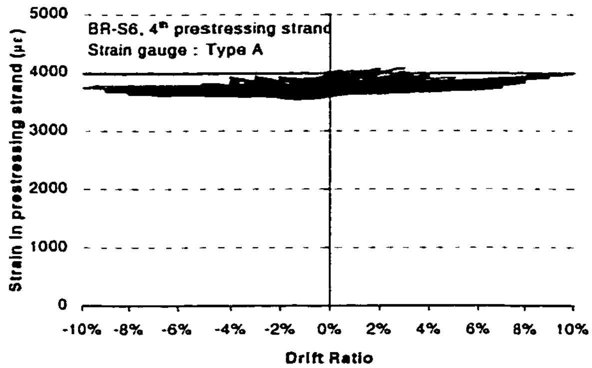

f) 4^{th} strand (Gauge:Type A)

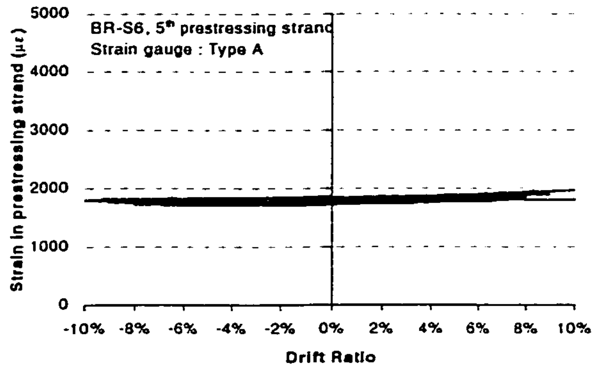

g) 5^{th} strand (Gauge:Type A)

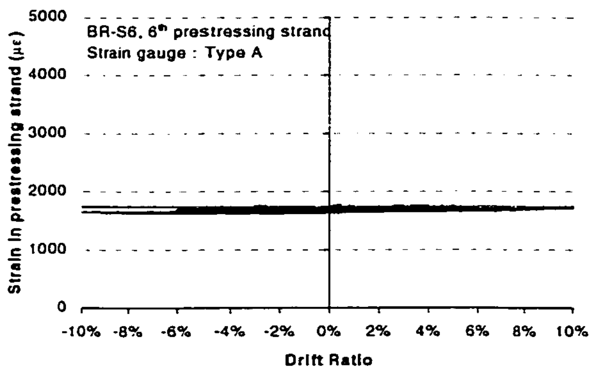

h) 6^{th} strand (Gauge:Type A)

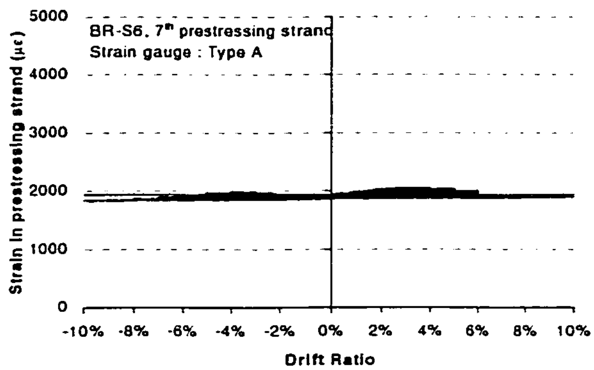

i) 7^{th} strand (Gauge:Type A)

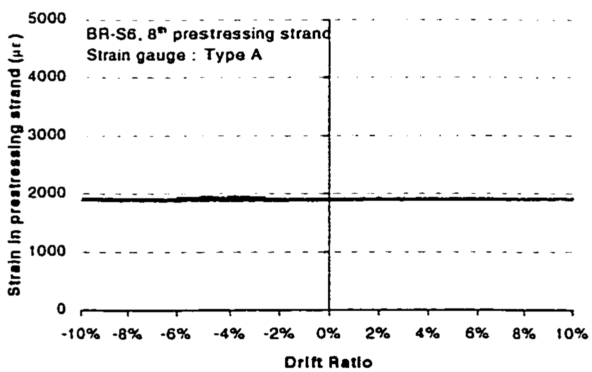

j) 8^{th} strand (Gauge:Type A)

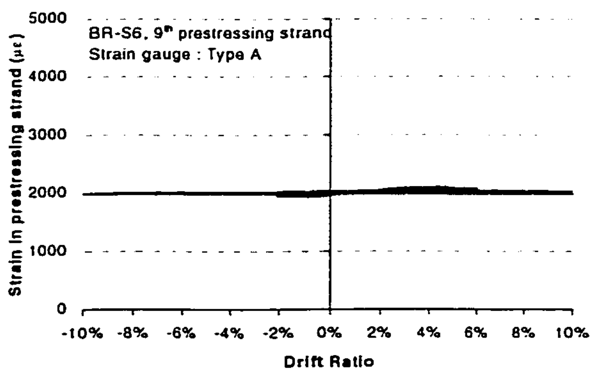

k) 9^{th} strand (Gauge:Type A)

Figure 3.27 Prestressing strand strains for column BR-S6 (Continued)

a) Column BR-S5 (East) b) Column BR-S6 (East)

Figure 3.28 Comparison of columns BR-S5 and BR-S6 (End of the test)

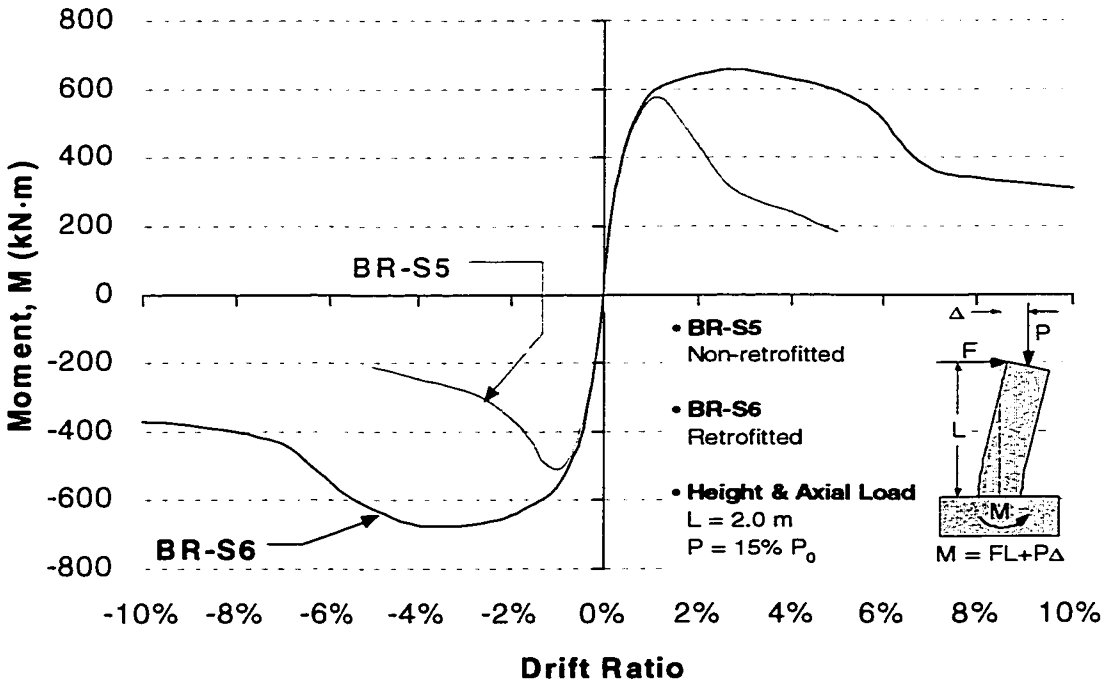

Figure 3.29 Moment-Drift envelope of columns BR-S5 and BR-S6

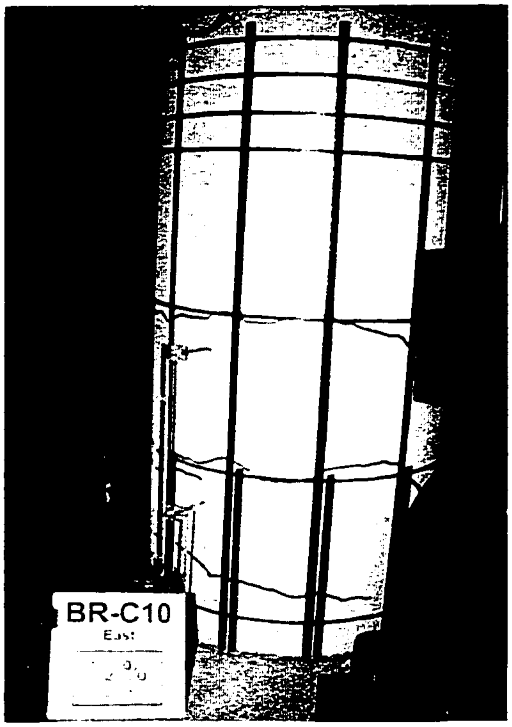

a) ½% drift

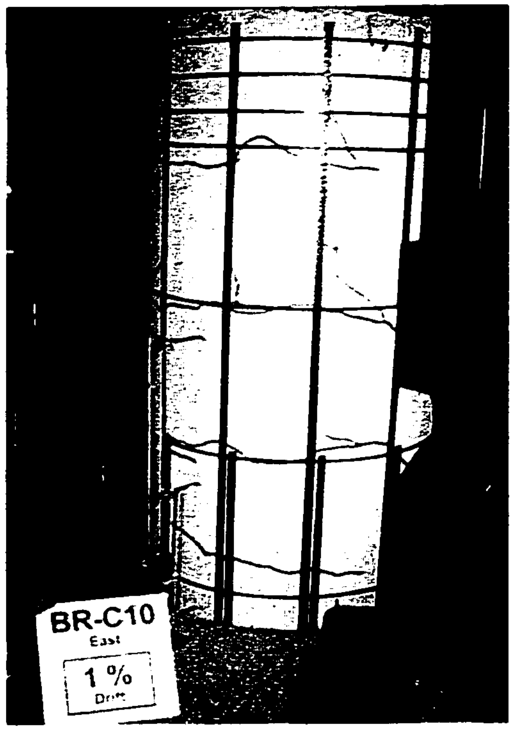

b) 1% drift

c) 2% drift

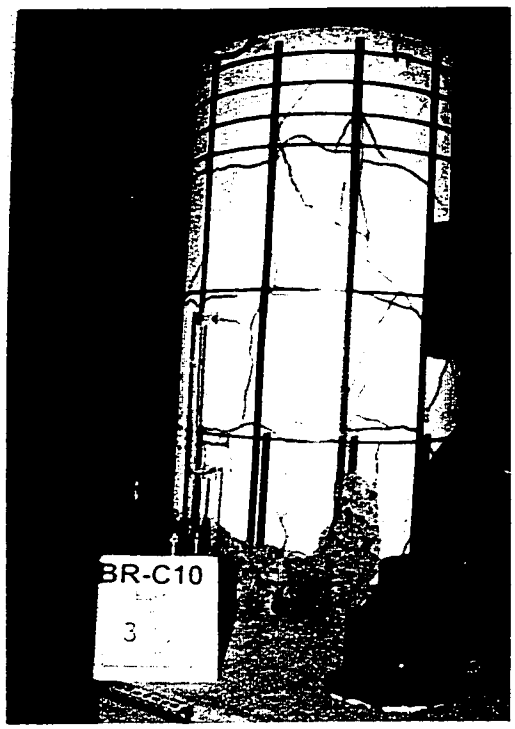

d) 3% drift

Figure 3.30 Behaviour of column BR-C10

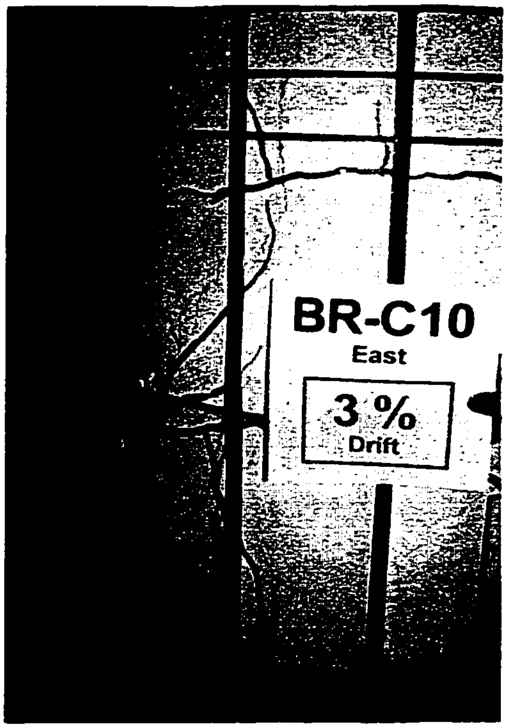

e) 3% drift, crushing of the concrete

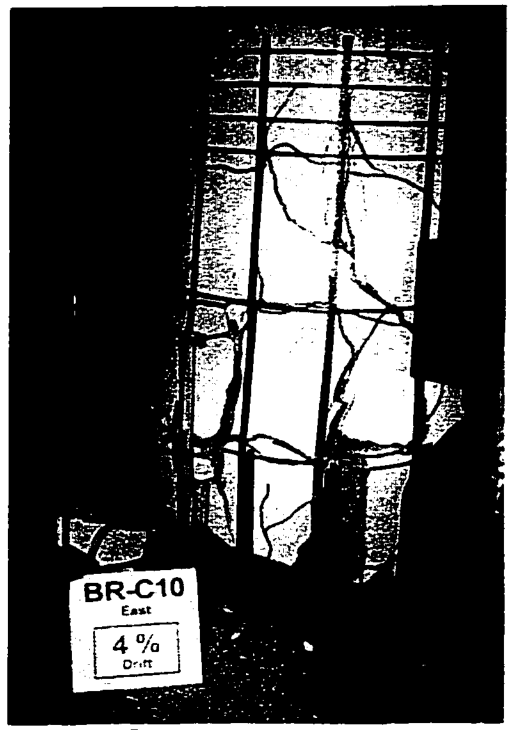

f) End of the test

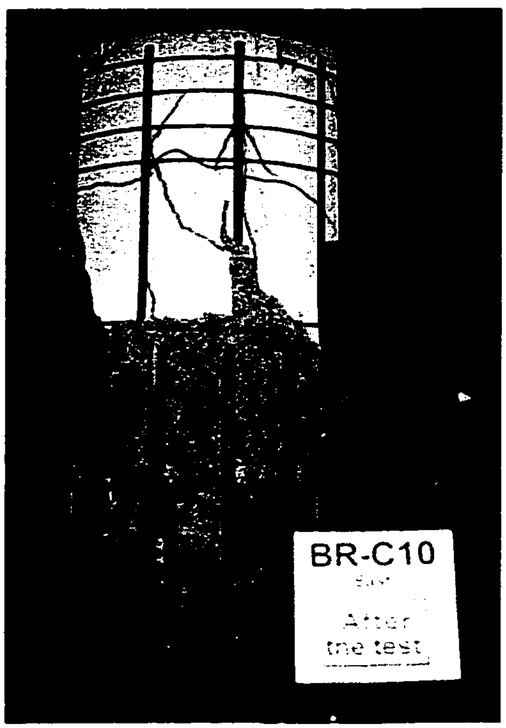

g) After the test

h) After the test, bukcling of bars

i) After the test, flexural crack

Figure 3.30 Behaviour of column BR-C10 (Continued)

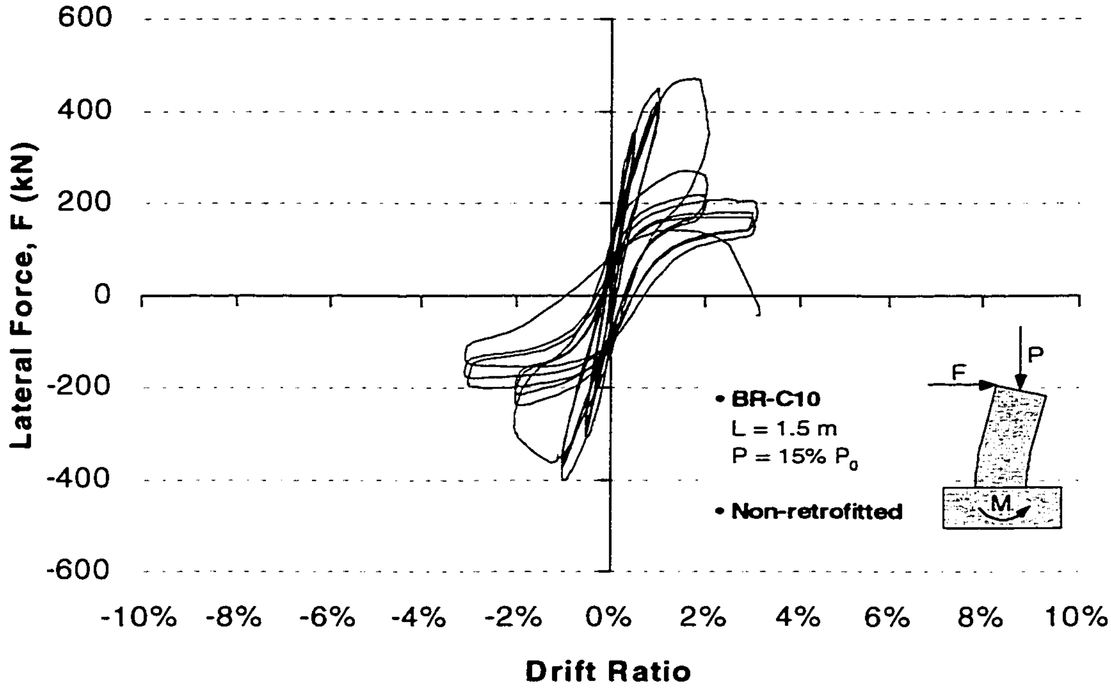

a) Force-Drift relationship

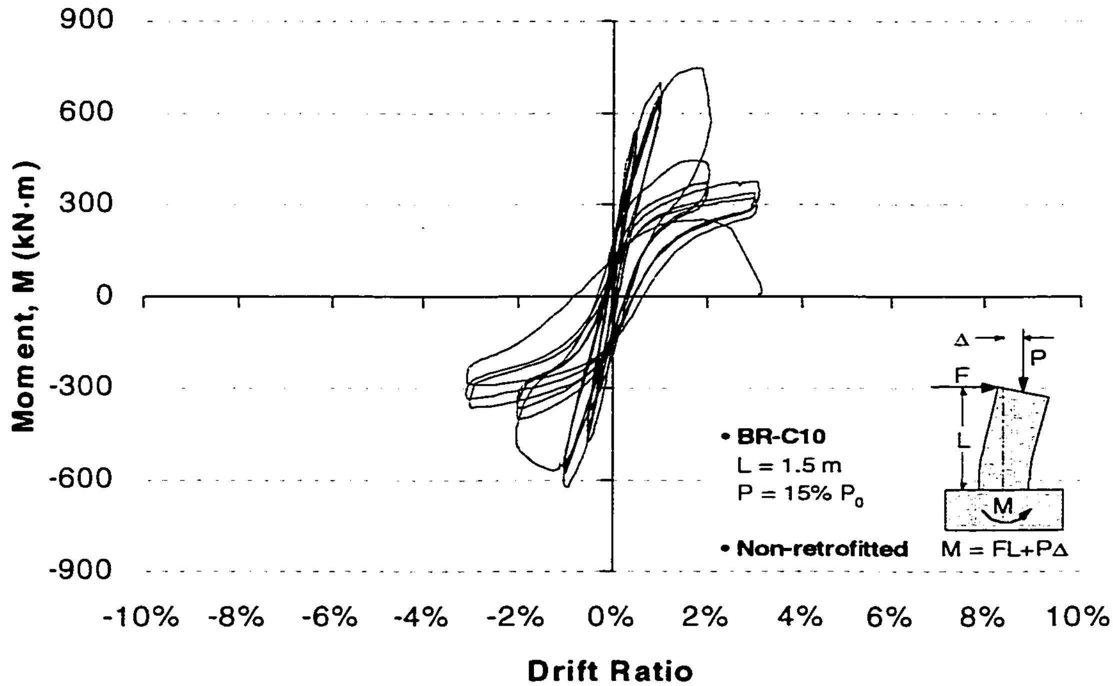

b) Moment-Drift relationship

Figure 3.31 Hysteretic relationships for column BR-C10

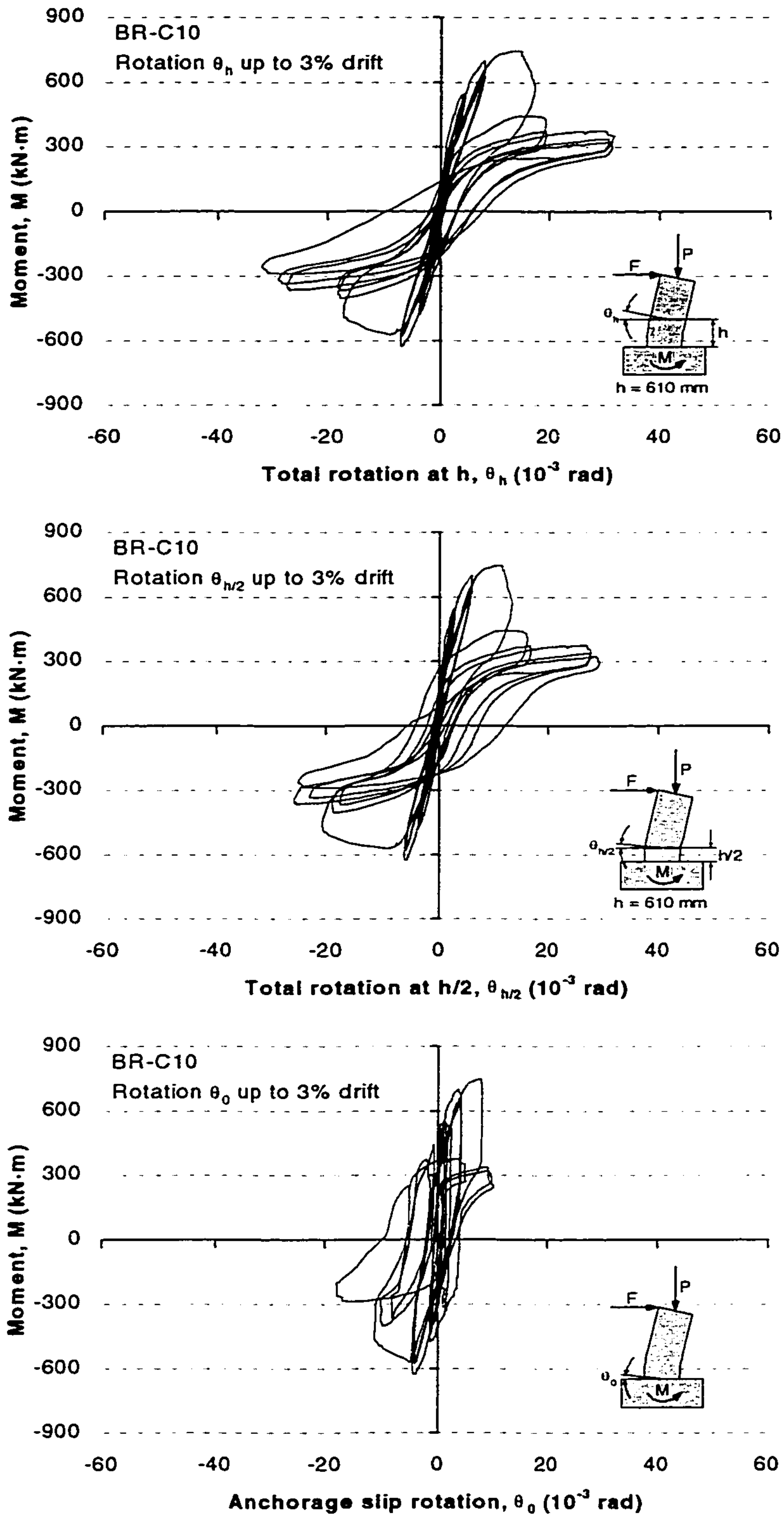

Figure 3.32 Rotation of the hinging region for column BR-C10

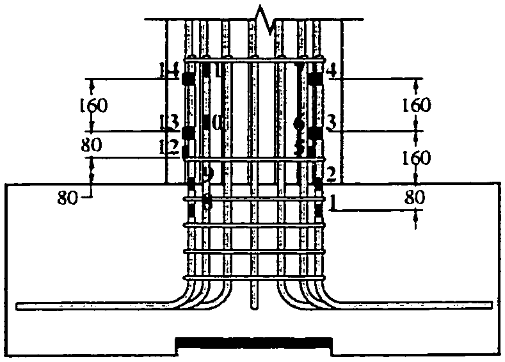

a) Strain gauge location on vertical bars

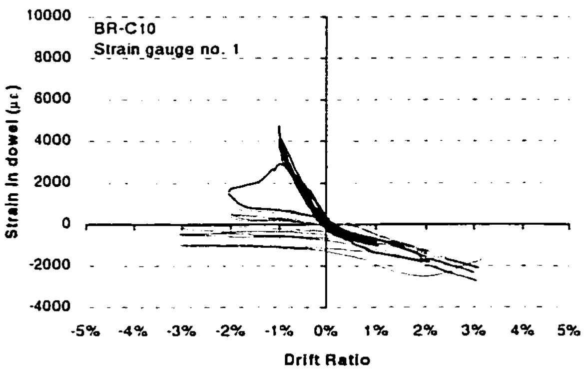

b) Strain gauge no. 1

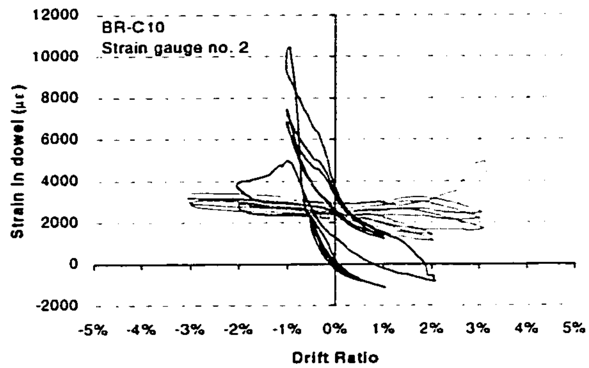

c) Strain gauge no. 2

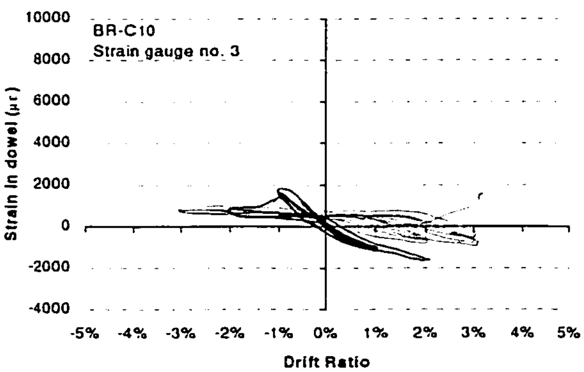

d) Strain gauge no. 3

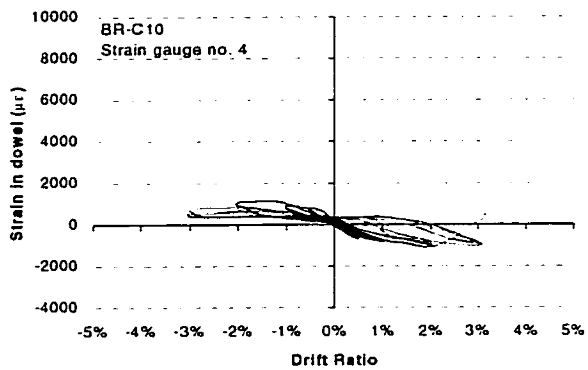

e) Strain gauge no. 4

Figure 3.33 Dowel strains for column BR-C10

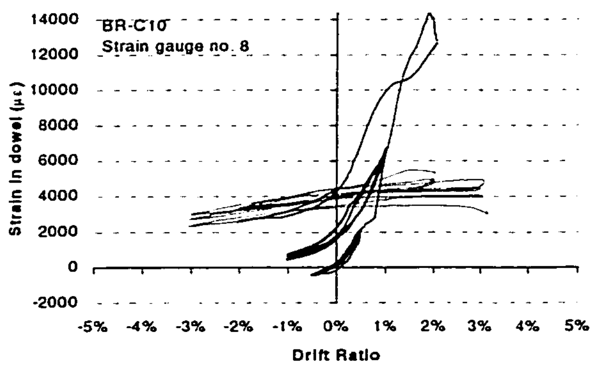

f) Strain gauge no. 8

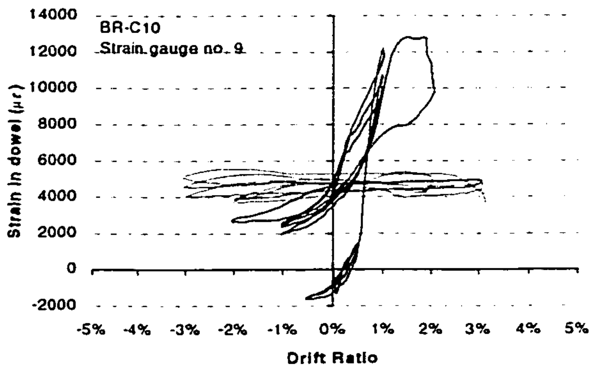

g) Strain gauge no. 9

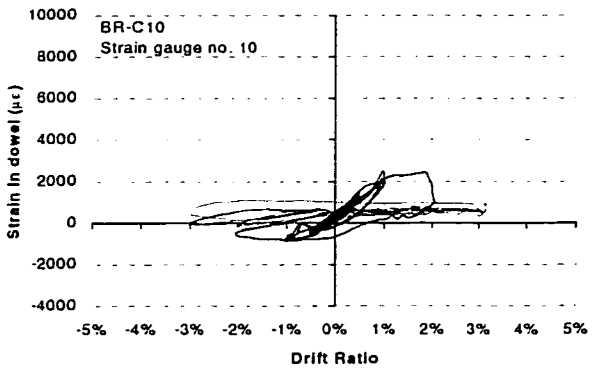

h) Strain gauge no. 10

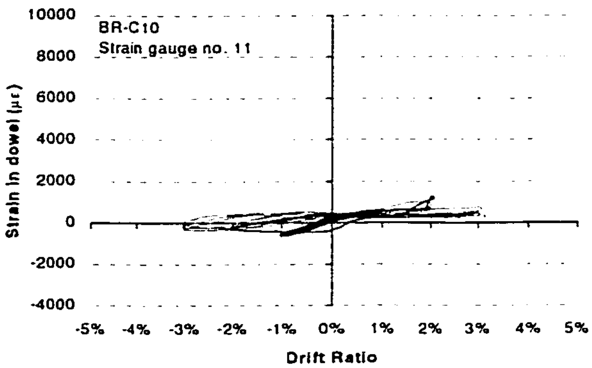

i) Strain gauge no. 11

Figure 3.33 Dowel strains for column BR-C10 (Continued)

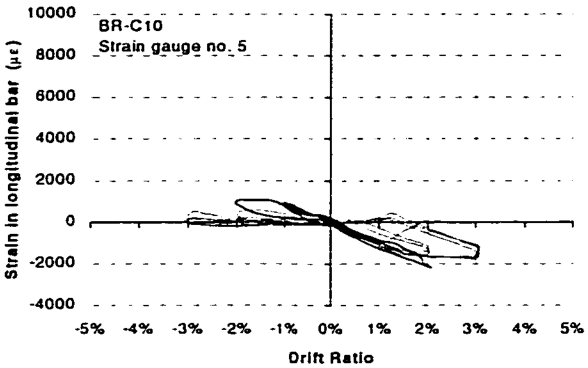

a) Strain gauge no. 5

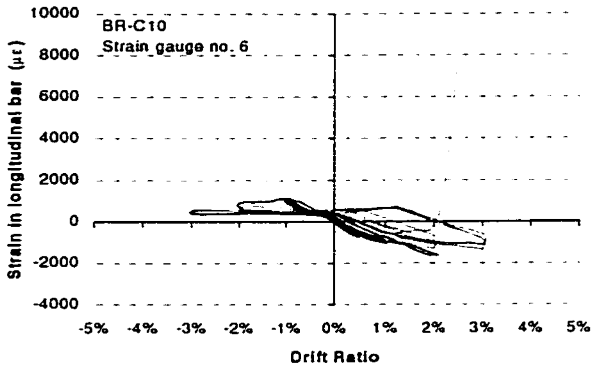

b) Strain gauge no. 6

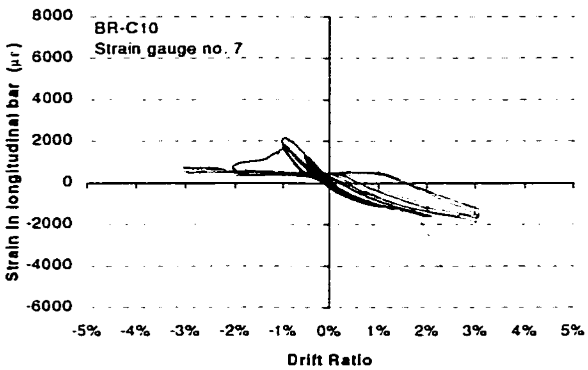

c) Strain gauge no. 7

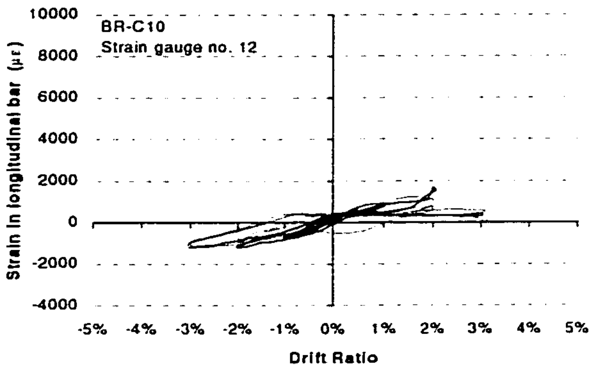

d) Strain gauge no. 12

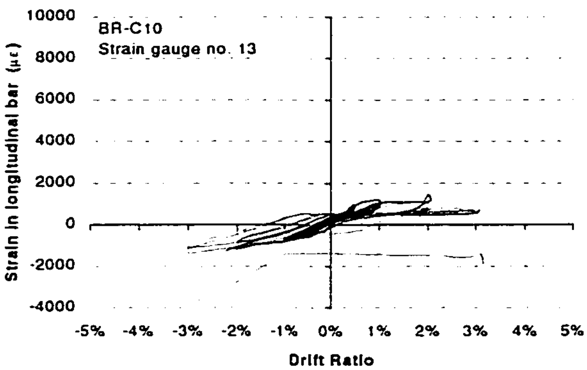

e) Strain gauge no. 13

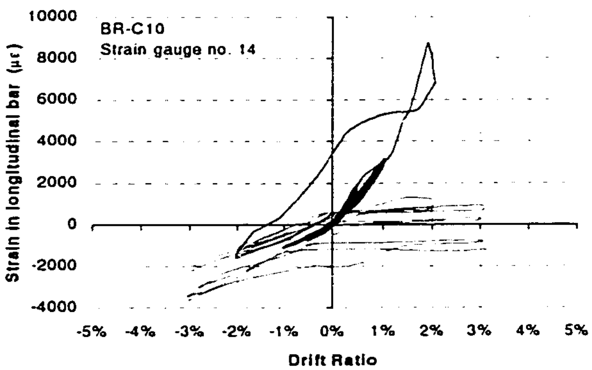

f) Strain gauge no. 14

Figure 3.34 Longitudinal reinforcement steel strains for column BR-C10

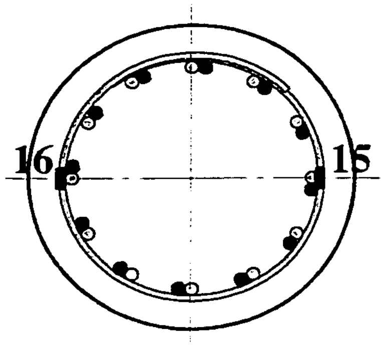

a) Strain gauge location on the 1^{st} hoop

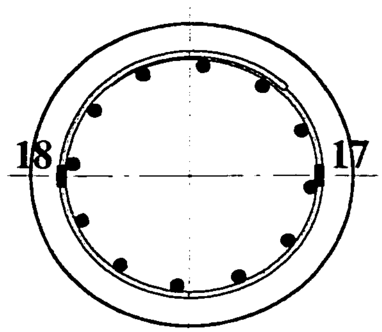

b) Strain gauge location on the 2^{nd} hoop

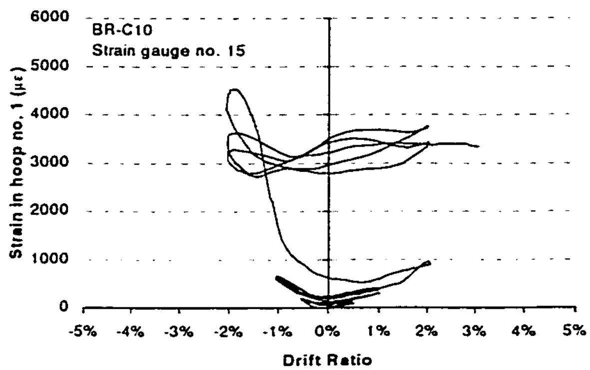

c) Strain gauge no. 15

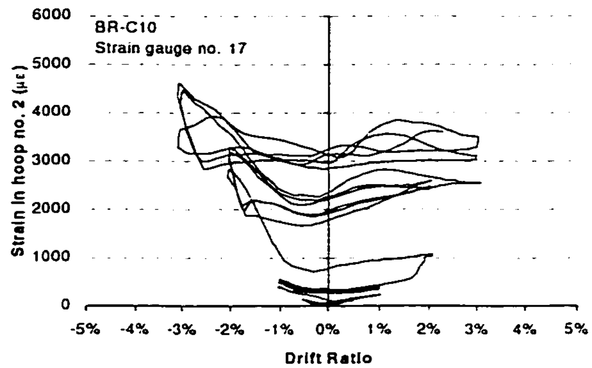

d) Strain gauge no. 17

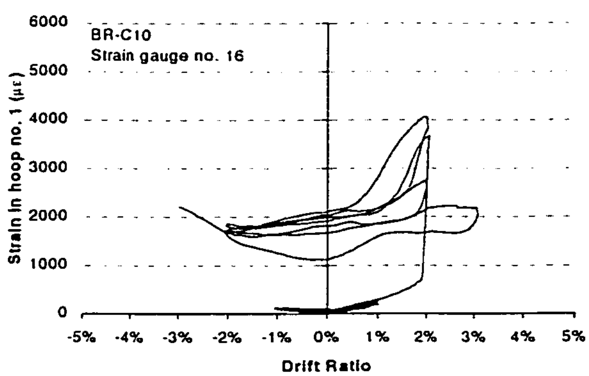

e) Strain gauge no. 16

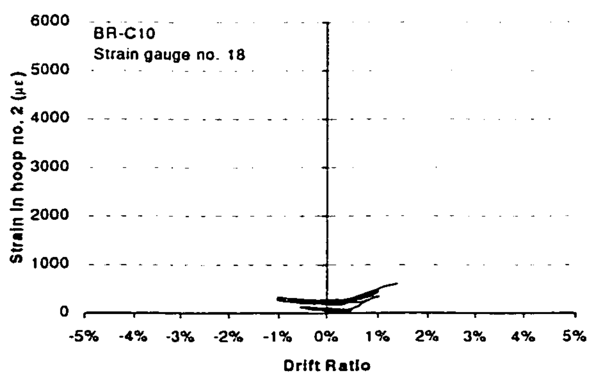

f) Strain gauge no. 18

Figure 3.35 Transverse reinforcement steel strains for column BR-C10

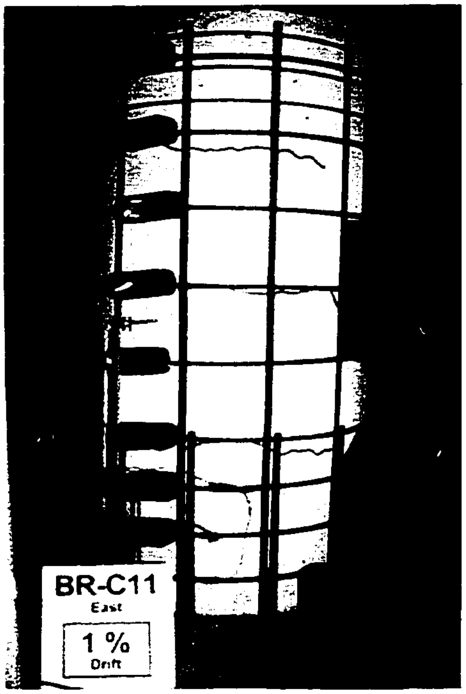

a) 1% drift

b) 3% drift, embedment of the 4^{th} prestressing strand and spalling of the concrete

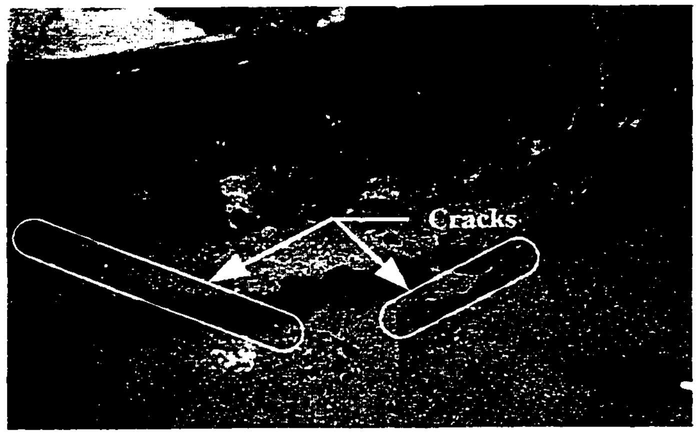

c) 4% drift, cracks into the footing

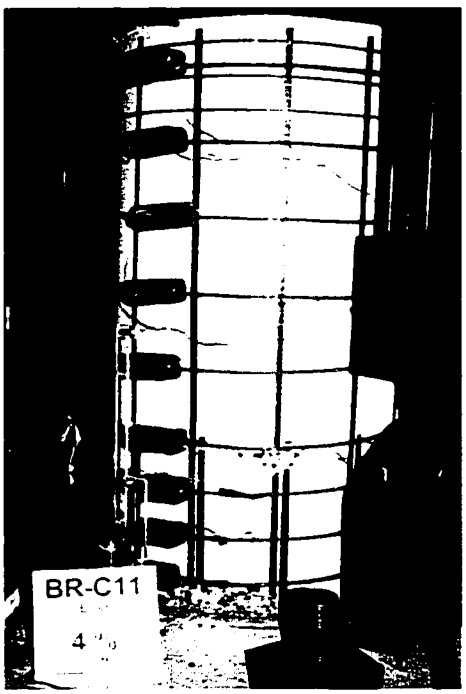

d) 4% drift

e) 5% drift, opening of 255 mm deep

Figure 3.36 Behaviour of column BR-C11

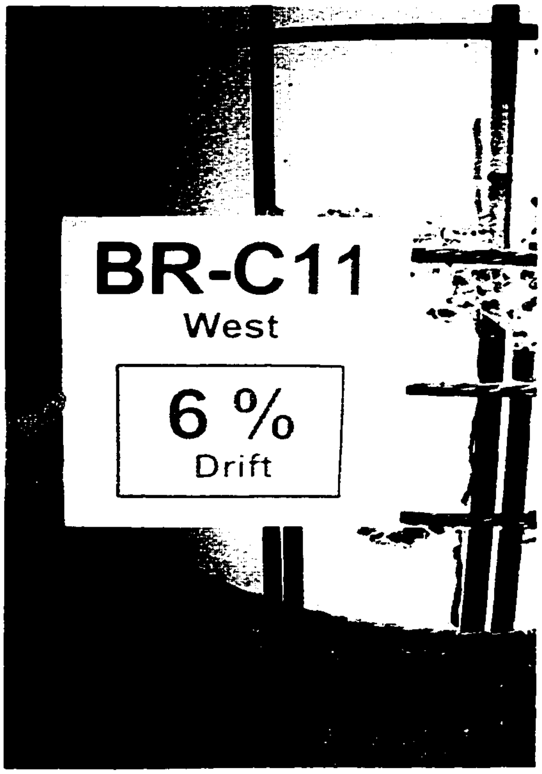

f) 6% drift, vertical crack formed in compression

g) 7% drift, large opening and slippage of the longitudinal reinforcement

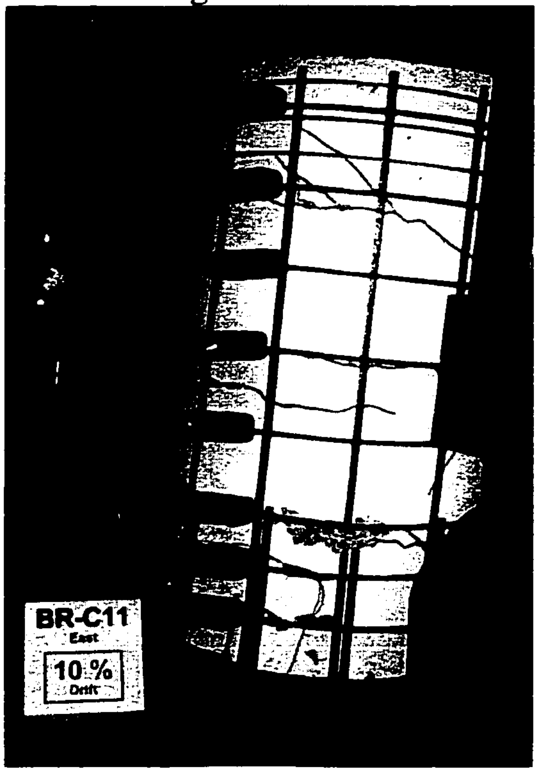

h) 10% drift

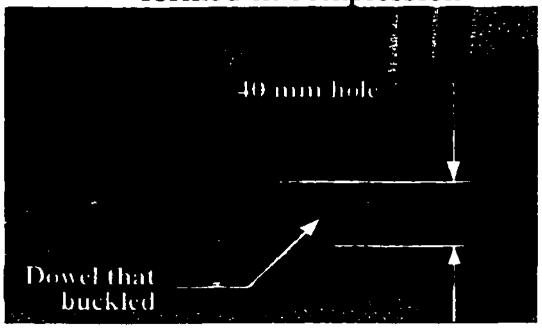

i) After the test

j) After the test, 4th prestressing strand embedded into the cover concrete

Figure 3.36 Behaviour of column BR-C11 (Continued)

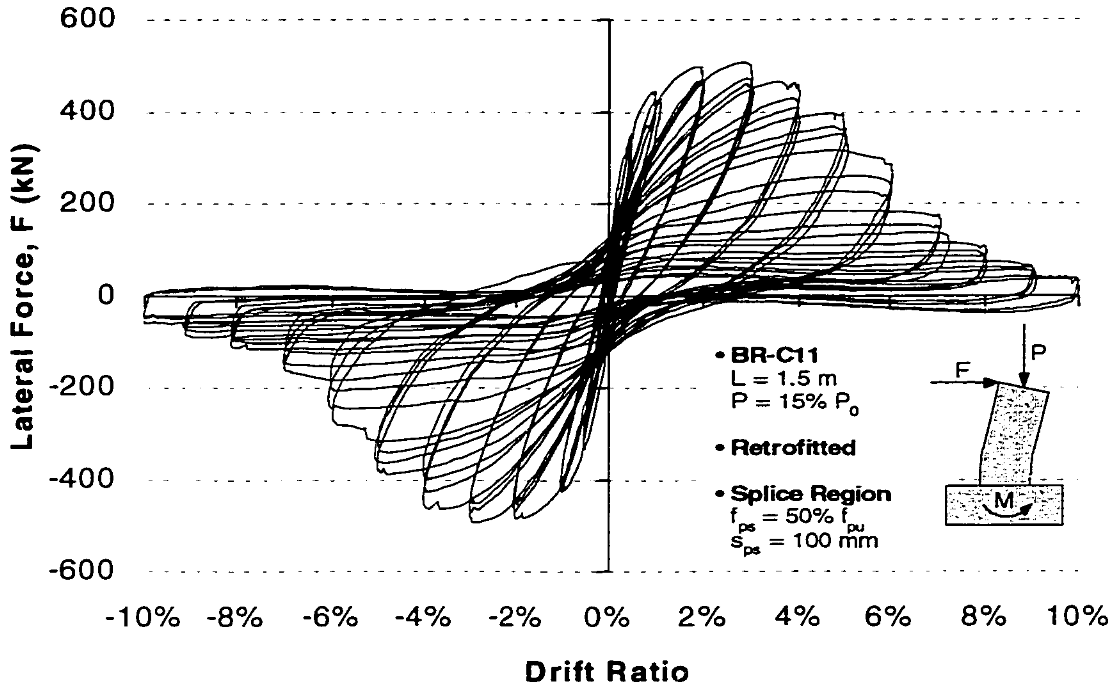

a) Force-Drift relationship

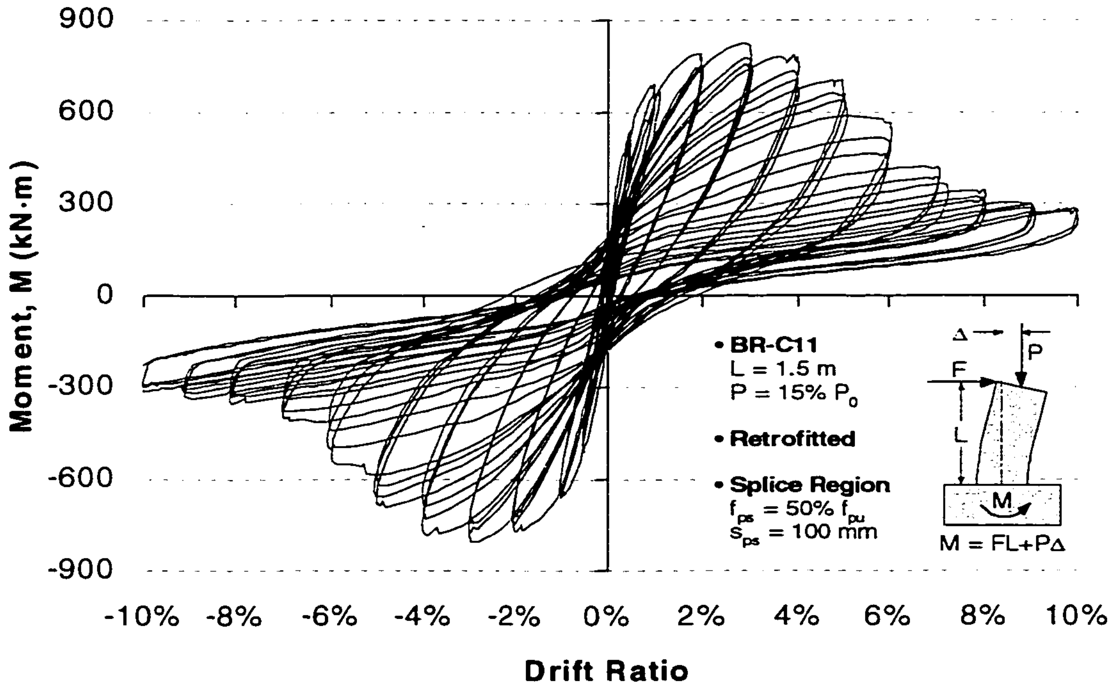

b) Moment-Drift relationship

Figure 3.37 Hysteretic relationships for column BR-C11

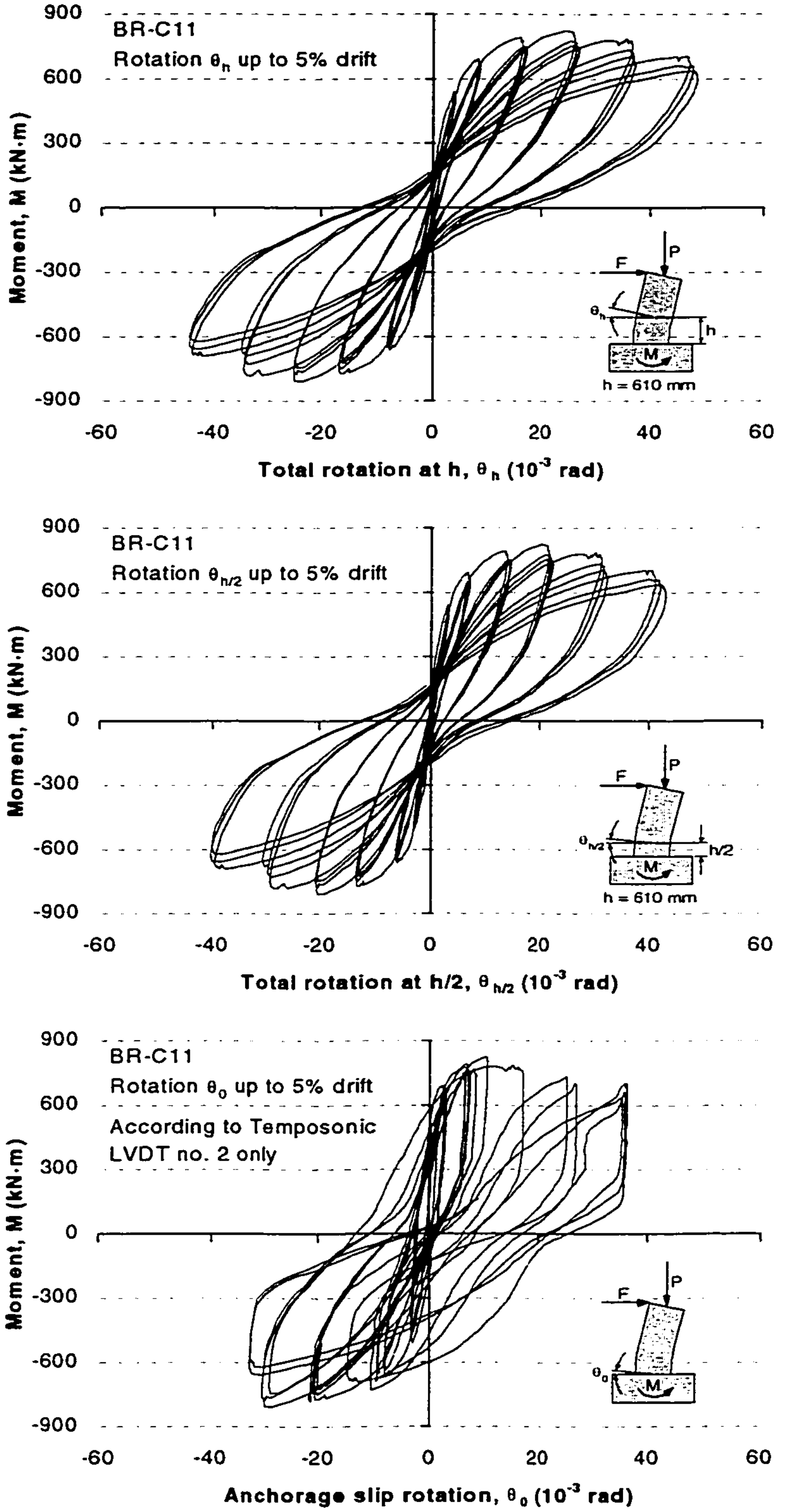

Figure 3.38 Rotation of the hinging region for column BR-C11

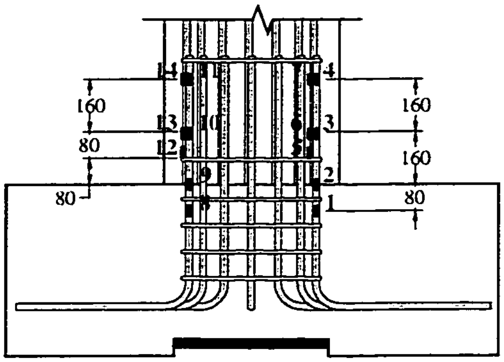

a) Strain gauge location on vertical bars

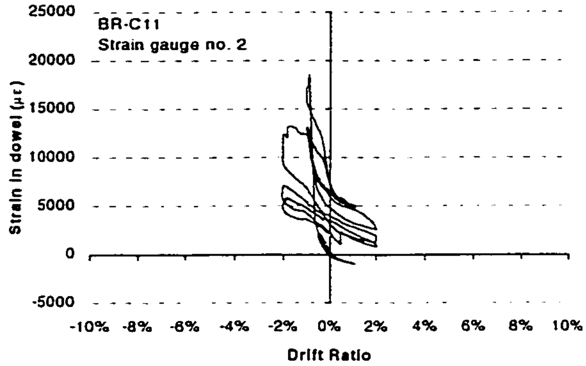

b) Strain gauge no. 2

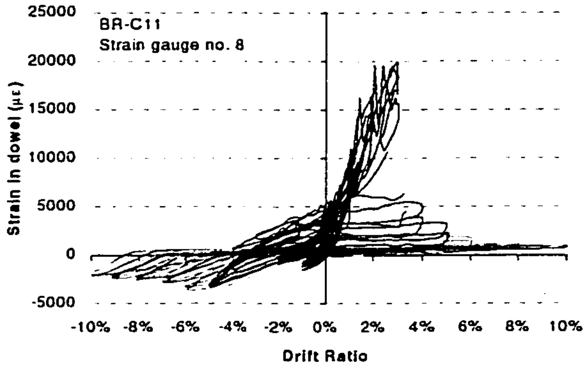

c) Strain gauge no. 8

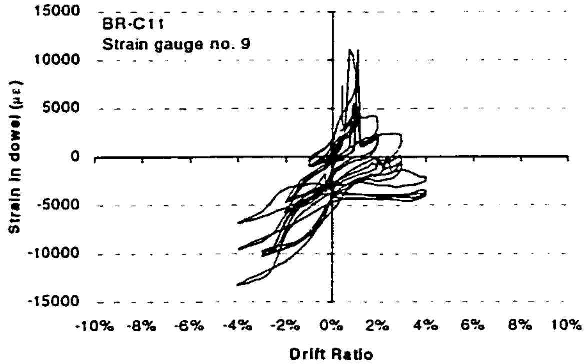

d) Strain gauge no. 9

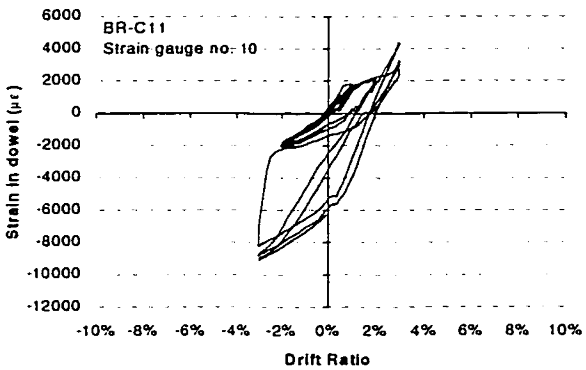

e) Strain gauge no. 10

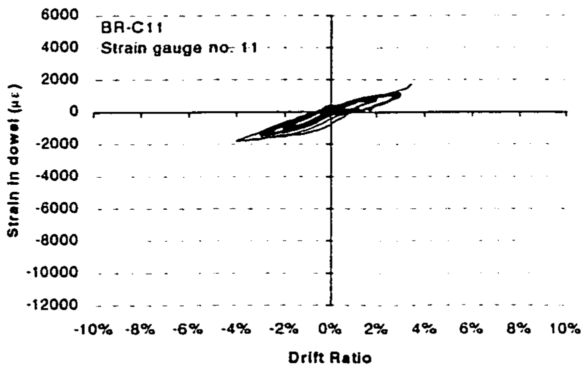

f) Strain gauge no. 11

Figure 3.39 Dowel strains for column BR-C11

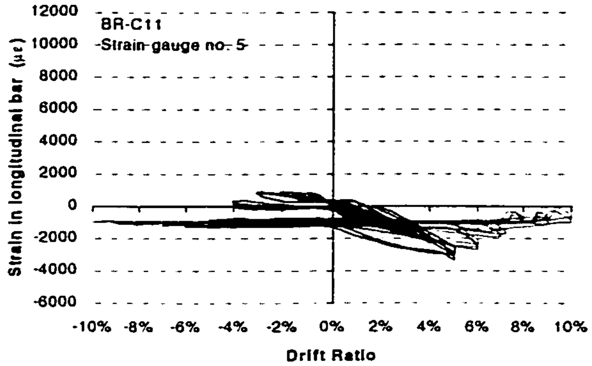

a) Strain gauge no. 5

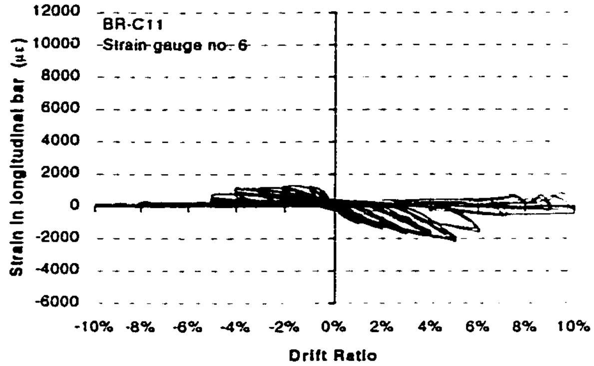

b) Strain gauge no. 6

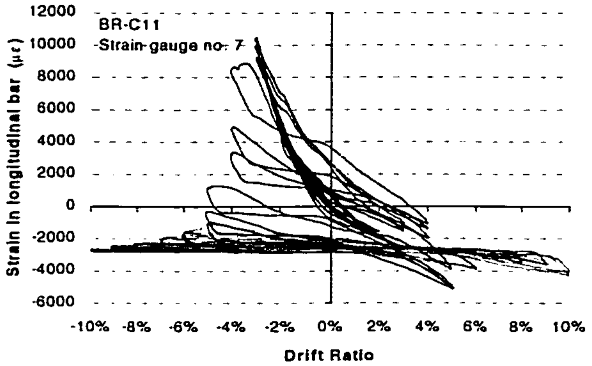

c) Strain gauge no. 7

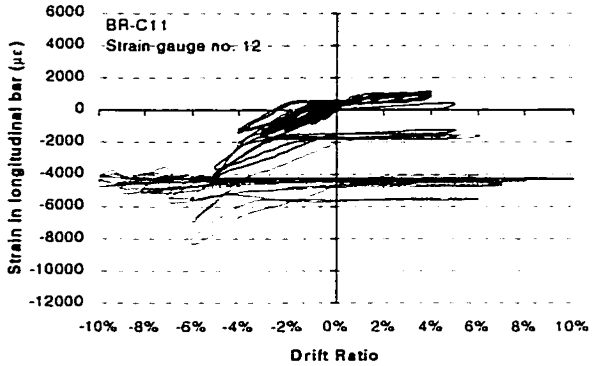

d) Strain gauge no. 12

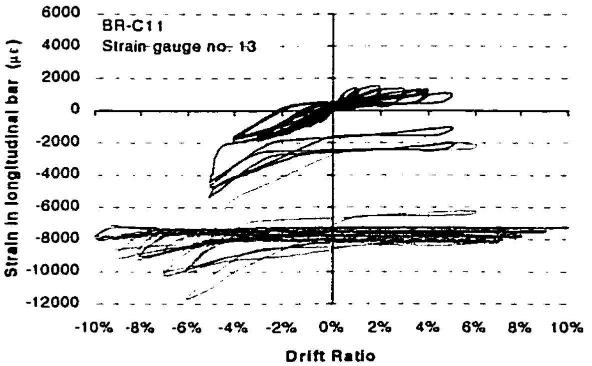

e) Strain gauge no. 13

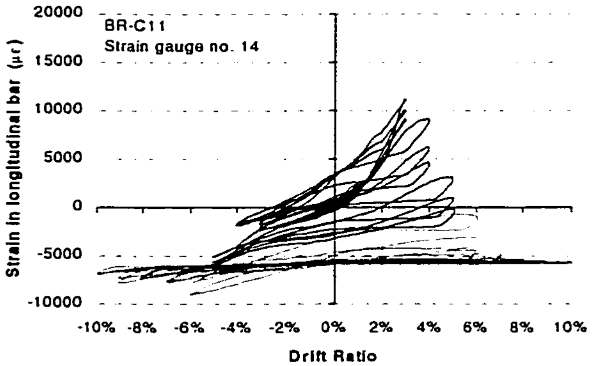

f) Strain gauge no. 14

Figure 3.40 Longitudinal reinforcement steel strains for column BR-C11

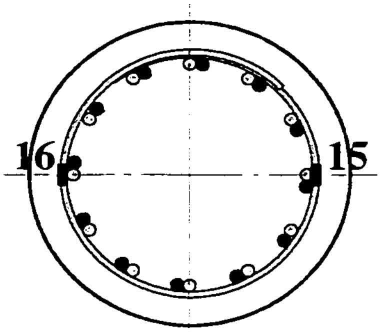

a) Strain gauge location on the 1st hoop

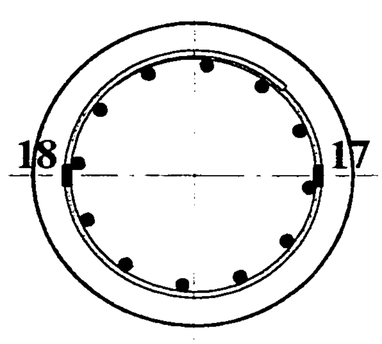

b) Strain gauge location on the 2nd hoop

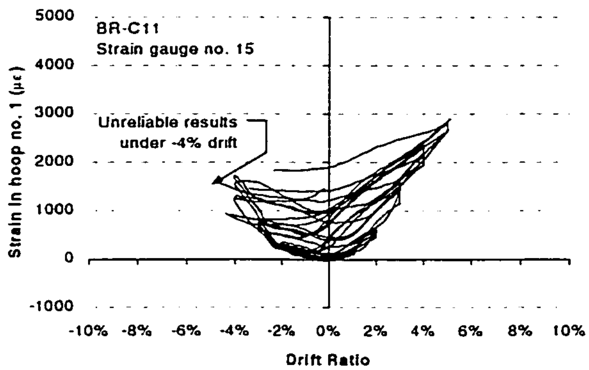

c) Strain gauge no. 15

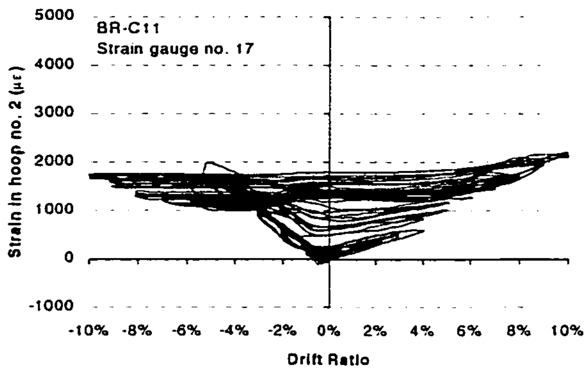

d) Strain gauge no. 17

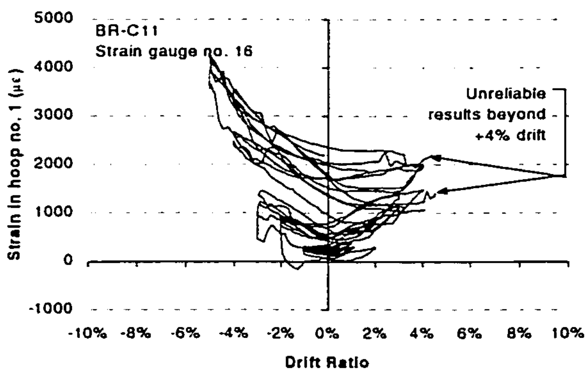

e) Strain gauge no. 16

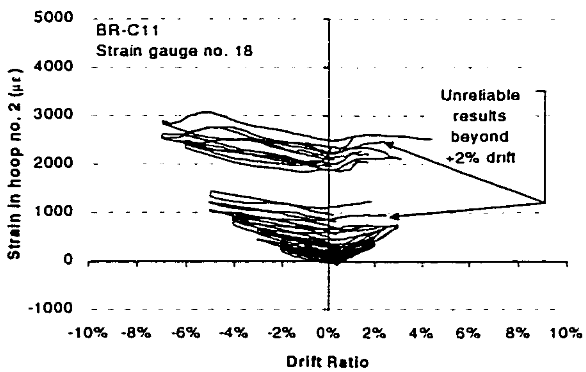

f) Strain gauge no. 18

Figure 3.41 Transverse reinforcement steel strains for column BR-C11

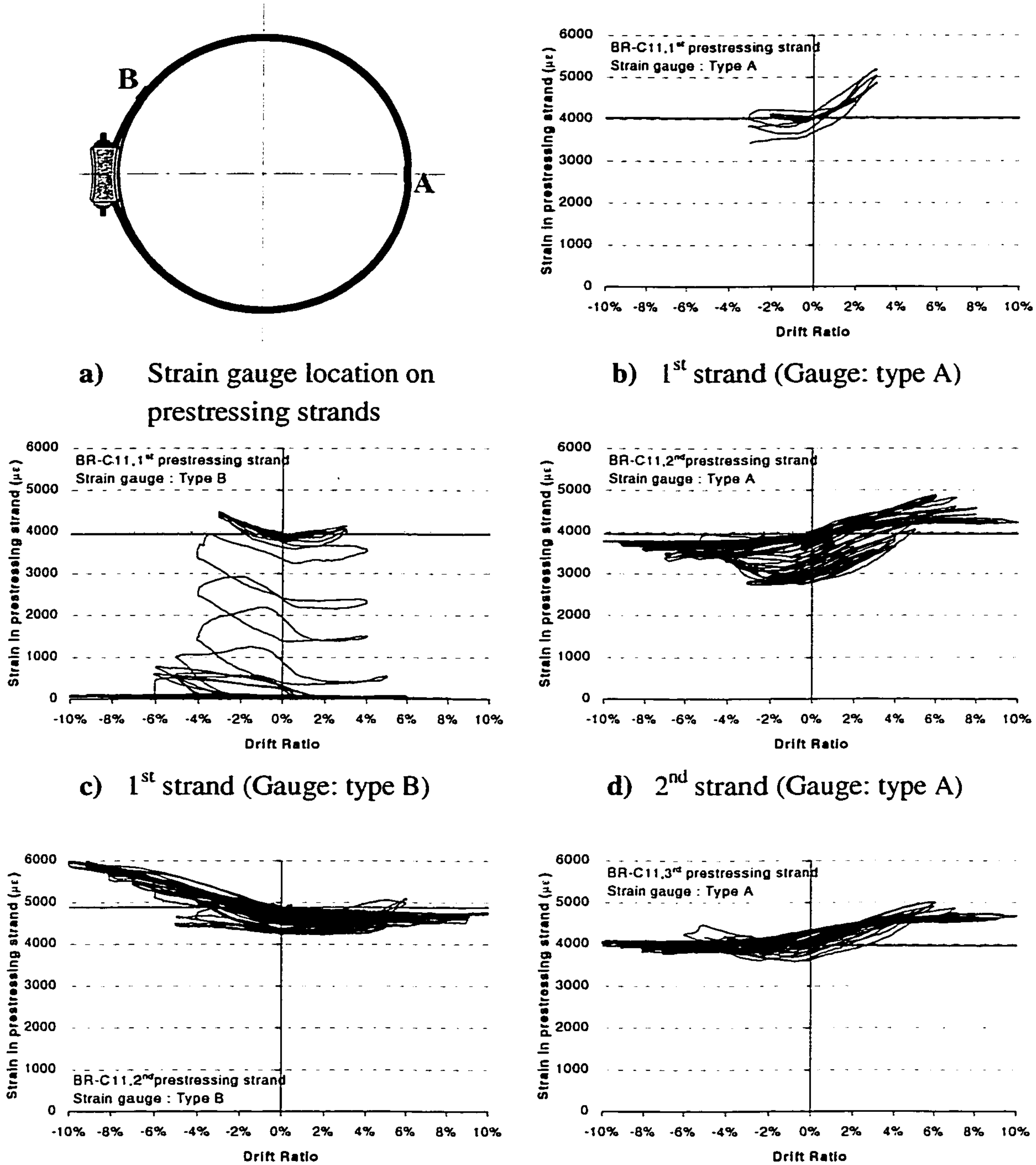

a) Strain gauge location on prestressing strands

b) 1st strand (Gauge: type A)

c) 1st strand (Gauge: type B)

d) 2nd strand (Gauge: type A)

e) 2nd strand (Gauge: type B)

f) 3rd strand (Gauge: type A)

Figure 3.42 Prestressing strand strains for column BR-C11

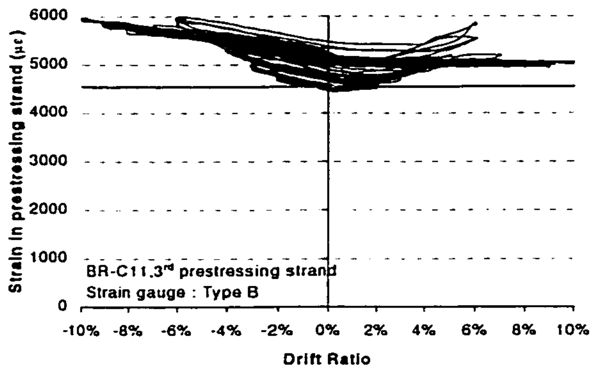

g) 3rd strand (Gauge: type B)

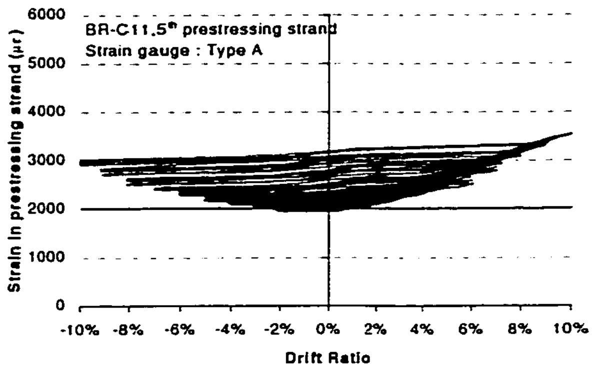

h) 5th strand (Gauge: type A)

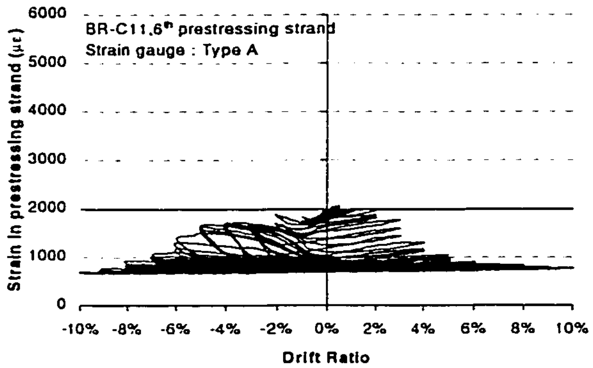

i) 6th strand (Gauge: type A)

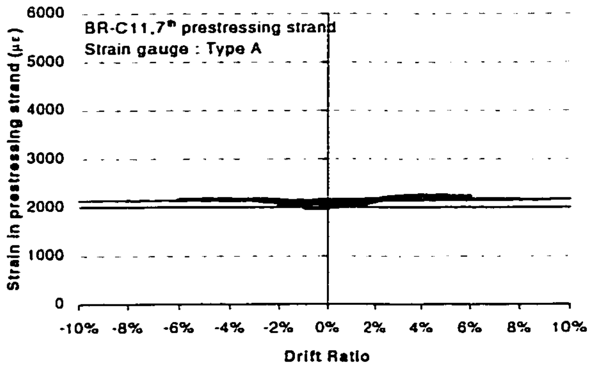

j) 7th strand (Gauge: type A)

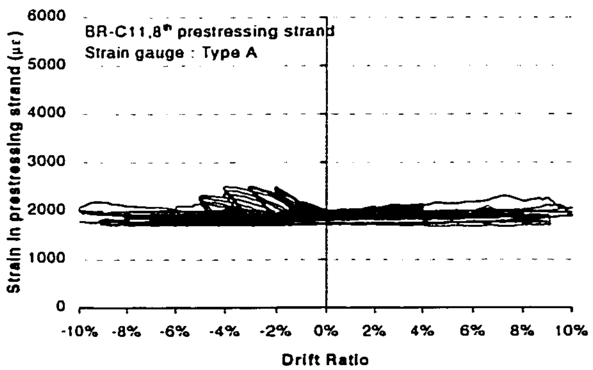

k) 8th strand (Gauge: type A)

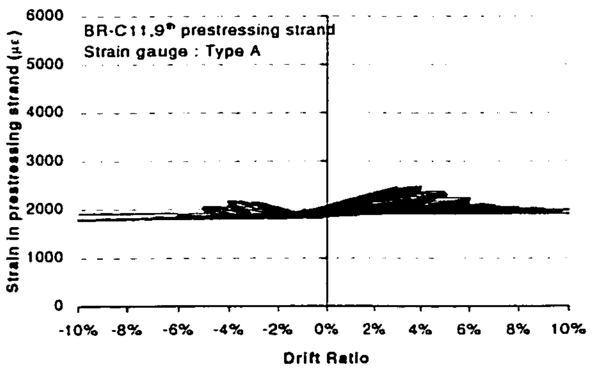

l) 9th strand (Gauge: type A)

Figure 3.42 Prestressing strand strains for column BR-C11 (Continued)

a) Column BR-C10 (South)

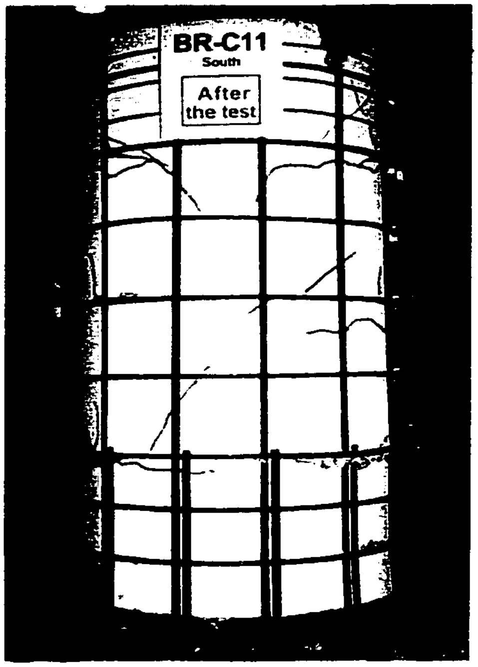

b) Column BR-C11 (South)

Figure 3.43 Comparison of columns BR-C10 and BR-C11 (After the test)

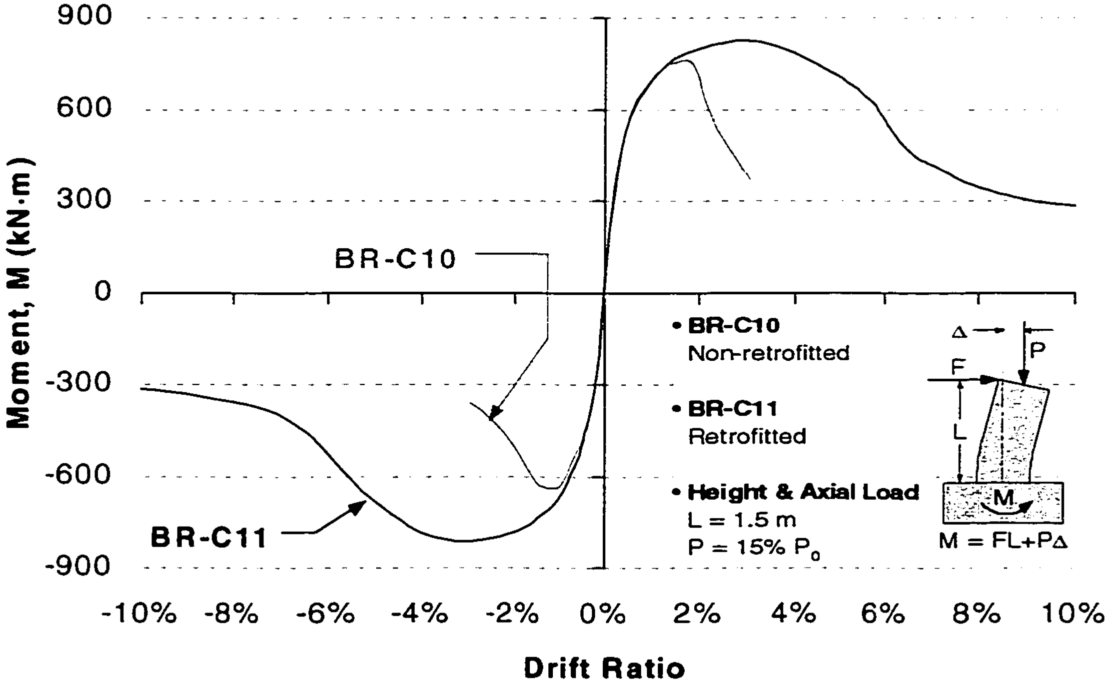

Figure 3.44 Moment-Drift envelope of columns BR-C10 and BR-C11

CHAPTER 4

EFFECTS OF TEST PARAMETERS AND COLUMN ANALYSIS

4.1 GENERAL

Failure mechanism, force and ductility capacities, as well as the comparison of six columns tested are presented and discussed in the previous chapter. The current chapter compares the six specimens with six others tested in the earlier phases of the same research program in order to assess the effectiveness of lap splices in potential plastic hinge regions of columns. The efficiency of the retrofitting strategies used in the splice region is also discussed. The columns tested in this project were analysed using computer software ***COLA***, developed at the University of Ottawa. The analytical results are compared to the experimental data recorded during testing.

4.2 EFFECT OF LAP SPLICE

The effect of insufficient lap splice length at the bottom of the columns is evaluated in this section. The behaviour of six other columns without lap splices is summarised. These columns were tested during the first and second phases of the same experimental investigation. The long columns, BR-C8, BR-C9, BR-S5 and BR-S6, are compared with companion columns BR-C6, BR-C7, BR-S3 and BR-S4 tested and analysed by Mes (1999). The two short columns, BR-C10 and BR-C11, are compared with two other specimens reported by Yalcin (1998) and labelled as BR-C1 and BR-C2.

The specimens tested by the previous researchers had similar geometry and reinforcing details as those presented in Chapter 3. The difference was the absence of longitudinal bar splicing. Otherwise, the reinforcing details were typical of the pre-1970's designed practice. The columns had twelve longitudinal bars continuous from the footing to the tip of the column, and were uniformly distributed along the perimeter. No. 10 hoops were spaced at 300 mm. The hoops for circular columns had overlapping ends, whereas the ends of the hoops used in square columns were bent 135°. The same retrofitting technique was used to strengthen the columns. Seven-wire strands of size 9 and grade 1860 MPa were installed around the columns, when retrofitted. They were spaced at 150 mm and prestressed to 25% of their ultimate strength f_{pu}. Other details for the columns tested in the earlier phases of the current research program are presented in Section 1.2.2.

4.2.1 LONG CIRCULAR COLUMNS

The long circular columns BR-C6 and BR-C7 tested by Mes (1999) had the same reinforcing details as for the specimens BR-C8 and BR-C9, except that the longitudinal reinforcement was continuous from inside the footing to the column. The diameter was 508 mm and the effective height was 2.0 m. The Moment-Drift hysteretic relationships of pairs of companion columns without retrofitting and with retrofitting are plotted in Figs. 4.1 and 4.2, respectively for comparison.

During testing of the as-built column, BR-C6, some flexural cracks formed at ½% drift. The longitudinal bars yielded at 1% drift cycles. The peak capacity occurred during the initial cycle at 2% drift, and reached an effective lateral load of about 221 kN and the corresponding moment capacity of 492 kN·m. Some shear cracks formed on the side faces of column at 2% drift. The column was considered to have failed at 3% drift because the lateral load dropped below 80% of peak. The longitudinal reinforcement buckled during the last cycle at 3% drift and the column collapsed. The failure was explosive.

Column BR-C8, with spliced bars, also reached the yield moment at 1% drift, but the maximum strength was at least 15% lower than the peak resistance of column BR-C6 without lap splice. The drift capacity of specimen BR-C8 was limited to 1%, instead of the 2% attained in BR-C6. The column with starter bars did not collapse, although a significant strength decay occurred at 2% drift due to the slippage of longitudinal reinforcement.

Columns BR-C7 and BR-C9 were both retrofitted with strands spaced at 150 mm and prestressed to 25% f_{pu}. The continuous reinforcement of the strengthened column BR-C7 yielded under cyclic loading at 1% drift. The lateral capacity reached a peak load of about 231 kN and a peak moment of 512 kN·m during the first cycle at 2% drift. The flexural capacity withstood up to 4% drift, but dropped by more than 20% at 5% drift. The specimen was considered to have failed at 5% drift, although the test was continued up to 6% drift. The column had a gradual failure. Figure 4.3 shows that the damage on specimen BR-C7 was minor compared to the as-built column BR-C6.

The retrofitted column BR-C9 with spliced reinforcement reached a similar flexural capacity as that for BR-C7. In fact, both retrofitted columns reached 477 kN·m when they were pulled. When they were pushed, however, the flexural capacity of BR-C7 exceeded the peak moment of specimen BR-C9 by 6%. The strengthened column with spliced reinforcement (BR-C9) could not maintain the peak moment after 2% drift. Its drift capacity was 2%, instead of the 4% observed for BR-C7.

Figure 4.4 illustrates Moment-Drift envelopes for the four long circular columns. The presence of lap splice at the bottom of long circular columns did not modify the stiffness. Although the retrofitting technique improved the column behaviour, the drift capacity was much lower for column BR-C9 than for BR-C7 because bond at lap splice started to deteriorate beyond the peak capacity. It is a sign that the clamping pressure was not sufficient and the confinement in the splicing region was not adequate.

4.2.2 LONG SQUARE COLUMNS

Mes (1999) tested another pair of long columns. The two specimens tested were labelled BR-S3 and BR-S4, and had a square cross-section of 500 mm × 500 mm, a shear span of 2.0 m. They were both reinforced with continuous longitudinal bars, starting from inside the footing and continuing up to the tip of the column. Figs. 4.5 and 4.6 show hysteretic Moment-Drift relationships for non-retrofitted (BR-S3 and BR-S5) and retrofitted columns (BR-S4 and BR-S6) to evaluate the difference in behaviour between columns with and without lap splices.

Column BR-S3, with continuous bars, had flexure dominant behaviour. The flexural cracks formed at ½% drift and became wider at 1% drift. The longitudinal reinforcement yielded at 1% drift. The column reached its maximum capacity during the first cycle at 2% drift. The peak effective lateral load was about 285 kN and the peak flexural capacity was approximately 630 kN·m. The column failed during the last cycle at 3% drift, since the lateral load could not maintain 80% of the maximum capacity. The resistance dropped during the initial cycle at 4% drift as the longitudinal reinforcement buckled and the column collapsed.

Column BR-S5, with starter bars, had a lower capacity than the companion column with continuous bars (BR-S3). The longitudinal bars of both columns yielded at 1% drift. The resistance of BR-S5 reached the peak value at 1% drift, but dropped under cyclic loading at 2% drift because the spliced bars started to slip. Its drift capacity was 1% instead of the 2% observed in BR-S3 with continuous reinforcement.

Mes retrofitted square column BR-S4 with prestressing strands spaced at 150 mm and stressed to 25% f_{pu} covering the bottom half of shear span. The yield capacity was reached at 1% drift. The flexural cracks started to widen during cycles at 2% drift and some shear cracks formed on the side of the column. The peak lateral load was approximately 273 kN at 2% drift. The peak flexural capacity was about 604 kN·m, and was maintained at 2% and 3% drift cycles. No major drop occurred in load resistance until 5% drift. The column was considered to have failed after the last cycle at 5% drift, since the lateral load became lower than 80% of peak. The concrete deterioration of BR-S4 was slow and essentially limited to the first 150 mm. The retrofitted column BR-S4 was subjected to less damage than the as-built column, BR-S3 (see Fig. 4.7).

The column with spliced reinforcement, BR-S6, was retrofitted and had a similar strength to that of BR-S4 with continuous bars. In fact, the capacity of BR-S6 was a little bit lower (4%) than the capacity of BR-S4, as the columns were pulled, but it was higher when the columns were pushed (9%). BR-S6 failed during the second cycle at 5% drift and BR-S4 failed after the last cycle at 5% drift.

Figure 4.8 illustrates Moment-Drift envelopes for the four long square columns and shows that inadequate splicing at the bottom of the columns did not significantly change the column stiffness. The seismic behaviour of both retrofitted specimens BR-S4 and BR-S6 was improved since the ductility and the energy dissipation increased. The strength and the shape of the Moment-Drift envelope were similar up to 6% drift for both retrofitted columns. It indicates that the clamping pressure provided by the strands in the splicing region was sufficient to prevent a complete loss of bond strength. The retrofitting layout seemed to provide enough confinement to compensate for the inadequate lap splice length.

4.2.3 SHORT CIRCULAR COLUMNS

The behaviour of columns BR-C1 and BR-C2, tested by Yalcin (1998) are summarised in this subsection. These specimens had a circular cross-section of 610 mm in diameter and an effective height of 1.485 m. The column aspect ratio was selected to produce shear dominant behaviour. No. 25 bars were used as longitudinal reinforcement, which was continuous from the footing to the tip of the columns. Figs. 4.9 and 4.10 show the hysteretic Moment-Drift relationships for non-retrofitted (BR-C1 and BR-C10) and retrofitted columns (BR-C2 and BR-C11) to evaluate the difference in behaviour between columns with and without lap splices. Since the columns with continuous reinforcement had no. 25 bars and the columns with lap splice had no. 20 bars, their capacity were not the same. Instead of comparing their capacity, the overall behaviour and the shape of the Moment-Drift relationships are compared. Note that a different scale is used for columns BR-C1 and BR-C2 than for columns BR-C10 and BR-C11 in Figs. 4.9 and 4.10.

Although the as-built column BR-C1 failed due to shear, some flexural cracks formed at ½% drift. Major diagonal shear cracks appeared during cycles at 1% drift. Peak lateral load and moment of 560 kN and 858 kN·m were respectively reached at 1% drift. The column could not complete the first cycle at 2% drift because a large shear crack formed and the longitudinal bars buckled. The failure of BR-C1 was brittle and sudden. The drift capacity was only 1%.

Column BR-C10, with spliced reinforcement, also had a drift capacity of 1%. The peak capacity was reached during the first cycle at 2% drift but dropped by 50% during the following two cycles due to the slippage of reinforcement. As compared to BR-C1, the collapse of BR-C10 was delayed and occurred after the last cycle at 3% drift. The failure of BR-C10 was also sudden and brittle.

The seismic behaviour of column BR-C2, with continuous reinforcement, improved due to retrofitting. Once again, external prestressing strands were used to strengthen the column. The strands were prestressed to 25% f_{pu} and spaced at 150 mm over the entire height of the specimen. During the test, the cracks were completely eliminated up to the last cycle at 1% drift. Some hairline flexural cracks appeared at 2% drift. At this stage of loading, the column reached its peak capacity. The maximum effective lateral load was about 614 kN and the flexural capacity was approximately 965 kN·m. The failure mode was no longer governed by shear, as in companion non-retrofitted column BR-C1, but by flexure. Only some hairline shear cracks were visible at 4% drift. The column was considered to have failed at 5% drift. The test continued up to the first cycle at 6% drift when the longitudinal bar started to buckle. Although the longitudinal reinforcement of BR-C2 buckled, the column has been subjected to less damage than its companion BR-C1, as shown in Fig. 4.11.

The drift capacity of both retrofitted specimens BR-C2 and BR-C11 was 4%. The peak capacity of column BR-C11 occurred at 3% drift. The peak capacity cannot be compared because of the different bar sizes that were used. The shape of the Moment-Drift envelope could be compared as long as the moment axis is normalised (dividing the moment by the peak moment). This was done for BR-C1 and BR-C2 to illustrate the improvement of the strengthened columns compared to companion as-built columns. The same normalisation was done for specimens BR-C10 and BR-C11. Figure 4.12 shows the normalised Moment-Drift envelopes of the four short circular columns. The retrofitting strategy improved the seismic behaviour of both retrofitted columns BR-C2 and BR-C11. The retrofitting allowed the formation of a plastic hinge at the bottom of the columns. The envelope of the strengthened columns is similar. It is an indication that the confinement provided by the external prestressing strands was sufficient to make up for the inadequate lap splice length of the column BR-C11. The retrofitting considerably increased the ductility and the energy dissipation of the columns with and without lap splice.

4.2.4 SIMILARITIES BETWEEN COLUMN BEHAVIOUR

From the analysis and comparison of twelve columns tested in the entire research program, some similarities were observed among different sets of columns. The following is not an exhaustive list of these similarities between columns with and without lap splices, but it presents similarities that repeated at least twice among the three sets of columns (long circular, long square, and short circular columns). The first list provides the effect of lap splice on as-built columns. The second list presents the behaviour of retrofitted columns with or without lap splices.

AS-BUILT COLUMNS

- Lower strength due to insufficient lap splice length.
- Significant strength decay at 2% drift due to lap splice debonding.
- Lower drift capacity for the long columns; similar drift capacity for short columns.
- Less ductility and energy dissipation for the long columns; similar ductility and energy dissipated for the short columns.

COLUMNS RETROFITTED WITH EXTERNAL PRESTRESSING STRANDS

- Formation of a plastic hinge at the bottom of the column.
- Similar peak capacity.
- Similar drift capacity (excluding BR-C9).
- Similar energy dissipation (excluding BR-C9).

It should be recalled that the retrofitted column BR-C9 did not have similar drift and energy dissipation characteristics as column BR-C7, because the confinement (clamping force) in the splicing region was not sufficient.

All the columns with inadequate lap splices could reach their flexural capacity M_y, even if they were not retrofitted. Finally, the stiffness for each set of columns was similar whether or not the column had starter bars.

4.3 EFFECT OF RETROFIT ARRANGEMENT

The results obtained from the column tests reported in this research program show that retrofitting non-ductile columns with external prestressing strands does improve the seismic behaviour, as long as enough lateral clamping force is provided. Yalcin (1998) tested and analysed the behaviour of shear dominant columns with a circular cross-section of 610 mm and a square cross-section of 550 mm. He concluded that the best results were provided by prestressing strands spaced at 150 mm and stressed to 25% f_{pu}. Mes (1999) showed that flexural dominant columns with a circular or a square cross-section of about 500 mm could also effectively be retrofitted with prestressing strands spaced at 150 mm and stressed to 25% f_{pu}.

The current research project emphasized the effect of prestressing strands on columns with inadequate lap splices in potential hinging regions (near the base). Specimens with circular and square cross-sections were investigated as well as long and short columns. Column BR-C9 was retrofitted with the same arrangement as that used by Yalcin (1998) and Mes (1999). Test data showed that the retrofitting strategy was less effective in the splicing region where the lap splice length was only 20 times the longitudinal bar diameter. Using prestressing strands spaced at 150 mm and stressed to 25% f_{pu} for column BR-C9 provided lateral confinement pressure f_l of 0.63 MPa. In order to increase the clamping pressure, the spacing was reduced to 100 mm and the stress level increased to 50% f_{pu} in the splice region of retrofitted columns (BR-S6 and BR-C11), resulting in lateral pressure three times higher. The increased confinement provided much better results. The lateral pressure applied for each strengthened column is summarized in Table 4.1.

Table 4.1 Lateral pressure f_l applied on the retrofitted columns

Retrofitting Arrangement		**Long Circular Column**	**Long Square Column**	**Short Circular Column**
Stress Level	**Spacing**			
25% f_{pu}	150 mm	0.63 MPa	0.64 MPa	0.53 MPa
50% f_{pu}	100 mm	—	1.92 MPa	1.57 MPa

Retrofitting columns with prestressing strands performed very well for long and short columns with and without lap splices. For the circular columns, the prestressing strands can be installed directly on the concrete, whereas for the square columns, some raisers have to be introduced between the strand and column surface to confine the column as uniformly as possible. Strands spaced at 100 mm and prestressed to 50% f_{pu} in the splicing region provided the best results.

4.4 COLUMN ANALYSIS

A ***COL****umn* ***A****nalysis* software named ***COLA*** was developed by Yalcin (1999), and was used to compute strength and deformation of six columns tested in this research project. The experimental data were compared to the analytical results to evaluate if the predicted deformation at failure and the strength of the column were close to the actual values, since the program did not consider lap splice of the longitudinal reinforcement.

COLA was developed to evaluate the force-displacement and moment-displacement relationships of a reinforced concrete column under constant compression and monotonic lateral loading. The drift ratio at failure could be established from the results of circular, square and rectangular cross-sections. The software first analysed the sectional behaviour of column to compute moment-curvature relationship. Important features of inelastic material models were used; such as confinement, anchorage slip and buckling of longitudinal bars. ***COLA*** also took into account the P-Δ effect, as well as the formation and progression of plastic hinging in the column. Two input files were required to evaluate the inelastic behaviour of columns. The first one included column geometry and reinforcement details, and the second included material properties and the level of constant axial load. The data obtained from testing concrete cylinders and steel coupons (see Section 2.4) were used to describe the material properties. Once the analysis was completed, all the output used by the software were available for further investigation.

The computer program ***COLA*** was not intended to analyze columns retrofitted with external prestressing strands, so realistic approximations had to be introduced in the input files. These approximations included the simulation of the additional confinement action provided by the strands, and could be specified as the contribution of transverse reinforcement. The software modelled passive confinement provided by internal hoops, but not the active confinement produced by external prestressing, so the active confinement had to be neglected.

The moment-drift relationship computed by ***COLA*** is based on monotonic loading, but researchers showed that the monotonic curve was a good estimation of the envelope of the hysteretic relationship (Fafitis and Shah, 1985 and Saatcioglu, Salamat and Razvi, 1995). This section compares the computed response with that recorded during testing. At the end of the chapter, the hysteretic Moment-Drift relationships are plotted and compared to the monotonic Moment-Drift curves computed by the software. The drift ratio at failure is determined from these graphs as the drift at which the flexural capacity drops to 80% of the peak moment. Note that the strength decay does not include the P-Δ effect, in Moment-Drift relationships.

4.4.1 COLUMN BR-C8

Moment-Drift relationships computed by ***COLA*** and recorded during the test are plotted in Fig. 4.13. The relationships show that the analytical behaviour of non-retrofitted column BR-C8 was very similar to the actual behaviour, up to the peak capacity. The maximum predicted flexural resistance was close to the experimentally recorded value, although the capacity was overestimated beyond 1% drift. Such an analytical inelastic response was anticipated because the software could not model the splicing of the longitudinal reinforcement. The difference in capacity occurred at 2% drift as the lap splice de-bonded. Once the reinforcement started to slip, the descending branch of the Moment-Drift relationship had the same slope experimentally and analytically. ***COLA*** indicated that the column failed at 2.7% drift, since moment resistance decreased to 80% of peak flexural capacity at this stage. The drift level at failure was overestimated since column BR-C8 failed at 2% drift during the test. The larger computed deformation at failure was expected because of lack of modelling of the lap slice in ***COLA***.

4.4.2 COLUMN BR-C9

The effects of prestressing strands were input in analysing column BR-C9, as contributions of transverse reinforcement to simulate the behaviour of a retrofitted column. Unfortunately, the lateral pressure provided by the strands into the software was passive confinement, instead of active confinement. The computer program underestimated the peak flexural capacity by about 9%. It may be argued that the difference in capacity was caused by the differences in active and passive pressure effects on column.

The analytical response was very accurate up to 1% drift, as illustrated in Fig. 4.14. During the test, it was observed that bond was destroyed at 3% drift, causing the slippage of longitudinal reinforcement. It was at this drift level that the software overestimated the resistance. The analytically computed drift capacity was 4.3% as compared with 3% observed experimentally at 80% of peak resistance.

4.4.3 COLUMN BR-S5

Analytical Moment-Drift relationship generated by ***COLA*** is compared with Moment-Drift hysteretic relationship measured during the test in Fig. 4.15. The computed response correlated well with measured response until the peak capacity of ¾% drift was attained. The measured peak flexural capacity was higher by about 5% of the maximum analytical resistance. The actual capacity dropped below the computed capacity during the first cycle at 2% drift as the longitudinal reinforcement started to slip. The analytical drift capacity was 2.4% as compared to 2% measured during the test.

4.4.4 COLUMN BR-S6

The software ***COLA*** was not intended to evaluate the behaviour of retrofitted columns. Even though the square column BR-S6 did not have cross-ties, closely spaced cross-ties were added to the analytical model to simulate the confinement effect provided by external prestressing. Analytical and experimental Moment-Drift relationships of specimen BR-S6 are compared in Fig. 4.16. The response was the same in both cases up to the ¾% drift level. The computed peak flexural capacity was 81% of the peak capacity measured during the test. Since the software could only model passive confinement, the active confinement that was provided by the prestressing strands had to be neglected. This approximation was most likely responsible for this difference of 19% between the peak capacities. The analytical drift capacity was 4.7% as compared with 6.0% measured during the test.

4.4.5 COLUMN BR-C10

Analytical and experimental inelastic responses of column BR-C10 are shown in Fig. 4.17 in terms of Moment-Drift relationships. The computed resistance and the experimental capacity were the same until ½% drift. The peak moment determined by the software was 80% of the peak flexural capacity measured during testing. The double reinforcement due to the splicing at the bottom of the column could be responsible for this underestimation of 20% since the software did not model the lap splice. Such a difference was not observed for the two long as-built columns.

COLA analyzed the column as if the longitudinal bars were continuous and estimated failure of the column at 1.8% drift. The lateral drift level at failure was slightly underestimated by the software as failure of the column occurred at 2% drift during testing. Similar trends of failure deformations were obtained for short non-retrofitted columns, with and without lap splice, as presented in section 4.2.3 (comparison of recorded data for BR-C10 to BR-C1).

4.4.6 COLUMN BR-C11

Analytical and experimental behaviour for column BR-C11 were similar up to ¾% drift, as illustrated in Fig. 4.18. The software computed a peak load corresponding to 78% of the actual peak flexural capacity. Two factors could explain this underestimation of 22%.

First of all, the software considered twelve longitudinal continuous bars but in reality there was twice the amount of reinforcement at the bottom of the column due to the lap splice. Secondly, the active confinement was neglected in the analysis. The computer program estimated that the drift capacity at failure was 4.1%. During the test, failure of the column occurred at 5% drift.

4.4.7 SUMMARY OF THE COLUMN BEHAVIOUR COMPUTED BY COLA

The software ***COLA*** is a powerful tool to evaluate the maximum strength and deformation at failure of a conventional reinforced concrete column with continuous bars. The following summarizes the observations previously mentioned from the analysis of six columns. These observations are based on the comparisons made between the analytical and experimental results, and provide some insight as to whether software can be used to determine seismic adequacy of an existing column with lap splices. The analytical results as compared to experimental data were:

- Similar up to the computed peak moment and showed similar stiffness (for the ascending branch);
- Slightly lower in strength for long as-built columns;
- Lower in strength for both short columns. This was probably because the lap splice at the bottom of the column was not modelled, though provided twice the amount of reinforcement used in the analysis;
- Lower in strength for the retrofitted columns probably because the active confinement was not modelled in the analysis;
- Higher in lateral deformation at failure of the long as-built columns because the lap splices were not modelled;
- Similar in terms of deformation at failure of the short as-built column even if the analysis did not model the reinforcement splice;
- Lower in deformation at failure for retrofitted columns except for column BR-C9, which was not properly confined in the splicing region.

The peak flexural capacities, measured experimentally and computed with ***COLA***, are summarised in Table 4.2. The table also includes the drift levels at failure. These values were established from the data presented in Figs. 4.13 to 4.18. Therefore, the P-Δ effect was not considered as part of the strength decay. In comparison, Table 4.3 shows the peak lateral load and the drift ratio at failure determined analytically by the software or experimentally from graphs shown in Chapter 3. Results in Table 4.3 include the P-Δ effect in strength decay.

Table 4.2 Experimental and analytical results *excluding* P-Δ effect

COLUMN	EXPERIMENTAL		ANALYTICAL	
	PEAK MOMENT	FAILURE*	PEAK MOMENT	FAILURE*
BR-C8	420 kN·m	2%	415 kN·m	2.7%
BR-C9	481 kN·m	3%	440 kN·m	4.3%
BR-S5	569 kN·m	2%	539 kN·m	2.4%
BR-S6	661 kN·m	6%	537 kN·m	4.7%
BR-C10	746 kN·m	2%	595 kN·m	1.8%
BR-C11	825 kN·m	5%	645 kN·m	4.1%

* Drift ratio at failure illustrates the column deformation as the moment capacity decreased to 80% of the peak flexural resistance.

Table 4.3 Experimental and analytical results *including* P-Δ effect

COLUMN	EXPERIMENTAL		ANALYTICAL	
	PEAK LOAD	FAILURE**	PEAK LOAD	FAILURE**
BR-C8	195 kN	2%	198 kN	1.9%
BR-C9	221 kN	3%	209 kN	2.4%
BR-S5	271 kN	2%	259 kN	1.8%
BR-S6	295 kN	5%	258 kN	2.0%
BR-C10	470 kN	2%	389 kN	1.5%
BR-C11	507 kN	5%	418 kN	2.5%

** Drift ratio at failure illustrates the column deformation as the lateral load resistance decreased to 80% of the peak lateral load.

The analytical drift ratios at failure, shown in Table 4.2, were more reliable and closer to the experimental results than the analytical drift level in Table 4.3. For instance, the analytical drift ratio of long columns without retrofitting should have been higher than the experimental values because the computer program did not model lap splices, but they were slightly underestimated in Table 4.3. It would be recommended to exclude the P-Δ effect from strength decay while determining the drift capacity with software ***COLA***.

According to the analysis of the three as-built and three retrofitted columns, the current version of ***COLA*** should not be used to accurately determine the behaviour of a retrofitted column with lap splice reinforcement. However, the computer program can provide guidance to engineers as to whether an existing column with lap splices require retrofitting or not.

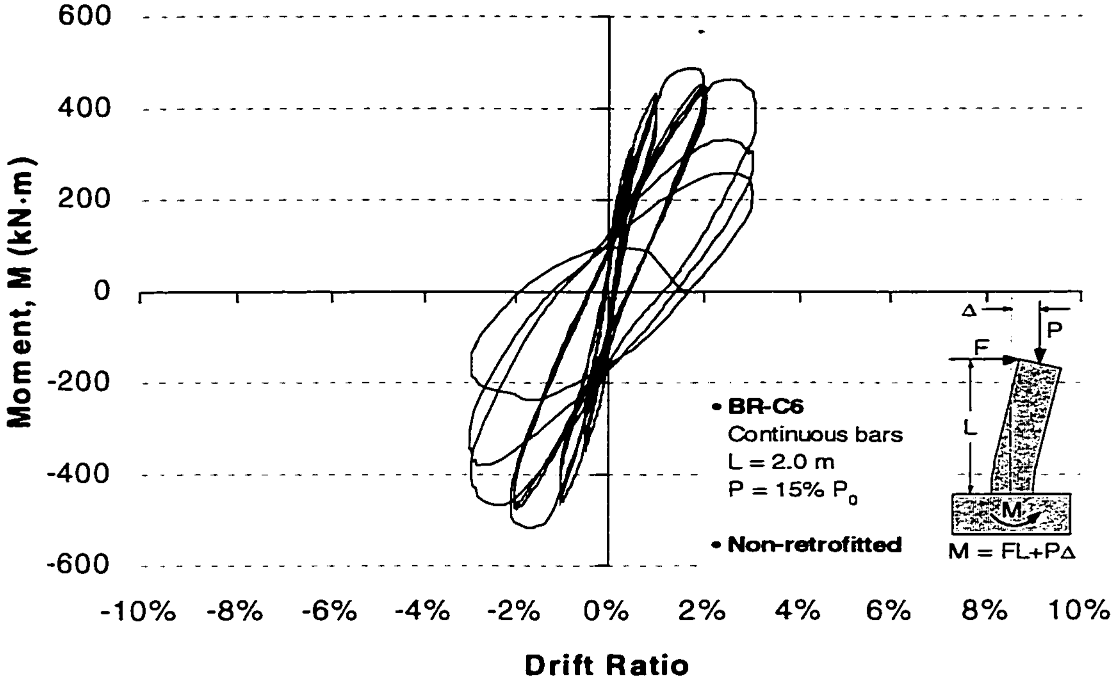

a) Column BR-C6 with continuous bars

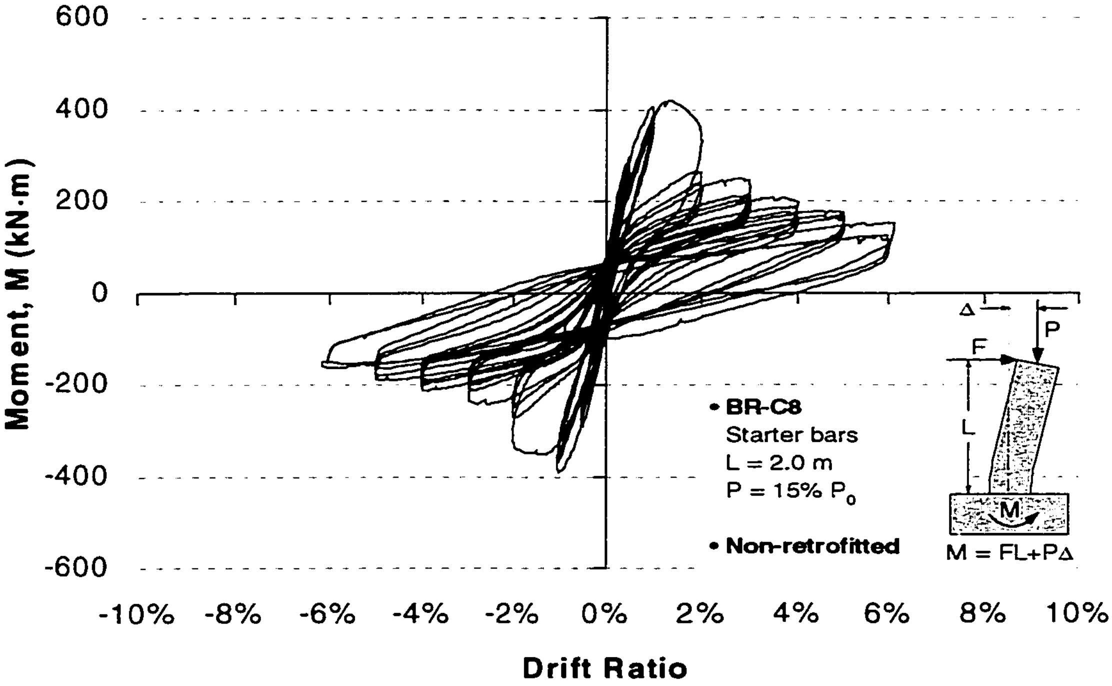

b) Column BR-C8 with lap spliced bars

Figure 4.1 Moment-Drift hysteretic relationships of the as-built columns BR-C6 and BR-C8

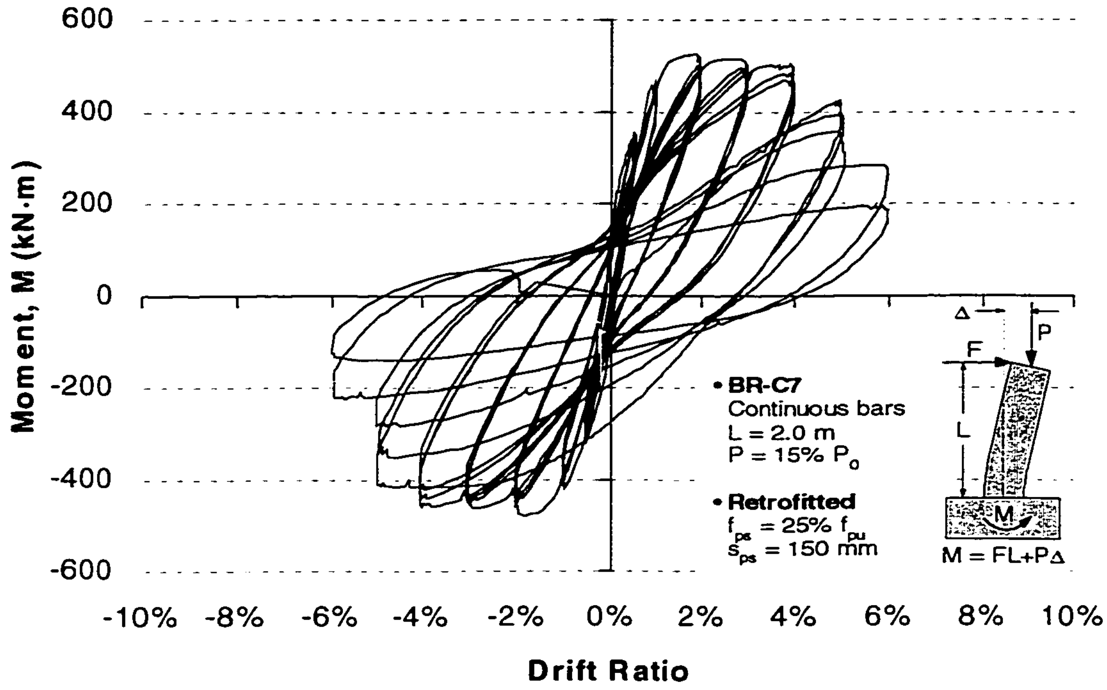

a) Column BR-C7 with continuous bars

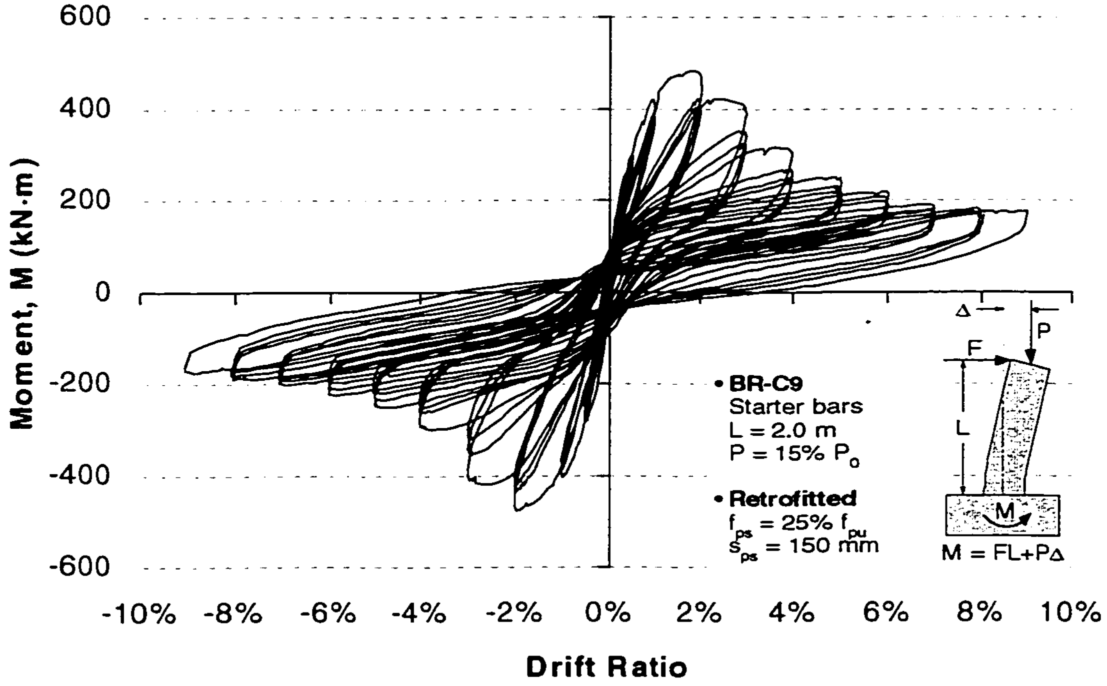

b) Column BR-C9 with lap spliced bars

Figure 4.2 Moment-Drift hysteretic relationships of the retrofitted columns BR-C7 and BR-C9

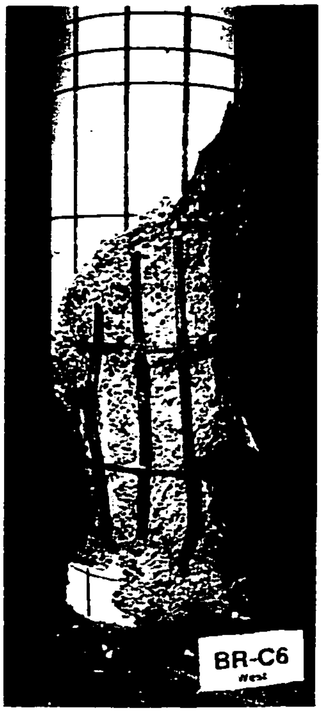

a) Column BR-C6

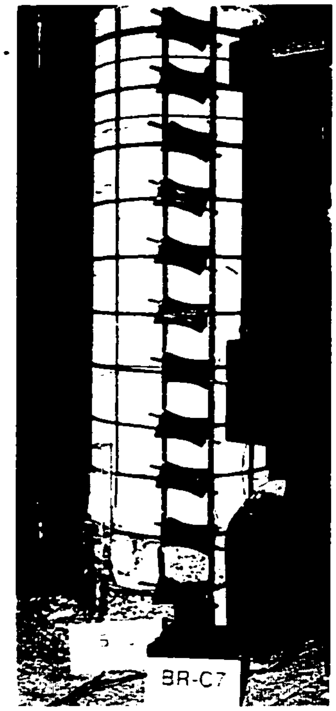

b) Column BR-C7

Figure 4.3 Comparison of columns BR-C6 and BR-C7

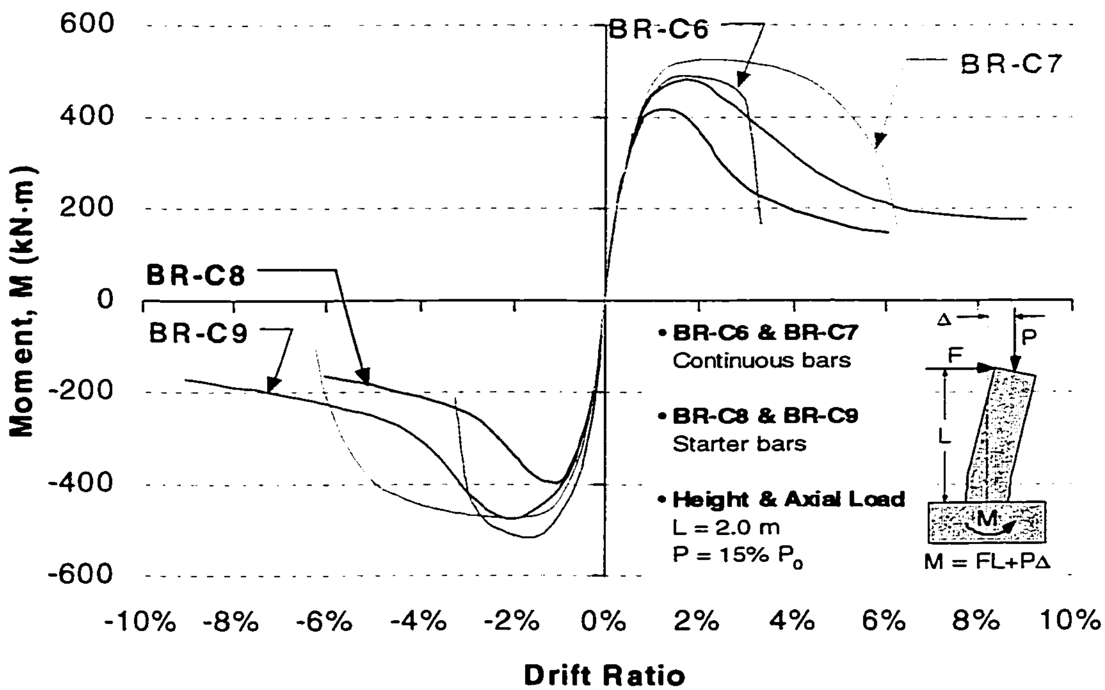

Figure 4.4 Moment-Drift envelope of the long circular columns

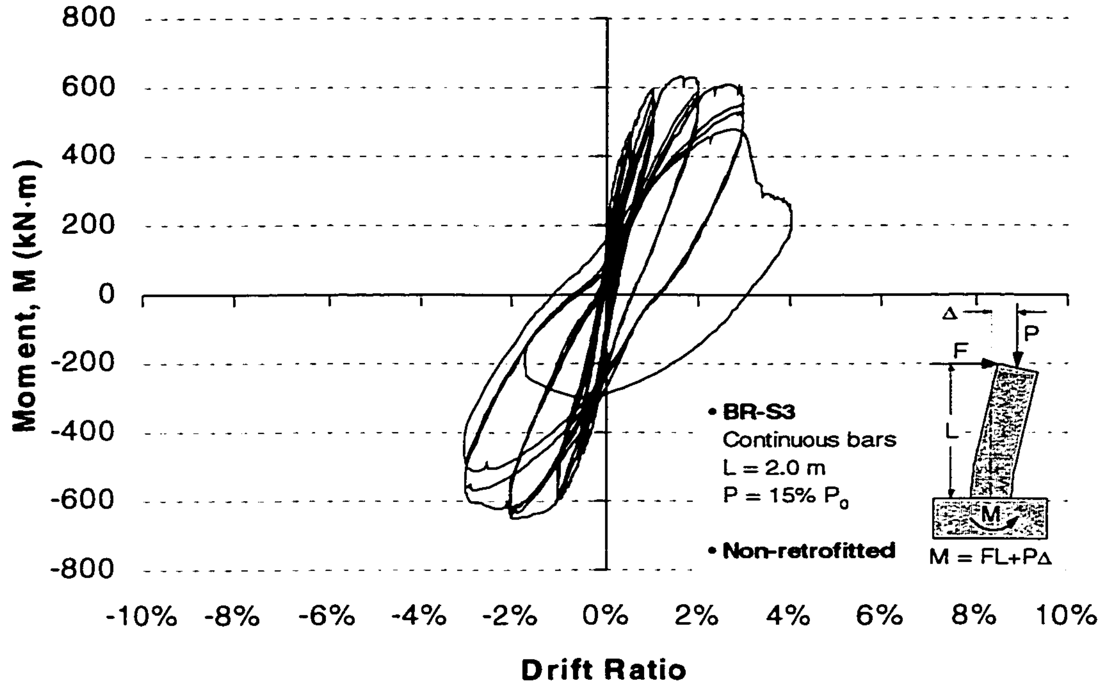

a) Column BR-S3 with continuous bars

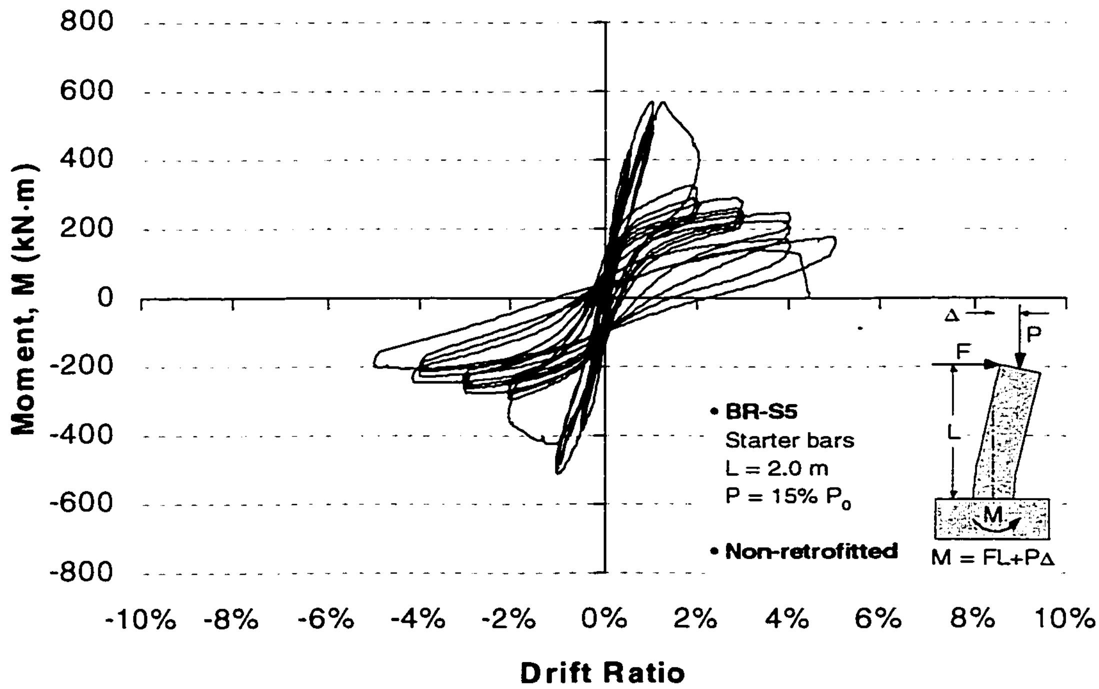

b) Column BR-S5 with lap spliced bars

Figure 4.5 Moment-Drift hysteretic relationships of the as-built columns BR-S3 and BR-S5

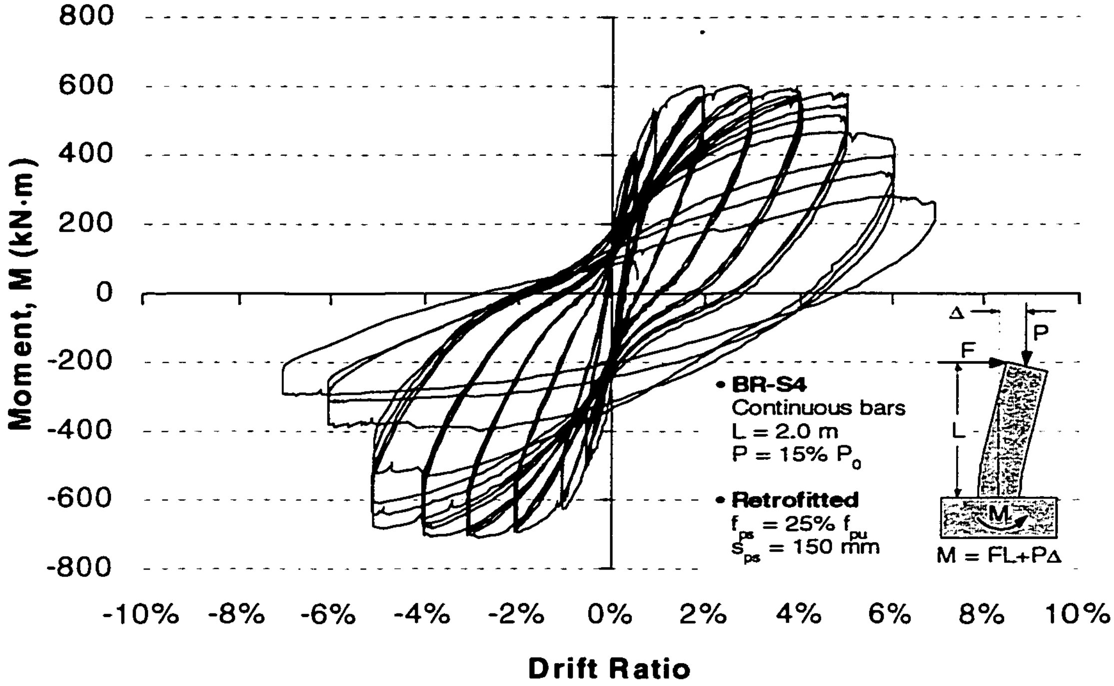

a) Column BR-S4 with continuous bars

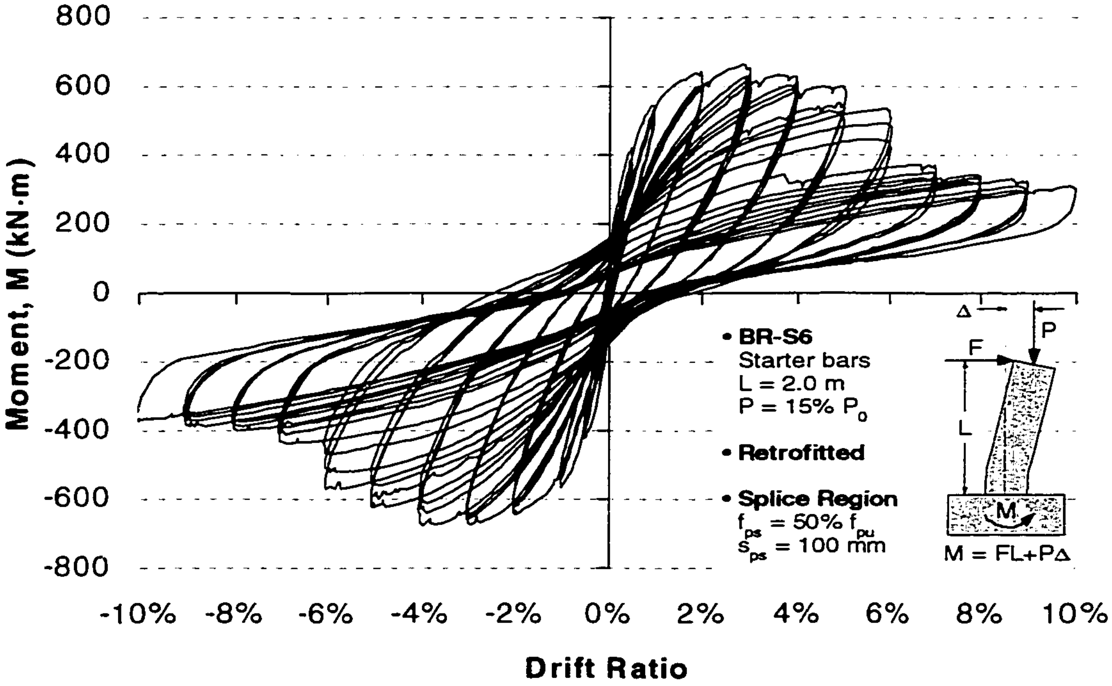

b) Column BR-S6 with lap spliced bars

Figure 4.6 Moment-Drift hysteretic relationships of the retrofitted columns BR-S4 and BR-S6

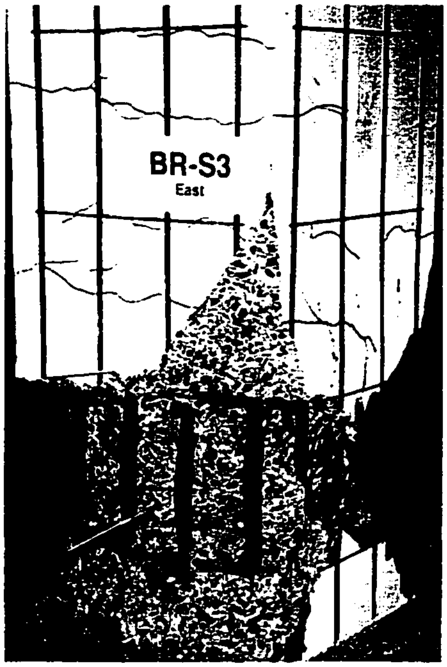

a) Bottom half of column BR-S3

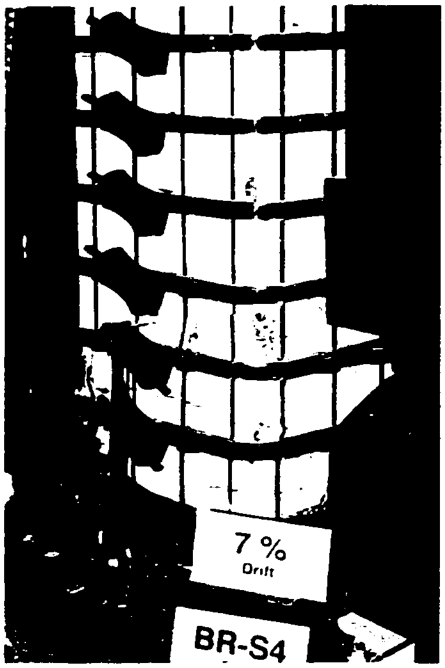

b) Bottom half of column BR-S4

Figure 4.7 Comparison of columns BR-S3 and BR-S4 (After the test)

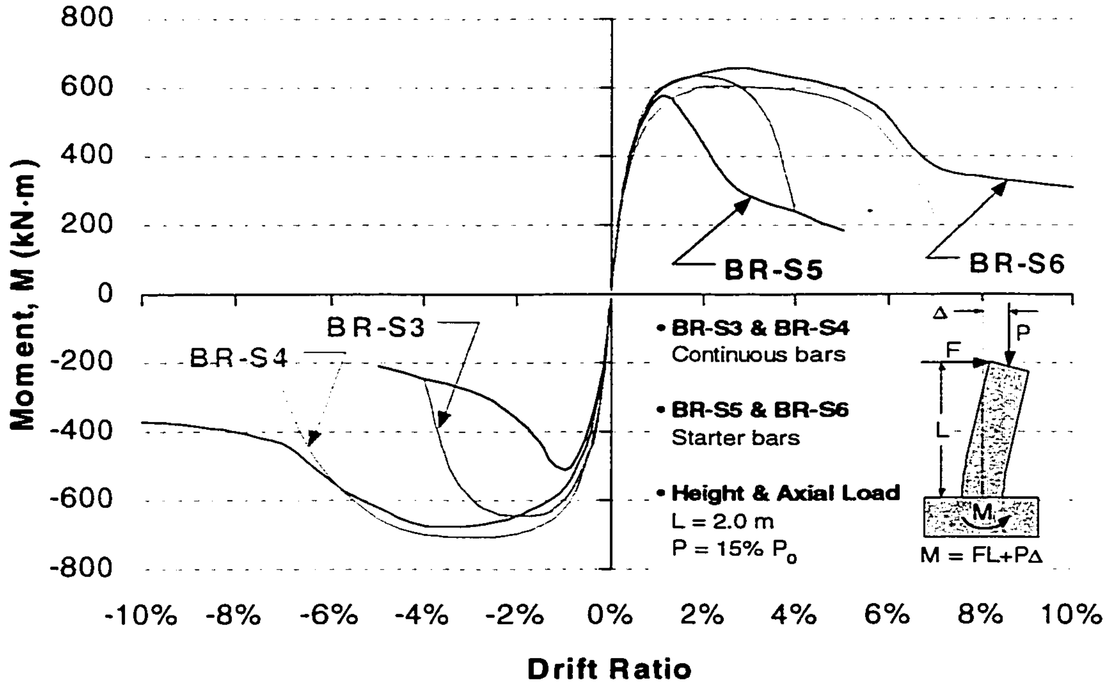

Figure 4.8 Moment-Drift envelope of the long square columns

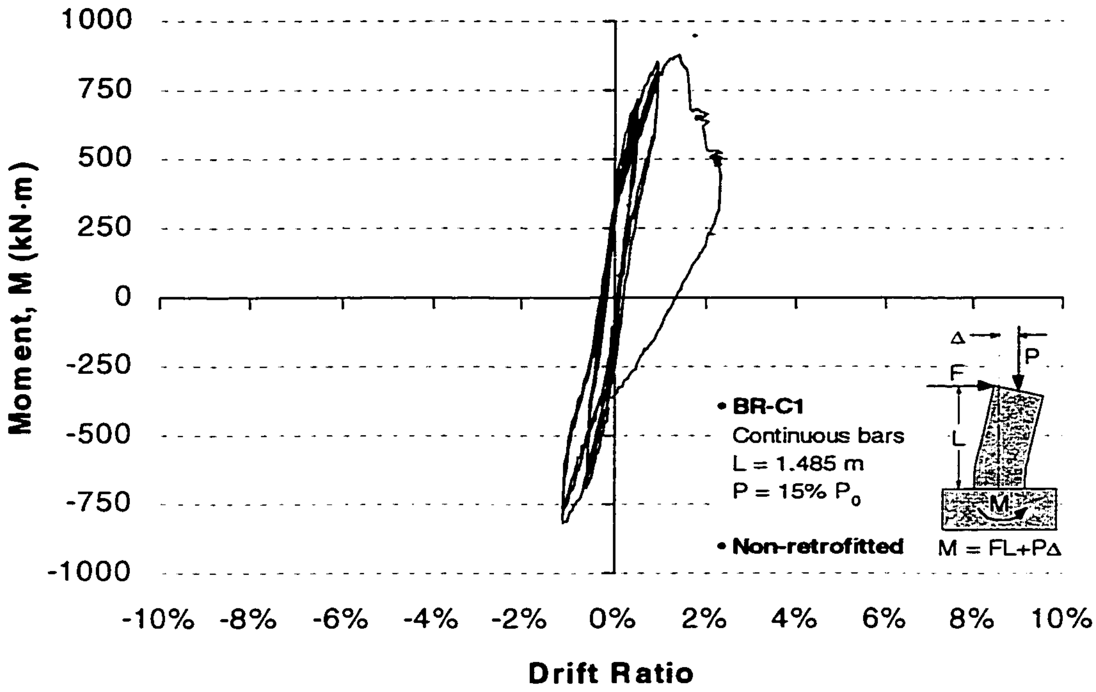

a) Column BR-C1 with continuous bars

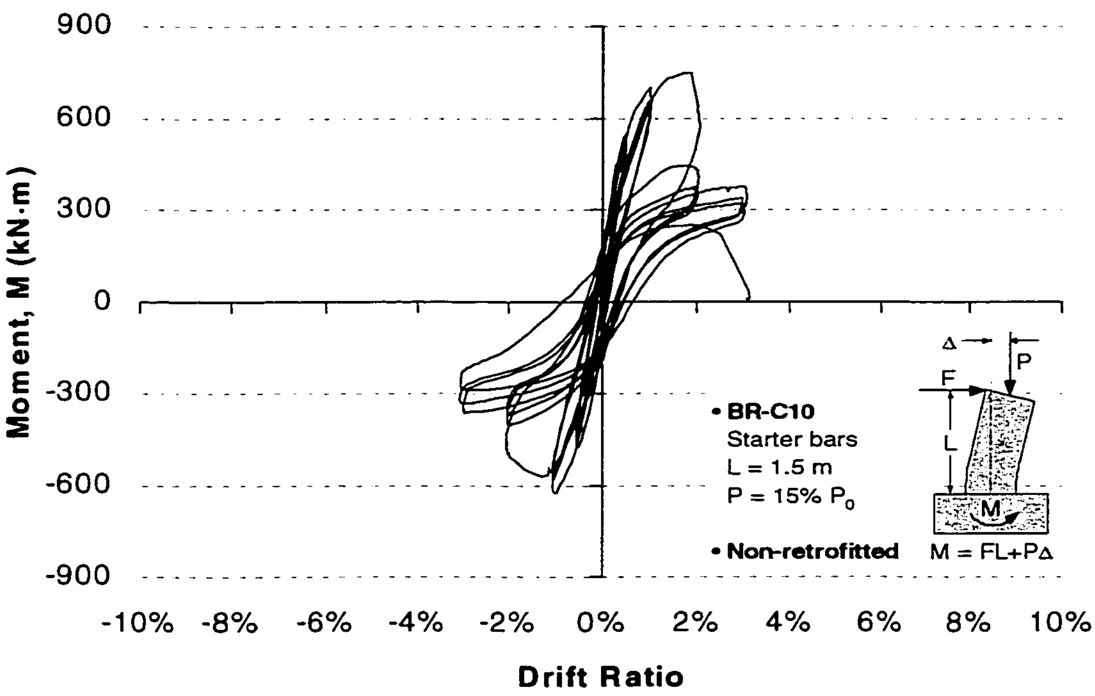

b) Column BR-C10 with lap spliced bars

Figure 4.9 Moment-Drift hysteretic relationships of the as-built columns BR-C1 and BR-C10

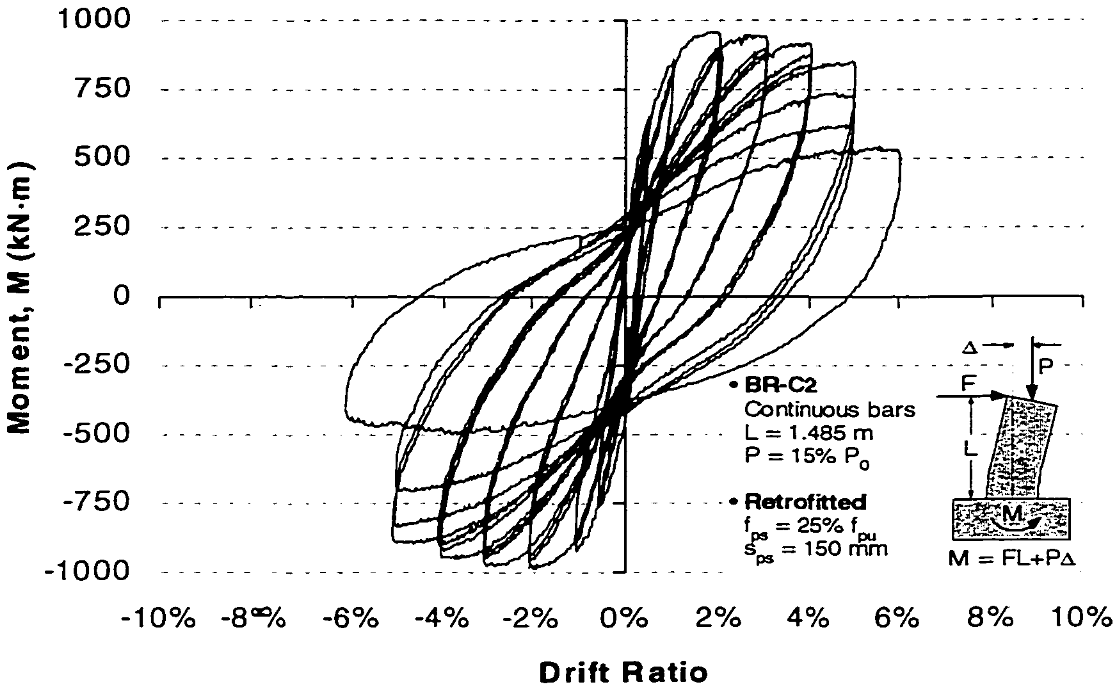

a) Column BR-C2 with continuous bars

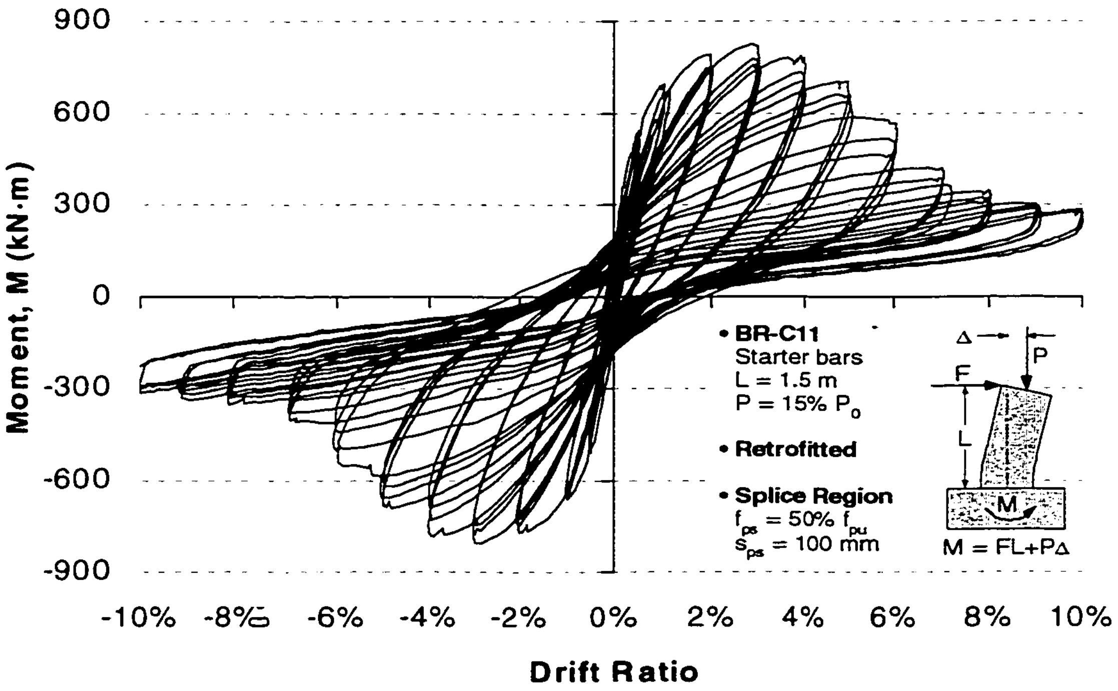

b) Column BR-C11 with lap spliced bars

Figure 4.10 Moment-Drift hysteretic relationships of the retrofitted columns BR-C2 and BR-C11

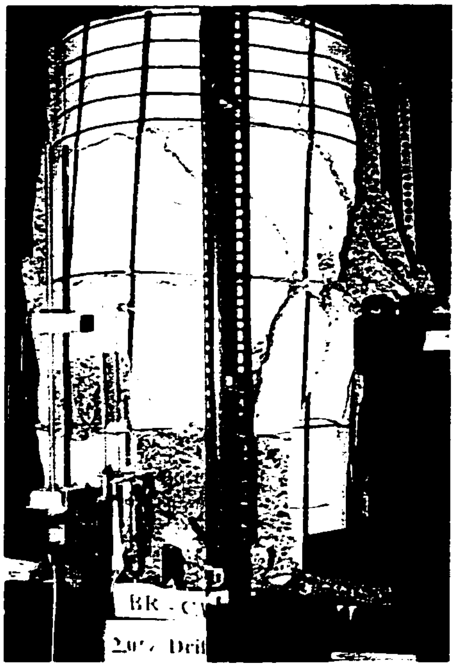

a) Column BR-C1

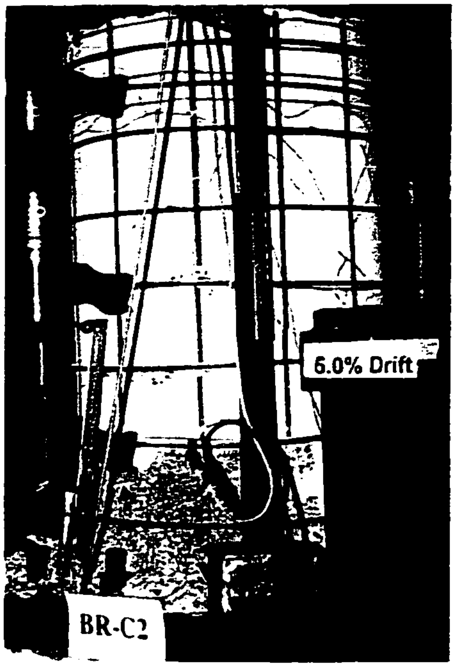

b) Column BR-C2

Figure 4.11 Comparison of columns BR-C1 and BR-C2 (End of the test)

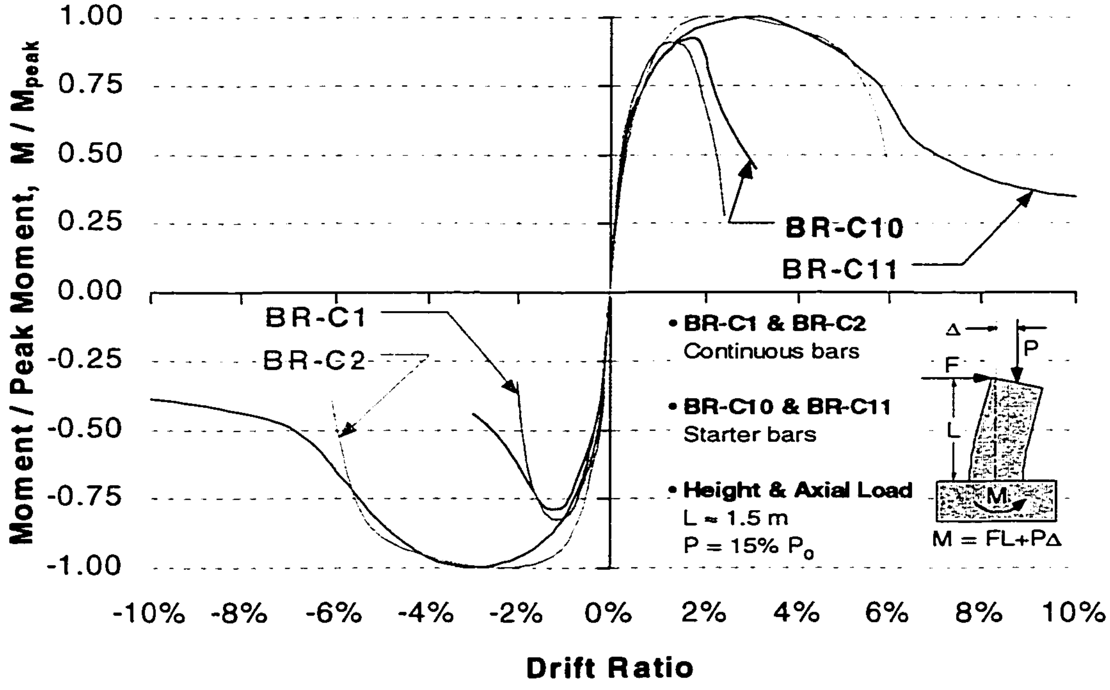

Figure 4.12 Moment-Drift envelope of the short circular columns

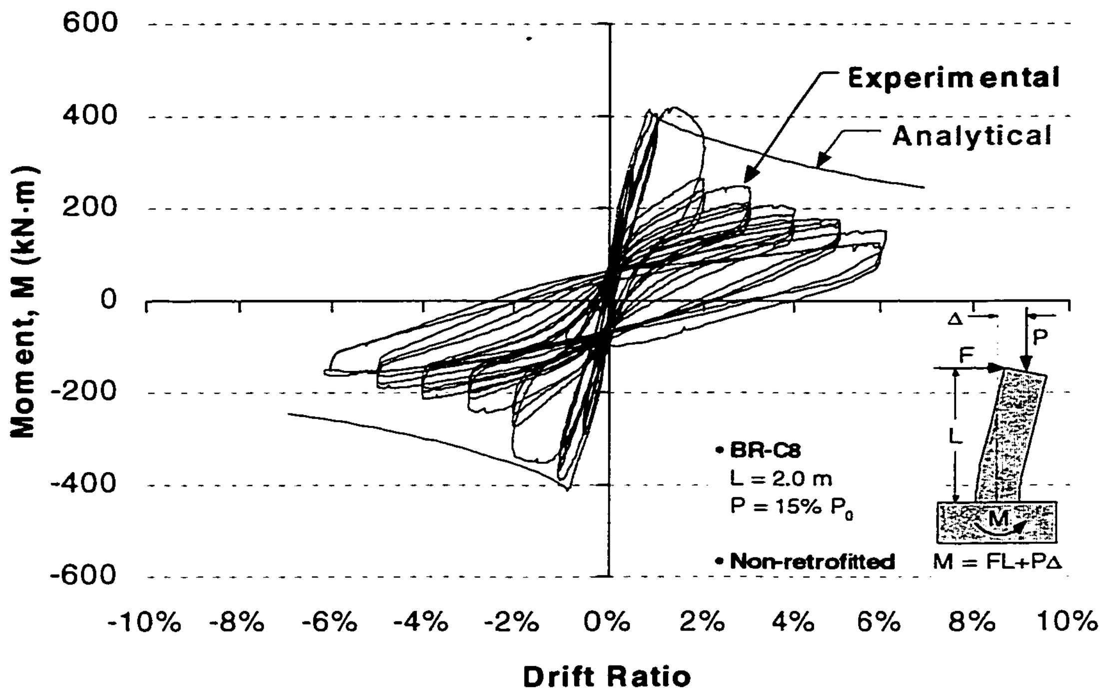

Figure 4.13 Comparison of analytical and experimental Moment-Drift relationships for the column BR-C8

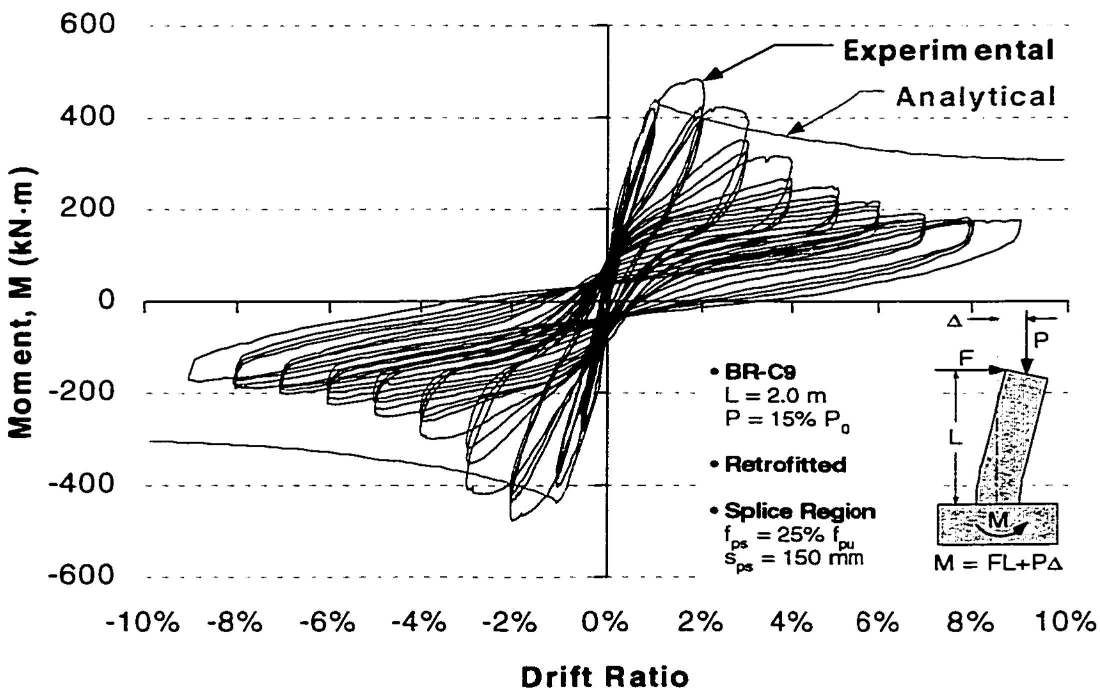

Figure 4.14 Comparison of analytical and experimental Moment-Drift relationships for the column BR-C9

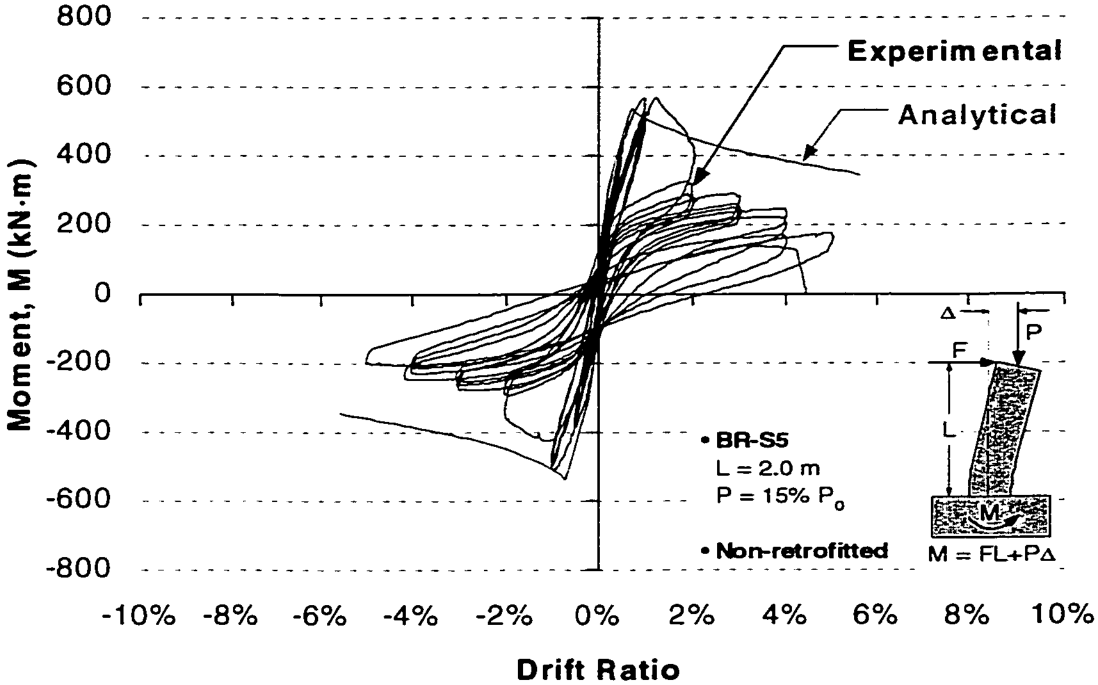

Figure 4.15 Comparison of analytical and experimental Moment-Drift relationships for the column BR-S5

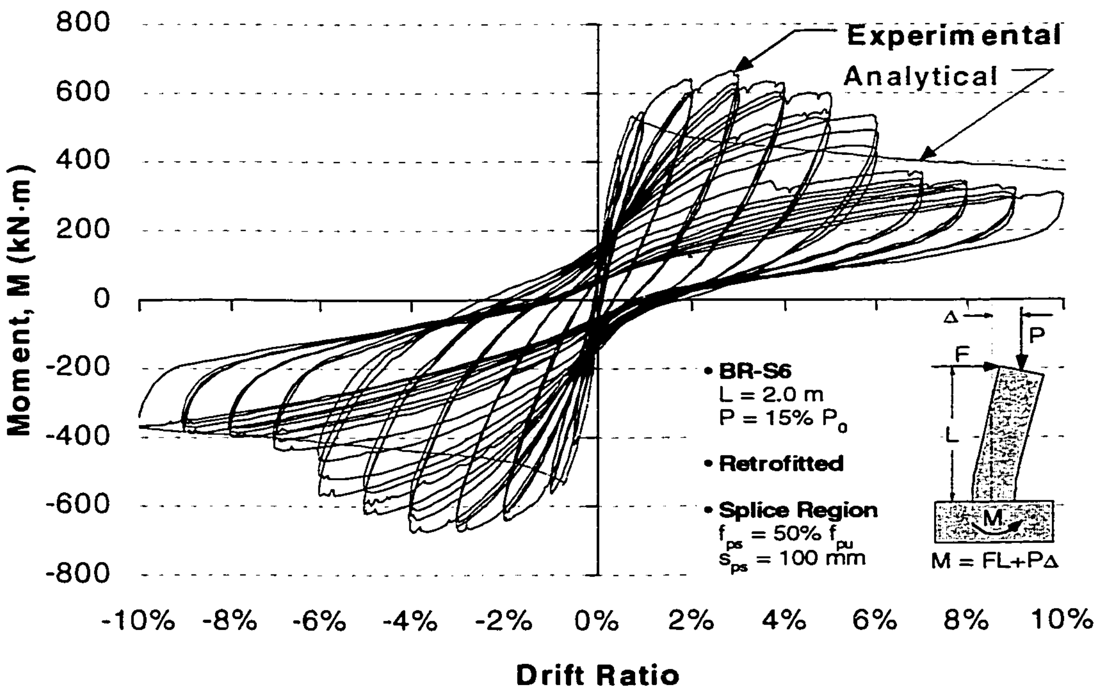

Figure 4.16 Comparison of analytical and experimental Moment-Drift relationships for the column BR-S6

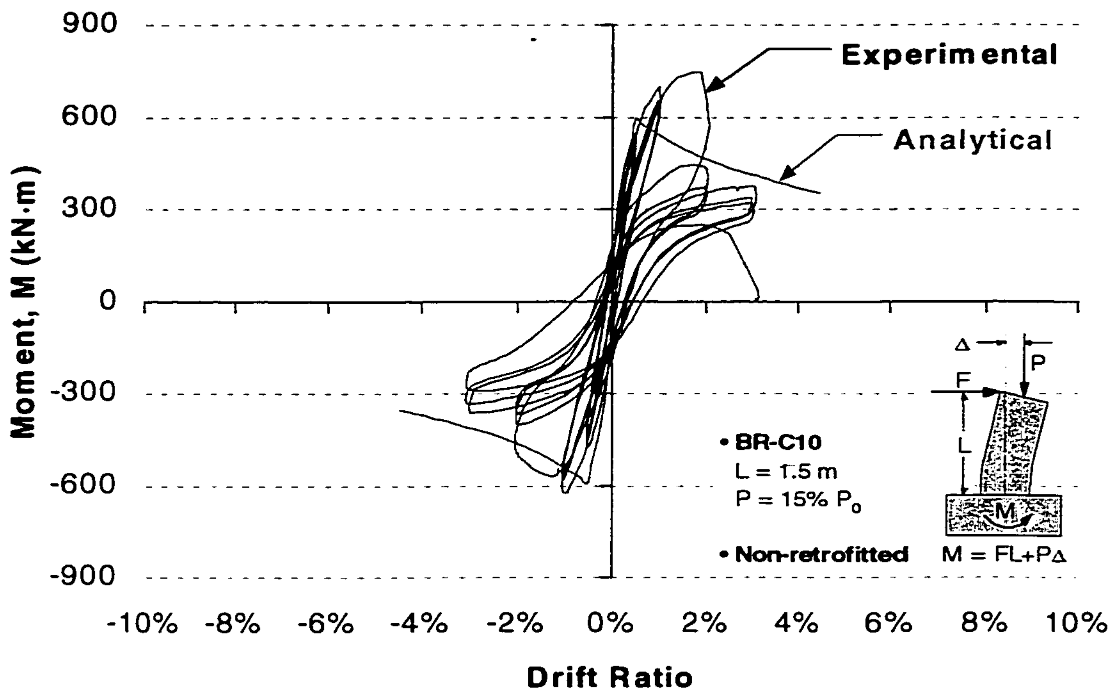

Figure 4.17 Comparison of analytical and experimental Moment-Drift relationships for the column BR-C10

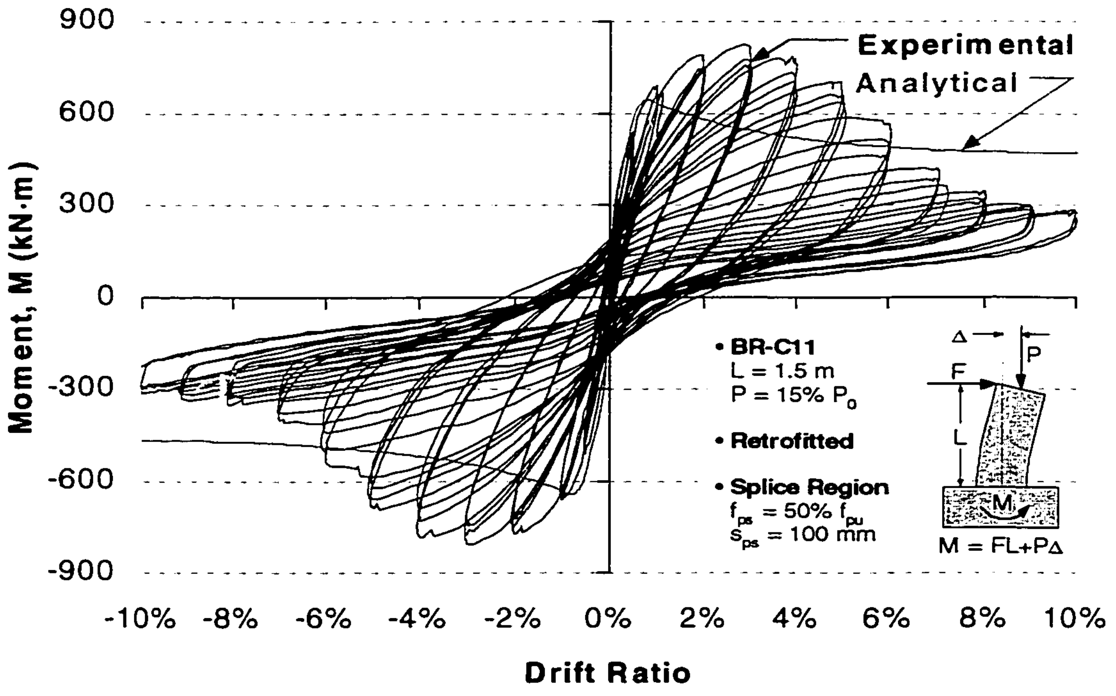

Figure 4.18 Comparison of analytical and experimental Moment-Drift relationships for the column BR-C11

CHAPTER 5

DESIGN RECOMMENDATIONS AND CONCLUSION

5.1 SUMMARY

Structures with reinforced concrete columns located in major seismic zones are subjected to high inertia forces during strong earthquakes. To resist these seismic lateral loads, a reinforced concrete column should have sufficient ductility to dissipate the energy and maintain its strength. However, most of the existing columns with reinforcing details of the pre-1971 design codes have brittle behaviour and cannot resist strong earthquakes. Additional confinement should be provided to these columns to enhance their ductility. The overall research program, which had three phases, had the objective of investigating the effectiveness of external prestressing on seismically inadequate columns for improving their seismic resistance. A total of 19 large-scale columns have been tested. First and second phases respectively studied shear dominant and flexural dominant columns, and were conducted by others. The third phase, presented in this thesis, essentially investigated the inelastic response of columns with inadequate reinforcement splices. A total of six columns were tested in this phase, under simulated seismic loading. Three columns were retrofitted, and compared with companion three non-retrofitted columns. The overall behaviour of the columns has been improved by the retrofitting scheme proposed in this research program. Some guidelines are provided below to retrofit non-ductile columns with external prestressing strands. Conclusions drawn from the results are also summarized in the chapter.

5.2 DESIGN RECOMMENDATIONS

Based on the experimental investigation and on analysis results, guidelines have been developed for seismic retrofitting existing reinforced concrete columns with external prestressing. The column drift capacity as well as the drift demand should first be checked by following the procedures presented in Chapters 3 and 4 of Yalcin (1998). The columns should be retrofitted if the demand is larger than the capacity.

For shear dominant or flexure dominant columns, the external prestressing strands should provide an active lateral confinement pressure f_l of 0.7 MPa. Equation 5.1 should be used to evaluate the required parameters to reach such a level of confinement:

$$f_l = \frac{2\, A_{ps}\, f_{ps}}{D\, s_{ps}} = 0.7 \text{ MPa} \qquad [5.1]$$

where, D = Column diameter or outside dimension of the column

A_{ps} = Nominal area of the prestressing strands

f_{ps} = Stress level applied on prestressing strands

s_{ps} = Spacing between prestressing strands

The parameters are illustrated in Fig. 5.1 for retrofitted columns with a circular or a square cross-section.

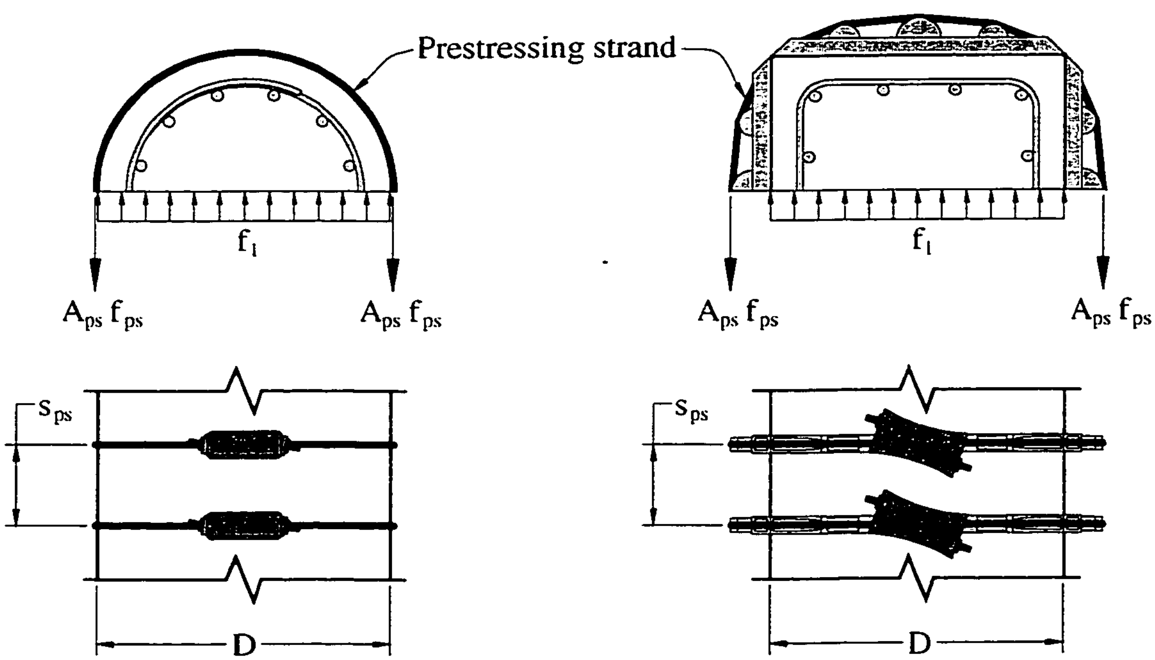

Figure 5.1 Parameters for the computation of lateral confinement pressure f_l

The lateral confinement pressure f_l given above is an average of the pressure applied on concrete. The maximum spacing for prestressing strands should be the lesser of $^D/_4$ and 150 mm, in order to provide as uniform of pressure as possible, and to avoid buckling of longitudinal reinforcement. The prestressing strands are installed directly on the column face, for circular columns. Raisers have to be introduced between the strand and the column face in square and rectangular columns to improve the uniformity of lateral confinement pressure.

The confinement should be higher for columns with inadequate splicing at their base. The lateral pressure f_l should be 2.0 MPa in the splicing region. Again, a maximum spacing of $^D/_4$ or 150 mm should be chosen. The remaining part of the retrofitted column should be actively confined to develop a lateral stress level of 0.7 MPa.

The design recommendations are intended to increase column ductility. The retrofitting strategy enhances the overall behaviour by:

- providing additional transverse reinforcement in the shear dominant columns;
- providing additional confinement in the flexural dominant columns;
- increasing the clamping pressure to avoid lap splice slippage.

It is recommended that the design stress level applied on prestressing strands f_{ps} should not exceed 50% of the ultimate strength f_{pu} to prevent the possibility of excessive straining and subsequent rupturing during a strong earthquake.

5.3 CONCLUSIONS

The literature review showed that columns designed prior to early 1970's had inadequate reinforcement details. It can be concluded that these columns were designed without adequate consideration of seismic effects. The hoops were usually placed at a large spacing of 12" (305 mm), resulting in inadequate confinement of concrete. Splicing of longitudinal reinforcement was done within the potential plastic hinge region, near the column critical section at the base. Jacketing strategy can be used to retrofit columns with inadequate seismic resistance. Steel, concrete and composite jackets showed that they could increase seismic behaviour of non-ductile columns. The steel jacket was widely used since the1971 San Fernando Earthquake.

The retrofitting strategy that is proposed in this thesis is less expensive and less labour intensive than steel jacketing. It is effective for different column cross-sections and aspect ratios. The following conclusions are drawn from the experimental and analytical investigation reported in this thesis:

- The columns which were built with reinforcement details typical of the pre-1970's designed practice, with spliced longitudinal had a limited drift capacity of 1%. These columns failed during inelastic reversals at 2% drift because of significant strength decay.

- A lap splice length of 20 times the diameter of longitudinal bar, within a potential hinging region, is insufficient. Columns designed to reflect this design practice failed prematurely as the reinforcement debonded during the first cycle at 2% drift, resulting in the slippage of bars and failure of columns. Although the splicing was inadequate, all the columns could reach their flexural yield capacity, M_y.

- The as-built columns had brittle behaviour, and the failure was usually sudden and even explosive. The retrofitted columns with lap splice reinforcement did not experience a sudden collapse, and had gradual failure. Damage on the columns, properly confined in the splicing region, was mainly limited to the first 75 mm at the bottom of the columns.

- The lap splice in columns did not significantly change the initial stiffness. The stiffness was similar for all columns, irrespective of whether they were retrofitted or not.

- Columns properly retrofitted by external prestressing, sustained a drift capacity of 4%. The retrofitting strategy provided a clamping pressure on inadequate splicing and improved inelastic response to a level comparable to that of columns with continuous reinforcement. The columns with and without lap splice had similar peak capacity, ductility and energy dissipation characteristics.

- Columns that were retrofitted with external strands, prestressed to 25% f_{pu} at 150 mm spacing showed some improvement and the drift capacity increased from 1% to 2%. It was observed that higher confinement pressure had to be applied in the splice region. Significantly improved results were obtained when a column was prestressed to 50% f_{pu} with strands at 100 mm spacing in the splice region. This retrofitting arrangement provided lateral confinement pressures f_l up to 1.92 MPa and resulted in a column drift capacity of 4%.

- Retrofitting enhanced the energy dissipation capacity. Column strength was increased only slightly. The major improvement was in inelastic deformability.

- The location of the anchors did not affect the results. The anchors were all on the East side, and similar results were recorded as columns were pushed or pulled towards the West or East, respectively.

- External prestressing enabled the formation of plastic hinging near the bottom of the columns. Columns without retrofitting experienced excessive rotations at column-footing interface. Prior to retrofitting, the designer has to ensure that the footing is strong enough to allow the formation of plastic hinges in the column before the footing fails.

- The computer program ***COLA***, developed at the University of Ottawa, slightly underestimated the strength of as-built long columns. The computed strength for the short as-built column with spliced reinforcement was much lower. Although this software can be used as a tool in judging as to whether seismic retrofitting is required or not, it should not be used to evaluate accurately the strength and deformabilty of columns with lap splices.

- The software ***COLA*** did not model the lap splice reinforcement. Consequently, it overestimated the drift level at failure of the as-built columns. Better results were provided by the program when the P-Δ effect was excluded from strength decay.

5.4 RECOMMENDATIONS FOR FUTURE RESEARCH

The following recommendations can be made for future investigation:

- Conduct additional tests on irregular columns with rectangular, hexagonal or octagonal cross-sections. Architectural features should also be included, such as flares, since it may cause migration of plastic hinging.

- Further investigate which products or materials should be used to cover the prestressing strands for effective protection against corrosion. The product or material would have to be easy to install and economical.

- Test and analyse typical building columns with inadequate reinforcement details. The main difference with earlier research would be the level of axial compression, as building columns should be subjected to higher axial load.

- Add a module to software ***COLA*** to take into consideration lap splicing of longitudinal reinforcement.

- Analyse the effect of active confinement provided by prestressing strands in order to add a module to computer program ***COLA*** that would allow analysis of retrofitted columns.

REFERENCES

- Aboutaha, R.S., M.D. Engelhardt, J.O. Jirsa and M.E. Kreger (1996). *Retrofit of concrete columns with inadequate lap splices by the use of rectangular steel jackets.* Earthquake Spectra, 12(4), Nov. 1996, 693-714.

- Aboutaha, R.S., M.D. Engelhardt, J.O. Jirsa and M.E. Kreger (1999). *Experimental investigation of seismic repair of lap splice failures in damaged concrete columns.* ACI Structural Journal, 96(2), March-April 1999, 297-306.

- Chai, Y.H. (1996). *An analysis of the seismic characteristics of steel-jacketed circular bridge columns.* Earthquake Engineering and Structural Dynamics, 25(2), Feb. 1996, 149-161.

- Chai, Y.H., M.J.N. Priestley and F. Seible (1991). *Seismic retrofit of circular bridge columns for enhanced flexural performance.* ACI Structural Journal, 88(5), Sept.-Oct. 1991, 572-584.

- Coffman, H.L., M.L. Marsh and C.B. Brown (1993). *Seismic durability of retrofitted reinforced-concrete columns.* Journal of Structural Engineering, 119(5), May 1993, 1643-1661.

- Daudey, X. and A. Filiatrault (2000). *Seismic evaluation and retrofit with steel jackets of reinforced concrete bridge piers detailed with lap-splices.* Canadian Journal of Civil Engineering, 27(1), February 2000, 1-16.

- Fafitis, A. and S.P. Shah (1985). *Predictions of Ultimate Behavior of Columns Subjected to Large Deformations.* ACI Structural Journal, July-August 1985, 423-433.

- Jaradat, O.A., D.I. McLean and M.L. Marsh (1996). *Strength degradation of existing bridge columns under seismic loading*. Transportation Research Record, 1541, 1996, 29-42.

- Mes, D. (1999). *Seismic retrofitting of concrete bridge columns by external prestressing*. M.A.Sc. Thesis, Department of Civil Engineering, University of Ottawa, Ottawa, Ontario, Canada, 1999, 125 p.

- Mitchell, D., M. Bruneau, M. Williams, D. Anderson, M. Saatcioglu and R. Sexsmith (1995). *Performance of bridges in the 1994 Northridge earthquake*. Canadian Journal of Civil Engineering, 22, 1995, 415-427.

- Mitchell, D., R. Sexsmith and R. Tinawi (1994). *Seismic retrofitting techniques for bridges — a state-of-the-art report*. Canadian Journal of Civil Engineering, 21, 1994, 823-835.

- Rodriguez, M. and R. Park (1994). *Seismic load tests on reinforced concrete columns strengthened by jacketing*. ACI Structural Journal, 91(2), March-April 1994, 150-159.

- Saadatmanesh, H., M.R. Ehsani and L. Jin (1996). *Seismic strengthening of circular bridge pier models with fiber composites*. ACI Structural Journal, 93(6), Nov.-Dec. 1996, 639-647.

- Saadatmanesh, H., M.R. Ehsani and L. Jin (1997). *Seismic retrofitting of rectangular bridge columns with composite straps*. Earthquake Spectra, 13(2), May 1997, 281-304.

- Saatcioglu, M., A.H. Salamat and S.R. Razvi (1995). *Confined Columns Under Eccentric Loading*. Journal of Structural Engineering, 121(11), November 1995, 1547-1556.

- Seible, F., M.J.N. Priestley, G.A. Hegemier and D. Innamorato (1997). *Seismic retrofit of RC columns with continuous carbon fiber jackets*. Journal of Composites for Construction, 1(2), May 1997, 52-62.

- Xiao, Y. and R. Ma (1997). *Seismic retrofit of RC circular columns using prefabricated composite jacketing*. Journal of Structural Engineering, 123(10), Oct. 1997, 1357-1364.

- Yalcin, C. (1998). *Seismic evaluation and retrofit of existing reinforced concrete bridge columns*. Ph.D. Thesis, Department of Civil Engineering, University of Ottawa, Ottawa, Ontario, Canada, 1998, 305 p.